2

GJBX-171 '79

REMOTE SENSING LABORATORY

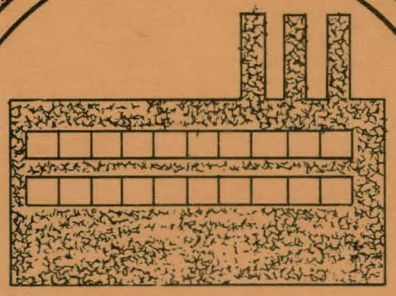

VIDEO PROCESSING OF REMOTE SENSOR DATA APPLIED TO URANIUM EXPLORATION IN WYOMING

R.A. Levinson
R.W. Marrs
Fred Crockell

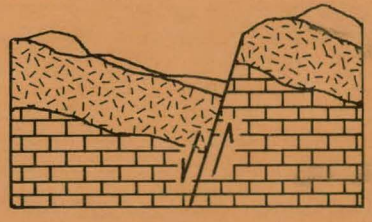

University of Wyoming

June 30, 1979

Department of Energy
Contract E(05-1)-1648

DISCLAIMER

VIDEO PROCESSING OF REMOTE SENSOR DATA APPLIED TO URANIUM EXPLORATION IN WYOMING

FINAL REPORT

Richard A. Levinson
Ronald W. Marrs
and
Fred Crockett

Department of Geology
University of Wyoming
Laramie, Wyoming 82071

June 30, 1979

PREPARED FOR THE UNITED STATES
DEPARTMENT OF ENERGY
GRAND JUNCTION OPERATIONS OFFICE
CONTRACT NO. E (05-1)-1618

NOTICE

ABSTRACT

LANDSAT satellite imagery and aerial photography can be used to map areas of altered sandstone associated with roll-front uranium deposits. Image data must be enhanced so that spectral contrasts related to alteration can be seen through masking contrasts of soil moisture and vegetation. Video image processing is a fast, low-cost, and efficient tool with which to accomplish this task. For LANDSAT data, the 7/4 ratio produces the best enhancement of altered sandstone. The 6/4 ratio is most effective for color infrared aerial photography. Field spectral reflectance data confirm the 7/4 ratio as the best discriminator between altered and unaltered surfaces, and show that altered surfaces display distinctive absorption of radiation characteristic of ferric iron.

Geochemical and mineralogical associations occur in unaltered, altered, and ore roll-front zones. Samples collected at the Pumpkin Buttes uranium district show that iron, in the form of an oxide stain on sand grains, is the primary coloring agent which makes alteration visually detectable. Eh and pH changes associated with passage of a roll front cause oxidation of magnetite and pyrite to hematite, goethite, and limonite in the host sandstone, thereby producing the alteration. Statistical analyses show that the detectability of geochemical and color zonation in host sands is weakened by soil-forming processes. Alteration can only be mapped in areas of thin soil cover and moderate to sparse vegetative cover, but can still provide a valuable exploration guide for roll-front uranium deposits.

ACKNOWLEDGMENTS

This study was generously funded by a grant from the U. S. Dept. of Energy. Drs. Dave Dahlem of the U. S. Dept. of Energy and Dave Emilia of Bendix Field Engineering Corp. were most helpful as contract monitors. Dr. Ron Chessmore of Bendix Field Engineering Corp. provided chemical analyses on a suite of samples. Dr. Steve Boese of the U. W. Geology Dept. provided much needed assistance and expertise for geochemical analysis. Dr. John Doerges, U. W. radiation safety officer, provided assistance for radiometric and x-ray analyses. The valuable assistance rendered by all the aforementioned people is greatly appreciated.

We would like to thank the following Powder River Basin ranchers and their families who kindly granted access to their land and broadened our horizons: Bud Christensen, John Christensen, Larry Gilbertz, John Groves, Ron Innes, Albert Schlautmann, and Wendell Schlautmann.

TABLE OF CONTENTS

	Page
INTRODUCTION	1
PREVIOUS WORK	2
CHOICE, LOCATION, AND ACCESS OF STUDY AREA	8
REGIONAL SETTING	11
Geomorphology	11
Climate and Vegetation	11
Soils	13
GEOLOGY	16
Geological Setting	16
Stratigraphy	16
Wasatch Formation	16
White River Formation	25
Structural Development	25
URANIUM DEPOSITS	28
Geometry of Roll-Front Deposits	28
Color	30
Sources of Uranium	31
Paleoenvironment	33
Mineralogy	34
Geochemistry	36
Roll-Front Zonation	37
Mode of Emplacement	39

Page

Age of Deposits 42

METHODS 44

IMAGE PROCESSING 46

Scale adjustment 46

Color separation 46

Contrast stretching and brightness level adjustment 46

Image Subtraction 47

Image Ratioing 47

Density Contouring 48

Compositing 48

ANALYSIS OF LANDSAT DATA 50

ANALYSES OF AIRCRAFT SENSOR DATA 56

URANIUM ALTERATION MAP 68

EVALUATION OF THE VIDEO IMAGE ANALYSIS SYSTEM 70

ANALYSIS OF FIELD SPECTRA 72

CHEMICAL ANALYSES 82

DETECTABILITY OF IRON OXIDE 87

RADIOMETRIC SAMPLING 95

ANALYSIS OF MINERALOGY 96

STATISTICAL ANALYSES 101

CONCLUSIONS 113

REFERENCES CITED 116

APPENDICES 126

LIST OF FIGURES

Figure		Page
1	Occurrence of red sandstone in the Powder River Basin, Wyoming	6
2	LANDSAT mosaic of Wyoming showing location of Pumpkin Buttes study area and outline of the Powder River Basin	9
3	Map of Pumpkin Buttes study area, Campbell County, Wyoming	10
4	View looking west to North Butte, showing typical vegetation and physiography in the study area	12
5	Geological Map of the Pumpkin Buttes region, central Powder River Basin, Wyoming	17
6	Uranium deposit on the south flank of North Butte which demonstrates the effect carbonaceous beds have on localization of uranium	19
7	Sedimentary structures of the Wasatch Formation: A. Channel and Fill, B. Large-scale trough cross stratification	21
8	Sedimentary structures of the Wasatch Formation: A. Soft sediment deformation, B. Weathered epigenetic concretion	22
9	Sedimentary structures of the Wasatch formation: A. Pipy concretions, B. Schmoos or pumpkins	23
10	Sharply defined color contact in Jeanette mine pit	24
11	Structural geological map of the Pumpkin Buttes area	27
12	Idealized cross-section through roll-front deposit	29
13	Contact between altered and unaltered sandstone expressed at the surface near the Jeanette mine	32
14	Paleogeography of the Powder River Basin during the Eocene	35
15	Eh-pH diagram showing the increased field of stability of uraninite indicated by Langmuir and Applin (1977) compared to that indicated by Hostetler and Garrels (1962)	38

Figure		Page
16	Chemical, mineralogical, and color zonation across a roll-front deposit	40
17	LANDSAT false-color composite of study area from a late October scene	52
18	Alteration map of the Pumpkin Buttes study area interpreted from LANDSAT	53
19	Unenhanced, high-altitude, color infrared photograph of study area	57
20	Ratio color composite enhanced from a color infrared aerial photograph at a medium scale	59
21	Video ratios of the CH anomaly produced from a color infrared aerial photograph at a large scale. A. Second generation 6/4 ratio, B. Third generation 6/4 ratio	61
22	Colored video enhancements of the CH anomaly produced from a color infrared photograph at a large scale. A. Density contoured 6/4 ratio, B. Ratio color composite	62
23	Night thermal/day thermal ratio of airborne multispectral scanner bands	67
24	Mean and standard deviation of spectral reflectivity in the Pumpkin Buttes uranium district	74
25	Mean and standard deviation of spectral reflectivity in the Crook's Gap uranium district	75
26	Mean and standard deviation of spectral reflectivity in the Southern Powder River Basin uranium district	76
27	X-ray fluorescence of finely-ground Fe_2O_3 pellets	89
28	Fe_2O_3 pellets used in the iron oxide experiment	90
29	Photometric reflectance determinations of Fe_2O_3 pellets	91
30	Laboratory-generated spectral curves for coarsely-ground Fe_2O_3 pellets	92
31	Laboratory-generated spectral curves for Fe_2O_3 powders	93
32	Magnetite altering to hematite in the Wasatch Formation. A. Thin section #16, unaltered sandstone. B. Thin section #12, altered sandstone	100

LIST OF TABLES

TABLE		Page
I	Entisols in the Pumpkin Buttes Area	14
II	Major Uranium Minerals Present at Pumpkin Buttes	36
III	Sample Areas in the Pumpkin Buttes Study Area	45
IV	Spectral Bands Derived From Color Separation of Color and Color Infrared Films	47
V	LANDSAT Imagery Used for Seasonal Analysis	50
VI	Comparison of the Alteration Map Interpreted from Enhanced LANDSAT Imagery to a Geological Map	54
VII	Spectral Bands Available on Multiband Photography	64
VIII	Spectral Bands Available on Airborne Multispectral Scanner Coverage	65
IX	Comparison of the Uranium Alteration Map Interpreted from Enhanced Aerial Photography to a Geological Map	69
X	Spectral Bands, Subtractions, and Ratios Derived from Field Spectra	77
XI	Optical Filters Used to Limit Photometer Sensitivity	79
XII	Geochemical Analyses	83
XIII	Comparison of Bendix and UW Geochemical Analyses	84
XIV	Mixes and Concentrations of Fe_2O_3 in Pellets	87
XV	Mineralogical Composition of Selected Rock Samples	97
XVI	Statistics on Variables Used in Correlation and Regression Programs	102
XVII	Correlation Matrix for all Variables in Soil Subfile	106
XVIII	Correlation Matrix for all Variables in Rock Subfile	107
XIX	Statistical Regressions with U_3O_8 as the Dependent Variable	110
XX	Statistical Regressions with Munsell Hue as the Dependent Variable	111

LIST OF APPENDICES

Appendix		Page
A	Descriptions of sample sites in the Pumpkin Buttes study area	127
B	Results of geochemical analyses for sample transects...	133
C	Results of geochemical analyses and photometric measurements for sample grids	156
D	Spectral curves collected in the Pumpkin Buttes area with the portable field reflectance spectrometer and geological sketch maps and cross-sections of spectrometer sample areas	173
E	Descriptions of petrographic thin sections, x-ray diffraction analysis, and mineral abundance estimates..	184

LIST OF PLATES

Plate		Page
1	Stratigraphic sections measured on North Butte	pocket
2	Uranium Alteration map	pocket

INTRODUCTION

The development of the roll-front model has been a powerful tool for exploration of sandstone-type uranium deposits in Wyoming. The model includes many facets of the deposits such as: geometry, color of the host sandstone, source of uranium, paleoenvironment, mineralogy, geochemistry, roll-front zonation, mode of emplacement, and age. The zone of altered sandstone behind a roll front is extremely important from a remote sensing point of view, for it offers the possibility for detection by satellite and airborne sensor systems.

The spectral contrasts related to uranium deposits are subtle and often masked by stronger contrasts related to variations in soil, soil moisture, and vegetation. Digital image processing has been employed to enhance remote sensor data, thus, enabling alteration to be "seen" through these interfering contrasts. Unfortunately, the potential of these enhancement techniques for uranium exploration has not often been realized because the cost of digital analysis is beyond practicality for many users. A video/analog system for image analysis was developed at the University of Wyoming with support from the U.S. Dept. of Energy. This system can provide low-cost image analysis and can create enhancements of a type and quality comparable to many digital image processing systems (Levinson, Marrs, and Grantham, 1976).

This study is a comprehensive investigation of altered sandstone associated with uranium deposits near Pumpkin Buttes in the Powder River Basin of Wyoming, and the detection of such alteration using remote sensing technology. The purpose of this study is two-fold: 1) to develop video image processing techniques that will preferentially enhance areas of alteration associated with uranium deposits and enable mapping of these areas, and 2) to investigate the spectral, geochemical, and mineralogical characteristics of altered areas which make them detectable on remote sensor data. Once these video processing techniques have been defined, they may be applied as exploration tools to new areas with similar surface and geological environments. In this way, remote sensing can serve as a valuable tool for uranium exploration.

PREVIOUS WORK

Attempts to use unenhanced remote sensor data in mineral exploration have been largely unsuccessful because the alteration patterns associated with mineral deposits are often subtle and variable. Compounding this problem is the fact that alteration patterns are usually masked by stronger contrasts related to differences in soil type, soil moisture and vegetation. The most successful endeavors to map alteration associated with uranium deposits have 1) taken advantage of spectral characteristics of the alteraton, 2) used digital processing of multispectral image data, and 3) applied the imagery in arid environments where interference from soil, soil moisture, and vegetation is minimal. These few successful studies have shown that the full spectral and spatial potential of image data may be realized only if the interpreter employs specialized image enhancement and analysis techniques. These techniques have included the following:

(1) seasonal image analysis
(2) atmospheric (dark level) correction
(3) contrast stretching
(4) density contouring (slicing)
(5) edge enhancement
(6) spatial frequency filtering
(7) digital classification and pattern recognition
(8) factor (principal component) analyses
(9) band addition and multiplication
(10) band subtraction and ratioing
(11) color additive viewing and composite display
(12) multiple operations of the above

Of these procedures, a combination of contrast stretch and ratio functions have produced the most significant enhancement of desired image contrasts (Vincent, 1973; Piech and Walker, 1974; Rowen, et al., 1974; Spirakis and Condit, 1975; Salmon and Pillars, 1975, Abrams, et.al., 1977; Offield, et.al., 1977).

Rowen, et.al, (1974) have shown that LANDSAT multispectral scanner (MSS) data can be used to discriminate ferric oxides from other materials, in their south-central Nevada test area. They constructed an uncalibrated ratio color composite from 4/5, 5/6, and 6/7 ratios of LANDSAT MSS bands where each ratio was displayed in a different color. Not only were they able to locate areas of hydrothermal alteration (commonly limonitic rocks), but they also had some success using this ratio to discriminate among ferric oxides (e.g. hematite versus limonite). The computer processing and enhancement techniques demonstrated by Rowen, et. al. (1974) may be applicable to exploration for sandstone-type uranium deposits commonly found associated with ferric oxide alteration.

Salmon and Vincent (1974) have demonstrated that detection of all ferric oxides can be enhanced by computer processing of a single LANDSAT

band ratio, the 5/4 ratio. They worked with data from the semi-arid, sparsely vegetated Wind River Basin of Wyoming. Their processing functions included 1) atmospheric correction, 2) construction of the 5/4 ratio, 3) automated recognition of materials displaying low image densities (high amounts of ferric oxides, particularly hematite), and 4) density slicing to enhance specifically the low-density areas.

Salmon and Pillars (1975) continued this work in the Wind River Basin, addressing the problem of enhancing ferric oxides specifically related to uranium deposits (as opposed to enhancing all ferric oxides). Their methods included collecting samples of altered surface material and subjecting these to laboratory analyses of spectral reflectance, Munsell color coordinates, mineralogy, and iron content. Results of these analyses were compared to LANDSAT ratios. They found that the 5/4 ratio could separate hematite-stained surface materials but not limonite-stained materials. However, when visually strong, yellow, limonite alteration correlated with high concentrations of free ferric oxide, the visible and infrared absorption in LANDSAT bands 4 and 7 could be strong enough to be recognized. Therefore, a combination of LANDSAT 5/4 and 7/6 ratios may detect some areas of limonitic stain.

Salmon and Pillars' (1975) study also showed that, for eighteen selected samples, Munsell color coordinates and ferric iron content decreased with a general shift in Munsell hue from 10YR to 5YR. This same general shift in hues correlated with increasing 5/4 ratio values. The ratios were generated from laboratory spectra of the individual samples. There was, however, no correlation between ferric iron content, and 5/4 ratio values.

Vincent (1977) continued the Wind River Basin work by constructing a representative spectral signature from LANDSAT digital data for oxidized topsoil found on or adjacent to known, near-surface uranium deposits. He used this signature in an automatic recognition mapping program for LANDSAT imagery. His "false alarm" rate was lower with this method than with photo-interpretation of a single ratio (including the 5/4 ratio) or with color composite ratio images. However, this method was unable to provide discrimination between secondary ferric oxides commonly associated with uranium deposits and some "uninteresting" primany ferric oxides. Vincent developed recognition contour maps based on regions of equal percentage of ground area covered by his "oxidized topsoil" signature represented on LANDSAT imagery. He constructed these maps for areas around the Gas Hills, and Southern Powder River Basin uranium districts in Wyoming, and for the Jackpile mine area in New Mexico. All maps showed recognition of "oxidized topsoil" in undisturbed areas adjacent to mine complexes. This suggests that his "oxidized topsoil" signature might be applied to other LANDSAT scenes collected at different times and places.

R. M. Hoffer and his staff at the Laboratory for Applications of Remote Sensing (LARS) at Purdue University performed a comprehensive investigation on computer-aided analysis of Skylab MSS data in the San

Juan mountains of southwestern Colorado (Hoffer and staff, 1975). In one of their studies, they attempted to enhance hydrothermal alteration consisting of iron oxide gossans using both SKYLAB and airborne MSS data. They produced ratios and ratio color composites similar to those used successfully by Rowen, et. al. (1974) and Salmon and Vincent (1974). While altered areas could be enhanced by using these methods, so were the noise characteristics of the data. Computer classification techniques proved to be the most definitive and consistent approach for delineating altered areas. However, successful application of these techniques required much fore-knowledge of the area, adequate training sets, and much computer time.

Spirakis and Condit (1975) used computer-enhanced LANDSAT data to locate alteration zones associated with uranium deposits in the Painted Desert near Cameron, Arizona. Their methods included digital processing of LANDSAT data for removal of electronic noise and atmospheric haze, then contrast stretching, ratioing, and constructing ratio color composites. Field work showed that the altered rocks were similar throughout the mining district, but that the alteration (a light brown-yellow color) was not uniquely related to ore deposits. Two ratio composites were effective in enhancing the alteration zones; they were the 5/4, 6/4, 7/6 combination and the 4/7, 6/4, 7/4 combination. The 6/4 ratio was most influential in accentuating alteration for both composites (Spirakis and Condit, 1975). Examination of the study area showed that many alteration zones were obsecured by alluvium and vegetation. Also, other rock units in the area produced anomalies similar to those produced by alteration on the ratioed imagery. Their technique resulted in a 75% success rate for observable alteration, and it demonstrated that ratios other than 5/4 could be effective in enhancing altered areas.

Offield, et. al. (1977) worked with computer-enhanced LANDSAT MSS data on geological studies related to uranium deposits in the southern Powder River Basin of Wyoming. They found that various enhancements and color presentations of the 4/5 ratio provide a reasonably good discriminator of exposed hematite alteration associated with uranium roll-front deposits there.

They used the portable field reflectance spectrometer (PFRS) developed by the NASA/Jet Propulsion Laboratory (JPL) at the California Institute of Technology (Goetz and others,1975, Appendix E) to measure spectral reflectance of altered and unaltered surface materials. The field spectra of altered rocks and their overlying residual soils showed absorption bands characteristic of ferric iron near 0.55 and 0.9 μm (Hunt, Salisbury, and Lenhoff, 1971) which were absent or minimal in spectra of unaltered materials. These patterns measured in the field agreed with controlled laboratory spectral measurements of selected samples. The spectra measured by Offield, et. al. (1977) also show that other spectral bands not available from LANDSAT should permit even better discrimination of altered materials associated with uranium roll-front deposits. On a 5/6 ratio, a large lineament marked by changes in vegetation and stream course patterns seemed to correlate with the western limit of

known economical deposits in the region. Other lineaments mapped from LANDSAT imagery correlated with the trend of mapped subsurface folds and ore-sand isopachs. Offield, et. al. (1977) suggest that many of these lineaments are related to structures which controlled the flow of uranium-bearing solutions.

Houston, et. al. (1973) studied uranium mineralization in coarse-grained, oxidized, arkosic sandstones in the Powder River Basin of Wyoming. They attempted to map altered areas from a LANDSAT false-color composite scene. Houston's map was compared to a geological map of the area compiled by Sharp and Gibbons (1964). Correlation between the image interpretation and mapped zones was slight (fig. 1). Because of the marginal success, Marrs, et. al. (1973) made several additional interpretations of the same area. There was fair to good agreement among interpreters with respect to location of altered areas, but little agreement as to the boundaries of the altered zones. Still, the interpretations only roughly corresponded to Sharp and Gibbons' (1964) map.

The most obvious color anomalies in the area correspond to altered sandstone mapped by Sharp and Gibbons (1964). The Pumpkin Buttes uranium district in the central Powder River Basin is one such area. In this area, several individual altered sands were recognized as color anomalies (fig. 1). These anomalies compared more favorably to a detailed large-scale geological map of the Pumpkin Buttes mineral district by Sharp and White (1957). Several of the individual color anomalies coincided with known uranium occurrences.

Video/analog image processing is a new technology which can provide an alternative to costly digital image processing for image enhancement. Many of the digital procedures described previously can also be accomplished in an analog mode.

Only two investigations have used video/analog image processing to evaluate uranium districts. Neither attempted to map uranium alteration directly.

Kober and Procter-Gregg (1977) used LANDSAT 19-cm (7.5-in) transparency sets to enhance alteration halos in fifty areas of known uranium occurrences in the western United States. Their hybrid-analog video processor enabled them to analyze great volumes of data with comparatively little expense and time. They also demonstrated th utility of density contouring to enhance changes in brightness on LANDSAT imagery.

Marrs and King (1978) demonstrated that video processing can be economically used as part of a program to assess regional uranium resource potential. Like Kober and Procter-Gregg (1977), they analyzed LANDSAT imagery for many diverse areas in the western United States. Their processing functions included ratios, band subtractions, edge enhancements, density contours, and color composites. These were applied selectively, depending on characteristics of each study area. Results

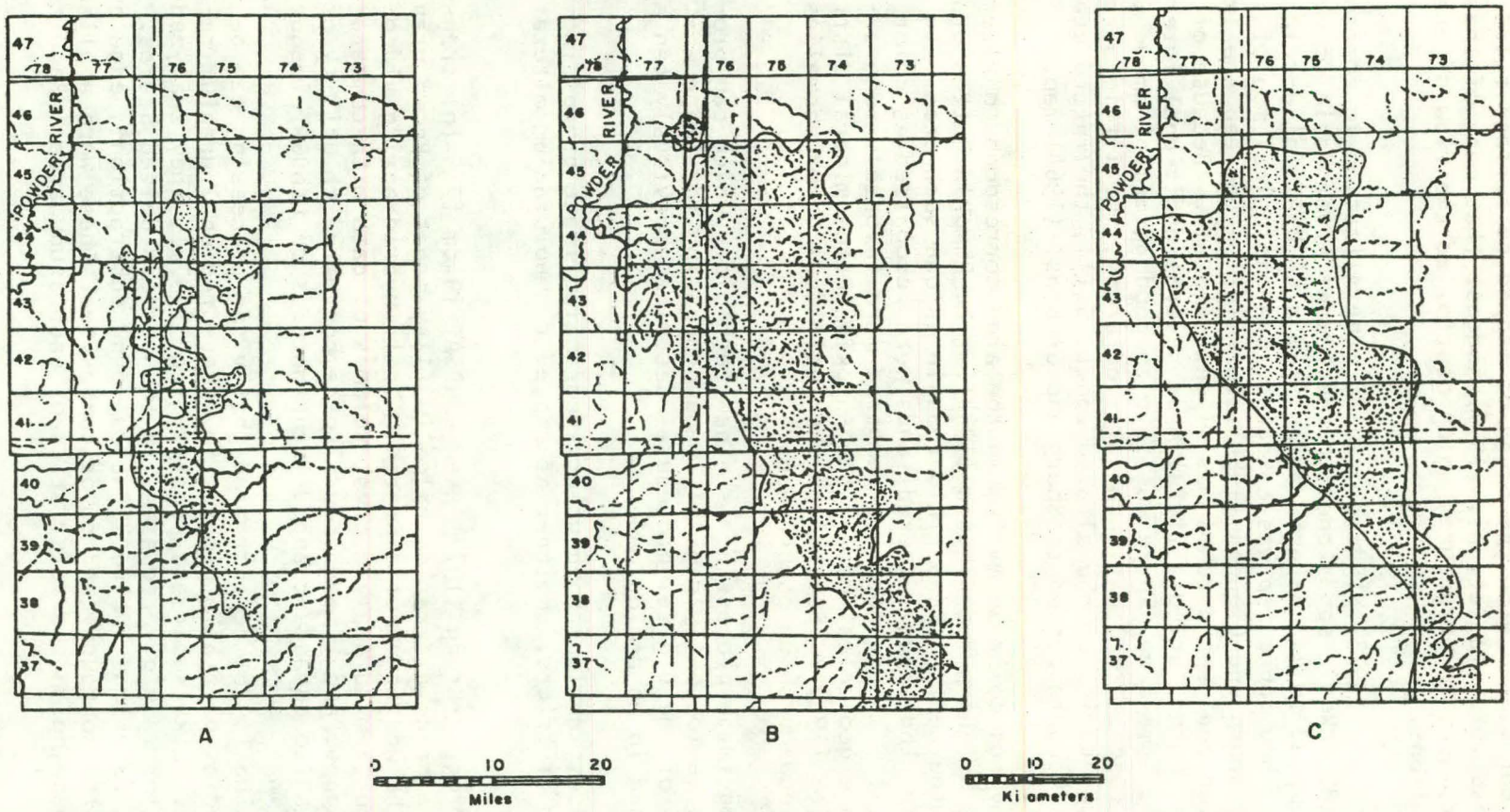

Figure 1 Occurrence of red-colored sandstone in the Powder River Basin, Wyoming.
A. Interpreted from an unenhanced LANDSAT color composite (Houston, et. al., 1973).
B. Interpreted from a video-enhanced LANDSAT color composite.
C. Field occurrence as mapped by Sharp and Gibbons (1964).

from their enhancements were mixed. In areas where geologic structure played a major role in ore emplacement (e.g. calderas), structural enhancements and geomorphic interpretations proved more successful than spectral analyses. In other areas, which involved shallow sandstone-type uranium deposits, various spectral band combinations proved more effective (though not always successful) in locating favorable environments for mineralization. Vegetative cover was often the limiting factor in determining the success of video analyses, though quantitative and qualitative information on vegetative cover was generally lacking. The exact effect of vegetation in any particular enhancement was not documented, though in several cases the 5/7 ratio was used to enhance differences in vegetation which seemed to indicate favorable lithologic environments for uranium deposition.

Townsend (1979) attempted to identify alteration associated with uranium mineralization in the Crooks Gap district from processed LANDSAT multispectral imagery. He found much of the altered ground characterized by a "bleached" condition with no diagnostic color. Smaller areas within the altered zone are pale red in color and exhibited high values in the LANDSAT 5/4 band ratio; but sand dunes and outcrops of red-colored Triassic rocks also produced high 5/4 ratio values. Townsend concluded that the altered ground in the Crooks Gap district is not spectrally identifiable (1979, p. 46). However, the LANDSAT multispectral data could still be used as a reconnaissance tool for identifying all areas rich in ferric iron oxides, some of which would be altered ground.

CHOICE, LOCATION, AND ACCESS OF STUDY AREA

The Pumpkin Buttes uranium district (fig. 2) was chosen for study because previous work by Houston, et. al. (1973) and Marrs, et. al. (1973) provided a basis from which the contribution of video processing technology could be evaluated. Scientists at JPL were, at that time, considering the Pumpkin Buttes area for study of the spectral characteristics of altered rocks and soils. The potential availability of their PFRS data further encouraged selection of the Pumpkin Buttes area as a test site. Some mining activity took place in the area between 1953 and 1964. This early development consisted of a few small open pits and scattered scrapings of surface material. At the start of this investigation, the study area was relatively undisturbed. A year after the start of fieldwork, the Hartzog Draw oilfield was developed southward through the study area. New roads, pipelines, drilling, and production facilities have now destroyed some of the natural cover.

The physiography of the Pumpkin Buttes area is favorable for remote sensing studies. The gently rolling, vegetated uplands east of the buttes are typical of Wyoming basin topography and range conditions. In the western part of the study area, badland topography provides good exposure of lithologies and enables fairly good stratigraphic control for ground-based and remote studies.

The Pumpkin Buttes stand in the southwestern corner of Campbell County, Wyoming, in the central portion of the Powder River Basin. The study area (fig. 3) covers 373 km^2 (144 mi^2), centered around T. 45 N., R. 75 W. This area comprises most of the Savageton, Wyoming 15-minute quadrangle (U.S. Geological Survey, 1959), and includes the northeast portion of the Pumpkin Buttes uranium district as well as areas outside the district. North (Pumpkin) Butte is in the southwest corner of the study area, and Black Butte is in the extreme northeast corner. The study area is located 56 km (35 mi) southwest of Gillette, Wyoming on Wyoming State Highway 50. The area may also be approached from Wyoming Route 387, which passes south of the Pumpkin Buttes. From this direction, the study area is located 29 km (18 mi) north on State Highway 50 from Pine Tree Junction. A county road intersects State Highway 50 at Savageton, Wyoming, and leads westward into the study area. Ranch and oilfield roads give reasonably good access to the rest of the study area.

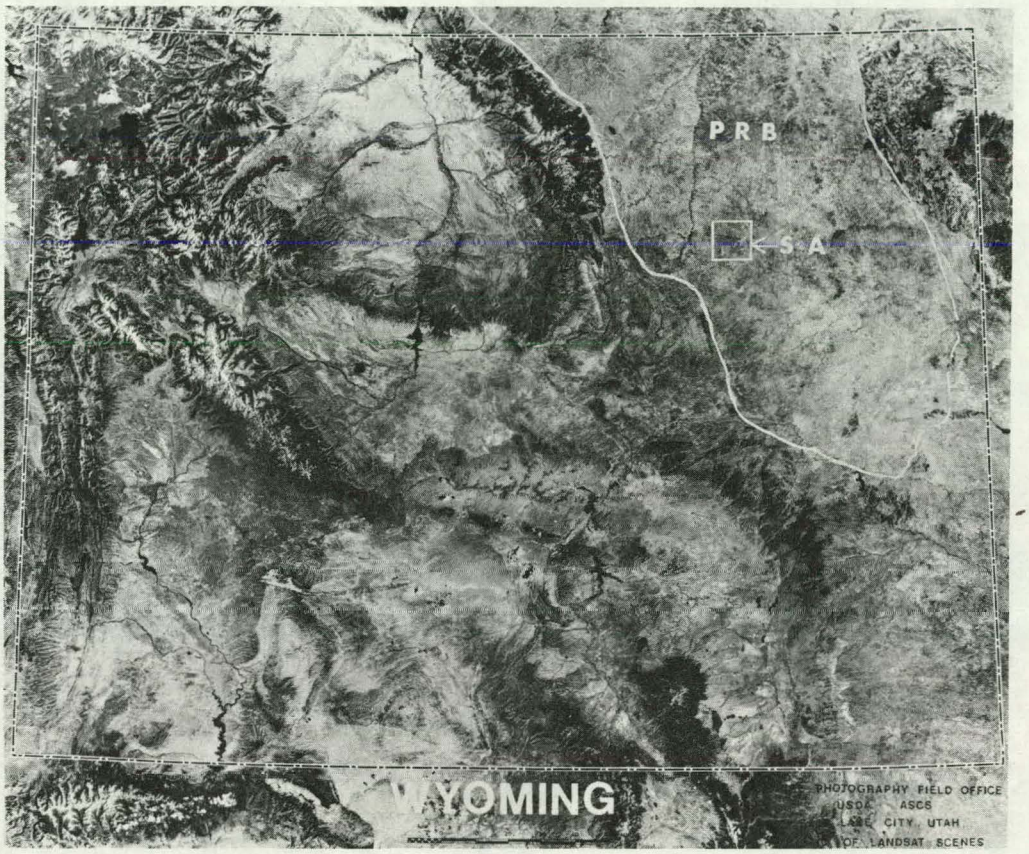

Figure 2. LANDSAT mosaic of Wyoming showing location of Pumpkin Buttes study area (SA) and outline of the Powder River Basin (PRB).

Pumpkin Buttes Study Area, Campbell County, Wyoming

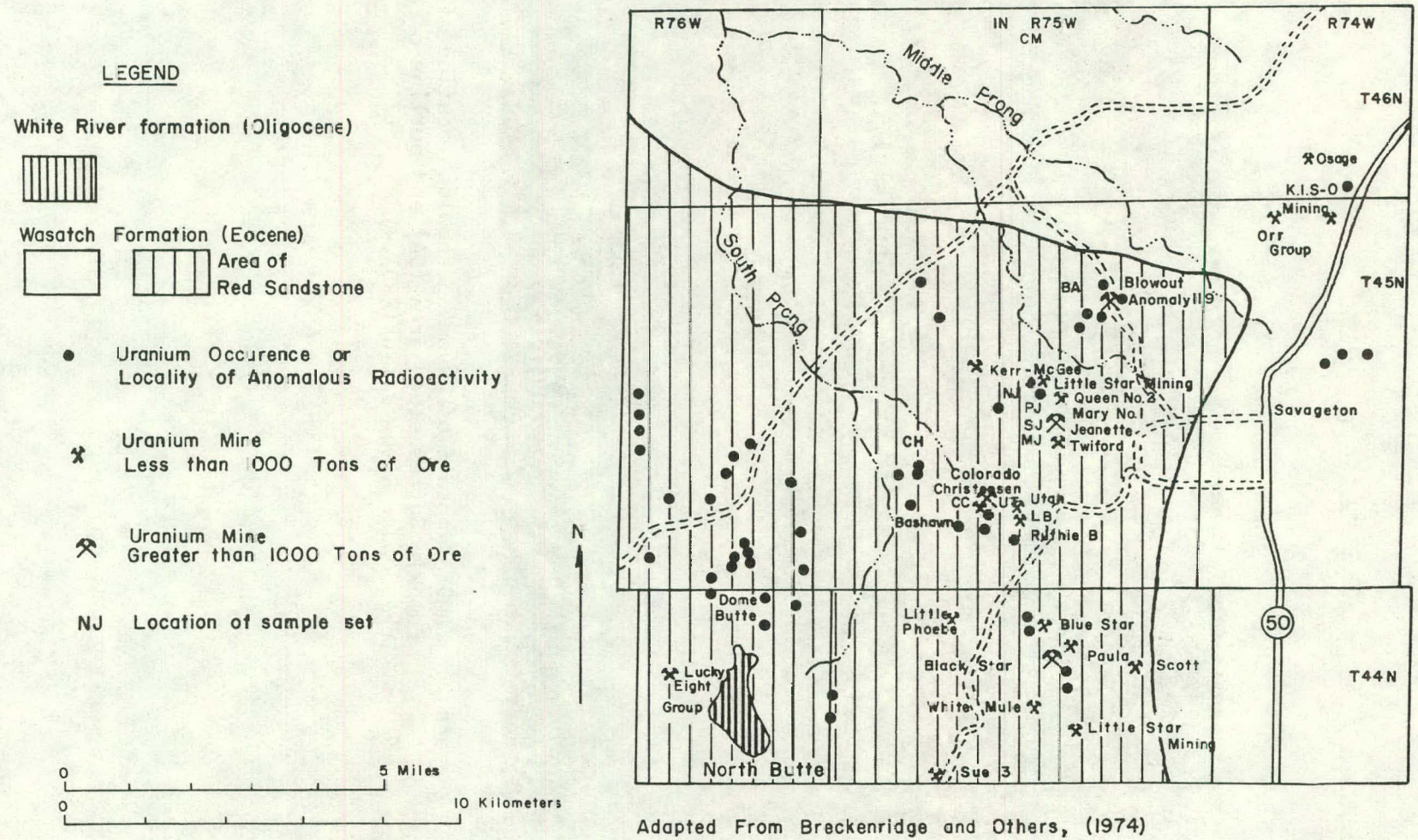

Adapted From Breckenridge and Others, (1974)

Figure 3

REGIONAL SETTING

Geomorphology

The study area lies within the unglaciated portion of the Missouri Plateau Section in the Great Plains Geomorphic Province (Fenneman, 1931). The Pumpkin Buttes are on the drainage divide between the Belle Fourche River and Powder River watersheds. Most of the study area has been classified as "rolling divide", characterized by smooth rolling topography (fig. 4). The extreme western portion of the study area is dissected upland, characterized by the moderate badland topography of the Powder River Breaks (Breckenridge and others, 1974). Elevations range from 1848 m (6062 ft) on North Butte to 1399 m (4589 ft) at the northwest corner of the study area where Pumpkin Creek exits.

The Pumpkin Buttes are prominent landmarks in the Powder River Basin, towering over 305 m (1000 ft) above the surrounding prairie. They are unique in that they are the last preserved remnants of an older erosion surface. The only remnants of mid-Tertiary (Oligocene) rocks in the Powder River Basin cap the Pumpkin Buttes. The Pumpkin Buttes include 5 major flat-topped mesas and several smaller buttes. Slumping, landslides, and solifluction are very common on the flanks of all buttes. Thick accumulations of allumium and colluvium lie at the base of the slopes. These deposits are deeply dissected. Several gullies contain natural bridges of alluvium--evidence of extremely rapid downcutting in recent years.

Regional variations in geomorphic pattern are caused primarily by differences in erosional characteristics of the nearly flat-lying Tertiary bedrock as the various units respond to downward and lateral dissection by fluvial channels and by eolian erosion and deposition.

Climate and Vegetation

Interactions between climate and hydrology have a major influence on transport and deposition of uranium deposits. For a detailed discussion of climate in the Powder River Basin and its implications concerning uranium deposits, the reader should refer to Morris (1977).

The climate of the Powder River Basin is temperate and semi-arid. The Pumpkin Buttes area receives 30.5-35.6 cm (12-14 in) of precipitation (WRRI, 1974), most of which occurs in the spring and early summer. The average January temperature for the area is -6°C (22°F), and the average July temperature is 25°C (77°F) (Becker and Alyea, 1964). Temperatures vary widely in both diurnal and seasonal cycles. The region has a growing season averaging about 120 days (Breckenridge and others, 1974).

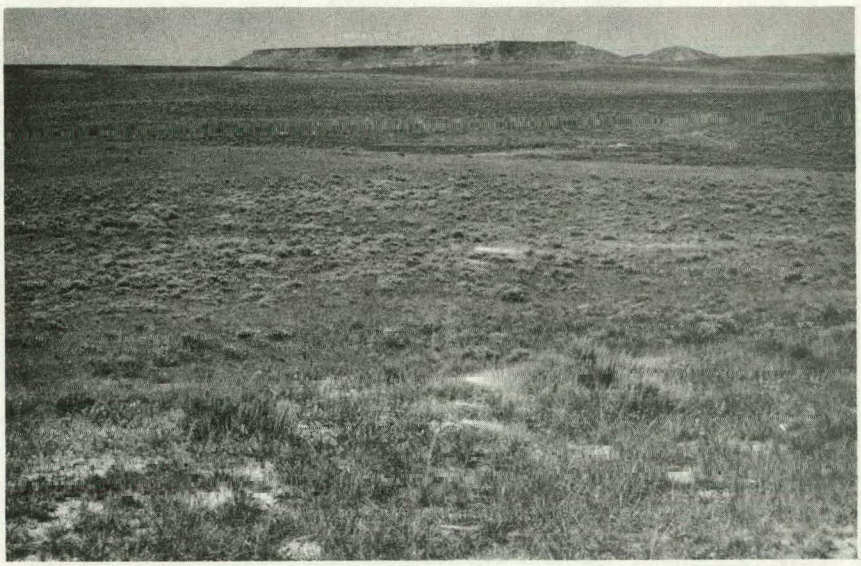

Figure 4. View looking west to North Butte, showing typical vegetation and physiography in the study area.

Vegetation in the Pumpkin Buttes area consists primarily of sagebrush-grassland communities. Vegetative cover typically ranges from 15 to 40 percent. In narrow alluvial valleys, where moisture is abundant, vegetative cover often exceeds 85 percent. Occasional cottonwood trees can be found along these valleys. Grasses are mainly grama-needlegrass-wheatgrass associations (Küchler, 1964). Common sagebrush species and subspecies include silver sagebrush, basin big sagebrush, and Wyoming big sagebrush. These are typical of plant species found throughout the Wyoming basins (Knight, Hill, and Harrison, 1976). Other ground vegetation include threadleaf sedge, rabbitbrush, and prickly pear cactus (Glassey and others, 1955). These species are uniformly distributed on favorable upland sites. Figure 4 shows typical vegetation of the rolling divide topography which constitutes most of the study area. Alluvial lowlands are covered with dense grasses, sedges, willows, and occasional cottonwood trees, while ridgetops support only sparse herbaceous plants and occasional yucca. Sagebrush is distributed over most upland sites, but is generally absent on ridgetops. Limber pine, ponderosa pine, and Rocky Mountain juniper grow on the flanks of the Pumpkin Buttes. Department of Interior (1974) and Ziemans and Walker (1977) provide lists of flora and descriptions of vegetation communities in the Powder River Basin. Readers should refer to those publications for further information on vegetation.

Soils

Soils in the test region are grouped according to similarities in geologic substrata and topography (Glassey and others, 1955). Much of the eastern study area has a cover of Ulm and Renohill series soils. Ulm soils are mature, derived from sandy and silty bedrock, and are characterized by a grayish-brown color, loamy or slightly sandy surface layers, and by friable, silty to clayey, calcareous, subsoils. They occupy upland areas of gentle relief and absorb most of the precipitation that falls.

Renohills soils occur in uplands of moderate relief throughout the study area. These soils are mature, noncalcareous, and are characterized by a light gray to brown color, compact, loamy or silty upper layer, and a more friable clay-loam subsoil. They are found on moderately sloping hillsides and on broad, flat ridgetops. Moisture permeates slowly through Renohill soils.

The bottomlands and draws contain soils of the Arvada series and the Banks fine sandy loam. These are light-colored, clayey to fine sandy soils developed from water-transported material. Soil consistency varies from compact to loosely coherent and water permeability rates vary from fast to slow. These soils are scabby where eolian erosion has removed the surface soil and exposed the more compact clayey subsoil.

An association of shallow, immature soils (entisols) occur on dissected uplands in the western part of the study area and on most

rolling divide ridgetops. The nature of the parent material largely controls the character of the thin soil mantle that overlies the original strata. The result is a complex pattern of soils differing from one another in texture, reactions, and color (Singleton and Cline, 1976). Soils that make up the entisol complex are the Tassel, Lessat, Shingle, Wibaux, Shake, Samsil, and Louviers series. These are classified according to texture and presence of calcareous material (table 1). Soils of the Wibaux series have not been included in table 1 as they are similar to soils of the Shake series in texture and calcareous habit; they differ in that they have a more yellow hue than Munsell 5YR (Singleton and Cline, 1976).

Table 1
Entisols in the Pumpkin Buttes Area

Texture	Calcareous	Non-Calcareous
Moderately coarse texture predominantly sandy loams, sandy clay loams	Tassel	Lessat
Medium to moderately fine texture sandy clay loams, light clay loams	Shingle	Shake
Fine texture predominantly clay loams	Samsil	Louviers

Most of the soils in the region have developed in place and are shallow -- usually less than 76.2 cm (30 in) in thickness (Glassey and others, 1955). On steep slopes and on ridgetops, soil thickness of only a few centimeters is common.

Due to prevailing climate and relatively sparse vegetative cover, organic matter has accumulated slowly. Therefore, soils are usually light-colored, and variation of soil color may be principally attributed to chemical weathering of underlying rock units (Birkland, 1974). Compounds released through weathering of bedrock form pigmenting materials which occur as colloidal coatings on soil particles. The concentration of pigmenting materials may be indicated by the color intensity. Common pigmenting agents include compounds of iron, manganese, aluminum, and calcium carbonate. Gray-blue colors often indicate the presence of pigments in a chemically reduced state; while red, yellow, and brown colors indicate the presence of oxides and hydrous-oxides (Birkland, 1974). Other factors affecting soil color are texture and moisture. Because a fine-grained soil has more surface area per unit volume than a coarse-grained soil, a greater quantity of pigment material is required to produce the same color in a fine-grained soil. The exact effect of texture on soil depends on the nature of the pigmenting agent. A darkening agent, such as manganese oxide, will produce a darker color in a

coarse soil than in a fine soil, because less pigmenting agent is required to coat coarse soil particles. By the same reasoning, a light pigmenting agent such as calcium carbonate will produce a lighter color in a coarse soil than in a fine soil. Moisture content also affects color, in that wet soils are usually darker and more vividly colored than dry soils. They have lower Munsell brightness values and greater Munsell chromas (G.S.A., 1975). Physical properties of soils, such as texture and moisture content, will affect the value and chroma of reflected light, but the hue (the basic color of a soil) depends solely on the pigmenting agents present in the soil.

Generally, only immature, shallow soils will exhibit colors of the parent material. Therefore, detecting and mapping of uranium alteration is possible only in entisols. As soils develop, organic material accumulates and decomposes. Groundwater movement causes leaching and circulation of chemical components (including pigmenting agents). Through time, a progression of soil colors in a well-developed soil reflects chemical changes as ions are leached out of surface horizons. For example, oxidized iron is soluble in an acidic environment, but will remain in place until all calcium carbonate ($CaCO_3$) has been leached and removed. Removal of $CaCO_3$ may actually enhance iron oxide coloration in these soils. However, it will eventually lower the pH of the soil, enabling iron oxide to be leached. Hence, its effect on soil color will subsequently diminish.

GEOLOGY

Geological Setting

The Powder River Basin is a large, topographic and structural basin in northeastern Wyoming which extends northward into Montana (fig. 2). The basin is bounded on the east by the Black Hills, on the southeast by the Hartville Uplift, on the south by the Laramie Range and Casper Mountain, on the southwest by the Casper Arch and on the west by the Bighorn Mountains. Topographically, the Powder River Basin is open-ended to the north. Structurally, the basin is bounded to the north by the Miles City Arch and Porcupine Dome.

Stratigraphy

The Pumpkin Buttes study area contains continental sedimentary rocks of the Wasatch Formation (early Eocene age) and the White River Formation (Oligocene age). A band of Fort Union Formation, of Paleocene age, crops out along Great Pine Ridge, 29 km (18 mi) southwest of the Pumpkin Buttes. Several Cretaceous units are exposed even farther to the southwest. The extent and lithologic characteristics of these formations are shown graphically in figure 5 and plate 1.

Wasatch Formation

The Wasatch Formation displays an array of lithologies and colors. It comprises drab, brown to gray claystone, siltstone, and carbonaceous shale, interbedded with buff to gray sandstone, fresh-water limestone, and black coal beds. In the Pumpkin Buttes area, the Wasatch may have a total thickness of over 915 m (3000 ft) (Mrak, 1958; Love, 1978). It thins out to the south, having a thickness of less than 305 m (1000 ft) (Sharp and Gibbons, 1964). A geological map by Sharp and White (1957) shows that the ratio of coarse- to fine-grained rocks of the Wasatch Formation in the Pumpkin Buttes vicinity is about 1:3. This agrees with the figure stated by Troyer and others (1954). Regional studies by Davidson (1953) have shown that the Wasatch Formation contains more abundant coarse-grained sediments in the southern part of the Powder River Basin and contains predominantly fine-grained sediments in the northern part of the basin. This fining northward trend indicates that the major source of sediments was to the south. All known uranium deposits occur where the formation contains a mixture of interbedded coarse- and fine-grained units.

In the Pumpkin Buttes area, the claystones and siltstones are variegated. Though they are predominantly drab, in places, purple, green, yellow, brown, and red tints occur. Lateral changes in composition and grain size are common and sometimes abrupt. Claystone, siltstone, fine-grained sandstone and carbonaceous shale commonly grade laterally into one another. These units are usually thinly bedded, though claystone units are sometimes massive and blocky. Ironstone and nodules of

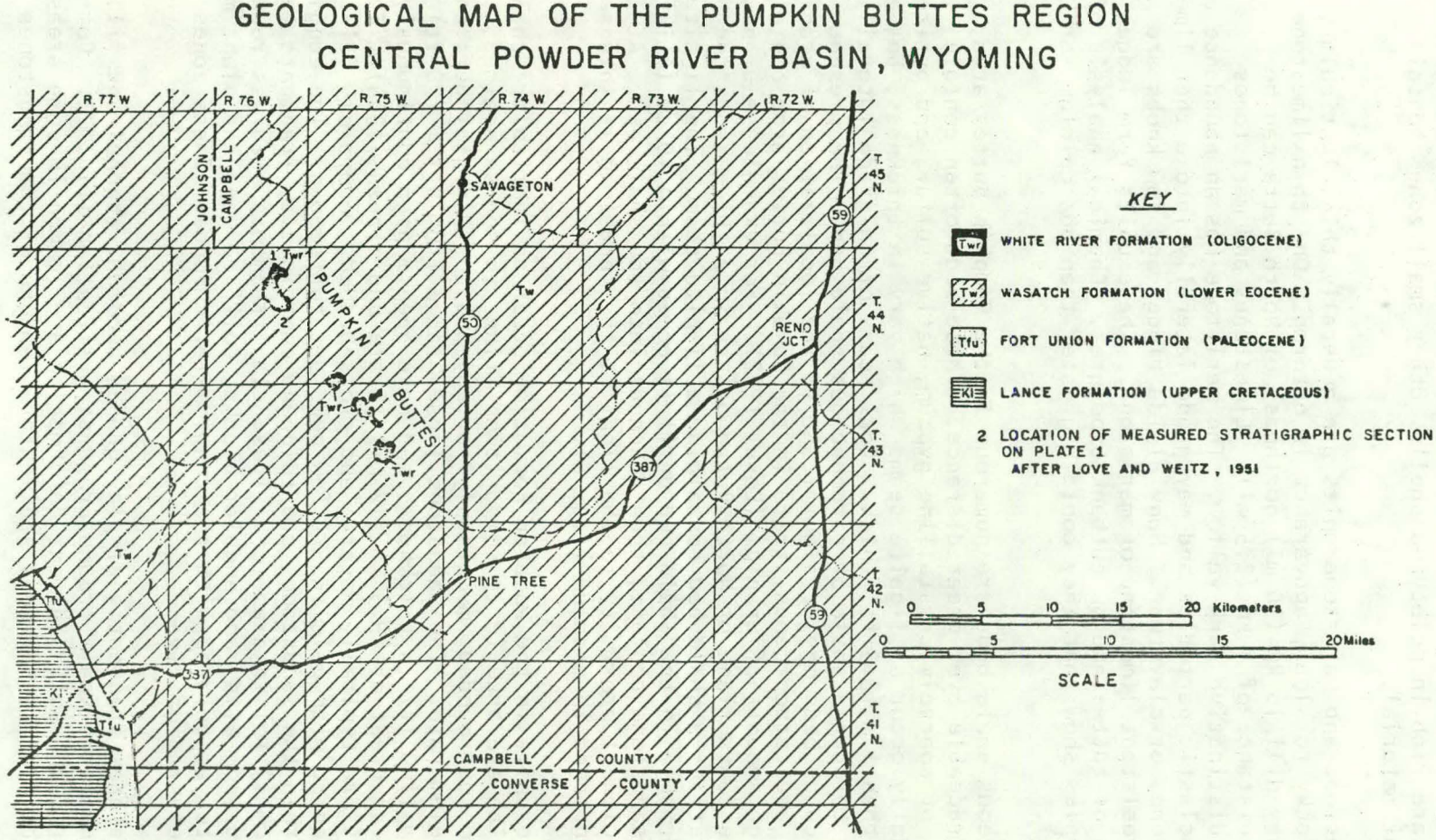
GEOLOGICAL MAP OF THE PUMPKIN BUTTES REGION
CENTRAL POWDER RIVER BASIN, WYOMING
R. 77 W
R. 76 W
R. 75 W
R. 74 W
R. 73 W
R. 72 W
T. 45 N.
T. 44 N.
T. 43 N.
T. 42 N.
T. 41 N.
JOHNSON
CAMPBELL
SAVAGETON
PUMPKIN BUTTES
RENO JCT
PINE TREE
CAMPBELL COUNTY
CONVERSE COUNTY
Twr
Tw
Tfu
Kl
KEY
WHITE RIVER FORMATION (OLIGOCENE)
WASATCH FORMATION (LOWER EOCENE)
FORT UNION FORMATION (PALEOCENE)
LANCE FORMATION (UPPER CRETACEOUS)
2 LOCATION OF MEASURED STRATIGRAPHIC SECTION ON PLATE 1 AFTER LOVE AND WEITZ, 1951
0 5 10 15 20 Kilometers
0 5 10 15 20 Miles
SCALE

Figure 5

pyrite-cemented clastic material are locally abundant. Some small lenses of siltstone are rich in pelecypod shells. Other small zones contain abundant plant material.

The limestone and marlstone units are generally thin, lenticular, and have a blocky to slabby appearance in outcrop. One thin limestone unit on Chimney Hill, 16 km (10 mi) northeast of North Butte, can be traced for a distance of 4 km (2.5 mi). Limestones and marlstones weather to a distinctive dark yellow. The marlstone has an abundance of fine-grained clastic particles and may grade laterally into either limestone, siltstone, or claystone. Many divide ridges and low knobs are capped with resistant limestone or marlstone. These units form ledges on the flanks of buttes and on cutbank exposures. Chemical analysis of limestone samples show that they contain greater than 60% calcium carbonate ($CaCO_3$).

Carbonaceous shale beds are numerous in the Pumpkin Buttes area, but few are traceable over great distance. These beds often contain large amounts of coarsely crystalline gypsum, native sulfur, and pyrite. Coal beds usually occur as lignite seams which vary in thickness, but are usually less than 1 m (3.3 ft) thick. Coal seams often grade laterally or vertically through a shale or carbonaceous shale bed. The presence of these carbonaceous beds may be significant to the localization of uranium. All coal and carbonaceous strata in the Pumpkin Buttes area contain abnormally high amounts of uranium (Love, 1952). For example, a uranium deposit on the south flank of North Butte occurs in a thick sandstone unit which overlies a shale bed containing a lignite seam. The lignite rises unconformably in the shale bed until it comes within 10 cm (4 in) of the shale/sandstone contact, then descends into the shale bed. At the point of closest proximity to the lignite, the sandstone is intensely altered and enriched in uranium (fig. 6).

Sandstone units in the Wasatch Formation occur as lenticular "channel" sands which are arkosic in composition, fine- to coarse-grained, sub-angular to sub-rounded, moderately sorted, and contain stringers and lenses of conglomerate. The sandstone lenses range from 6.1 m (20 ft) to over 30.5 m (100 ft) in thickness, and have been mapped continuously for distances as great as 19.3 km (12 mi) (Sharp and others, 1964). The sandstone beds are typically massive and cross-bedded, moderately friable, and cemented with calcite. A few beds are tuffaceous. The conglomerate beds within the sandstones are thin and contain clay fragments as large as 7.6 cm (3 in) in diameter. These clay fragments occur as rounded pebbles, curved galls, and angular blocks. Colified wood and plant material are often associated with the conglomeratic zones. These zones may be extremely radioactive.

The sandstones frequently display graded bedding, channel and fill structures, and large-scale trough cross-stratification (fig. 7). Compaction features and soft sediment deformation are common in some areas (fig. 8A). The most conspicuous sedimentary feature of the sandstones

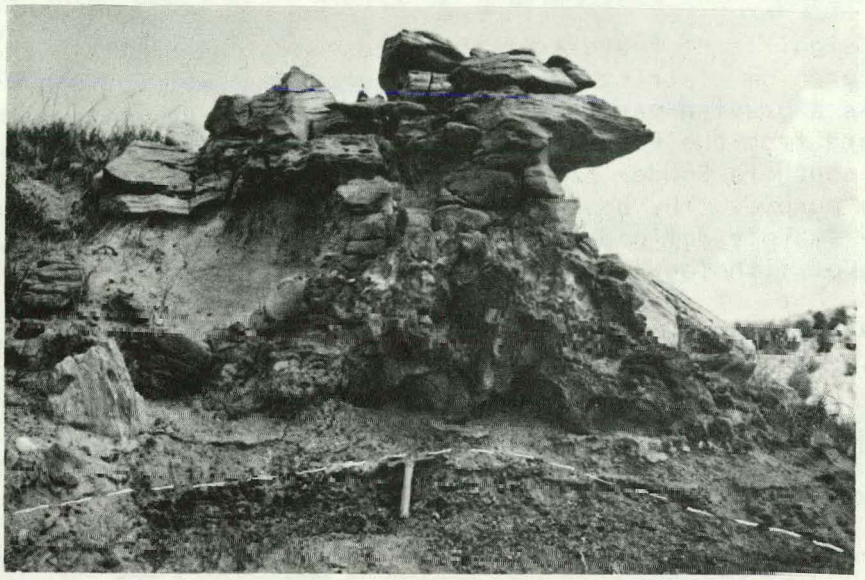

Figure 6. Uranium deposit on the south flank of North Butte which demonstrates the effect carbonaceous beds have on localization of uranium. The line is drawn along the top of a coal seam.

in the Pumpkin Buttes area is the epigenetic concretions of sand grains cemented by $CaCO_3$. The variations in size, shape, cementation, and weathering, provide many interesting forms (fig. 8B). The largest concretions are up to 30 m (100 ft) long and 1.8 m (6 ft) in diameter and resemble the lobate, pipy concretions in western Nebraska and eastern Wyoming described by Schultz (1941) (fig. 9A). Other forms include concentric masses and spherical forms locally known as "schmoos", "cannon balls", and "pumpkins" (fig. 9B). It is these concretions to which Pumpkin Buttes owe their name (Sharp and Gibbons, 1964; Steidtmann, 1978). Calcite concretions are believed to have their origin in migrating groundwaters. Study of their distribution and orientation may be a useful indicator of groundwater movement, and may provide a clue to the origin of uranium deposits (Meschter, 1958).

A significant feature of the sandstone lenses within the Pumpkin Buttes uranium district is color. The predominant color of the sandstone is a grayish-tan (buff), but within a narrow zone, extending southward from the Pumpkin Buttes area to the Box Creek uranium district in the southern Powder River Basin, sandstone color varies from yellow to deep purple. The boundary between the colored and buff sandstone is usually sharply defined and transects sedimentary structures and small changes of lithology within the sandstone (fig. 10).

- Pyrite nodules are common in some buff sandstone units which, apparently, have not been long exposed to weathering. Ironstone is abundant in the colored sandstone and uncommonly occurs in the buff sandstones. Fossil and coalified wood, leaves, grass, and other plant material occur locally. Fossil wood is replaced by silica, goethite, or hematite, and occasionally shows pseudomorphs of pyrite.

Sandstone units are resistant to erosion and usually cap ridges and knobs, and form ledges on the flanks of the Pumpkin Buttes. The surface overlying sandstone units is characteristically pockmarked by blowouts.

Vertebrate fossils collected by the author and by Love (1977) indicate an early Eocene age for the Wasatch Formation in the Pumpkin Buttes area. Those fossils occur only near the top of the Wasatch Formation (plate 1). Fossils collected lower in the formation are older and probably do not belong to the Wasatch Formation as currently defined (Delson, 1971; Taylor, 1975). The type locality of the Wasatch Formation, in Utah, is over 483 km (300 mi) away from the Pumpkin Buttes area. Comparable strata in intervening basins have different names (e.g. Wind River, Indian Meadows, Battle Springs, and Willwood formations). It is unlikely that rocks deposited by rivers flowing north from the southern Powder River Basin were derived from the same source as those of the type Wasatch. It is also questionable that the base of the Wasatch Formation, as mapped in the Powder River Basin, coincides with the boundary between rocks of Eocene and Paleocene Age. For these reasons, use the term "Wasatch Formation" for the Powder River Basin is inappropriate and should be reconsidered or abandoned. It will be used in this report because a

A

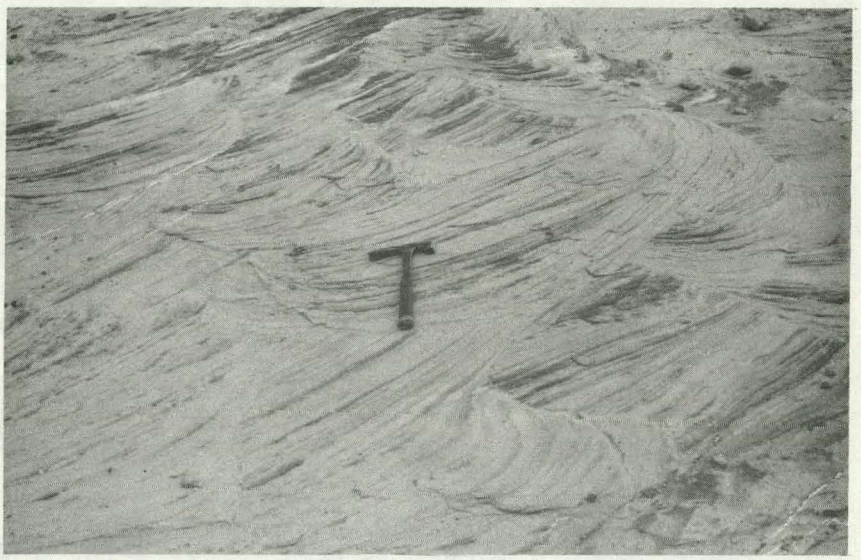

B

Figure 7. Sedimentary structures in the Wasatch Formation.
A. Channel and fill
B. Large-scale trough cross stratification

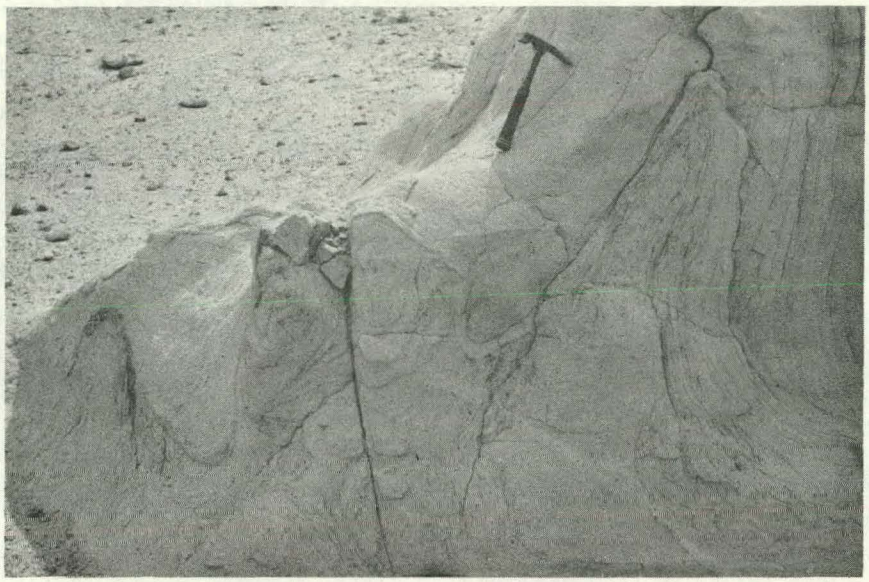

A

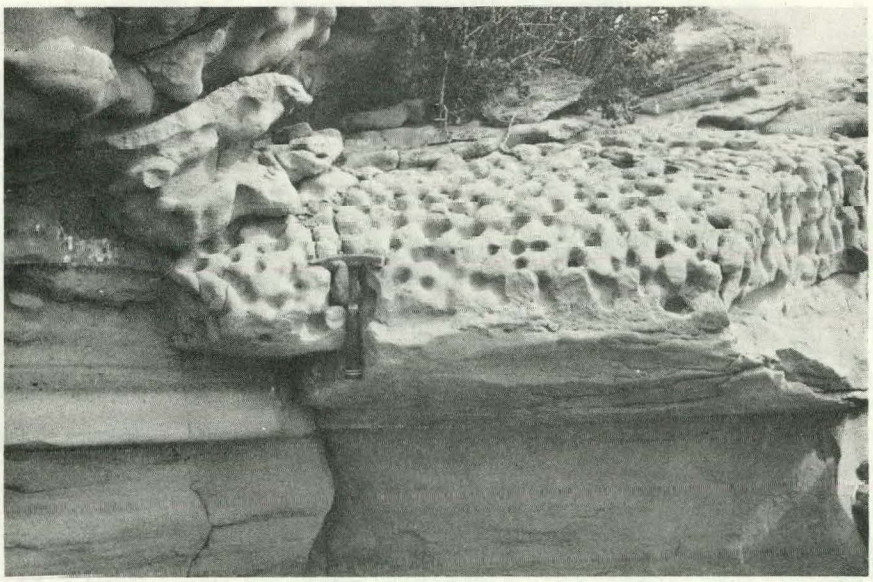

B

Figure 8. Sedimentary structures of the Wasatch Formation.
A. Soft sediment deformation.
B. Epigenetic concretion; differential cementation affects the weathering patterns

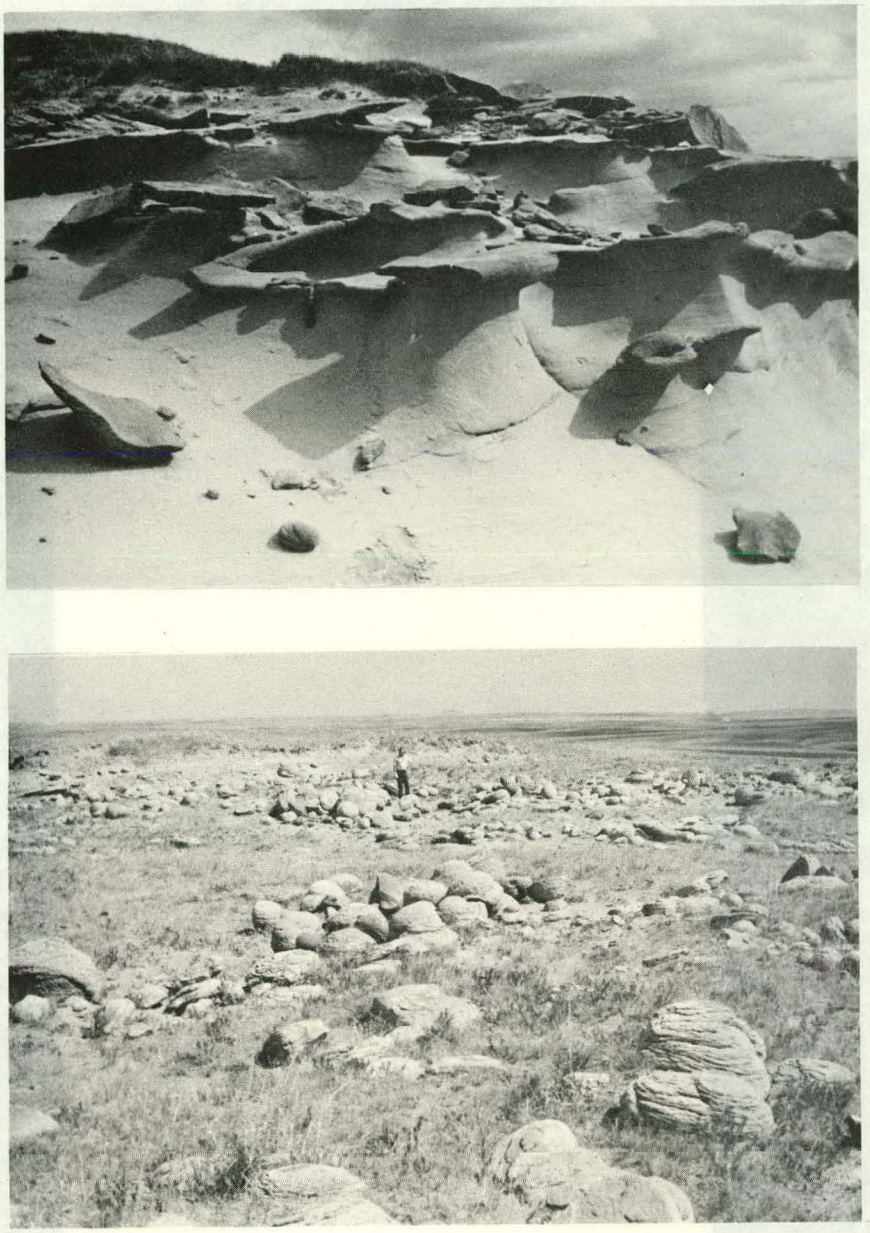

A

B

Figure 9. Sedimentary structures of the Wasatch Formation.
A. Pipy concretions.
B. Schmoos or pumpkins.

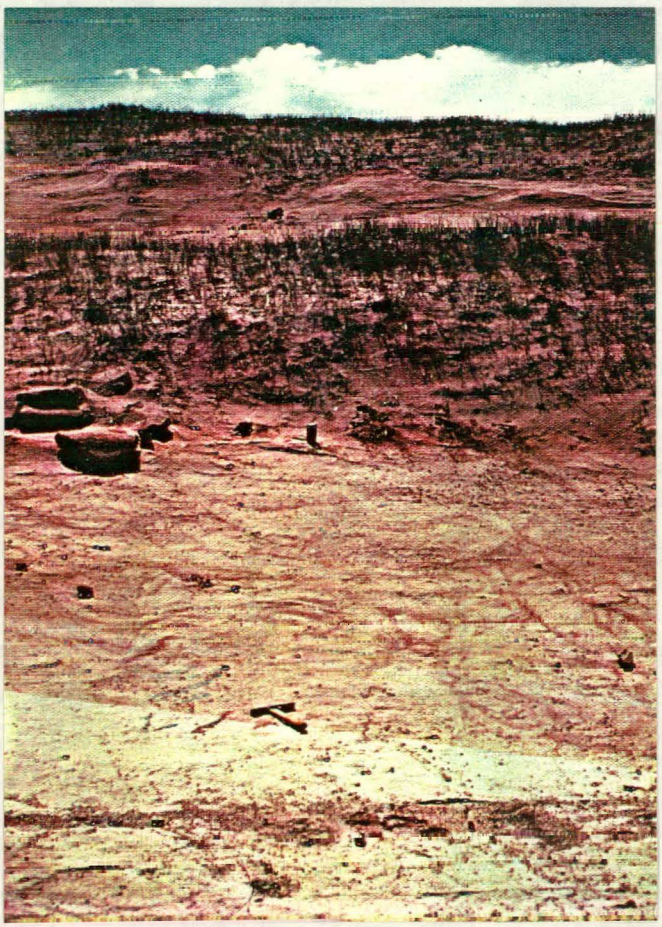

Figure 10. Sharply defined color contact in Jeannette mine pit.

new term has not yet been formally defined. J. D. Love of the U.S.G.S., has proposed the term "Pumpkin Buttes Formation" for the lower Eocene rocks in the Powder River Basin based on a type exposure on North Butte (plate 1, column 2) (Love, 1977). His proposal has been accepted by the U.S.G.S., but is still unpublished.

White River Formation

A basal member of the White River Formation caps the five major buttes and is 9 to 23 m (30 to 75 ft) thick. An erosional disconformity separates the resistant White River Formation from underlying friable sandstones of the Wasatch Formation. Two lithological units are present on the Pumpkin Butes: a caprock unit and an overlying tuffaceous claystone facies. The caprock consists of coarse- to very coarse-grained conglomeratic sandstone with a silicious cement. The pebbles present in conglomeratic zones are rounded and range in size from 2.5 to 10 cm (1 to 4 in) in diameter. The conglomerates contain pebbles of quartzite, limestone, chert, gneiss, hornblende, hypersthene, and augite. These rocks and minerals are similar to those found in rocks of Paleozoic and Precambrian age in the Big Horn mountains and in Tertiary volcanic rocks in the Absaroka Range (Love, 1952). The mineralogy, grain-size, and siliceous cement combine to make the caprock a resistant cliff-former which is responsible for preservation of the Pumpkin Buttes. The tuffaceous clay-stone unit consists of remnants of soft, white and pink tuff and bentonitic claystone. It is easily eroded and is found only in a few areas overlying the caprock and filling fractures in the caprock. Vertebrate fossils found in this unit confirm an Oligocene age for these sediments.

The areal extent of the White River Formation and overlying Miocene sediments was originally much greater than at present. These formations probably draped across the entire Powder River Basin and connected individual occurrences to the northwest, east and south of the Powder River Basin (Darton, 1905; Love, 1952). Black Butte, a hill 21 km (13 mi) northeast of North Butte is capped by large slumped blocks of hard, hematite stained, very-coarse, silicious sandstone, believed to be of White River origin. These blocks were apparently let down more than 183 m (600 ft) by erosion of the less resistant Wasatch formation. Other blocks of White River lithology occur on hills in the vicinity of Black Butte and at a location 8 km (5 mi) south of North Butte.

Structural Development

The Powder River Basin is a broad asymmetrical syncline with its Precambrian axis in the western part of the basin. The axis shifted eastward as the basin filled; and the present axis (as measured from dips on Tertiary rocks) now lies several miles east of the basement axis (Dahl and Hagmaier, 1976). This reflects a regional tilting of the basin in Tertiary time.

In the Pumpkin Buttes area, data from wells indicate Tertiary basin fill of at least 1829 m (6000 ft). Below this are 2134 m (7000 ft) of Cretaceous rocks, 305 m (1000 ft) of Jurassic and Triassic rocks, and 610 m (2000 ft) of Paleozoic rocks. The estimated depth of sedimentary rocks is about 44,878 m (16,000 ft) in the Pumpkin Buttes area (Love, 1952).

Except for local diagenetic and depositional features, the beds in the Pumpkin Buttes area lie almost horizontally; dips range from 4 to 8 m per km (20 to 40 ft per mile) on the east side of the buttes, to more than 20 m per km (100 ft per mi) in the area west of the buttes (Troyer and others, 1954). Two jointing trends are common; one set trends N. 60° E. and one set trends N. 30° W. Some joints are filled with white punky calcium carbonate ($CaCO_3$). No significant faulting is recognized in the Pumpkin Buttes area, although several minor reverse faults offset coal beds on cutbank outcrops along the Powder River, west of the study area (Sharp and others, 1964).

Several minor structures are present in the Pumpkin Buttes area (fig. 11). These are described by Wegemann and others (1928), Troyer and others (1954), Osterwald and Dean (1961), and Sharp and others (1964). These structures consist primarily of small, very gentle anticlines and synclines which approximately follow the general northwest-southeast structural trend of the Powder River Basin. Osterwald (1955) believes these folds are related to tectonic patterns in the Precambrian basement which have influenced later movements. Through repeated deformation, the Tertiary rocks have become slightly deformed and jointed. Thus, tectonic activity has provided a favorable structural environment for uranium transport and deposition.

It seems more likely that most of these minor structures are related to differential compaction of the underlying sediments (Law, 1976; Blackstone, 1977). The unusually thick coal seams of the Lower Wasatch and upper Fort Union Formations together with burned coal beds and facies changes in coal and non-coal lithologies could provide the necessary environment for differential compaction and deformation. The results of these processes are readily visible as contorted sedimentary structures (fig. 8A). Regardless of the mechanism which created these minor folds, they certainly exerted control over sedimentation patterns and location of paleostream channels during deposition of the host sands. Joint patterns created by subsequent deformation provided conduits for uranium-bearing groundwaters.

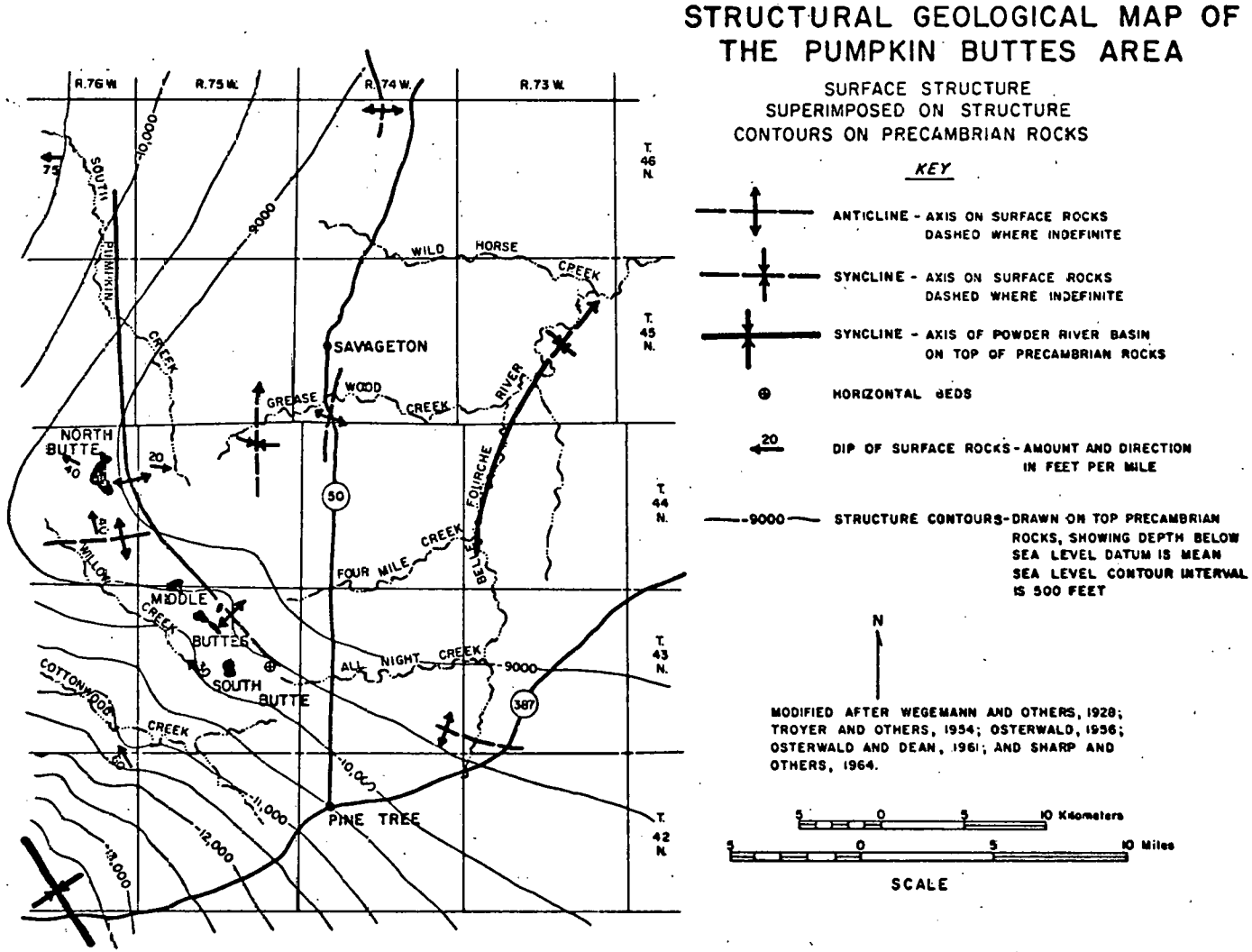
STRUCTURAL GEOLOGICAL MAP OF THE PUMPKIN BUTTES AREA
SURFACE STRUCTURE SUPERIMPOSED ON STRUCTURE CONTOURS ON PRECAMBRIAN ROCKS
KEY
ANTICLINE - AXIS ON SURFACE ROCKS DASHED WHERE INDEFINITE
SYNCLINE - AXIS ON SURFACE ROCKS DASHED WHERE INDEFINITE
SYNCLINE - AXIS OF POWDER RIVER BASIN ON TOP OF PRECAMBRIAN ROCKS
HORIZONTAL BEDS
20 DIP OF SURFACE ROCKS - AMOUNT AND DIRECTION IN FEET PER MILE
-9000- STRUCTURE CONTOURS - DRAWN ON TOP PRECAMBRIAN ROCKS, SHOWING DEPTH BELOW SEA LEVEL DATUM IS MEAN SEA LEVEL CONTOUR INTERVAL IS 500 FEET
N
MODIFIED AFTER WEGEMANN AND OTHERS, 1928; TROYER AND OTHERS, 1954; OSTERWALD, 1956; OSTERWALD AND DEAN, 1961; AND SHARP AND OTHERS, 1964.
5 0 5 10 Kilometers
5 0 5 10 Miles
SCALE
R.76 W.
R.75 W.
R.74 W.
R.73 W.
T. 46 N.
T. 45 N.
T. 44 N.
T. 43 N.
T. 42 N.
SAVAGETON
WILD HORSE CREEK
SOUTH PUMPKIN CREEK
WOOD CREEK
GREASE
NORTH BUTTE
MIDDLE BUTTE
SOUTH BUTTE
FOUR MILE CREEK
WILLOW CREEK
ALKALI NIGHT CREEK
COTTONWOOD CREEK
FOURCHE
BELLE
RIVER
PINE TREE
-10,000
-9000
-11,000
-12,000
-13,000
50
387

Figure 11

URANIUM DEPOSITS

Ore-grade uranium was first discovered in the Pumpkin Buttes area in 1951 by J.D. Love of the U.S.G.S. during a ground check of radioactive areas located by an airborne radiometric survey. The early descriptions by Love (1952), Troyer and others (1954), Sharp (1955) and Sharp and others (1956, 1964) were of near-surface oxidized deposits. Deeper, unoxidized deposits have been described by Davis (1969), Rackley and Johnson (1969), and Schafer (1977).

Two types of uranium deposits have been observed in the Pumpkin Buttes district; concretionary and disseminated deposits.

In the concretionary deposits, oxidized uranium minerals are associated with pyrite or manganese oxide nodules. The deposits are small in size (less than 61 cm (2 ft) in diameter), round to irregularly shaped, very rich in uranium and often display a concentric arrangement of minerals (Sharp, et. al., 1964). Coalified and ferruginous woody material is common in or near some nodules. The concretions are generally isolated within zones of red-colored host sandstones.

Disseminated deposits occur as shells between interpenetrating tongues of buff or colored sandstones. Green, yellow, and black uranium minerals interstitial to sand grains are usually in buff or yellow sands along color contacts or around calcite concretions. Mineralization also occurs in porous sandstones where red sandstone intersects underlying or overlying fine-grained clastic rocks at a low angle. Mineralization also occurs where concentrations of carbonaceous material are present in the host sand or in underlying or overlying sediments. Though disseminated deposits are usually of lower grade than concretionary deposits, they are much larger in size. They may be economically important, and can be sought using a variety of techniques, including remote sensing.

The similarities between disseminated uranium deposits in Tertiary sandstones of many Wyoming basins has given rise to the "roll-front" emplacement model for Wyoming sandstone uranium deposits. Though specific factors in the model are disputed among geologists, the development and application of the roll front model has proven to be a powerful tool for the exploration geologist.

Geometry of Roll-Front Deposits

The idealized geometry of a roll-front deposit is shown in figure 12. The host sandstone beds may range from 3 to 18 m (10 to 60 ft) in thickness. These are lenticular sand bodies which are usually tongue-like extensions of major sandstone units. The ideal shape of the deposit, in cross-section, resembles a crescent roll in which the concave side encloses altered, and often colored sand, and the convex side points toward fresh or unaltered (buff colored) sands. The upper and

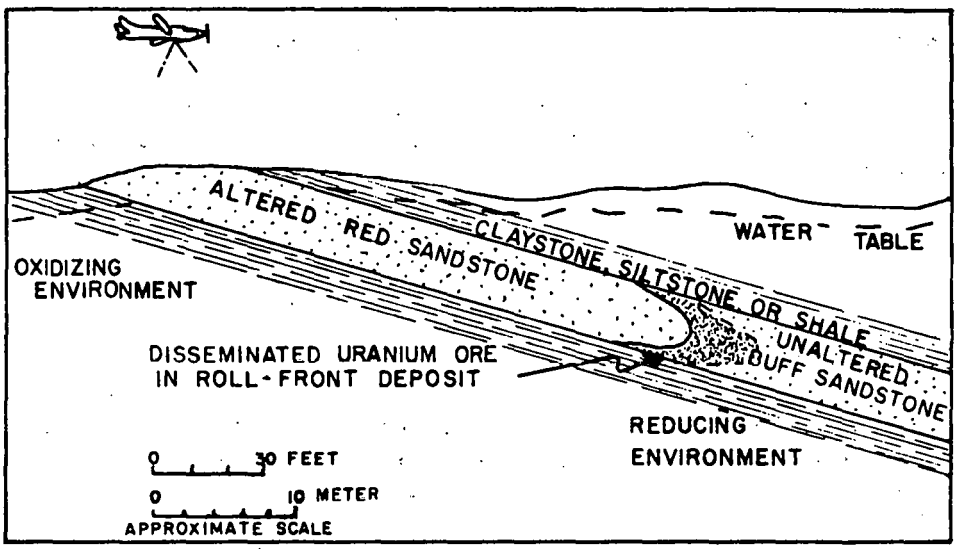

Figure 12. Idealized cross-section through roll-front deposit.

lower edges of the crescent or "limbs" may extend back some distance from the roll. Vertical distance between the limbs typically ranges between 1 to 10 m (3 to 33 ft). Often, limbs are bounded by less permeable lithologies, such as claystone, siltstone, or shale. In plan view, the deposits are irregularly lobe-shaped. Often, fingers of altered ground extend into unaltered ground. Uranium mineralization occurs at the altered-unaltered interface in these fingers and in "pseudo-blankets" along the upper and lower limbs (DeNault, 1974). The ore bodies vary greatly in thickness, but are usually thickest at the front and thin at the limbs.

Actual geometry of the roll-front deposits varies greatly from the idealized crescent and may trend more towards hour-glass, tube, or "S" shapes (Shaw, 1956). Local variations in geometry and distribution of rolls appear to be related to differences in permeability, fracture density, and dip of the host rock (Alder and Sharp, 1967).

Roll-front uranium deposits, everywhere, are associated with large tongues of altered sandstone which were produced by the passing of ore-bearing solutions (Harshman, 1970). Though the character of the resultant alteration differs from place to place the most common effect is that of oxidation.

Color

Color associated with uranium alteration can be spectacular, as with deposits in the Powder River Basin (Sharp and others, 1964; Sharp and Gibbons, 1964). Unfortunately, alteration colors vary within a mineral district, as well as between mineral districts.

The color of the host sandstone is largely a function of chemical and mineralogical redox changes affecting iron and organic matter (Adler and Sharp, 1967). When sandstone is subjected to oxidation, notable color changes take place. The sandstone may become yellowish due to presence of hydrous ferric oxides (limonite, goethite) or purple or red due to presence of ferric oxides (hematite). Altered ground can also take on a bleached appearance relative to buff-colored unaltered rocks, or it may become greenish due to concentration of ferrous iron and montmorillonite.

In the Pumpkin Buttes area, colors of altered rocks range from purple to red, pink, orange, or yellow. The color cross-cuts many primary sedimentary structures as does the disseminated ore, showing clearly that the ore minerals and alteration are epigenetic (fig. 10). An alteration zone may be entirely red, or it may contain thin red stringers and red nodules interspersed throughout the sandstone. Hematite stained sand has been shown, by exploration drilling, to extend to depths of more than 457 m (1500 ft) in areas where movement of ground-water has been inhibited (Bailey and Childers, 1977; Childers, 1974).

The spectral reflectivity of the alteration is especially important from a remote sensing point of view. Reddish pigments from altered sandstones are incorporated into the soil and show anomalous patterns with respect to buff-colored unaltered ground and non-host lithologies (fig. 13). Reddish anomalies, interpreted within the framework of the local geology, geomorphology, and the roll-front model, can provide a valuable clue to the location of ore bodies.

Sources of Uranium

Before the discovery of uranium in Tertiary sandstones of the Wyoming basins. a magmatic-hydrothermal model was used as an explanation for origin of most uranium ores. The Wyoming roll-front deposits are far-removed from sites of plutonic activity, making a magmatic source quite improbable. This gave considerable impetus to the theories of secondary enrichment by groundwater.

Weathering and leaching of granite rocks could provide uranium for deposition in the Wyoming basins. Surficial oxidation, acting on fractured granitic rocks, makes loosely bound uranium soluble. Uranium can be leached by meteoric waters and groundwaters, enter the aquifer systems, and migrate basinward great distances to sites favorable for deposition. It is probable that greater amounts of granite were exposed during the Laramide orogeny. High concentrations of uranium in hypothermal and mesothermal veins now removed by erosion, may have contributed large amounts of uranium to the Tertiary basins (Houston, 1969).

An area of provenance for host sandstones of most major uranium districts in Wyoming is the Sweetwater Arch. Some granites there have uranium contents of 10-20 ppm, which is three to five times the average content of igneous rocks (Masursky, 1962, p. B95; Stuckless, et. al., 1977). Lead isotope studies and material balance of lead, thorium, and uranium for the Sweetwater granites indicate that 75% of the amount of uranium required to produce the radiogenic lead found in these granites has been removed from these rocks during the Cenozoic. This may constitute a major source of uranium now in ore deposits in Wyoming basins (Rosholt, et. al., 1973).

A similar concept holds that uranium was leached from arkosic sandstones which were deposited from weathering and disaggragating granitic uplands (Rackley, 1972). The roll-front model would then provide a means of concentrating uranium already present in the host rock.

Another theory for the origin of uranium involves leaching of uranium from tuffaceous material either within or above the host sands. As volcanic ash devitrified, groundwaters may have leached silica, alkalis, uranium, vanadium, molybdenum, selenium, arsenic, phosphorous, and other substances (Waters and Granger, 1953; Denson and others, 1956; Grutt, 1971). Much of the original volcanic material is now altered to montmorillonitic clays. Tuffaceous material is present in sparse amounts in

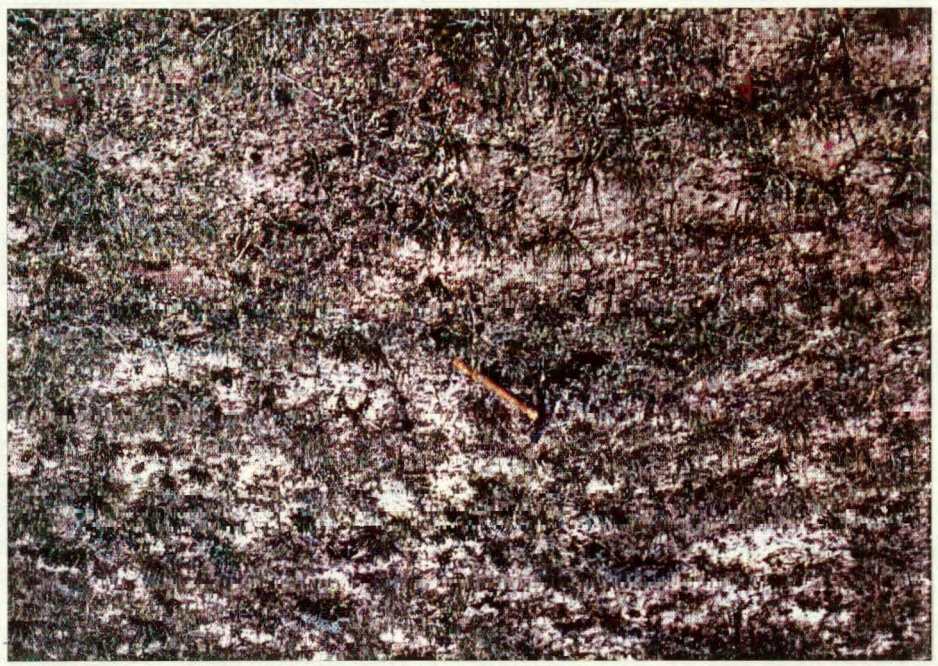

Figure 13. Contact between altered (bottom) and unaltered (top) sandstone expressed at the surface near the Jeannette mine.

the Wasatch formation. Montmorillonite is much more common. Deposition of the host sands of most major Wyoming sandstone uranium deposits is roughly time equivalent to the eruption and deposition of the Absaroka volcanic supergroup in northwest Wyoming (Smedes and Prostka, 1972). The tremendous volume of volcanic material erupted there, could have supplied all of northern Wyoming with abundant, uranium-rich tuffaceous sediments. Volcanic activity was wide-spread in later Tertiary times as well, as is evident in tuffaceous sediments of the Oligocene White River formation and Miocene Arikaree formation. The rock units of Oligocene and Miocene age are noted for the high uranium content in groundwater issuing from them (Denson and others, 1956). The presence of the White River formation, capping the Pumpkin Buttes, provides evidence that the Powder River Basin was blanketed by, at least, Oligocene sediments.

Groundwater analyses have demonstrated that either granitic rocks or tuffaceous rocks could have provided enough uranium for all uranium deposits discovered to date in the Tertiary basins of Wyoming (Childers, 1974). It is probable that uranium was leached out of both tuffs and arkosic sands; for deposits in close proximity to granitic uplifts, a granitic source is also possible.

Paleoenvironment

Uranium deposits in the Pumpkin Buttes area occur only in fluvial sandstones that are at least 198 m (650 ft) down from the top of the Wasatch formation. The locations of ancient river valleys, which formed these "channel" sands, were probably influenced by geologic structure in the area.

The most favorable lithofacies for the known uranium deposits are characterized by coarse fluvial facies which intergrade into finer variegated facies (Webb, 1969). It is believed that aggrading streams which deposited these sediments were probably part of a very large river system (by Pleistocene and Holocene standards). Streams ranged in size from .8 km (.5 mi) to as much as 8 km (5 mi) in width during normal stages, and covered much larger areas during flood stages (Webb, 1969). The massive sandstones deposited from these large rivers are typically scoured with large, complex interchannel and intrachannel cut-and-fill structures and large-scale cross stratification (fig. 8). While many channel sands display discrete lenticular forms, other channel sands merged together to form large "blanket" sandstone units which can be traced laterally for many kilometers.

Floodplain deposits developed laterally along the margins of the main channel and lapped onto the valley sides. Lakes, temporary ponds, and swamps developed on the floodplain and these are responsible for the deposition of limestones, marlstones, mudstones, carbonaceous shales, and lignites.

A warm, temperate, and moderately humid climate must have prevailed during the early Eocene, but the climate probably did fluctuate (Webb, 1969; Childers, 1974).

Vegetation was plentiful along the main channels, regardless of the climatic period, and often plant fragments were buried during flood stages. These organic-rich deposits, plus paludal overbank deposits, decomposed to produce chemically reduced sediment layers adjacent to and interfingering with the oxygenated sediment of the main channel.

Comprehensive studies on sand-grain elongation, regularity, mean size, and crossbedding directions of sandstones in the Wasatch Formation in the Powder River Basin have provided information about the Eocene sedimentation patterns and paleodrainage (Seeland, 1976). Figure 14 shows the paleogeography of the Powder River Basin during the Eocene. At that time, the ancestral Wind River flowed across what is now the Casper Arch and became the major drainage of the Powder River Basin. Another major river system, with tributaries flowing out of the Black Hills, Hartville Uplift, and Laramie Range, flowed directly through the Pumpkin Buttes area. It joined the ancestral Wind River at a site approximately 25 km (16 mi) southeast of Buffalo, Wyoming (Seeland, 1976).

Mineralogy

The host sands of the Wasatch formation show variation in mineral composition, but are generally arkosic and cemented by calcite. Calcite is present in varying amounts up to 50%. Quartz, feldspar and lithic fragments (including chert) make up approximately 40, 10, and 10 percent, respectively, of the rock composition. Accessory minerals, carbonaceous fragments, and voids make up the remainder of the rock.

Major accessory minerals in the sandstones include the following: biotite, muscovite, pyrite, magnetite, marcasite, amphibole, pyroxene, epidote, garnet, apatite, and chlorite. Minor accessory minerals include: zircon, tourmaline, sphene, hypersthene, gypsum, and zeolite. The assemblage of accessory minerals show that the sandstones are mostly first-cycle sediments derived from Precambrian plutonic and metamorphic rocks with little volcanic input (Denson and Pipiringos, 1969).

Hundreds of uranium-bearing minerals are known. A systematic listing of common uranium mineralogy may be found in Frondel (1958). Table II lists the major uranium minerals in the Pumpkin Buttes district along with their chemical formulas. Of those minerals listed, the uranium vanadates are the most common (Troyer and others, 1954; Sharp and others, 1964). These minerals usually occur as irregularly shaped aggregates of microcrystals which typically coat sand grains, replace calcite, and fill interstices. They also fill fractures in both calcite and detrital minerals. Uranium mineralization is often associated with iron and manganese oxides which have partially replaced calcite as a cementing agent. Uranium minerals occur at the interface zone between the iron-manganese

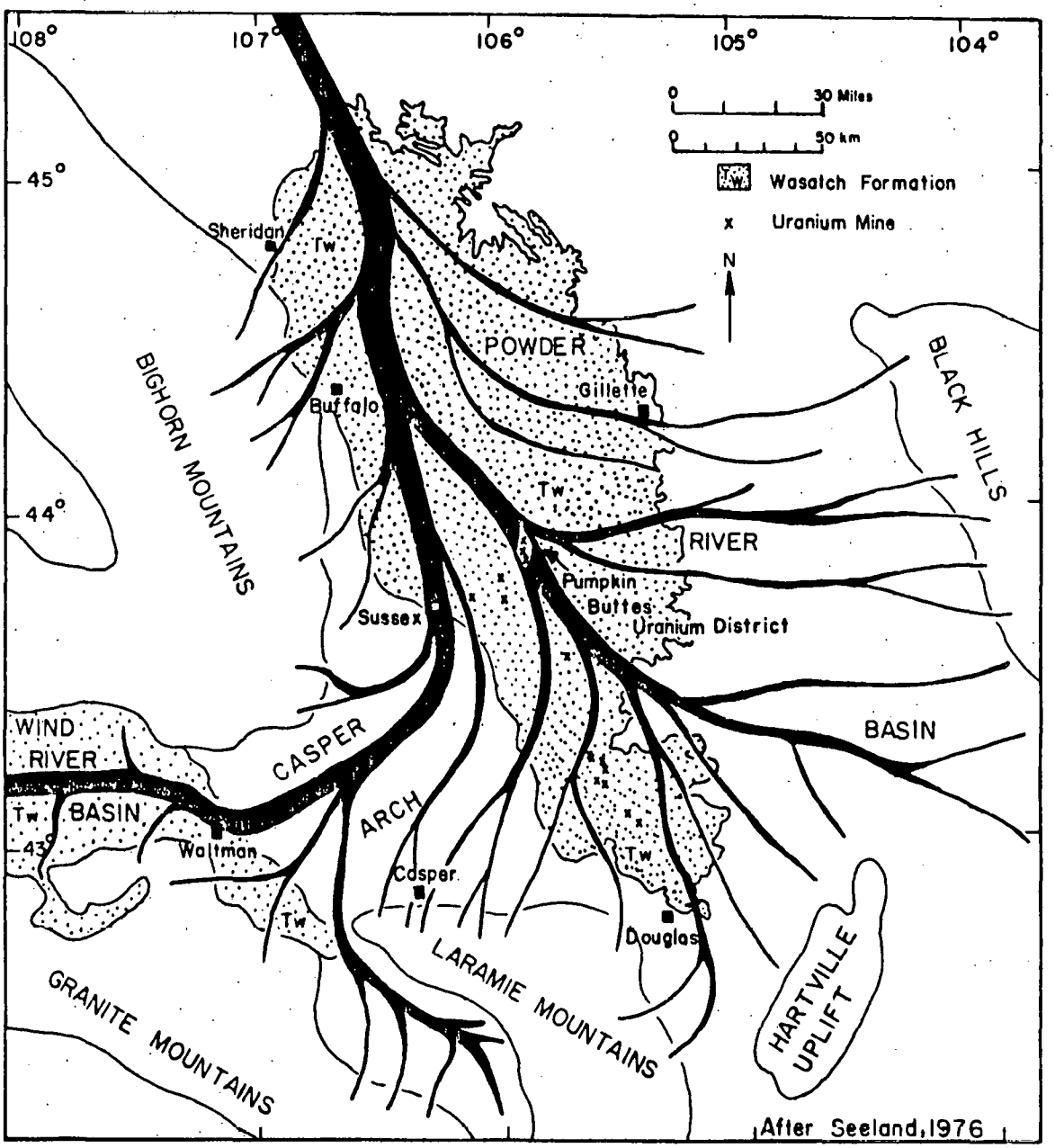

Figure 14. Paleogeography of the Powder River Basin during the Eocene. Paleodrainage was reconstructed using sand-grain elongation, regularity, mean size, and cross bedding direction studies.

oxides and the calcite, replacing calcite, but not the iron-manganese oxides (Troyer and others, 1954).

Pyrite marcasite, hematite, molybdenum (as jordisite) and selenium (both native selenium and ferroselite) are associated with uranium minerals (Harshman, 1968b; Granger, 1966). These are all considered epigenetic, and are related to the ore-forming process.

TABLE II

Major Uranium Minerals Present At Pumpkin Buttes

Mineral Name	Chemical Formula
Uraninite	UO_2
Uranophane	$Ca(UO_2)_2(SiO_3)(OH)_2 \cdot 5\ H_2O$
Coffinite	$U(SiO_4)_{1-x}(OH)_{4x}$
Carnotite	$K_2(UO_2)_2(VO_4)_2 \cdot 1\text{-}3\ H_2O$
Tyuyamunite	$Ca(UO_2)_2(VO_4)_2 \cdot 5\text{-}8\ H_2O$
Metatyuyamunite	$Ca(UO_2)_3(VO_4)_2 \cdot 8\text{-}10\ H_2O$
Liebigite	$Ca(UO_2)(CO_3)_3 \cdot 10\ H_2O$
Bayleyite	$Mg_2(UO_2)(CO_3)_3 \cdot 18\ H_2O$

Thin section and x-ray diffraction studies on selected samples collected in the study area indicate that alteration color of the sandstones in the Pumpkin Buttes uranium district is caused primarily by hematite and goethite, which is derived, in part, from the alteration of magnetite. The mode of occurrence of iron minerals in altered rocks (i.e. grain coatings and cement) strongly influences the degree of coloration.

Geochemistry

The abundance of epigenetic calcite in the Wasatch formation, and its apparent local control of much uranium deposition suggests that mineralizing solutions had a high carbonate and bicarbonate content (Sharp, 1964). Slightly alkaline, oxidizing, bicarbonate-sulfate groundwater,

similar to modern groundwaters in the Powder River Basin, is thought to have been the agent that transported uranium in the fluviatile sandstones (Butler, 1969).

Hostetler and Garrels (1962) studied the thermodynamics of uranium compounds dissolved in water. They concluded that uranium and vanadium could be transported as highly stable uranyl bicarbonate and tricarbonate complexes. Uranium and vanadium would precipitate as a result of reduction of hexavalent aqueous uranium species and tetravalent vanadium species. They constructed Eh-pH stability diagrams for both the $U-O_2-H_2O-CO_2$ system and the $U-V-K-O_2-H_2O-CO_2$ system at 25°C (77°F) which clearly showed how the presence of CO_2 causes both the formation of stable uranyl complexes, and a significant increase in the solubility of uraninite in natural waters. Carnotite stability was more sensitive to changes in ionic activity than to changes in Eh or pH (except for distinctly reducing conditions). Its precipitation was controlled by the amounts of uranium, vanadium, and CO_2 in solution.

Langmuir and Applin (1977) and Langmuir (1978) updated the landmark studies by Hostetler and Garrels. Using the same free energy data listed by Hostetler and Garrels (1962), Langmuir showed that uraninite and coffinite solubility is about 8 to 10 orders of magnitude less than that indicated by Hostetler and Garrels. This suggests that for a given Eh and pH, these minerals can precipitate from groundwaters far more dilute in uranium than previously assumed. The enlarged stability field for uraninite is shown in figure 15. Langmuir and Applin also stressed the importance of different complexes for the uranyl (UO_2^{2+}) and uranous (U^{4+}) ions in natural waters. Their work showed that for pH values less than 4.5, fluoride and sulfate complexes predominate and where fluoride complexing occurs, uraninite solubility is greatly increased. If the uranyl phosphate complex is present, it dominates through the pH range 4.5-7.5; if absent, uranyl carbonate complexes dominate this range. The uranyl carbonate complex always dominates where pH values are greater than 7.5.

Roll-Front Zonation

A geochemical cell is a dynamic system in which oxygenated water invades reduced, carbonaceous, pyrite-bearing sandstones resulting in an interface (or solution front) at which ore bodies may form (Shockey and others, 1968). As the oxidizing front advances, marked changes occur in Eh, pH, mineralogy, chemistry and microrganisms. This results in a systematic zonation across the "roll-front" which can be used as an exploration guide. In general, there are three major zones: the unaltered zone, the ore zone, and the altered zone (also called the barren interior). Rubin (1970) recognized six zones. As one progresses from outside to inside the geochemical cell, there is an increase in Eh. pH drops off sharply as one progresses from the unaltered zone to the ore zone and rises again in the altered zone (DeNault, 1974). These changes probably control much of the mineralogical and chemical variations across a roll-front.

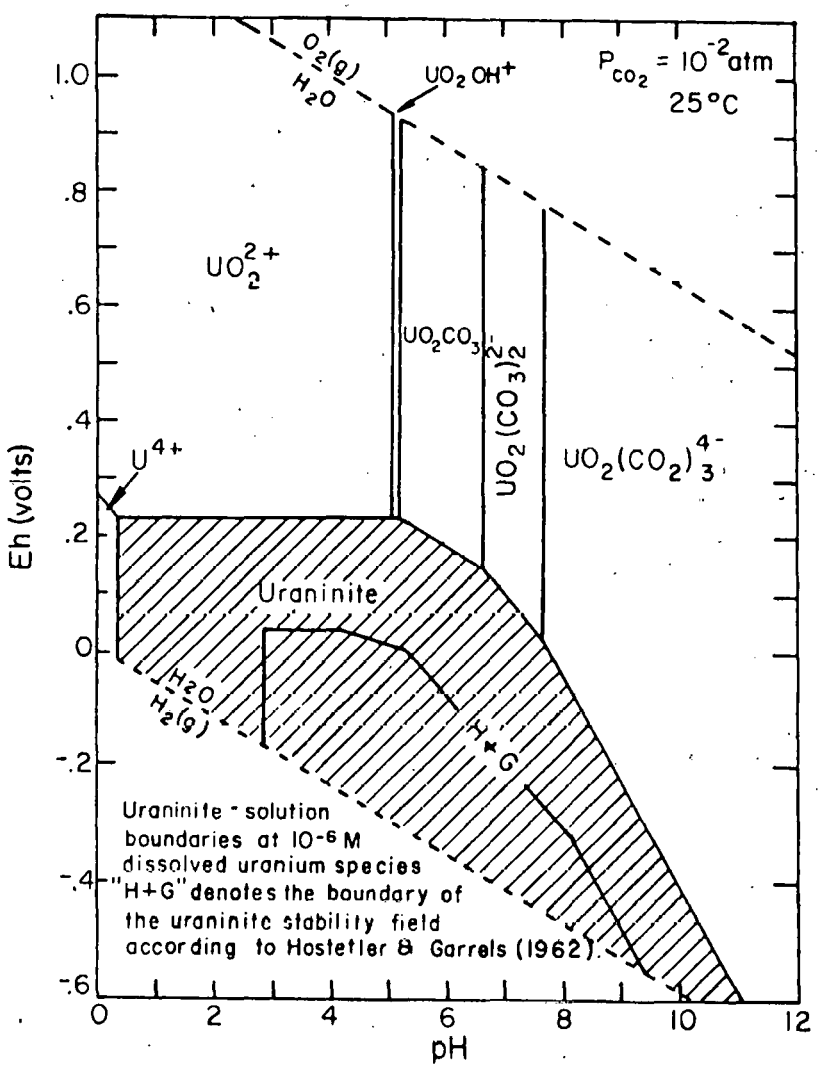

Figure 15. Eh-pH diagram showing the increased field of stability of uraninite indicated by Langmuir and Applin (1977) compared to that indicated by Hostetler and Garrels (1962).

Bacteria, which might be present in the reducing and oxidizing environments, could offer further control over zonation (Rackley, 1972). Bacteria of the genus Clostridium and of the genus Desulfovibrio thrive in reducing environments. Clostridium is a fermentor of cellulose, lignin, and other organic material, and it produces CO_2, H_2, and succinic acid (which is required by other bacteria). Desulfovibrio is especially important because it also consumes organic material, inorganic sulfates, and products of Clostridium to produce hydrogen sulfide (H_2S). Bacteria of the genus Thiobacillus thrive in an oxidizing environment where sulfides are present. These bacteria use oxygen and ferrous sulfate to oxidize pyrite, and produce sulfuric acid, ferric sulfate, and iron hydroxides. They create an acidic environment which is capable of leaching uranium and other susceptible elements (Rackley, 1972).

Mineralogical, geochemical, and color changes across a roll-front are shown graphically in figure 16. Geochemical zonation is also illustrated by data from samples collected along transects over roll-front deposits at the Pumpkin Buttes (Appendix B). Trace elements such as U, V, Se, Mo, P_2O_5, and As are concentrated at the interface between the oxidizing and reducing environments. Other soluble metals such as copper or silver could also be concentrated in this zone by the geochemical cell if they are present in the mineralizing solution. This would essentially be a supergene enrichment process (Houston, 1978). Major elements, such as Fe, Mn, and Al are present throughout the host rock, but change oxidation states upon passage of the roll-front.

Mode of Emplacement

The favored theory for the emplacement of roll-front uranium deposits will vary from district to district. Local geology, paleoenvironment, and preferred source usually dictate the favored mode of emplacement.

Rackley (1972) supports the geochemical cell concept that begins at a point where oxygenated waters enter and react with a reduced sandstone. The cell expands to form a three-dimensional finite body. The shape and size of the geochemical cell is controlled by shape and permeability of the host sands, presence of fracture systems, hydrological activity, and availability of carbon and pyrite. Biochemically controlled reactions take place at the advancing edge of the cell, producing changes in chemical conditions of the host rock. Uranium may be leached from the arkosic sands, transported to the reducing zone by groundwater, and precipitate only to be taken into solution again as the cell advances. Uranium is continuously enriched in the roll-front as the geochemical cell expands.

Harshman (1970) studied the roll-front deposits in the Shirley Basin of Wyoming. He believed that both granitic rock from the surrounding mountains and volcanic ash, which once overlaid the basin, were the

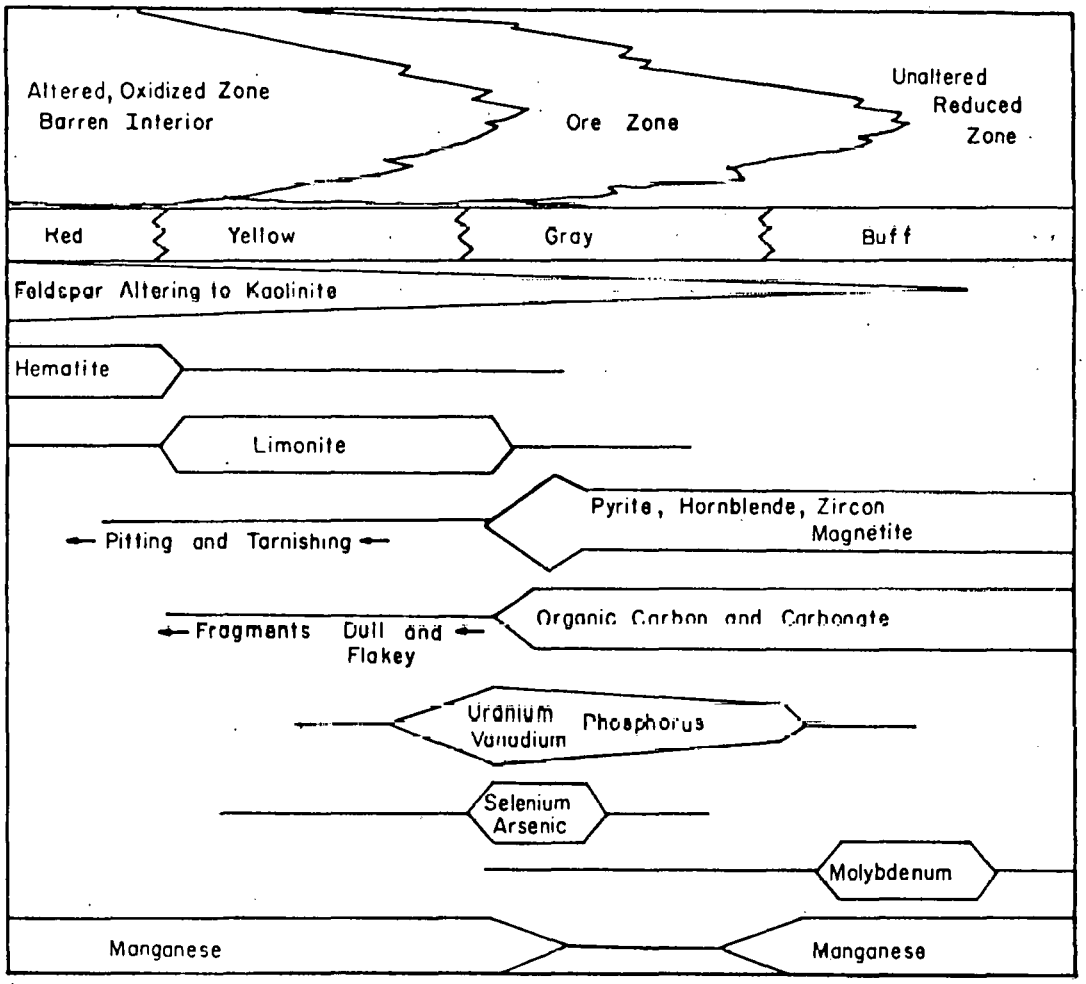

Figure 16. Chemical, mineralogical, and color zonation acros a roll-front deposit.
Compiled from Davis (1969), DeNault (1974), Rackley (19?2, Rubin (1970), and personal data.

sources of the metals. Uranium was transported in an oxidizing, alkaline solution and precipitated where hydrogen sulfide, and possible other reductants, caused a drop in Eh.

Adler and Sharp (1967) describe two prerequisites necessary for the formation of ore rolls. One factor is the occurrence of a reduzate facies in fluviatile sandstones. This forms when pyrite and/or large quantities of organic debris are buried in an oxygen-depleted environment below the water table. Low dip, low permeability, and other factors that inhibit the flow of water, would preserve the reducing capacity of this environment. Geologic activity or climatic change would enable oxygenated water to invade the reduzate zone, causing chemical reactions and alteration, such as oxidation of pyrite, oxidation and destruction of organic material, and oxidation of any chemically susceptible material in the groundwater. The second factor is the presence of uranium in adequate amounts in the groundwater. The mineral and chemical changes occurring in the sandstone can take place with or without the presence of uranium. A uranium ore body will form only if uraniferous waters penetrate or make contact with the chemical reduction zone.

Granger and Warren (1969) have proposed a process whereby the oxidation of pyrite in the host rock produces a series of unstable sulfur species, such as sulfite. These sulfur species, along with hydrogen sulfide, are active reducing agents capable of precipitating metals out of groundwater. Some of the sulfur products may recombine with ferrous iron at the roll-front to form the iron sulfide minerals associated with the ores. An important aspect of Granger and Warren's (1969) work is that they have demonstrated the formation of a well-defined reduction barrier in a biologically sterile environment.

Cheney and Jensen (1966), studied sulfur, carbon, and oxygen isotopes of samples from the Gas Hills uranium district in Wyoming. Sulfur isotope studies showed that pyrite cement associated with uranium mineralization is isotopically similar to sulfides produced by anerobic bacteria. Both have significantly lighter δS^{32} values than magmatic hydrothermal sulfides. They suggest that the extremely light isotopic composition on the leading edges of roll ore bodies is caused by oxidation and re-reduction of previously formed biogenic sulfides. Further evidence of biogenic origin for the deposits was furnished by carbon isotopes from the epigenetic calcite cement of the sandstones. δC^{13} values were very light, similar to the δC^{13} of calcite associated with asphalt and coalified wood.

Hydrocarbons may also play an important role in localizing uranium ore bodies. Natural gases seeping from pre-Tertiary rocks often contain hydrogen-sulfide (H_2S) -- a powerful reductant. In addition to direct precipitation of uranium, natural gas may be responsible for the formation of much of the widely distributed pyrite. When iron-bearing groundwaters contact natural gas seeps, precipitation of disseminated iron sulfide can occur. Chemical analyses of samples around seeps in

the Gas Hils of Wyoming, show that the flow of natural gas has raised the carbon content of the surrounding soils, and that much of the localized carbon has become fixed in the sandstones of the Eocene Wind River Formation (Grutt, 1957).

The association of H_2S-bearing oil and gas and uranium occurrences is well-documented in the Coastal Plain of southeast Texas (Eargle and Weeks, 1961). Grutt (1957) points out the close association of uranium deposits and occurrences of oil and gas in the Gas Hills, Crook's Gap, and Baggs mineral districts in Wyoming, and in the Maybell area of northwestern Colorado. The recent extension of the Hartzog Draw oilfield through the study area, and the presence of other major oilfields to the northeast and southwest of the study area, suggests that an association between hydrocarbons and uranium also exists in the Pumpkin Buttes uranium district. It should be noted, however, that while associations between uranium deposits and petroleum occurrences exist in many districts, oil- and gas-producing beds have not been spatially related to uranium ore bodies, and an exact link between the two has not been proven.

Gruner (1956) proposed a process of multiple migration accretion where uranium would be deposited and concentrated in a series of oxidation-solution-migration-precipitation cycles. The earliest stage was the extraction of uranyl ions from weathering tuffaceous or granitic terrain (including detrital material weathered from the granite). Uranium was carried in groundwater until it encountered a reductant (such as organic matter, H_2S, hydrocarbons, etc.) where it precipitated. This first accumulation was low in uranium content, but extensive. A second stage began when these precipitates were exposed, oxidized, redissolved, and carried into a new carbonaceous environment for reduction. Each new stage yielded higher concentrations.

Though Gruner's hypothesis is a general one, it may readily be applied to all roll-front deposits regardless of variations in local geology, source of uranium, and reducing agent. Diversity of lithological environment, climate, erosion rates, and periodicity of recurrence may be responsible for the observed differences in sandstone-type uranium deposits.

Age of Deposits

There are two prevailing schools of thought concerning the age of the uranium deposits: one has the deposits forming in middle Tertiary time, and the other has deposits forming in late Tertiary-Quaternary time.

Those that believe in an arkose source for uranium usually favor an Eocene-early Oligocene (Chadron) age for the deposits. They site evidence such as the paleoenvironment of an oxidized channel sand adjacent to reduced over-bank deposits. Uranium-bearing groundwaters flowing through such an environment would be able to leach, redistribute,

precipitate, and concentrate the uranium as ore deposits, especially if climatic fluctuations occurred. Conditions were more favorable for uranium transport in massive groundwater movement, with higher oxidation potentials, and over a longer time period, during the Eocene and early Oligocene than in any subsequent epoch (Bailey and Childers, 1977; Childers, 1974). Deep burial of reduced uranium subsequently froze it into place. No alteration complexes have been found in post-Chadron strata, and some roll-fronts were clearly developed before normal faulting which occurred in mid- to late-Tertiary time (Childers, 1974).

Those that favor a volcanic tuff source for uranium, believe the age of uranium deposits is late Oligocene or later, when a sufficiently large volume and widely distributed supply of volcanic ash was provided (Langen and Kidwell, 1974). Widespread normal faulting, which occurred in the late Tertiary (McGrew, 1971), could have furnished conduits for downward transport of uranium by oxygenated waters, thus enabling the eventual concentration of uranium in Wasatch sandstones.

Results of radiometric dating techniques have been inconsistent. Uraninite samples from the Blowout Anomaly deposit in the Pumpkin Buttes area have been analyzed for Pb^{206}/U^{238} and Pb^{207}/U^{235} isotope ratios. Age determinations range from 4.5 to 13 million years. Pb^{207}/Pb^{206} age determinations of the same samples have been less consistent with one sampling yielding an age of 425 million years (Sharp and others, 1964). This anomalous age value probably indicates that older radiogenetic lead was carried to the roll front, and probably approaches that of the source material of the host sands. Harshman (1968a) reports an age of 10 to 15 million years for uranium samples from the Shirley Basin of Wyoming, based on total lead/uranium ratios. Other age determinations from the same area, based on both U^{234}/U^{235} and Th^{230}/Pa^{231} ratios, indicate a minimum age of more than 250,000 years (Dooley and others, 1964). Oxygen isotopic composition of epigenetic calcite associated with uranium mineralization in the Gas Hills district of Wyoming show an extremely light O^{18}/O^{16} ratio, similar to that derived from polar snow. This indicates a Pleistocene age greater than 500,000 years (Cheney and Jensen, 1966).

There are considerable possibilities for error in these age determinations. Many samples used for analyses have been taken from the surface or near surface where the deposits have been exposed to oxidation and remobilization. The assumption must be made that all radiogenic lead resulted from decay of uranium in the deposits. Sharp and others (1964) have shown that some lead was introduced with the uranium. Daughter products of uranium could also have been introduced at the time of deposition; and certain daughters could have been preferentially leached since that time (Harshman, 1968b). If processes of multiple migration-accretion were indeed active, then it is probable that ages of uranium deposits may vary from Eocene to Holocene, and we should expect variability in age determinations.

METHODS

Satellite and aircraft imagery of the Pumpkin Buttes study area were analyzed using the University of Wyoming's video image analysis system. Specific techniques were defined which succeeded in enhancing known areas of uranium-associated alteration. Results were compared to digitally processed (VICAR) LANDSAT scenes provided by NASA/JPL.

A field program was conducted to confirm image interpretations and to provide spectral, radiometric, and geochemical data. Field sampling localities are shown in figure 3. Table III contains geographical and physical descriptions of the sampled features. Descriptions of field sample sites are contained in Appendix A.

Two sample grids (CH, CC) were set up over alteration zones which appear anomalous on enhanced imagery (Fig. 20); one of these areas (CC) contains a known uranium deposit. Three coarsely spaced sample transects crossed sandstone units (NJ, LB, IN). NJ covers an area which appears anomalous on enhanced imagery and contains a known uranium deposit. LB crosses a mapped altered sandstone which does not appear anomalous on enhanced imagery. IN covers an unaltered area, north of the mineral district, which does not appear anomalous on enhanced imagery. The following data were taken at each sample site: radiometric and spectral photometric measurements, percent vegetative cover, soil color (Munsell standard), surface slope and aspect, and soil pH. Soil samples were collected at a depth of 15 cm (6 in) where effects of surface oxidation are less pronounced. Geochemical analyses were performed on these samples.

Three closely spaced sample transects were set up across roll-front deposits exposed in mine pits (PJ, MJ, UT). Radiometric measurements and soil color determinations were made at each of these sites. Rock samples were also collected for geochemical and mineralogical analyses.

Three traverses were made with JPL's portable field reflectance spectrometer (PFRS) (Goetz, et. al., 1975, Appendix D) across roll front deposits (SJ, BA, LR*). Samples of surface material were collected at each spectrometer site for geochemical analyses.

Radiometric measurements, and rock and soil samples were also collected at spot locations throughout the study area. Many of these samples were submitted for geochemical analyses. A selected group were mineralogically analyzed using optical and X-ray techniques.

Geochemical, radiometric, color, and photometric data were treated statistically to determine correlations between color, uranium concentrations, and geochemical variables.

* Laur Mine Transect (LR) was located 11.3 km (7 mi) south of the study area.

TABLE III Sample Areas in the Pumpkin Buttes Study Area

Name	Abrev.	Location	Type of Sample	Number of Sample Sites	Spacing	Description
Christensen Grid	CH	E½, sec.20, T45N, R75W	Soil	44	100 m	Distinctive "Finger" shaped alteration zone not associated with uranium deposit.
Colorado Christensen Grid	CC	SW¼, SE¼, sec. 28, T45N, R75W	Soil	27	100 m	Area includes Colorado Christensen Mine, dumps, and undisturbed area downstream from Mine.
Lauby Transect	LB	SW¼, sec 27, T45N, R75W	Soil	14	100 m	Altered sandstone area mapped by Sharp, et. al., (1964) but non-anomalous on video enhanced aerial photography.
North Jeannette Transect	NJ	NE¼, NE¼, sec 22, T45N, R75W	Soil	5	100 m	Undisturbed area north of Jeannette I Mine, underlain by roll-front deposit.
Innes Transect	IN	NE¼, NE¼, sec 21, T46N, R75W	Soil	5	100 m	Unaltered sandstone area north of mineral district used for control data. Area is unmapped by Sharp, et. al., (1964) and is non-anomalous on video enhanced aerial photography.
Jeannette I Mine Transect	PJ	SE¼, NE¼, sec 22, T45N, R75W	Rock	13	Irregular	Samples from color zones in Jeannette I Pit.
Mid-Jeannette Transect	MJ	SE¼, NE¼, sec 22, T45N, R75W	Rock	3	4 m	Fine sampling of roll-front zones in wall of secondary pit south of main Jeannette I Pit.
Utah Mine Transect	UT	SE¼, SW¼, sec 27, T45N, R75W	Rock	7	Irregular	Samples from roll-front zones in south wall of trench near Utah Mine.
Jeannette Spectrometer Transect	SJ	SE¼, NE¼, sec 22, T45N, R75W	Rock	10	Irregular	Sample transect with PFRS, 4 m(13 ft) south and parallel to PJ Transect.
Blowout Anomaly #114 Transect	BA	NW¼, SE¼, sec 11, T45N, R74W	Rock	10	Irregular	Samples from roll-front zones with PFRS.
Laur Mine Transect	LR	SW¼, sec 19, T43N, R74W	Rock	7	Irregular	Samples from roll-front zones with PFRS. Transect is south of Study Area.
Spot Sample Locations	SL	Throughout Study Area	Rock	7	Irregular	Samples of various lithologies from various strata within Wasatch and White River Formations.

IMAGE PROCESSING

The video image analysis system has several attributes which make it a very effective tool for alteration mapping. Input to the system is non-digital so that image data of many different types and formats may be used. Scale-change capability allows matching and comparison of different types of image data. Instantaneous display ("real-time" viewing) allows on-the-spot corrections and changes in enhancement procedure. A number of different image processing functions can be performed (Levinson, Marrs, and Grantham, 1976). Processed scenes may be stored on a video disc, or may be photographed for hardcopy output.

Several basic image processing functions were applied to the Pumpkin Buttes imagery using the video image analysis system. These include: 1) scale adjustment, 2) color separation, 3) contrast stretch and brightness level adjustment, 4) image subtraction, 5) image ratioing, 6) density contouring, and 7) compositing.

Scale adjustment: The video scanner has a graduated, height adjustment to provide a variable field-of-view. The scanner is also equipped with a standard objective lens and a bellows-mounted close-up lens. These make image analysis possible over wide range of scales and allow registration of images having different scales.

Color separation: Each of the three emulsion layers on color films is sensitive to a specific spectral band and records the intensity of reflected light in that particular wavelength band as a primary color. A color separation filter can be placed between the video scanner and the color film to allow only information from a particular film layer to be viewed (table IV). In this way, color and color infrared films may be separated into their component spectral bands for spectral analysis.

Contrast stretching and brightness level adjustment: Contrast stretching is a procedure in which a selected brightness range (graylevel) of the image is expanded or "stretched" to fill the dynamic range of the display medium. Digital image processing systems accomplish this by constructing frequency histograms of image density numbers (DN). The peak of the histogram, corresponding to the feature of interest, is shifted to the center of the output graylevel range (brightness level adjustment). Then it is expanded to fill the entire black-and-white range of the output medium (contrast stretch). This expansion may be either linear or non-linear. Contrast stretching and brightness level adjustment are accomplished on the video system by simply selecting the mode (linear or logarithmic), then adjusting the gain and level controls to achieve optimal contrast. More complex stretches can be approximated by adjusting gain and level controls to overdrive or underdrive the signal, recording the resulting image, and playing it back at more neutral gain and level settings. The process can be repeated through several record/reproduce cycles if necessary.

TABLE IV

Spectral Bands Derived from Color Separation of Color and Color Infrared Films

Filter Color	Kodak Filter Number	Color Reversal Film (Kodak Extrachrome MS Aerographic Film 2448)*	Color Infrared Reversal Film (Kodak Aero-chrome Infrared Film 2443)*
Blue	No. 25	400-510 nm	500-580 nm
Green	No. 58	470-580 nm	560-675 nm
Red	No. 47B	560-680 nm	650-830 nm

Compiled from Eastman Kodak Company (1971)

* Spectral range limits represent the 10% transmission threshold of the filters.

Image Subtraction: Image subtraction is a normalization process which enhances differences between scenes. It is accomplished digitally by subtracting the DN of a particular picture element (pixel) in one spectral band from the DN of the same pixel in another spectral band. This is done for every pixel in the image. On the video system, a band subtraction is accomplished by mixing the negative transform signal of one band with the positive signal of the other band. This process could be represented by the following formula:

$$A - B = (m)(A) + (100 - m)(- B)$$

where A and B represent brightness values of the two scenes and m is the mixing proportionality coefficient.

The mixing coefficient is completely variable, and can be set at any proportion that yields the optimal enhancement for a desired purpose. Due to the differences in brightness and contrast of the two original scenes, a 50/50 mix rarely produces the optimal enhancement. The presentation of image subtractions is usually improved with contrast stretching and brightness level adjustment.

Image Ratioing: The ratio is a normalization process which clusters regions of like tonal value regardless of image brightness. It effectively mutes the strong contrasts so that subtle spectral contrasts may be seen. It often removes differences caused by minor atmospheric

effects or photographic defects. The ratio is accomplished digitally, by dividing the DN of a particular pixel in a given spectral band by the DN of the same pixel in a different spectral band. This division is performed on a pixel-by-pixel basis over the entire image. The video ratio function is similar to the video subtraction function except that both the positive and negative signals are stretched logarithmically. The formula for the video ratio is:

$$\log(A/B) = (m)(\log A) + (100 - m)(-\log B)$$

Again, the mixing proportion (m) is a subjective factor based upon what yields the most desirable enhancement. Like the subtraction, the ratio is best presented with the contrast stretch and brightness level adjustment. Since strong brightness contrasts are muted by ratioing, the brightness distribution in the ratioed image is much narrower than that of either original spectral band. A much greater contrast stretch is usually necessary for optimum presentation of a ratio (Goetz and Billingsley, 1973).

Density Contouring: Density contouring enhances changes in graytone of an image by presenting selected graytone ranges as contrasting colors. It is accomplished by separating the image graylevels into density intervals or "density slices". Density slices may be displayed in black, in the original graytone, or in a color. The bandwidths of the density slices are completely variable so that the most subtle density contrast of an image may be defined and displayed (Levinson, Marrs, and Grantham, 1976).

Compositing: Scenes may be combined in the video system in several ways. They may be added together,

$$A + B = (m)(A) + (100 - m)\ (B)$$

or they may be multiplied

$$\log(A \times B) = (m)(\log A) + (100 - m)\ (\log B)$$

Both these functions enhance contrasts that are similar to both spectral bands. Because the human eye can discriminate many more hues than graylevels, a color image can effectively display more information than either a single black-and-white picture, or a set of three black-and-white pictures from which a color composite is made (Goetz, et. al., 1975). Some critical spectral contrasts only become distinct when spectral bands or band combinations are presented as a color composite. Color composite scenes are produced on the video system by displaying each spectral band through a different color gun of the color monitor. Each scene may be adjusted individually for contrast and brightness. Any color combination may be used to produce a pleasing "false-color" presentation. The scenes are usually pre-registered and recorded on the video disc; but one of the scenes may be "live" from the scanner. In

this way, a map or other non-image overlay may be scaled and displayed with images in a composite scene. This allows easy comparison of images and other data, such as geological maps, contoured geochemical data, mine locations, etc.

ANALYSIS OF LANDSAT DATA

The LANDSAT satellite system offers tremendous potential for analysis and mapping of large altered areas associated with uranium deposits. The LANDSAT satellites provide synoptic, sun-synchronous, repetitive, multispectral coverage from a stable platform. LANDSAT orbits at an altitude of 918 km (570 mi), and produces small-scale imagery with nominal ground spatial resolution of 79 m (259 ft).

Video image analysis of the study area involved processing of LANDSAT 18.8 cm (7.4 in) transparency sets of multispectral scanner (MSS) data. A multi-seasonal approach was used in which five images, representing bimonthly observations during the snow-free seasons, were evaluated. The images are listed in table V.

TABLE V

LANDSAT imagery used for seasonal analysis

LANDSAT image number	Date
1228-17251	March 8, 1973
1300-17245	May 19, 1973
1353-17183	July 11, 1973
1047-17182	September 8, 1972
1461-17163	October 27, 1973

Each of the five images has relatively low contrast. Consequently, contrast stretching was applied to enhance spectral differences between features on the ground. Unfortunately, contrast stretching accentuated scan-striping and image processing noise, as well as enhancing image detail. The scan-striping became a severe problem in close-up examination of the imagery.

Video functions were applied to each image data set. The following functions were used: scale adjustment (enlarge study area to full screen size), band registration and recording, contrast stretching and brightness level adjustment, band subtractions, band ratioing, and color-compositing. The presentation of known occurrences of altered sandstone was evaluated with application of each video function.

Of all the possible band combinations, the 7/4 ratio shows the greatest potential for enhancement of areas of known alteration. The 4/5 ratio is generally bland, but displays broad, indistinct anomalies corresponding to altered ground. The 4/6 ratio has higher contrast than the 4/5 ratio, and yields more detail. Altered zones appear as

light-toned anomalies in these ratios, but their boundaries are generally indistinct. Many small alteration zones in the study area are beyond the resolution capability of LANDSAT.

Though alteration is enhanced using ratios, contrast stretched band color composite images provided better enhancement of known alteration zones (fig. 17). Ratios have lower spatial resolution, than color composites, because mutli-generation processing, which is necessary for construction of ratios, reduces spatial resolution. Also, alteration anomalies appear clearer and more pronounced in a color format rather than a gray tone format.

The late October scene clearly gave the best enhancement of soil color contrasts (fig. 17). The spring vegetation bloom produced a mottled effect on spring images which masked important soil contrasts. The mottling progressively decreased through the summer and fall as vegetation became senescent. Therefore, the latest fall imagery before snowcover provides the best enhancements of soil and rock anomalies.

An alteration map was constructed from a contrast-stretched, band color composite of the LANDSAT scene acquired on October 27, 1973 (fig. 18). On this composite, band 4 was colored blue, band 5 was colored green, and band 6 was colored red. Areas of altered sandstone appear as pale-yellow anomalies (fig. 17). Anomalous areas corresponding to areas of known alteration were mapped first; then, similar features were mapped. Detail on the color enhancement was often poor, so mapped anomalous areas were classified as distinct or indistinct. Because roll-front uranium deposits are confined to sandstone units, this map (fig. 18), was compared to a geologic map of the area compiled by Sharp, et. al. (1964). The two maps were brought to the same scale (1:62,500), and were superimposed. A 320-dot grid was laid over both maps. All dots superimposed on mapped sandstone or on distinct or indistinct anomalies were counted. The results are shown in table VI. Of the areas mapped as anomalous on the LANDSAT composite 52% corresponded to areas mapped as sandstone by Sharp, et. al. (1964). Visual observation showed many discrepencies between the two maps. The shapes of anomalous areas of the LANDSAT map differ greatly from the shapes of sandstone occurrences on the geological map. Often, color anomalies and mapped sandstone units were offset. This is partially due to geometric distortions on the LANDSAT enhancement. Many small areas of sandstone were not observed nor mapped because they exceeded the resolution limit of the video processed LANDSAT composite. These unmapped areas were usually less than 150 m (492 ft) across.

A regional analysis of occurrence of altered sandstone was conducted using enhanced LANDSAT imagery. A computer-enhanced LANDSAT image of the southern Powder River Basin was used as a data base (LANDSAT image #E-5 505-16264, September 5, 1976). Digital pre-processing of these data was performed at the EROS Data Center, Sioux Falls, S.D., and included edge enhancement, contrast stretching, scan-stripe removal, and

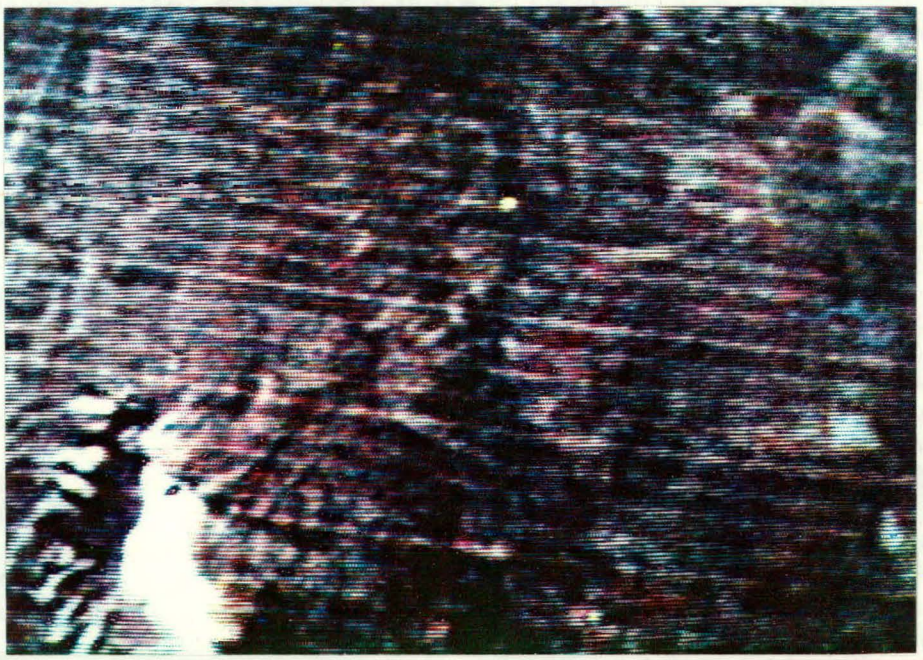

Figure 17. LANDSAT false-color composite of study area from a late October scene. Band 4 is colored blue, band 5 is colored green, and band 6 is colored red. Large areas of altered sandstone appear as pale-yellow anomalies.

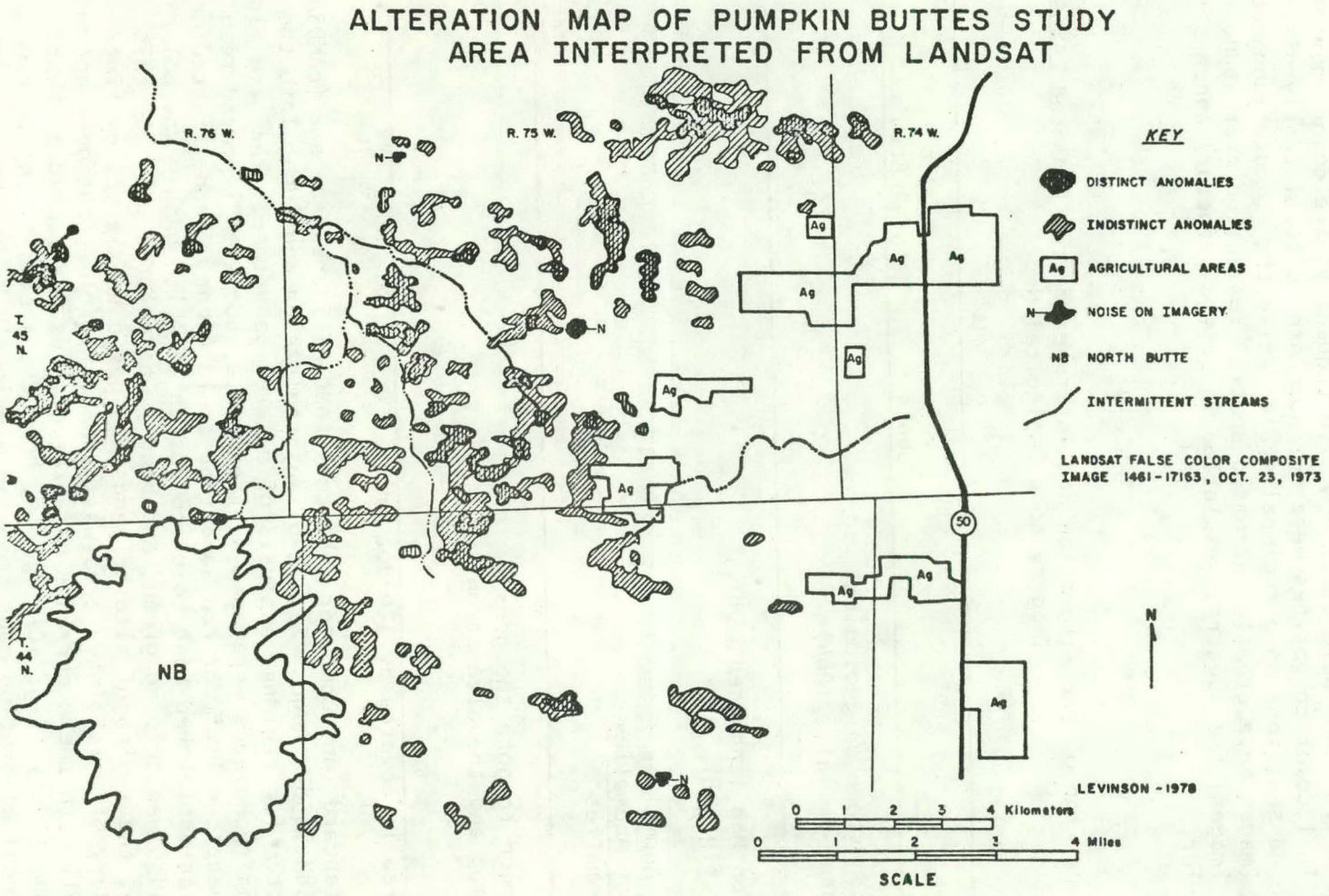
ALTERATION MAP OF PUMPKIN BUTTES STUDY AREA INTERPRETED FROM LANDSAT
R. 76 W.
R. 75 W.
R. 74 W.
T. 45 N.
T. 44 N.
NB
Ag
N
50
KEY
DISTINCT ANOMALIES
INDISTINCT ANOMALIES
AGRICULTURAL AREAS
NOISE ON IMAGERY
NB NORTH BUTTE
INTERMITTENT STREAMS
LANDSAT FALSE COLOR COMPOSITE IMAGE 1461-17163, OCT. 23, 1973
LEVINSON - 1978
0 1 2 3 4 Kilometers
0 1 2 3 4 Miles
SCALE

Figure 18

geometric corrections. Video processing of this image included color separation, additional contrast stretching and brightness level adjustment, and construction of band color composites, ratios and ratio color composites. Contrasts on the color-separated bands and spectral contrasts between bands were quite low. Consequently, the color contrasts on the final color composites were not adequate to consistently distinguish altered sandstone on a regional scale. While the computer-enhanced LANDSAT images have greatly increased spatial resolution over standard LANDSAT images, the spectral resolution (a critical factor) appears to be inferior.

Table VI

Comparison of the Alteration Map Interpreted from Enhanced LANDSAT Imagery to a Geological Map

Map	Dot Counts	% of Total Area*
Mapped sandstone on geological map (Sharp, et. al., 1964)	50	16
Alteration Map (enhanced LANDSAT Imagery, fig. 18)		
Distinct Anomalies	13	4
Indistinct Anomalies	33	10
Total Anomalies	46	14
Areas Common to both the geological map and the alteration map	24	8

*Total area is covered by 320-dot grid.

A standard (not computer enhanced) LANDSAT image data set (LANDSAT image #2583-16584, August 27, 1976) was registered and input into the video system for regional analysis of altered sandstone. The same video processing techniques were used on these data, but with improved results. The northeastern limit of red sandstone could clearly be delineated on the contrast-stretched band color composite in which band 4 was colored blue, band 5 was colored green, and band 7 was colored red. On this composite, the region of altered sandstone has a subtle yellow tint. The boundary of this tinted area was mapped (fig. 1B), but does not correlate well with the occurrence of altered sandstone mapped by Sharp and Gibbons (1964) (fig. 1C). It is, however, a significant improvement over regional alteration maps compiled previously by Houston, et. al.

(1973) and Marrs, et. al., (1973) (fig. 1A) which were constructed from unenhanced, bulk-processed LANDSAT imagery. It should be noted that the interpretation of the regional alteration pattern from enhanced LANDSAT imagery may be more accurate than the map by Sharp and Gibbons (1964). This is especially true in the study area where subsequent detailed mapping of altered sandstones (using aerial photography) has established the limit of altered sandstones.

An analysis of the study area was performed using digitally processed (VICAR) LANDSAT data. Contrast stretched bands and ratios were produced from these data (courtesy of NASA/JPL). Each individual band and ratio was checked for anomalies corresponding to known alteration. The 7/4 and 6/4 ratios appear very similar. Both provide reasonably good enhancement of alteration throughout the study area. The 5/4 ratio provides adequate enhancement of alteration in the dissected, sparsely vegetated uplands, to the west of North Butte, but it does not reveal altered areas in the moderately vegetated, rolling divide area east of North Butte. This indicates that vegetative cover seriously reduces the effectiveness of the 5/4 ratio. The 6/4 and 7/4 ratios are not seriously affected because they are not so strongly influenced by vegetation.

ANALYSES OF AIRCRAFT SENSOR DATA

Aerial photography and airborne scanner data provide greater resolution than LANDSAT data. Therefore, the aircraft data have greater utility in establishing image analysis techniques where greater spatial detail and multi-generation processing are required. Such is the use for enhancement of small areas of altered sandstone associated with uranium deposits.

A high-altitude (1:130,000-scale) color-infrared aerial photograph (NASA Mission 72-138, Line C-D, Frame 4736, August 11, 1972) served as a test scene to define the most effective video image processing techniques. This frame covers the entire study area. However, vignetting is so strong on this photograph that the color contrasts appear washed out in the northern part of the study and too dark in the southern part (fig. 19). Known uranium mines, uranium occurrences, radiation anomalies, and altered sandstone outcrops in the area have been mapped previously (Breckenridge, et. al., 1974; Sharp, et. al., 1964) and many are shown in figure 4. These features were located on the aerial photograph and identified as control points in the subsequent analyses. Both open pit mines and smaller surface scrapes appear as bright spots which are devoid of vegetation. Reddish altered sandstone appears yellow on the color-infrared photograph, but this coloration is subtle and is often masked by vegetation, eolian cover, or the vignetting effect. Most uranium occurrences and radiation anomalies are associated with altered sandstone, and many are located in (or adjacent to) yellow areas on the photograph.

The aerial photograph was analyzed in the video system at three scales to determine the optimal scale for uranium alteration mapping. Small-scale regional analyses were performed first. A portion of the scene encompassing the entire study area was input (19.3 km (12 mi) across). Image processing functions included the following: color separation of the photograph into component spectral bands (equivalent to LANDSAT bands 4, 5, and 6), linear contrast stretch, logarithmic contrast stretch, brightness level adjustment, band addition, band subtraction, band ratioing, band color compositing, ratio color compositing, and combinations of these functions. These processing functions were applied to every possible band combination. Several "generations" of recording (enhance/record/reproduce cycles) were attempted in order to achieve increased spectral contrasts. The enhancement of the control points in the study area was evaluated with each processing function. Density contouring was applied to several bands and band combinations, but density contrasts due to vignetting were stronger than significant density contrasts related to alteration.

This approach to image analysis clearly showed the advantages of more complex image processing involving band computations and multi-generation processing. The increased resolving power and lack of scan-stripes enabled a far superior enhancement product to be produced. Ratios proved superior to single contrast-stretched bands, band additions,

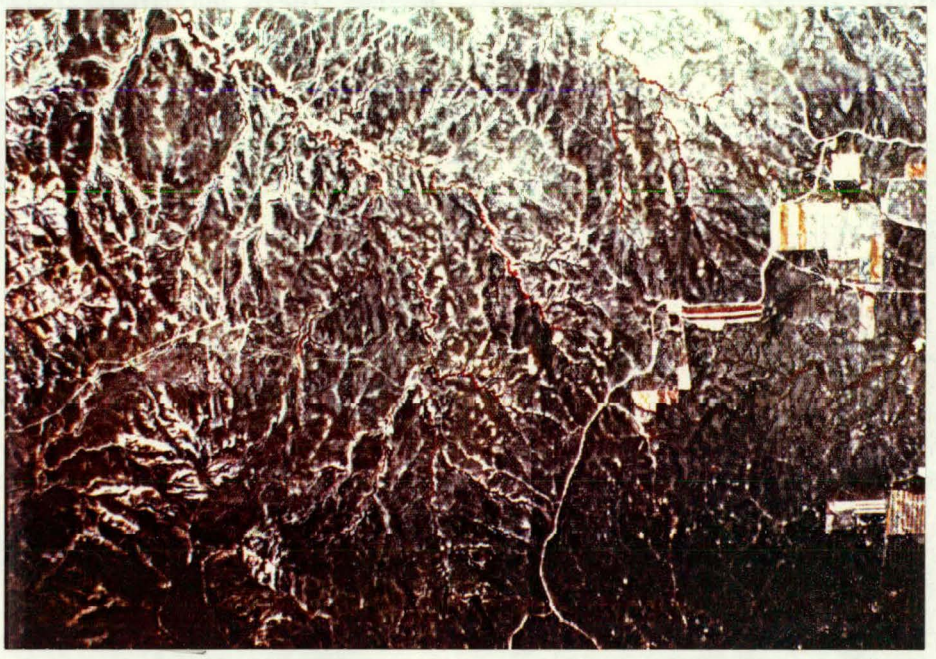

Figure 19. Unenhanced, high-altitude, color infrared photograph of study area. NASA Mission 72-138, line C-D, Frame 4736, August 11, 1972.

band multiplications, and band subtractions. Ratios eliminated most slope effects and also greatly reduced vignetting in the scene. Only the 5/4, 6/4, and 6/5 ratios could be constructed from the color-separated, color-infrared photograph. Of these, the 6/4 yielded the best enhancement of known alteration areas.

The 5/4 ratio, which was used successfully by previous workers (Rowen, et. al., 1974; Salmon and Vincent, 1974; Salmon and Pillars, 1975; Offield, et. al., 1977), produced only a bland product with very little contrast. This may be due to the moderate vegetative cover which occurs over most of the rolling divide terrain in the study area. At the time of the air-photo mission (mid-August), most vegetation in the area had dried and turned yellow. The senescent vegetation reflects almost equal amounts of red and green light. Hence, there should be little difference between bands 5 and 4, and their ratio should produce a low contrast image.

Ratio color composites also produced good enhancement of altered areas. In these composites, the 6/4 ratio was most influential in enhancing areas of known alteration. When second generation ratios were incorporated into ratio composites, the contrast between altered and unaltered areas became even stronger.

Vignetting was not completely removed from the image. Acceptable enhancement of altered areas was obtained only in the central 50% of the study area. While many known alteration zones appear anomalous, it is uncertain that all anomalous areas correspond to uranium alteration. The resolution of the enhanced imagery at this scale is too coarse to define all anomalous areas, or to locate accurately their boundaries.

As a test of video analysis for medium-scale processing, a smaller area in the central portion of the study area was enlarged to full screen on the video system, corresponding to a ground distance across the video screen of 6.4 km (4 mi). The same suite of processing functions were performed at the medium scale. The results were very similar. The 6/4 ratio provided the best enhancement of known altered areas, and ratio color composites in which the 6/4 ratio was most influential, delivered the best display of alteration (fig. 20). At this scale, it became clear that altered sandstone outcrops often have a unique geomorphic expression. The sandstones, being resistant to erosion, form broad ridgetops. These ridgetops usually have thin, immature soils and sparse vegetative cover. Often, they are pockmarked with blowouts. The sparse vegetative cover allows the soil to show through such that the ridgetops may appear "pink" regardless of whether they are formed from altered or unaltered sandstone. This is because all soils tend to have slightly stronger reflectance in the red band. Differentiation between altered and unaltered sandstone in ridgetop areas was not possible at small-scale, but was possible at medium-scale. Boundaries of alteration are clearly discernible at this scale (fig. 20). In many cases these boundaries extend well below the crest of the ridgetops, even into areas where vegetation is more dense. The vignetting problem is greatly reduced when a smaller portion of the

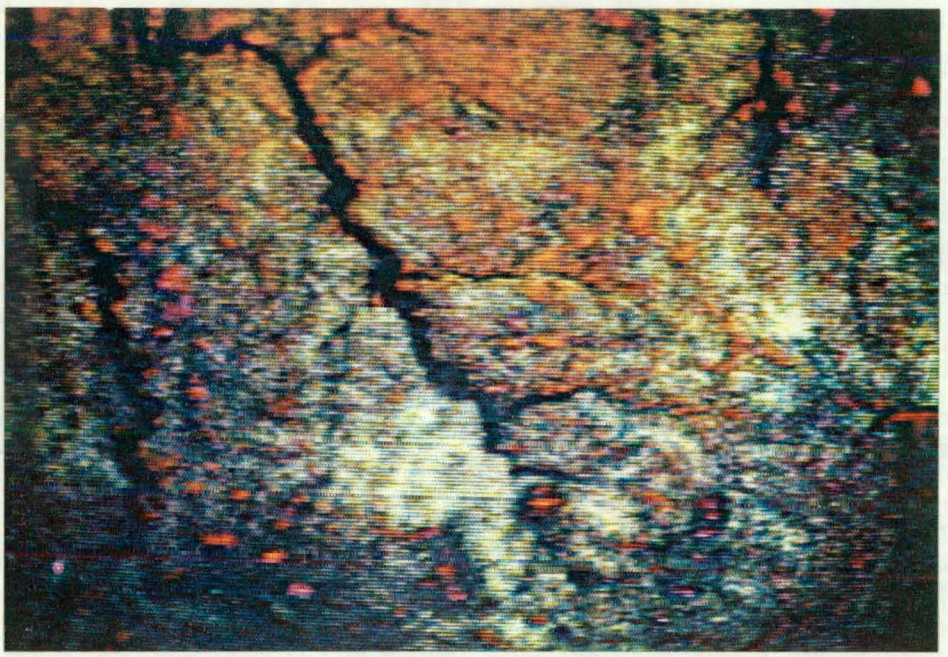

Figure 20. Ratio color composite enhanced from a color infrared aerial photograph at a medium scale. -(5/4) is colored blue, 6/5 is colored green, and 6/4 is colored red in this presentation. Altered sandstone appears reddish-orange.

photograph is analyzed. Ratios and ratio composites produce acceptable enhancement of altered areas throughout 80% of the scene. Because of the increased detail and reduced vignetting, video image processing at this scale is satisfactory for alteration mapping.

Video analyses were also performed at large-scale to provide a detailed evaluation of a single altered area. Horizontal distance across the video screen at this large-scale represents 2 km (1.2 mi) on the ground. The scene evaluated covered a distinct anomalous area whose shape resembled a hand with an extended index finger. It was designated the Christensen Anomaly (CH) because it occurred on Christensen ranch property. This area was later grid-sampled and subjected to chemical, photometric, and radiometric analyses. The CH anomaly was mapped as sandstone by Sharp, et. al. (1964), however, the shape of Sharp's mapped area differs greatly from that of the CH anomaly as it appears on video enhancements. No uranium occurrence or radioactive anomaly was known in the CH area. The same enhancement processing functions used at the small- and medium-sclaes, were employed at the large scale, yielding identical results. Thus, the 6/4 ratio was confirmed as the optimal enhancement for uranium alteration on this particular photograph. The detail obtainable at large scale enabled detection of changes in vegetation type and percent cover as well as changes in soil type. These effects produced a background "noise" which could be reduced to a black background through multi-generation contrast stretching and brightness level adjustment (fig. 21A). Multi-generation processing also increased the contrast between altered and unaltered areas, but a minor loss of spatial resolution accompanies each successive generation of recording (Levinson, Marrs, and Grantham, 1976) (fig. 21B). Ridgetops, blowouts, and cutbank exposures were easily identified at the large scale. These appear as areas of higher albedo and are distinctively different from altered areas on ratio color composites (fig. 22B). Because the vignetting effect was nearly eliminated at this scale an attempt was made to test the density coutour function. A contrast stretched 6/4 ratio image of the CH anomaly was divided into seven equi-density intervals and was color coded (fig. 22A). This display successfully enhanced altered areas which appear yellow. Blowouts, cutbank exposures, near-barren ridgetops and other areas of high albedo appear green. Unaltered areas appear brown and violet. Unfortunately, many small, unaltered areas also were displayed as yellow features. These spurious features represent primarily eroded Arvada series soils, entisols, some alluvial deposits, and areas of sparse vegetation cover. These areas can clearly be differentiated from altered areas on the contrast stretched 6/4 ratio and on ratio color composites (fig. 21 and 22B).

Large-scale color infrared aerial photography was made available through the U.S. Bureau of Land Management (BLM) who sponsored an aerial photo mission over Campbell County, Wyoming during May and June, 1976. This 1:33,500-scale photography offers significantly more detail than the NASA Mission 72-138 photography. The entire study area was covered in stereo on 23 frames. However, the color quality of the BLM photography is poor. The color of each is dominated by a blue tone with green tones

A

B

Figure 21. Video ratios of the Ch anomaly produced from a color infrared aerial photograph at large scale. A. Second generation 6/4 ratio. B. Third generation 6/4 ratio. Altered sandstone appears as light graytones on these ratios.

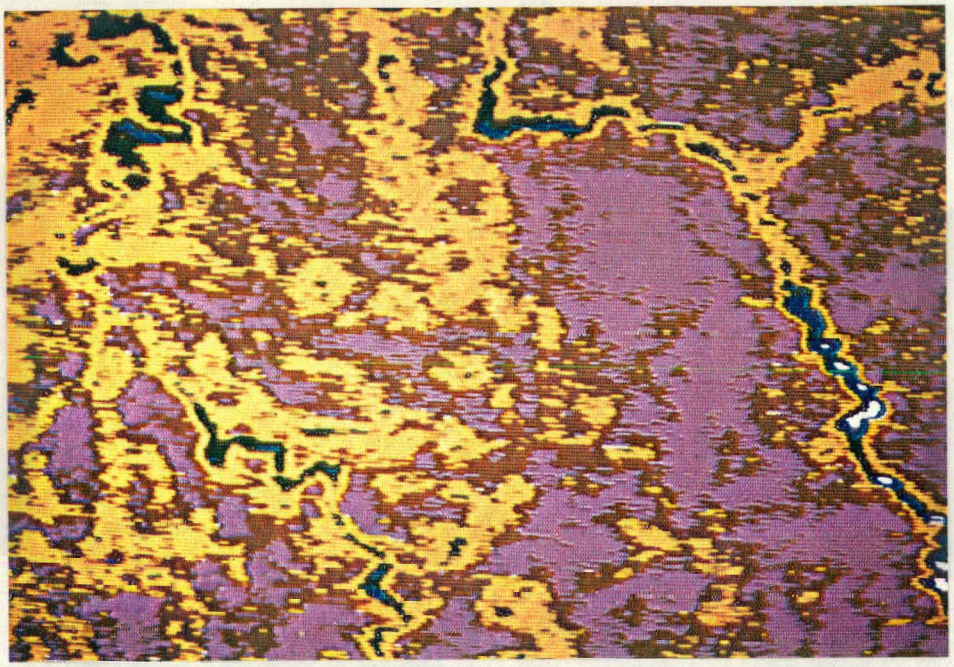

A

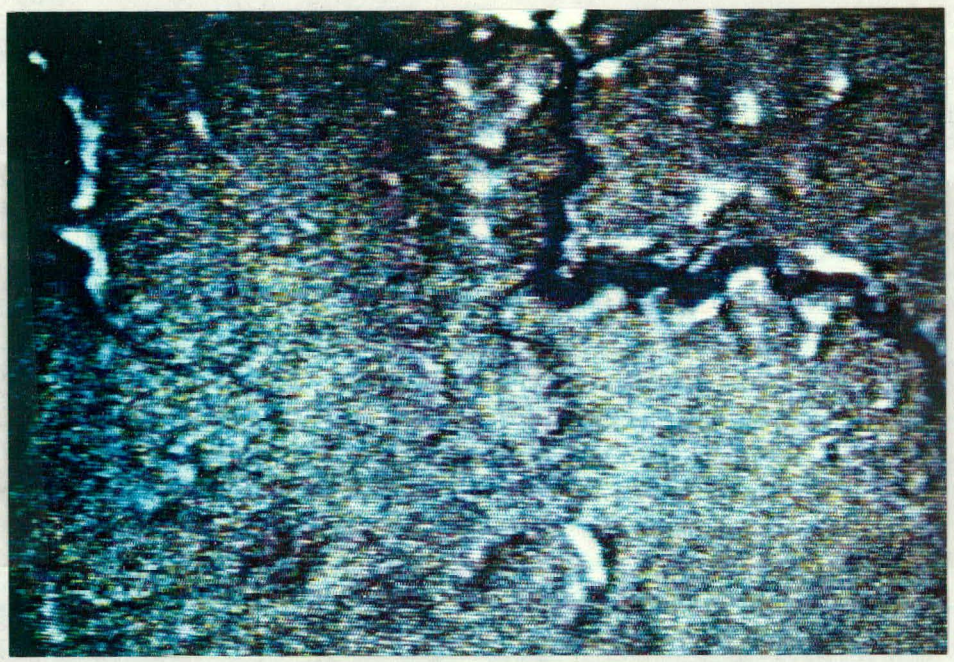

B

Figure 22. Colored video enhancements of the Ch anomaly produced from a color infrared aerial photograph at a large scale. A. Density contoured display of third generation 6/4 ratio. Altered sandstone appears yellow. B. Ratio color composite in which -(5/4) is colored blue, -)6/4) is colored green, and -(6/5) is colored red. Altered sandstone appears purple; blowouts, bare ridgetops, and cutbank exposures appear white.

nearly absent and red tones only present in densely vegetated areas (i.e. floodplains). Known areas of red sandstone which are readily visible on unenhanced NASA photography could not be visually detected on the BLM coverage due to the color imbalance. Color separation filters were applied to selected frames on the video system in an attempt to enhance the weaker spectral components. This proved unsuccessful because the red and green colors were not adequately recorded on the film. Further video processing seemed unlikely to yield positive results, so no further analyses were performed. This experience with BLM photography shows that high quality photography is essential for spectral analysis.

Video processing was also performed on multiband photography (NASA Mission 310, Line 6, Frames 159-160, June 2, 1975). The spectral bands represented by these data are listed in table VII. These multiband photos cover only the central 1/4 of the study area. Horizontal distance across the video screen for a single frame is 6 km (3.7 mi). Many known alteration areas and several roll-front deposits occur on this coverage. Unfortunately, this photography is not of sufficient quality to accurately record spectral contrasts. All bands were overexposed and lacked color contrast. The color and color infrared photography was seriously deficient in red and infrared components. Color separation and contrast stretching did not sufficiently enhance these bands to make them useful for further video processing. However, the blue band, which was color separated from the color photography (table VII), was used in conjunction with the green, red, and near infrared bands for multispectral analyses. A ratio composite in which 7'/6 was displayed in blue, 7'/4 was displayed in green and 6/4 was displayed in red produced the best enhancement of the area. On this enhancement, areas of high vegetative density appear white. Alteration areas appear as a reddish brown indicating that the 7'/4 and 6/4 ratios had a significant influence on the enhancement. However, because each individual band was of very low contrast, the resulting ratios and ratio composites also lacked contrast. Boundaries of altered areas are indistinct. Contrast stretching and multi-generation processing improved the enhancement of altered areas, but also increased the apparent graininess and processing noise in the photography.

Airborne multispectral scanner imagery covering a portion of the study area was made available for video analysis (courtesy U.S. Geol. Survey). The scanner system recorded in spectral regions equivalent to each of the four LANDSAT bands, plus a blue band, and two thermal infrared bands. These data were acquired on September 9, 10, and 11, 1976, from an altitude of 4,878 m (16,000 ft) above sea level. Thermal data was acquired on a separate night and morning flights. The spectral bands available from this scanner data are shown in table VIII.

Intensive multispectral analyses were performed on these data. Individual bands were contrast stretched and analyzed. All possible band subtraction and ratio combinations were constructed. But of these, the best enhancement was produced from the 7/4 ratio. The 6/4 also enhanced

altered areas well. The 5/4 ratio was, again, a bland image and produced relatively poor results.

TABLE VII

Spectral Bands Available on Multiband Photograhy*

Spectral Bands	Wavelengths	LANDSAT Equivalents
Green Band	.5 - .6 um	Band 4
Red Band	.6 - .7 um	Band 5
Near Infrared Band	.7 - .8 um	Band 6
Near Infrared Band	.8 - .9 um	Band 7' (Short wavelength portion of LANDSAT Band 7)
Color Photography	.4 - .7 um	Color separation into LANDSAT Bands 4 and 5, plus a Blue Band
Color Infrared Photography	.5 - .88 um	Color Separation into LANDSAT Bands 4, 5, and 6.

*NASA Mission 310, Line 6, Frames 159, 160, June 2, 1975

TABLE VIII

Spectral Bands Available on Airborne Multispectral Scanner Coverage*

Spectral Bands	Wavelengths	LANDSAT Equivalents
Blue Band	.4 - .5 um	----------
Green Band	.5 - .6 um	Band 4
Red Band	.6 - .7 um	Band 5
Near Infrared Band	.7 - .8 um	Band 6
Near Infrared Band	.8 -1.1 um	Band 7
Thermal Infrared Band - Low Resolution	7.5-12.5 um	----------
Thermal Infrared Band - High Resolution	7.5-12.5 um	----------

*Courtesy U.S. Geological Survey

Processing of thermal data produced some very interesting enhancements. Quantitative temperature determinations were easily acquired by calibrating the image densities to the blackbody and graybody stripes provided on the film. Density contouring was then used to display temperatures in a readily-interpretable form. Broad patterns became apparent on the night thermal band and night/day thermal ratio. These patterns followed the general outcrop of channel sands, showing them as slightly warmer areas (fig. 23). The cause of these thermal patterns is unknown, though it may be related to heat capacity, thermal inertia, texture and permeability, soil moisture, soil type, or vegetation. Ratios of standard spectral bands to the thermal band produced unusual and interesting results which are difficult to interpret. Specific characteristics of materials in the thermal wavelengths are not well defined. Interactions between emissive and reflective radiation are also poorly understood. Research on thermal inertia and on the interactions of visible and thermal radiation at the surface of the earth is currently underway at the U.S. Geological Survey (Miller and Watson, 1977), NASA/JPL (Kahle and others, 1977), and other institutions.

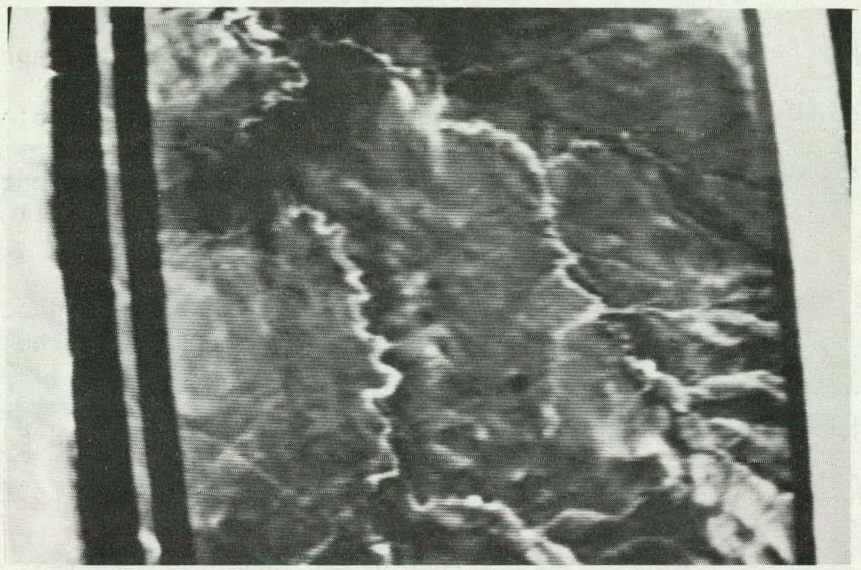

Figure 23. Night thermal/day thermal ratio of airborne multispectral scanner bands. Light tones, wich indicate warmer areas, generally follow the outcrop of channel sands.

URANIUM ALTERATION MAP

In order to demonstrate the effectiveness of the video-enhanced remote sensor data as an aid to uranium alteration mapping, a map of altered sandstone in the Pumpkin Buttes study area was constructed from aerial photography processed on the video system (plate 2). The NASA Mission 72-138 photography was used as a data base for the alteration map, because enhancements from that color infrared photography were superior to all other types of available imagery in terms of spatial resolution, spectral contrasts, and minimal image processing noise.

In order to minimize the vignetting effect and provide adequate detail, the study area was analyzed in nine separate sections, each covering an area of 6.4 X 8 km (4 X 5 mi). Each section was analyzed in an identical fashion. The processing and mapping procedure was as follows:

1. Set up for proper scale and location on photograph.
2. Color separate photograph into component spectral bands.
3. Construct band color composite. Each band is contrast stretched individually to provide best presentation of altered areas.
4. Map all anomalous areas. This stage of mapping accounts for 80% of the alteration zones identified on the final map.
5. Construct all ratio combinations (5/4, 6/4, and 6/5).
6. Map anomalous areas on contrast stretched 6/4 ratio (which have not been mapped previously). This accounts for 18% of the altered zones identified on the final map.
7. Construct ratio color composite and contrast stretch each ratio individually to provide maximum enhancement of altered areas.
8. Map additional anomalous areas. This accounts for 2% of the altered zones identified on the final map.
9. Photograph map both with and without band color composite background.
10. Transfer video map to base map.

Anomalous areas corresponding to areas of known alteration were mapped first; then anomalous areas which appeared similar to these were mapped. Boundaries of anomalous areas were marked directly on the screen of the color monitor. Photographs of each of the mapped quadrants were transferred to a 1:62,500-scale topographic base map (U.S. Geological Survey, 1959).

This alteration map (plate 2) was compared to the geologic map of the Pumpkin Buttes area by Sharp, et. al., (1964). Sharp's map is difficult to interpret because he only divided the Wasatch formation into sandstone units, carbonaceous units, and undifferentiated fine-grained sedimentary rocks. He identified sandstone units by their relative stratigraphic position, where possible. He did not designate sandstones as altered or unaltered, but mapped sandstones only within the region of red (altered) sandstone (Sharp and Gibbons, 1964). Some sandstone outcrops such as at the Innes transect site (IN), Chimney Hill, and other areas north and east of the mineral district, were not mapped. Sharp did show locations of major uranium occurrences. This aided in interpretation of video enhancements.

A 320-dot grid was superimposed on both the alteration map (plate 2) and Sharp's geological map (Sharp, et. al., 1964). Counts were made of all dots corresponding to sandstone or altered areas for both maps. Table IX shows the comparison of dot counts for the two maps. This comparison indicates that 60% of the areas mapped as sandstone by Sharp, et. al. (1964) appear altered on enhanced aerial photography. Of the altered areas, 22% do not correspond to mapped sandstone. There was generally good agreement between the shape of alteration zones and sandstone areas on the two maps. It should be emphasized that two different (but related) parameters are compared in Table IX; Sharp, et. al. (1964) mapped sandstone, while plate 2 shows uranium alteration. It is probable that not all sandstone in the study area is altered, and that some areas appearing altered do not correspond to sandstone. However, it is important to note that there is a strong correspondence between sandstone units and altered ground.

TABLE IX

Comparison of the Uranium Alteration Map Interpreted from Enhanced Aerial Photography to a Geological Map

Map	Dot Counts	% of Total Area*
Mapped Sandstone on Geological Map (Sharp, et. al., 1964)	75	23.4
Uranium Alteration Map (Interpreted from video enhanced color infrared photography, plate 2)	58	18.1
Areas Common to both the Geological Map and the Uranium Alteration Map	45	14.1

*Total Area is covered by 320-dot grid.

EVALUATION OF THE VIDEO IMAGE ANALYSIS SYSTEM

Video image analysis proved to be a fast and inexpensive tool for image enhancement. Marrs and King (1978) provide cost estimates of video image processing for several demonstration projects in which uranium resource areas were evaluated. They showed that video processing costs range from 1/4 to 1/10 that of similar digital processing. Initial, operating, and maintenance costs of the video system also are far less than that of digital systems which perform similar tasks. The flexibility of processing functions, speed of operation, and "real-time" viewing capability make video image processing extremely efficient as well as economical.

The video system adapts to many types of image data and also functions as a data storage device. Photography, multispectral scanner data, thermography, printed maps, and video enhancements were all stored on the video disc recorder, and recalled as needed during the course of image analysis. The high spectral resolution of the video system (.02 D) (Levinson, Marrs, and Grantham, 1976) enables consistantly good reproduction of these data.

The video image analysis system also serves as a mapping tool. New data from each enhancement can be quickly added or compared to existing information. Up to three images can be displayed simultaneously using the three primary colors. This enables a multitude of correlations and presentations. Features of interest can be interpreted and mapped directly from the screen, or hardcopy output may be obtained by photographing the screen. Image distortions (due to screen curvature and lack of convergence on edges) causes some difficulty in transferring data to base maps. However, if only the central 80% of the screen is used, distortion is minimal and information displayed on the screen can be transferred easily.

The major drawback to the video system is its loss of spatial resolution. Use of image data, which was originally in digital format (i.e. LANDSAT), restricts resolution of the data at the outset. Each cycle through the video processor degrades spatial resolution ∿5% (Levinson, Marrs, and Grantham, 1976). This becomes a major factor for complex image processing functions which require several "generations of recording". When fine detail is essential in the processed product, this loss of spatial resolution may limit the number of enhancement options. Digital image analysis systems have a distinct advantage of being able to maintain spatial resolution throughout the most complex image processing. It should be mentioned, however, that many types of data used in this study are not available in digital form. Digitization of these data would be expensive, time-consuming, and the end product would still be limited by the resolution of the original image.

The video system provides a great variety of processing functions. Among those used in this study were: 1) scale adjustment, 2) color

separation, 3) contrast stretch and brightness level adjustment, 4) image subtraction, 5) image ratioing, 6) density contouring, and 7) compositing. These functions enable complete spectral analyses to be performed in a minimal amount of time. All possible spectral band combinations, and all proportions of a particular band combination, may be easily displayed and analyzed. The best combination of processed products can then be identified and recorded. Image analysis requiring preprocessing, filtering, complex stretches, pattern recognition, statistical analyses, or exact spatial resolution must be handled through digital computer systems. However, many image enhancement techniques may be developed and applied more quickly, and at a much lower cost, using video image processing. Once the optimum processing procedures are defined through video processing, they may be applied via digital computer systems for complex or precision image processing.

ANALYSIS OF FIELD SPECTRA

Spectral reflectance of surface rocks, soils, and vegetation was measured in the field for both altered and unaltered areas. This was done to 1) establish an accurate spectral representation of surface materials, 2) provide a direct link between remotely detected broad-scale reflectivity and reflectivity of small samples collected for laboratory analyses, 3) determine the spectral effects of absorption by chemical compounds at the surface, and 4) establish a set of spectral criteria to be used as guidelines for quantitative image processing.

Data were collected using the portable field reflectance spectrometer (PFRS) developed by NASA/JPL. The PFRS has a wavelength sensitivity range of 0.4 μm to 2.5 μm and a spectral resolution of 0.02 to 0.04 (Goetz, et. al., 1975, Appendix D). It is sturdy, field-portable, self-contained, and operates over a wide range of temperatures. Spectral curves are generated as a circularly variable, band-pass filter rotates beneath a PbS detector. Data are recorded digitally on magnetic tape. The optical head is mounted on a tripod 1.3 m (4.3 ft) above the surface, and the field of view is approximately 200 cm^2 (31 in^2) (Goetz, et. al., 1975, Appendix D).

To generate a spectral curve, a measurement of the target surface brightness is taken, followed immediately by a measurement of a reflectance standard. Fiberfax, a ceramic wool, was used as a standard because of its high, spectrally flat, broad-band reflectance. A contaminant-free surface can be maintained on the fiberfrax by periodically peeling away the upper layer and pressing the newly exposed surface flat. The target and "standard" brightness values are ratioed to yield a normalized reflectance curve that is free of atmospheric variations.

Field reflectance data were collected in the Pumpkin Buttes, Southern Powder Basin, and Crook's Gap uranium districts in Wyoming. Areas of altered and unaltered sandstones were selected in each mineral district. A minimum of eight spectral curves were generated at each area. The field of view for each measurement included soil and natural cover (low-growing vegetation, dead vegetation, rocks, fecal material, etc.). Separate spectra, representative of larger vegetation (sagebrush, rabbitbrush, greasewood, saltbrush), were also generated. Because remotely sensed data integrate the combined effect of the exposed surface and natural cover, it was necessary to include these materials in the field spectra. Tests show that averaged spectral measurements made on the ground are nearly identical to those made from a helicopter (Conel and others, 1978). Vegetative ground cover was determined using a point-intercept method, and estimates were made of percent exposed soil and rock. All spectra in each area were averaged digitally with each cover type weighted according the cover estimates. The result was representative spectral curves for both altered and unaltered ground in each mineral district. Standard deviations of the mean spectral curves were also computed. These curves are shown in figures 24, 25, and 26. Individual spectral curves collected within the Pumpkin Buttes study area are given in Appendix D.

These spectral curves show that absorption bands characteristic of ferric iron near .55 μm and .9 μm (Hunt, et al., 1971) are present in the spectra of altered areas. This suggests that ferric iron is a key factor in discriminating (chemically) between altered and unaltered ground. It is also responsible for the characteristic pink coloration of altered sandstone. Ferric iron is found in the minerals hematite, goethite, and limonite; all of which typically form under oxidizing conditions as alteration or weathering products of iron-bearing minerals (magnetite, pyrite, marcasite, etc.).

An absorption band characteristic of ferrous (reduced) iron is present at 1.1 μm (Hunt, et. al., 1971). It occurs as a minor absorption band which is most prevalent in the spectra of unaltered areas. This indicates that unaltered areas contain more reduced iron than altered areas. However, surface oxidation and spectral mixing of different surface materials has greatly diminished absorption in this band.

Other absorption bands observable in these curves include a clay absorption band at 2.2 μm. X-ray diffraction analysis has shown that both illite and montmorillite are present as clays. A carbonate absorption band is present near 2.45 μm. This is often due to calcite cement in the sandstone. Substantial amounts of calcium carbonate in the soil at some sites may also produce this absorption band.

Each of the four LANDSAT bands and band 7' of the Mission 310 multiband photography were identified on each of the mean spectral curves (tables VII and VIII). Mean spectral reflectance values for each of these bands were determined (table X). These values were then manipulated digitally to calculate band subtractions and band ratios for an average altered and unaltered surface in each mineral district. Differences between the altered and unaltered values were calculated to determine what band computation could yield the greatest discrimination. Results are summarized in table X.

Individual bands and band subtractions did not yield consistent patterns in any of the sampled mineral districts. Consistent differences between altered and unaltered surfaces were obtained by ratioing. The 7/4 ratio and the 6/4 ratio were most successful in differentiating between altered and unaltered surfaces in the Pumpkin Buttes district. The 7/4, 7'/4, and 6/4 ratios (in that order) proved most successful in the Crook's Gap district. There were no consistently good discriminators in the Southern Powder River Basin district. The most successful ratios were the 5/4, 7/5, 7'/5, and 6/4 ratios (in that order). However the difference values (unaltered - altered) in the Southern Powder River Basin district were less than half the difference values obtained in the other two districts for the best discriminators. The lack of a good discriminator in the Southern Powder River Basin district may be attributed to the variable nature of the alteration and/or contrasting vegetative cover there. Where good differentiation between altered and unaltered surfaces is possible, the field spectral curves indicate that the 7/4 ratio is the best discriminator.

MEAN AND STANDARD DEVIATION OF SPECTRAL REFLECTIVITY IN THE PUMPKIN BUTTES URANIUM DISTRICT

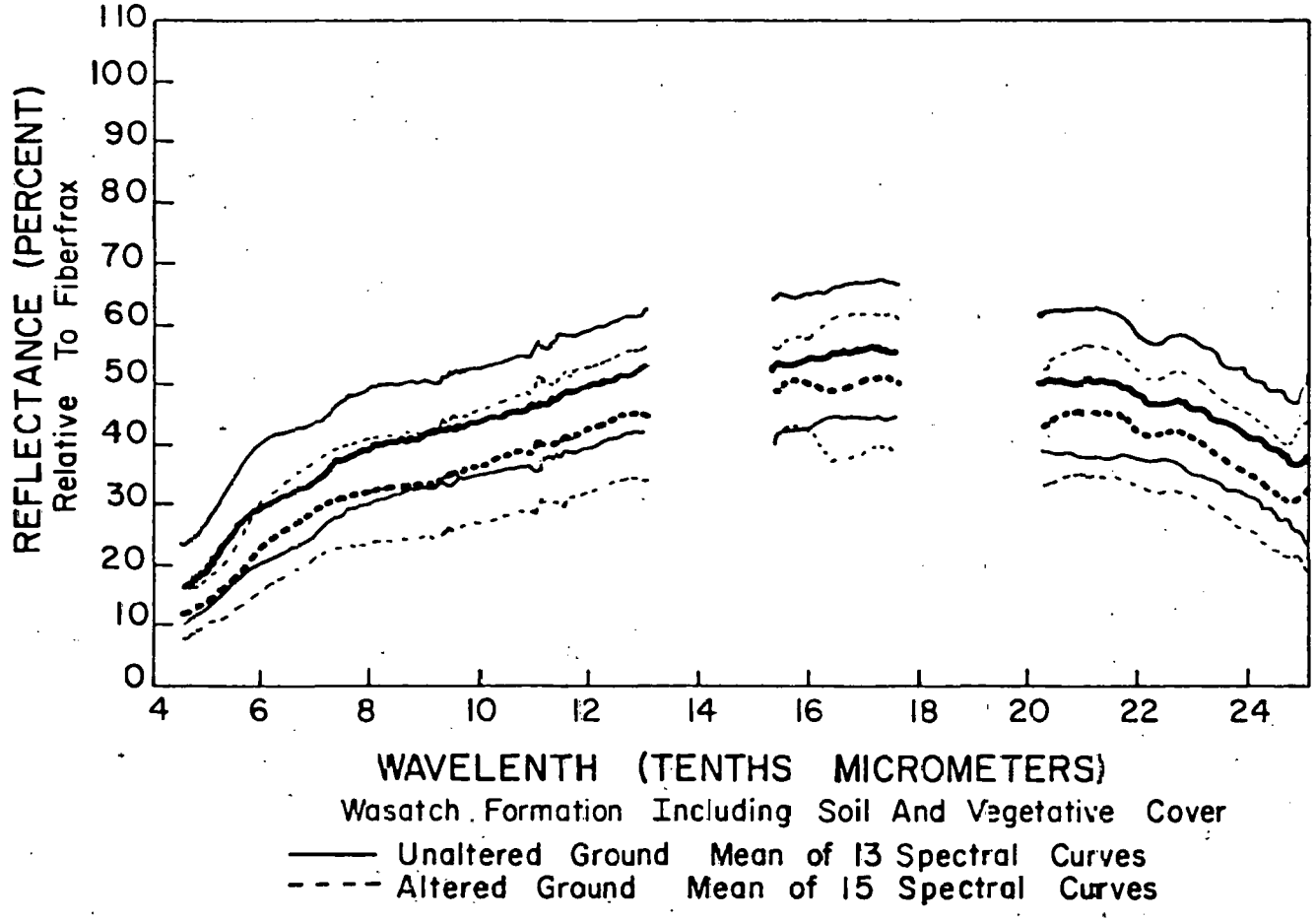

Figure 24

MEAN AND STANDARD DEVIATION OF SPECTRAL REFLECTIVITY IN THE CROOK'S GAP URANIUM DISTRICT

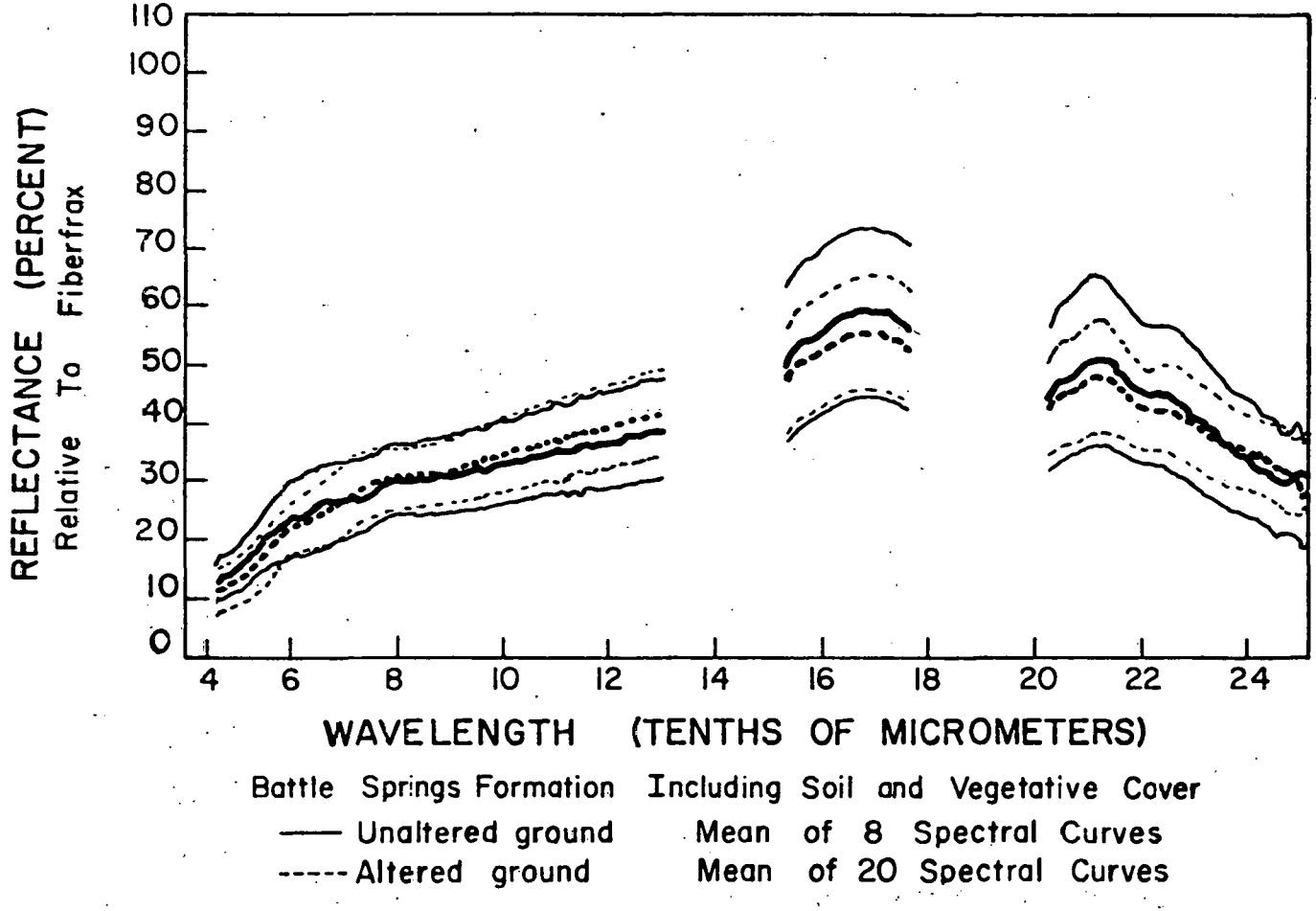

Figure 25

MEAN AND STANDARD DEVIATION OF SPECTRAL REFLECTIVITY IN THE SOUTHERN POWDER RIVER BASIN URANIUM DISTRICT

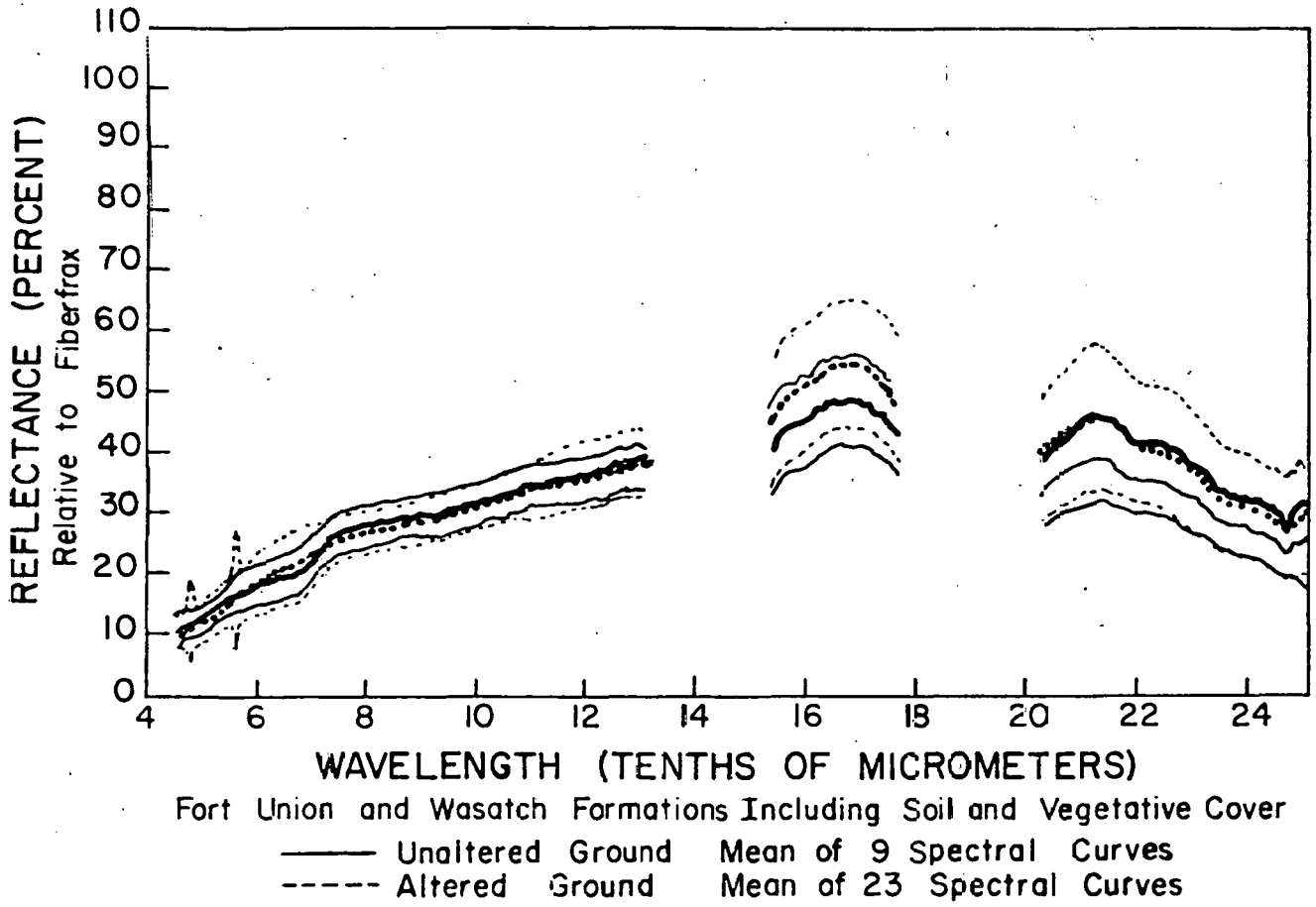

Figure 26

TABLE X Spectral Bands, Subtractions, and Ratios Derived from Field Spectra

Pumpkin Buttes				Southern Powder River Basin				Crook's Gap			
B*	A**	U***	Δ****	B*	A**	U***	Δ****	B*	A**	U***	Δ****
4	18	25	7	4	15	16	1	4	17	20	3
5	26	32	6	5	21	20	-1	5	24	26	2
6	31	37	6	6	26	26	0	6	29	29	0
7'	32	41	9	7'	28	29	1	7'	31	31	0
7	38	43	5	7	30	31	1	7	34	33	-1
5-4	8	7	-1	5-4	6	6	-2	5-4	7	6	-1
6-4	13	12	-1	6-4	11	10	-1	6-4	12	9	-3
6-5	5	5	0	6-5	5	6	1	6-5	5	3	-2
7'-4	14	16	2	7'-4	13	13	0	7'-4	14	11	-3
7'-5	6	9	3	7'-5	7	9	2	7'-5	7	5	-2
7'-6	1	4	3	7'-6	2	3	1	7'-6	2	2	0
7-4	20	18	-2	7-4	15	15	0	7-4	17	13	-4
7-5	12	11	-1	7-5	9	11	2	7-5	10	7	-3
7-6	7	6	-1	7-6	4	5	1	7-6	5	4	-1
5/4	1.44	1.28	-0.16	5/4	1.40	1.25	-0.15	5/4	1.41	1.30	-0.11
6/4	1.72	1.48	-0.24	6/4	1.73	1.63	-0.10	6/4	1.71	1.45	-0.26
6/5	1.19	1.16	-0.03	6/5	1.24	1.30	0.06	6/5	1.21	1.12	-0.09
7'/4	1.78	1.64	-0.14	7'/4	1.87	1.81	-0.06	7'/4	1.82	1.55	-0.27
7'/5	1.23	1.28	0.05	7'/5	1.33	1.45	0.12	7'/5	1.29	1.19	-0.10
7'/6	1.03	1.11	0.08	7'/6	1.08	1.12	0.04	7'/6	1.07	1.07	0.00
7/4	2.11	1.72	-0.39	7/4	2.00	1.94	-0.06	7/4	2.00	1.65	-0.35
7/5	1.46	1.34	-0.12	7/5	1.43	1.55	0.12	7/5	1.42	1.27	-0.15
7/6	1.23	1.16	-0.07	7/6	1.15	1.19	0.04	7/6	1.17	1.14	-0.03

B* Spectral Band or Band Computation
A** Values From Spectra of Altered Ground
U*** Values From Spectra of Unaltered Ground.
Δ**** Difference, Unaltered - Altered

In order to complete a broader study of surface reflectivity as it relates to specific zones of alteration, a simpler, less expensive method of deriving spectral reflectivity was needed. A Science and Mechanics filter photometer (model A-3) was used to collect spectral data because of its light weight, sturdy construction, accurate response to light intensity, and low cost. Raines and Lee (1975) have demonstrated the reliability of this instrument for measuring broad-band spectral reflectance. They determined the accuracy of the filter photometer and their procedure to be 20% of the average band reflectance. Recent work by Kaminsky (1977) has shown that precise field measurement of rock reflectance can be made using the Science and Mechanics photometer if field procedures are carefully standardized.

Photometric measurements were made at all soil sample sites. Filters were selected to approximate the four LANDSAT MSS bands plus a broad band covering the visible and near-infrared range corresponding to the total spectral region of color infrared films. Total reflectivity (no filters) was also determined at each site. The exact spectral intervals sampled and the filters used are shown in table XI. All photometric measurements were vertical-looking from a height of 50.8 cm (20 in). The receptor angle was 30° so the circular field-of-view encompassed a ground area of 582 cm^2 (90.2 in^2). A reading of the surface target was taken in each of the six spectral intervals sampled. These readings were followed immediately by readings of two calibration standards in each spectral interval. The standards used were Kodak 18% and 90% reflectance graycards which were calibrated to absolute reflectance (MgO standard) by the Beckman laboratory spectometer at U.S.G.S./Denver, Co. (Hunt, 1977). Several sets of photometer readings (at least 3) were made at different instrument gain levels. These readings were standardized to a uniform gain level and averaged to give a mean reflectance determination. The data calibration and normalization procedure used to reduce the photometric measurements is described by Kaminsky (1977). The method for collecting measurements differed from Kaminsky's work in that photometer readings were taken from a constant height above the surface and the look-angle was vertical (Kaminsky's readings were taken at oblique angles to the surface from varying heights).

Field reflectance was measured at each site in the CH and CC sampling areas to determine if altered and unaltered ground in these areas could be spectrally differentiated using photometric data. Calibrated photometric data for each of the bands were plotted on grids and contoured by reflectivity. Contour maps of the CH and CC areas in the LANDSAT bands are presented in Appendix C. These photometric "pictures" show great variation from site to site and from band to band. In no case, do they present a reflectance pattern similar to the enhancement of alteration provided by video processed aerial photography (compare Appendix C and fig. 21). Also, some photometric values appear "contradictory" when compared to spectral relationships recorded on LANDSAT. Certain grid sites were, apparently, represented by "bad" photometric data which caused contortion of contours and lack of agreement between ground-based photometric reflectance and video-enhanced imagery (especially the 6/4 ratio).

TABLE XI Optical Filters Used to Limit Photometer Sensitivity

Spectral Band	LANDSAT Spectral Interval	Filter Combination For Photometer	Spectral Region of Filter Transmittance Above 10%	Effective Photometer Spectral Interval
4 (Green)	500-600 nm	Kodak 57 Corning 3961	480-590 nm -660 nm	480-590 nm
5 (Red)	600-700 nm	Kodak 26 Corning 3961	595-1100 nm -660 nm	595-660 nm
6 (Near IR)	700-800 nm	Kodak 89B Corning 4602	700-1100 nm -880 nm	700-880 nm
7 (Near IR)	800-1100 nm	Kodak 87C Corning 3966	823-1100 nm no cut-off	823-1100nm
CIR	----------	Kodak 12 Corning 4602	508 nm - -880 nm	508-880 nm
Total	----------	None	----------	400-950 nm (sensitivity of photometer)

"Bad" photometric data may have been caused by a number of factors. These include: mechanical problems, insufficient field calibration data, rapidly changing light conditions, and sampling of small areas which are not characteristic of actual overall field conditions.

The latter factor represents a sampling problem and is far more important than instrumentation or calibration errors. Material covering the ground surface varies greatly in short distances. Because of the photometer's small field-of-view, only an incomplete portion of the ground cover (consisting of soil and living and dead herbaceous vegetation) could be sampled. Larger surface features (shrubby vegetation, tall sedges and forbs, rock outcrops, etc.) could not be included. A greater number of photometer measurements (both of surface targets and calibration graycards) taken at a much greater viewing height (3 m (10 ft)) might better represent the true reflectance at a given site. Raines (1974) suggests that the number of measurements required to select the best band(s) for the discrimination of two formations is between 150 and 300 measurements per band per formation. This is because rock band reflectances measured in situ, like the formations themselves, are highly variable due to mineralogical, cementation, lithological, geomorphological, moisture, surface cover, and color differences. Variation between altered and unaltered sandstones are primarily due to mineralogical and color differences and represent only a portion of the variation within two formations. Therefore, a significantly smaller number of photometric measurements per band may be required to produce reliable spectral values necessary for discrimination between altered and unaltered sandstones. Kaminsky (1977) demonstrates that the reflectance of standard color cards (blue, green, red, and brown) show distinctive spectra when sampled individually by filter photometer. However, combinations of colored cards introduced spectral inhomogeneity and loss of distinguishing spectral differences. This is analogous to the spectral mixing brought about under field conditions by combining the effects of varying soil conditions, rock outcrops, slope and aspect effects, and diversity of vegetation type and density.

Kaminsky (1977) could not correlate his rock reflectance measurements to LANDSAT data because the photometer's spectral intervals could not be precisely matched to the LANDSAT bands, and because exact calibration of the LANDSAT MSS bands is not provided. Kaminsky (1977) also noted that the photometer lacks sensitivity beyond 950 nm (.95 μm). Because LANDSAT band 7 extends out to 1,100 nm (1.1 μm), he recommends that all data in the photometer's spectral interval corresponding to band 7 be disregarded.

The same problems in correlating LANDSAT data to field reflectance are present in this study (table XI). Similar problems occur when trying to correlate photometric reflectance data to aerial photography. The bands derived from color-separated, color infrared, aerial photography do not precisely match the photometer's spectral intervals (compare table IV and table XI). Also, precise calibration of the light-sensitive film layers is not possible; variation in camera filters and film processing assures this.

All these problems detract from the value of the Science and Mechanics filter photometer as a tool to describe spectral changes in the field. These results show that photometric data should be used with caution. For this study, photometric reflectance measurements could not provide explanations of contrasts which the remote photographic and scanner systems detect spectrally; nor could they provide a field-oriented discriminator between altered and unaltered ground.

In contrast, the PFRS spectrometer produces curves with a high spectral resolution, and reflectance varies continuously with changing wavelength (not in discrete, broad bands). Because of this, individual spectral signatures of surface materials can be delineated. Digital averaging of several curves produces a composite curve in which spectral characteristics of many features can be recognized, rather than a curve composed of broad bands which have lost their ability for spectral discrimination due to spectral mixing. Exact intervals corresponding to the LANDSAT bands or color-separated aerial photography bands can be isolated and the field reflectance of the bands can be determined. The PFRS is subject to errors in obtaining a "representative" sample. In order to minimize this, spectra were taken of all surface materials covering the site. These curves were weighted according to percent cover of each surface material and then digitally averaged to determine and evaluate the degree of spectral mixing. A minimum of 8 curves were averaged for each mean curve. Because these mean curves take into account all surface cover types in a properly weighted fashion, and because the PFRS has a vertical look-angle (as do all remote sensor systems used in this study), the spectral curves should accurately record surface reflectivity in a fashion similar to remote detectors. Differences in the shape of the mean curves for altered and unaltered ground represent real spectral distinctions between these two rock types. Precise correlation of the field spectra to LANDSAT data or aerial photography is still not possible, because precise calibration of these image systems is not provided. However, the spectral curves do establish a relative correlation between field-measured, surface spectral reflectance and reflectivity recorded by remote detectors. The PFRS is the best tool available to accomplish this task.

CHEMICAL ANALYSES

Samples of soil and rock collected in the field were brought to the University of Wyoming (UW) geochemistry laboratory for chemical analysis. The particular chemical determinations and the procedures used are given in table XII. Results of these analyses are given in Appendices B and C. For the CH and CC sample grids, concentrations of elements and compounds were plotted and contoured.

In order to check the UW analytical procedures and results, a duplicate suite of sixty selected soil and rock samples were sent to the Bendix Field Engineering Corp. geochemistry laboratory, Grand Junction, CO for analysis. A comparison of Bendix and UW values shows that most results agree within the Bendix sensitivity range for each analysis (table XIII). Uranium analyses were an exception. Because of different preparation methods, many of the values obtained by the two laboratories differed substantially, though they were of the same order of magnitude. This is evident in table XIII. More samples were sent to the Bendix laboratory for uranium analysis using sample preparation identical to that of the UW laboratory. These values were similar to the UW values.

Many of the elements and compounds analyzed show a direct association with each other. Some elements show an association with specific roll front zones. Mobile Fe, total Fe, organic C, and TiO_2 are consistently related. All four show greater abundance in unaltered areas than in altered areas. Total Mn, Ca, inorganic C, and total C were least abundant in unaltered areas. U_3O_8, Mo, and V showed distinctive highs over uranium ore zones, and in some basal layers of sandstone units containing ore bodies.

The IN transect was used as a control set from which to evaluate geochemical values because it runs across an unaltered sandstone unit several miles north of the mineral district. The values of most elements analyzed from samples in the IN transect were of the same orders of magnitude as values from transects within the mineral district (appendix B). Most elements (especially total and mobile Fe) were somewhat more abundant in the IN transect than in altered areas. Ca, and all C values were influenced by a marlstone unit lying beneath the sandstone units in the IN transect. Consequently, Ca and C values were unlike the values determined for the rest of the study area.

Results of chemical analyses for the grid sample areas were superimposed on video-processed aerial photography for comparison. Large-scale enhancements of the CC grid area were not useful because most of the sample sites had been disturbed by mining activity. These disturbances produced areas of high albedo and correspondingly low spectral contrasts on the imagery. Samples from mine dumps contained unnatural chemical concentrations.

TABLE XII Geochemical Analyses

Element/Compound	Procedure	Reference	Precision
1. Total Fe	Wet Chemical-Atomic Absorption (AA)	Modification of Shapiro and Bannock (1952, 1956, 1962)	± 0.05% of sample
2. Mobile Fe	Sodium Dithionite - Citrite - Bicarbonate Method - AA	Aguilera and Jackson (1953,1954)	± 0.01% of sample
3. Total Mn	Wet Chemical - AA	Same as 1	±0.0005% of sample
4. Mobile Mn	Sodium Dithionite - Citrate -Bicarbonate Method - AA	Same as 2	±0.001% of sample
5. Mg	Wet Chemical - AA	Same as 1	± 0.02% of sample
6. Ca	Wet Chemical - AA	Same as 1	± 0.1% of sample
7. U_3O_8	Fluorometric	Centanni, Ross, and DeSesa (1956)	± 5% of value
8. V	Wet Chemical - AA	Same as 1	± 0.01% of sample
9. Acid Soluble Se	Wet Chemical - AA	Modification of Fernandez (1973)	± 20% of value
10. Base Soluble Se	Wet Chemical - AA	Same as 9	± 20% of value
11. Total Se	Wet Chemical - AA	Same as 9	± 20% of value
12. Mo	Wet Chemical - AA	Same as 1	±0.001% of sample
13. TiO_2	Wet Chemical - AA	Same as 1	± 0.02% of sample
14. P_2O_5	Wet Chemical - Spectrophotometric	Modification of Riley (1958)	± 0.05% of sample
15. Al_2O_3	Wet Chemical - AA	Same as 1	± 1% of sample
16. SiO_2	Wet Chemical - Spectrophotometric	Same as 1	± 2% of sample
17. Inorganic C	Wet Chemical - Coulometric	Modification of Jeffery (1970) and Boniface and Jenkins (1975)	± 0.01% of sample
18. Total C	Wet Chemical - Coulometric	Same as 17	± 0.01% of sample
19. Organic C	Difference between Total C and Inorganic C	Same as 17	± 0.01% of sample

TABLE XIII Comparison of Bendix and UW Geochemical Analyses

Lab	Sample	U_3O_8 ppm	Mg%	Total Mn%	Total Fe%	Total C%
Bendix	NJ-1	9.0	0.41	0.04	1.79	.76
UW	Unaltered Soil	8.2	0.40	0.04	1.57	.70
Bendix	NJ-2	5.0	0.38	0.04	1.36	.95
UW	Unaltered Soil	4.6	0.33	0.03	1.33	1.00
Bendix	NJ-3	10.7	0.38	0.07	1.24	1.57
UW	Ore Zone Soil	9.1	0.40	0.06	1.28	1.40
Bendix	NJ-4	4.7	0.47	0.18	1.73	6.69
UW	Altered Soil	3.8	0.50	0.16	1.78	3.50
Bendix	NJ-5	4.0	0.53	0.05	1.95	1.04
UW	Unaltered Soil	2.9	0.50	0.05	2.00	1.00
Bendix	MJ-1	4.0	0.59	0.02	1.20	0.32
UW	Unaltered SS	2.4	0.60	1.50	1.35	0.29
Bendix	MJ-2	9.0	0.43	0.14	1.30	2.07
UW	Ore Zone SS	8.2	0.49	0.08	1.25	1.10
Bendix	MJ-3	5.0	0.39	0.23	1.00	3.40
UW	Altered SS	3.1	0.42	0.33	1.01	3.90
Bendix	CH-51	3.0	0.53	0.04	1.83	0.86
UW	Unaltered Soil	0.8	0.52	0.04	1.65	1.10
Bendix	CH-52	4.0	0.51	0.04	1.45	0.88
UW	Unaltered Soil	2.2	0.52	0.06	1.41	1.40
Bendix	CH-53	3.0	0.50	0.03	1.68	0.80
UW	Altered Soil	0.7	0.53	0.03	1.66	1.10
Bendix	CH-54	3.0	0.47	0.04	1.37	0.52
UW	Altered Soil	1.3	0.43	0.04	1.19	0.90
Bendix	CH-55	4.0	0.54	0.04	1.87	0.60
UW	Unaltered Soil	0.6	0.61	0.04	1.97	1.00

Analysis for Mo, V, and Se were also performed at both laboratories. An unfair comparison of values for these trace elements would result due to different sample preparations.

Comparison of chemical distributions and image patterns was favorable on the CH grid because there was no significant man-caused alteration of the site (at the time of the sampling). In this area, distribution of total Fe, and (to a lesser extent) mobile Fe, show a good visual correlation to patterns corresponding to altered sandstone interpreted from the 6/4 image ratio (compare Appendix B to figure 21). No other elements or compounds show positive correlations to these image patterns. This indicates that, of all the elements and compounds analyzed, iron, especially total Fe, has the greatest influence on the ability to discriminate between altered and unaltered areas on multispectral imagery. This confirms that iron compounds (oxides) are largely responsible for the observed coloration of altered sandstones. However, the relationship is one in which altered (red) areas have lower concentrations of total iron while unaltered (buff) have higher concentrations.

It seems unusual, at first, that alteration zones can be chemically distinguished from unaltered areas by their lower concentration of total iron, when it is iron oxide that produces anomalies which enable altered areas to be detected visually and with multispectral sensors. This seemingly inverse relationship can be explained by considering alteration zones as part of the "barren interior" of a roll-front deposit. Iron is originally present throughout the host sandstone, commonly occurring in reduced or ferrous states as pyrite and magnetite. A redox change occurs as a roll front moves through the sandstone. Reduced iron dissolves into the groundwater and is mobilized as the pH decreases and Eh increases. Some iron is carried away in solution. Upon passage of the roll front, the pH rises, causing the remaining iron to be deposited as an oxide coating on sand grains. Iron may first be redeposited as the hydrous minerals limonite and goethite. With passage of time, the minerals may dehydrate, to hematite (Berner, 1969).

Mobile iron may be greatly affected by local permeability changes in the sandstone and surrounding sediments. Accumulations of organic material in the sandstone may create local zones of reduction which cause pyrite to be re-deposited. Some mobile iron may migrate out of the system through fractures. The hematite, pyrite, and ironstone concentrations, which are found throughout the study area, may account for much of the iron that is not re-deposited as a coating on sand grains.

The iron oxides have a strong spectral absorption band at .55 µm (550 nm) (Hunt, et. al., 1971). This is in the visible-green portion of the electromagnetic spectrum. Because green light is absorbed, iron oxides (especially hematite) have an orange-red color, which is sometimes quite subtle, but may be detected on color and color infrared films, and by multispectral scanner systems. Iron oxides also have an absorption band at .9 µm (900 nm) (Hunt, et. al., 1971). This is in the near-infrared portion of the electromagnetic spectrum, beyond the sensitivity range of photographic films, and can only be detected by scanner systems which sense this spectral region (e.g. LANDSAT). Reduced (ferrous) iron has an absorption band at 1.1 µm (1100 nm) (Hunt, et. al., 1971). This is also in the near-infrared spectral region, at the upper

boundary of detectability for LANDSAT (table XI). Because the end point of LANDSAT's band 7 is at 1.1 μm, and because band 7 is a broad band, reduced iron is not distinguishable by LANDSAT. Also, surface oxidation of ferrous iron may diminish or destroy this absorption to the extent that a scanner which might ordinarily sense absorption in the 1.1 μm region may not be able to detect reduced iron. Thus, the currently available systems cannot "see" reduced iron in unaltered areas. They can, however, detect altered areas (containing oxidized iron).

In review, a redox change, associated with passage of a roll front, causes a change in the iron mineral species. Some iron is redistributed or removed from the system while in the mobile state. This causes altered rocks to have slightly lower total Fe concentrations, but higher "visibility" due to iron oxide grain coatings.

DETECTABILITY OF IRON OXIDE

An experiment was performed to determine quantatively the minimum concentration of iron oxide necessary to be detected spectrally. Powdered iron oxide (Fe_2O_3) and MgO (a white powder used for spectral calibration) were combined in different proportions and thoroughly mixed in a laboratory ball mill to produce mixtures with different concentrations of Fe_2O_3. Mixtures varied by even orders of magnitude from pure Fe_2O_3 to 0.1 ppm Fe_2O_3 (table XIV). Pure MgO was used as a standard. Each mixture was split, and half of the powder was pulverized in a shatterbox. The shattered powder was labeled "fine"; unshattered powder was labeled "coarse". Both fine and coarse mixtures of each concentration were pressed into 2.5 cm (1 in) pellets using a 16-ton hydraulic press.

TABLE XIV Mixes and Concentrations of Fe_2O_3 in Pellets.

Fe_2O_3		MgO		Concentration of Fe_2O_3
1g	+	10g	→	100,000 ppm
0.1g	+	10g	→	10,000 ppm (Mix A)
1g Mix A	+	10g	→	1,000 ppm
0.1g Mix A	+	10g	→	100 ppm
0.01g Mix A	+	10g	→	10 ppm (Mix B)
1g Mix B	+	10g	→	1 ppm
0.1g Mix B	+	10g	→	0.1 ppm

X-ray fluorescence analysis of the pellets was performed. Only the finely ground pellets produced a surface suitable for x-ray analysis. Results of the analysis are shown in figure 27. Progressive decrease in x-ray counts occurs as the concentration of Fe_2O_3 decreases. However, the curve in figure 27 levels out at 100 ppm. This indicates that, using available equipment, iron oxide cannot be detected by x-ray fluorescence in concentrations less than 100 ppm.

Visual examinations of both coarse and fine pellets shows that the fine pellets have a dark, shiny surface, whereas the coarse pellets are light-toned and dull. The effect of the press on the finer powder produces the shiny surface. The darker tone of the fine pellets is probably due to the greater surface area of the finer powder (see page 14). The characteristic red color of iron oxide diminishes as concentration of Fe_2O_3 decreases (fig. 28). The 100 ppm pellet has a faint pink color, but all pellets with lower concentrations of Fe_2O_3 appear white. Thus, the visual limit of detectability of Fe_2O_3 is also about 100 ppm.

Spectral analysis was first performed on the pellets using the Science and Mechanics filter photometer. It was anticipated that with total control of the target, ideal atmospheric conditions, and careful calibration and operating procedure, the filter photometer could be used successfully to determine the spectral reflectance of the pellets under natural sunlight. The calibration and operating procedures used are described by Kaminsky (1977). Measurements were made in approximate LANDSAT bands 4, 5, and 6, and with no filters (table XI). Determinations were not made in LANDSAT band 7 spectral region, as recommended by Kaminsky (1977). Photometric determinations of reflectivity for both coarse and fine pellets are given in figure 29. These curves show that reflectivity increases as the concentration of Fe_2O_3 decreases. The curves, once again, level off starting at 100 ppm. Because reflectivity was measured in broad spectral bands, individual absorption bands for ferric iron cannot be recognized. Consequently, the curves for bands 4 and 5 are similar. Measurements from coarse pellets are probably most reliable because the shiny surface of the fine pellets produces a specular reflective component which is difficult to measure accurately. Every effort was made to avoid the specularly reflected light while taking photometric measurements.

The coarse pellets and samples of the original powder mixture were subsequently sent to the U.S.G.S. in Denver, CO, to be analyzed on the Beckman laboratory spectrometer. This spectrometer produces curves similar to J.P.L.'s PFRS, however, the field-of-view is 2.5 cm (1 in) square, and measurements are ratioed to a smoked MgO standard rather than fiberfrax. The spectrometer curves are given in figures 30 and 31. The water absorption bands at 1.4 μm and 1.9 μm are readily visible. Also apparent are the ferric iron absorption bands at .55 μm and .9 μm. Increasing concentrations of Fe_2O_3 show increasing absorption (decreasing reflectivity) in these bands. This clearly demonstrates how responsive the ferric iron absorption bands are to varying concentrations of Fe_2O_3. Due to instrumental problems, the spectra in figures 30 and 31 are offset at .75 μm, which is the instrumental change-over point from the visible to the near-infrared. The curve values are correct from .75 μm to 2.5 μm. However, from .4 μm to .75 μm, the absolute positions of the curves are incorrect, though the relative positions are accurate and reveal the iron absorption. The original, unpressed powder mixtures produce less noisy spectra than do the pellets. The spectra for pure Fe_2O_3 (both pellet and powder) do not contain water absorption bands. This indicates that the Fe_2O_3 reagent is pure, whereas the MgO reagent may contain some hydroxide. MgO is certainly more hygroscopic than Fe_2O_3. The 100 ppm samples display a minor absorption band at .55 μm, but lower concentrations of Fe_2O_3 do not display this iron absorption. The 0.9 μm spectral region appears to be more sensitive to iron absorption because even the 10 ppm samples display a very faint iron absorption in the 0.9 region. A sensor system which is sensitive from 0.85 μm to 0.9 μm (in addition to other bands) could be more useful for identifying iron oxides than the present LANDSAT system.

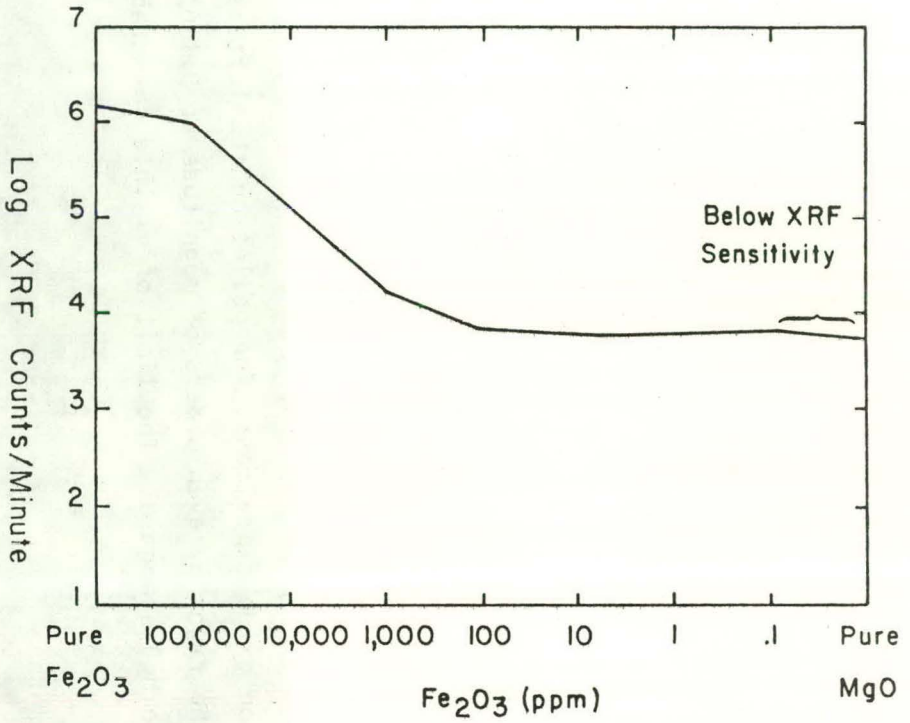

Figure 27. X-ray fluorescence (XRF) of finely-ground Fe_2O_3 pellets.

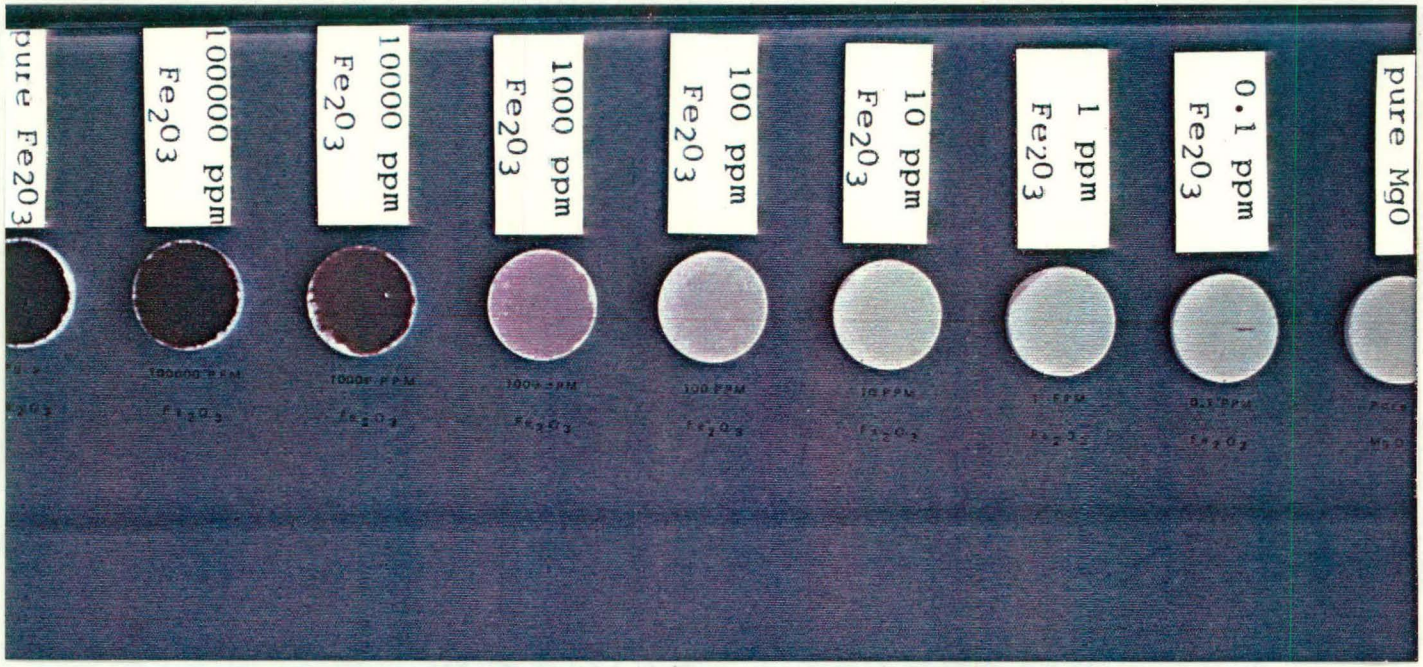

Figure 28. Fe_2C_3 pellets used in the iron oxide experiment. The pellet on the left is pure Fe_2O_3. Concentrations decrease to the right by even orders of magnitude to 0.1 ppm Fe_2O_3. The pellet on the right is a pure MgO standard. The limit of visible detectability is at 100 ppm.

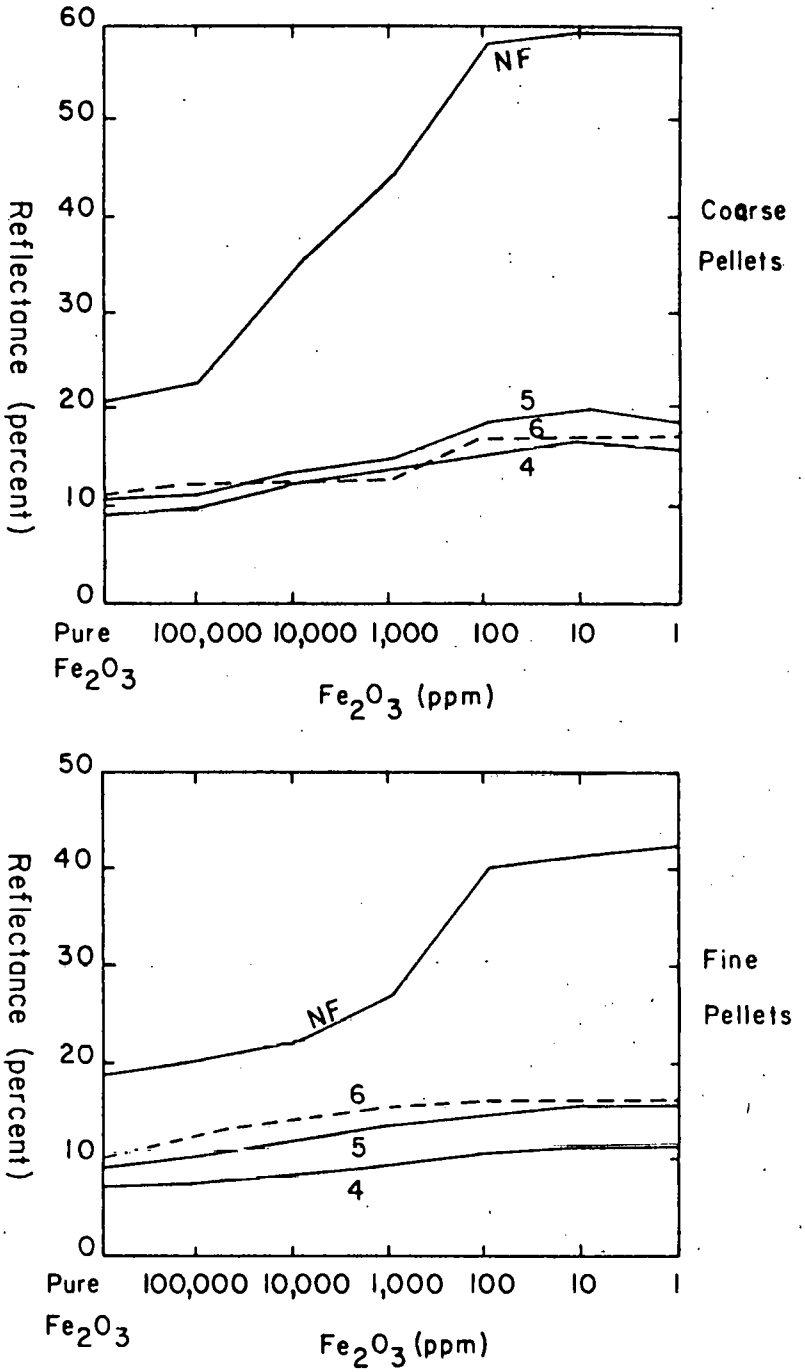

Figure 29. Photometric reflectance determinations of Fe_2O_3 pellets. Reflectivity in equivalent LANDSAT spectral bands is represented by lines 4, 5, and 6 (dashed). Total reflectivity (no band-limiting filters) is represented by line NF.

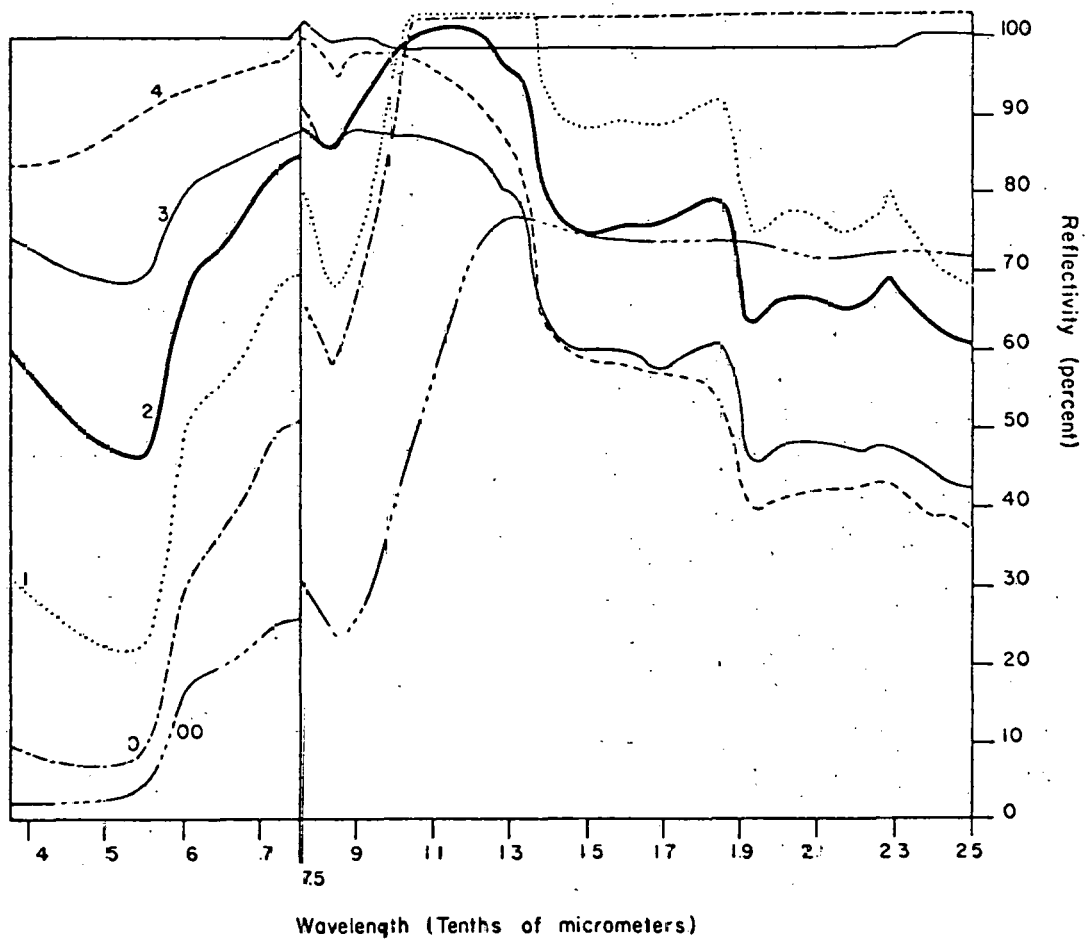

Figure 30. Laboratory-generated spectral curves for coarsely-ground Fe_2O_3 pellets. The lines shown have the following concentrations of Fe_2O_3: 00, pure Fe_2O_3; 0, 100,000 ppm; 1, 10,000 ppm; 2, 1,000 ppm; 3, 100 ppm; 4, 10 ppm. Note how ferric absorption bands at 0.55 um and 0.9 um increase with increasing concentrations of Fe_2O_3.

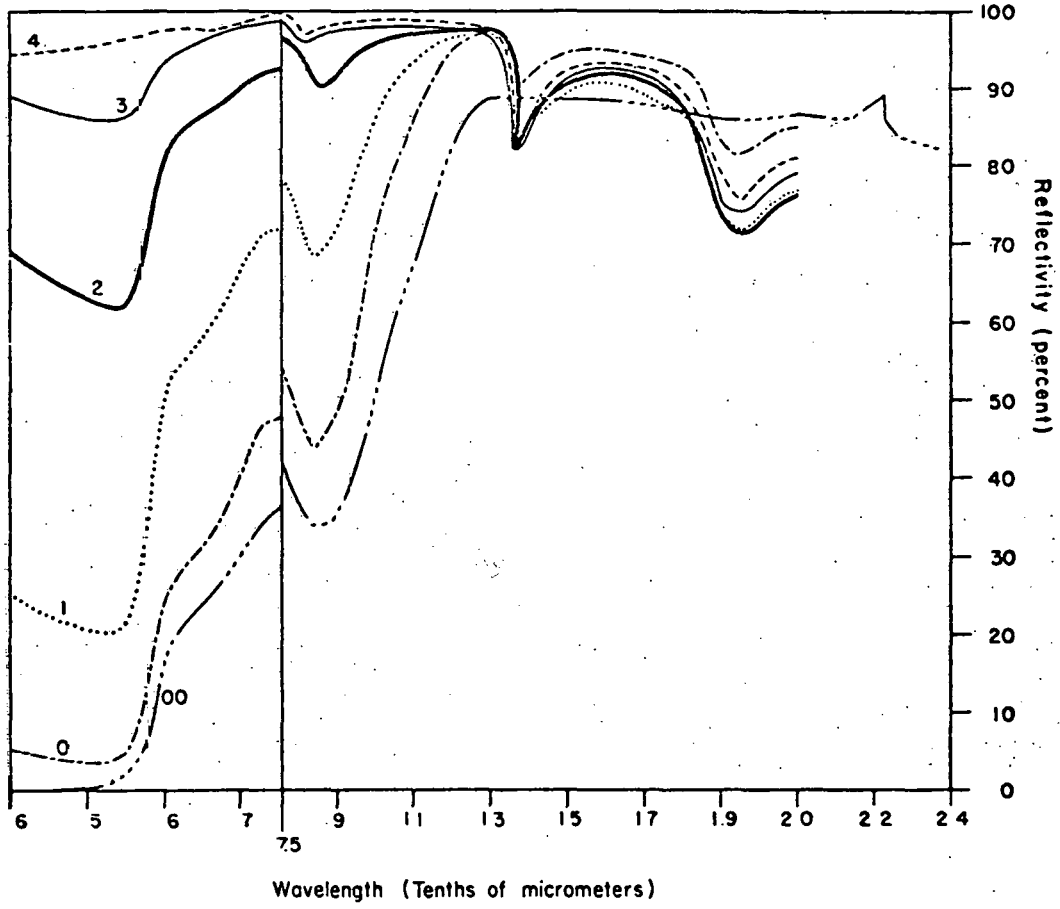

Figure 31. Laboratory-generated spectral curves for Fe_2O_3 powders. The lines shown have the following concentrations of Fe_2O_3: 00, pure Fe_2O_3; 0, 100,000 ppm; 1, 10,000 ppm; 2, 1,000 ppm; 3, 100 ppm; 4, 10 ppm. Note how ferric absorption bands at 0.55 um and 0.9 um increase with increasing concentrations of Fe_2O_3.

The purpose of the iron oxide experiment was to determine the limit of detectability for iron oxide. X-ray fluorescence, visual examination, and photometric analyses all indicate that this limit is at an approximate concentration of 100 ppm for pure iron oxide. Spectrometer analysis shows that, in the 0.9 μm absorption band, this limit may extend to 10 ppm. As iron content increases it becomes more spectrally distinct. The average total iron concentration in altered soil samples collected at Pumpkin Buttes is on the order 10,000 ppm. This is sufficiently high to produce a distinctive spectral signature. However, due to spectral mixing of all surface materials in an area, the effect of iron absorption bands is often muted or obliterated.

RADIOMETRIC SAMPLING

Radiometric data were collected at each sample site using a Mount Sopris portable scintillation counter (Model SC-131A) provided through the courtesy of Bendix Field Engineering Corp. Scintillometer measurements were made primarily for reconnaissance purposes. Measurements were taken of both high- and low-energy radiation. Counts of high-energy radiation were made using a lead filter over the sodium iodide detector. From these data, equivalent uranium (eU) values were calculated according to the formula:

$$eU = K\ (\Delta CPS)$$

where eU = equivalent uranium in parts per million.

ΔCPS = difference in counts per second between measurements taken with and without the lead filter.

K = Constant; a scale factor relating the two energy levels sampled. Previous calibration tests by Bendix Field Engineering Corp. determined, that for this instrument, K=0.450.

The eU values obtained with this calculation were used as a check for geochemical determinations of U and V. The eU values compare favorably with geochemical values for U and V, but are consistantly higher than the geochemically determined U values by a factor of 3-4. This is attributed to the fact that uranium, thorium, and their daughter products all emit radiation which is detected by the scintillation counter. The geochemical analysis was for uranium only.

Radiometric measurements were also used for identifying uranium concentrations in the field. The contacts of lithologic units and all abrupt soil-color changes were radiometrically checked for uranium. Because of erosion, the majority of altered areas at Pumpkin Buttes are discontinuous (plate 2), and are not directly related to roll front deposits. Occasionally, the base of some altered sandstones produced radiometric highs indicating proximity to a roll front. Several previously unmapped uranium concentrations were located in this manner.

ANALYSIS OF MINERALOGY

Thin sections and x-ray diffraction patterns of twenty-two surface samples from the Pumpkin Buttes area were examined in an attempt to determine the mineralogical nature of red-colored alteration detected on LANDSAT and aerial photography. The thin sections were made from rock samples collected from roll-front zones in the Jeannette and Colorado Christensen mines as well as from spot locations in the study area. Six samples were from the White River Formation, and sixteen samples were from the Wasatch Formation.

The thin sections were examined under transmitted light with a polarizing petrographic microscope. An external light source was used to help identify iron sulfide minerals, magnetite-ilmenite minerals, hematite, and goethite by their reflective behavior. Limonite was considered as part of the goethite class because the reflective behavior of limonite is optically similar to that of goethite. The percent abundance of the major minerals was derived by averaging approximately ten visual estimates. X-ray diffraction patterns for each sample were obtained by standard x-ray diffraction procedures. Thin section descriptions and estimates of abundance of various minerals derived from x-ray diffraction are given in Appendix E. A summary table of mineral abundance in the 22 samples is given in table XV.

The samples of White River Formation contain an average of 41 percent quartz, 21 percent feldspar, 18 percent cristobalite, and 11% lithic fragments. Voids and accessory minerals made up the remainder of these rocks. Grains are generally angular to sub-angular and less than 2 mm (0.1 in.) in size. Thin sections from the Wasatch average 40 percent quartz, 5 percent feldspar, 31 percent calcite, 14 percent lithic fragments, and 1 percent mica. The remainder of these rocks is made up of voids, accessory minerals and secondary minerals.

The red and yellow colors of altered samples are caused by hematite and goethite. These minerals are derived principally from the alteration of magnetite and pyrite. Figure 32 shows magnetite partially altered to hematite in both altered and unaltered sandstone in the Wasatch Formation. Buff-colored samples contain noticeably less hematite and goethite. The mode of occurrence of iron minerals strongly influences the color of the samples. In buff-colored samples iron oxide minerals are concentrated in localized areas, so they do not strongly color the rocks. In red or yellow sandstone, iron minerals are dispersed throughout the rocks as grain coatings or stain in cement. This causes altered rocks to be strongly colored.

TABLE XV. Mineralogical Composition of Selected Rock Samples

Sample #	Location	Formation	Description	Calcite	Christobalite	Quartz
1	North Butte	White River	Unalt. ss.	<<1	13	42[1]
2	North Butte	White River	Alt.(?) ss.	0	19[1]	45[1]
3	North Butte	White River	Alt. ss.	0	21[1]	39[1]
4	North Butte	White River	Unalt. ss.	0	35[1]	39[1]
5	North Butte	White River	Alt. ss.	0	35[1]	39[1]
6	Bad Lands Rdg.	Wasatch	Marlstone	50[1]	0	50[1]
7	Chimney Hills	Wasatch	Marlstone	60[1]	?	?[1]
8	Chimney Hills	Wasatch	Unalt. ss.	48[1]	0	31[1]
9	Col. Ch. Mine	Wasatch	Unalt. ss.	33[1]	0	54[1]
10	Col. Ch. Mine Grid 33	Wasatch	Alt. ss.	40[1]	0	29[1]
11	Col. Ch. Mine Grid 54	Wasatch	Alt. ss.	36[1]	0	33[1]
12	Col. Ch. Mine Grid. 24	Wasatch	Alt. ss	34[1]	<1	35[1]
13	Powder River Breaks	Wasatch	Alt. ss.	27[1]	0	41[1]
14	Hill West of CC Grid	Wasatch	Alt. ss.	?	?	?[1]
15	Mid Jeanette	Wasatch	Unalt. ss.	<1	0	57[1]
16	Mid Jeanette	Wasatch	Unalt. ss.(ore)	16[1]	0	51[1]
17	Mid Jeanette	Wasatch		32[1]	0	41[1]
18	West Jeanette Monument Pk	Wasatch		34[1]	0	35[1]
19	West Blowout Anomaly	Wasatch	Unalt. ss.	50[1]	0	22[1]
20	Black Butte	White River	Alt. ss.	?[1]	0	39[1]
21	North Butte Amphitheatre	Wasatch	Pyrite cemented sandstone	0	0	37[1]
SL105-2 Blowout Anomaly		Wasatch	Roll Front	0	0	44[1]

[1] Detected by x-ray diffraction

[2] Biotite and/or muscovite detected as illite by x-ray diffraction

TABLE XV. Continued

#	Feldspar	Lithic Fragments	Biotite[2]	Muscovite[2]	Chlorite	Pyroxene	Amphibole	Garnet	Epidote
1	12[1]	2	0	1	0	0	<1	0	0
2	31[1]	3	0	<1	0	0	<<1	0	<1
3	24[1]	6	<<1[1]	<1	<<1	0	<1	0	<1
4	4[1]	22	<1[1]	<1[1]	0	0	0	0	<1
5	4[1]	22	<1[1]	<1[1]	0	0	0	0	<1
6	0	<1	<1	<1	0	0	0	0	0
7	?[1]	?	?[1]	?[1]	?	?	?	?	?
8	9[1]	12	<1[1]	<<1[1]	<1	0	0	0	<<1
9	1	<1	3[1]	<1[1]	<1	0	<<1	0	<<1
10	14[1]	8	1[1]	<1[1]	<1	<<1	0	0	<1
11	4[1]	16	2	1	<1	<1	0	<<1	<1
12	3[1]	22	<1	<1	0	<1	<1	0	<1
13	2[1]	22	<1[1]	<1[1]	<1	0	<<1	<1	<<1
14	?	?	?	?	?	?	?	?	?
15	8[1]	10	3[1]	<1[1]	1	0	<1[1]	0	<1
16	2[1]	22	2[1]	<1[1]	2	0	<1[1]	<1	0
17	5[1]	15	1[1]	<1[1]	<1	0	<1	0	<1
18	3[1]	18	2	<1	<1	<1	0	0	<1
19	8[1]	7	2[1]	<1[1]	<1	0	<1	0	0
20	23[1]	2	<1	0	0	0	<1	<1	0
21	2[1]	6	1	<1	<1	0	0	0	<<1
SL-105-2	6[1]	27	<1	<1	<1	<1	0	<<1	<1

TABLE XV. Continued

#	Magnetite Ilmenite	Pyrite	Hematite Goethite	Clay	Zeolite	Void	Remarks
1	?	0	?	0	5[1]	0	Black opaque material, possibly petroleum, forms cement locally.
2	<<1	0	<1	0	0	0	
3	<<1	0	4[1]	0	0	3	
4	<1	<<1	<1	0	0	0	
5	<1	0	5	0	0	0	
6	<1	0	<1	0	0	0	Dolomite[1].
7	<<1	?	<<1?	?	?	?	25% Clastic grains. Dolomite[1].
8	<1	0	<1	?[1]	0	0	
9	<1	0	1	0	1	6	
10	<<1	0	1	2	0	6	Schmoo concretion.
11	<1	0	<1	1	0	3	
12	¼	0	2	1	0	<1	Difficult to estimate percent because of small grain size.
13	<1	0	3	0	0	1	
14	<<1	0	70[1]	?	?	?	Goethite[1] forms cement. Silicate minerals 30%.
15	<1	0	<<1	3[1]	0	19	
16	¼	0	<1	1[1]	0	0	No radioactivity detected on autoradiograph.
17	<1	0	2	?[1]	0	1	
18	<1	0	2	2	0	<1	Aragonite[1].
19	<1	0	<1	2	0	7	
20	<<1	0	12	0	0	22	Hematite much more abundant than goethite.
21	?	53	<1	<1	0	0	
SL105--2	<1	<<1?	<1	2	0	20	

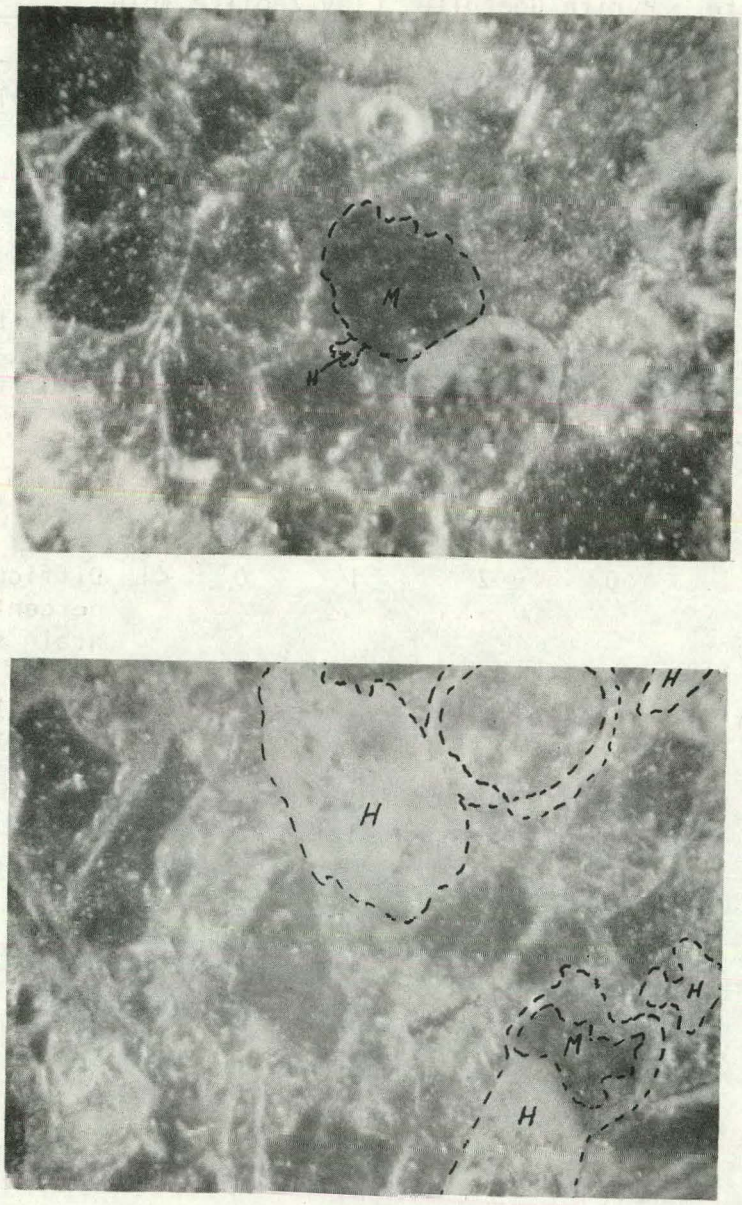

Figure 32. A. Unaltered magnetite in the Wasatch Formation. M--magnetite, H--Hematite. Thin section #16. Photo taken in oblique light. 320X. B. Magnetite altering to hematite in the Wasatch Formation. Hematite stained silicate grains and hematite coating on grains is outlined. M--magnetite, H--hematite. Thin section #12. Photo taken in oblique light. 320X

STATISTICAL ANALYSES

Favorable preliminary comparison of spectral and chemical data indicated that these parameters should be quantitatively compared. Photometric, radiometric, geochemical, and Munsell color data were evaluated statistically by computer. Two data subfiles were created: one contained all data from soil sample sites (CH, CC, LB, NJ, and IN), the other contained all data from rock and mine sample sites (PJ, UT, LR, BA, MJ, SJ, SL). Each of these two data subfiles was analyzed for associations and dependence among the variables by correlation and multiple regression.

Correlation coefficients estimate the degree of interrelation between variables in a manner not influenced by measurement units (Davis, 1973). In this way, unrelated variables, such as photometrically determined reflectivity in LANDSAT bands, percent vegetation cover, pH, total Fe concentration, and Munsell hue, may be compared. The correlation coefficient, r, is the ratio of the covarience (COV) of two variables to the product of their standard deviations (S):

$$r_{jk} = \frac{COV_{jk}}{S_j S_k}$$ (Davis, 1973)

Correlations range from +1 to -1. A positive correlation coefficient indicates a direct relationship between two variables while a negative coefficient indicates that one variable is inversely related to the other. All coefficients between the extremes (+1 and -1) represent less-than-perfect correlations. A correlation coefficient of zero indicates that no linear relationship exists between the two variables.

The variables used in the statistical analyses, explanations of their abbreviations, number of samples considered, and variable means and standard deviations are given in table XVI. Some variables are "second generation" variables created by permutation of one or two existing variables. This was done in order to analyze, at the same time, pairs of variables which behave in similar fashions, and to increase statistical variance. Correlation coefficients for combinations of variables are given in correlation matrices (tables XVII and XVIII). Also given in the matrices are the number of common cases for each correlation. The symbol "--" indicates that there are insufficient cases to make a meaningful correlation. The correlation matrix in table XVII represents all soil data; the correlation matrix in table XVIII represents all rock data. The rock subfile produced stronger correlations (higher positive and negative coefficients). Weathering and mixing effects of soil formation, erosion, and transportation could have reduced the strengths of many correlations in the soil subfile. Some data, such as photometric spectral bands, pH, and TiO_2, were not obtainable from all rock sample sites. Consequently, correlations were made from small populations for these variables and should be used with caution.

Table XVI. Statistics on Variables Used in Correlation and Regression Programs

Soil Subfile - CH, CC, LB, NJ, IN

Variable	Mean	Standard Deviation	Number of Samples
U3O8 (U_3O_8, ppm)	2.7	4.9	95
Gamma (Total radiometric gamma counts)	114.	87.	88
EU (eU, ppm)	14.3	9.7	83
V (V, ppm)	66.	56.	95
MO (Mo, ppm)	9.	10.	95
ORGC (Organic C, ppm)	10,000.	5,000.	95
TC (Total C, ppm)	13,000.	6,000.	95
INORGC (Inorganic C, ppm)	21,000.	39,000.	95
CA (Ca, ppm)	11,000.	13,000.	95
TIO2 (TiO_2, ppm)	3,000	1,000.	10
GAMEU (GAMMA x EU)	1,723.	4,389.	95
GAM2 ($GAMMA^2$)	18,900.	62,450.	95
EU2 (EU^2)	260.4	773.7	95
GAMEU2 ($GAMEU^2$)	22,029,000.	169,947,000.	95
VMO (V x MO)	690.	1,190.	95
V2 (V^2)	7,420.	9,910.	95
MO2 (MO^2)	180.	460.	95
ORGC2 ($ORGC^2$)	135,986,000.	196,409,000.	95
ORGCTC (ORGC x TC)	156,902,000.	201,669,000.	95
TC2 (TC^2)	205,786,000.	250,402,000.	95
CAINOR (CA x INORGC)	550,747,000.	1,463,090,000.	95

Table XVI. Statistics on Variables Used in Correlation and Regression Programs (continued)
(cont)

Soil Subfile - CH, CC, LB, NJ, IN

Variable	Mean	Standard Deviation	Number of Samples
PH (Soil pH)	7.5	0.8	81
HUE (Munsell hue)	19.	2.	95
TFE (total Fe, ppm)	17,900.00	4,600.	95
MFE (Mobile Fe, ppm)	4,600.	1,400.	95
TMN (Total Mn, ppm)	397.	160.	95
MMN (Mobile Mn, ppm)	190.	90.	95
VEGCOV (Vegetative cover %)	36.	18.	95
B4 (Photometric Band 4)	18.7	10.3	85
B5 (Photometric Band 5)	23.9	14.8	85
B6 (Photometric Band 6)	28.6	22.1	78
B504 (B5/B4)	1.2	0.6	95
B604 (B6/B4)	1.3	1.1	95
B605 (B6/B5)	1.1	0.9	95
B5M4 (B5 - B4)	4.6	8.9	95
B6M4 (B6 - B4)	6.7	19.8	95
B6M5 (B6 - B5)	2.1	19.0	95
TFETMN (TFE x TMN)	7.227,000.	3,550,904.	95
TFE2 (TFE^2)	341,200,000.	172,700,000.	95
TMN2 (TMN^2)	182,800.	260,200.	95
MFEMMN (MFE x MMN)	945,000.	555,000.	95
MMN2 (MMN^2)	45,800.	42,200.	95
MFE2 (MFE^2)	23,390,000.	12,820,000.	95

Table XVI. (cont) Statistics on Variables Used in Correlation and Regression Programs (continued)

Rock Subfile - PJ, UT, LR, BA, MJ, SJ, SL

Variable	Mean	Standard Deviation	Number of Samples
U3O0 (U_3O_8, ppm)	165.2	353.3	48
GAMMA (Total radiometric gamma counts)	920.	1,980.	16
EU (eU, ppm)	100.2	179.2	17
V (V, ppm)	290.	540.	50
MO (Mo, ppm)	9.	14.	50
ORGC (Organic C, ppm)	1,800.	2,800.	42
TC (Total C, ppm)	11,400.	13,800.	48
INORGC (Inorganic C, ppm)	77,400.	119,400.	50
CA (Ca, ppm)	29,500.	41,200.	49
TIO2 (TiO_2, ppm)	2,300.	860.	14
GAMEU (GAMMA x EU)	139,900.	897,600.	50
GAM2 ($GAMMA^2$)	1,470,000.	9,733,000.	50
EU2 (EU^2)	13,700.	82,800.	50
GAMEU2 ($GAMEU^2$)	----------	----------	50
VMO (V x MO)	4,090.	9,940.	50
V2 (V^2)	367,000.	1,290,000.	50
MO2 (Mo^2)	260.	760.	50
ORGC2 ($ORGC^2$)	9,080,000.	40,560,000.	50
ORGCTC (ORGC x TC)	19,320,000.	51,300,000.	50
TC2 (TC^2)	304,200,000.	615,300,000.	50
CAINOR (CA x INORGC)	6,786,000,000.	15,664,000,000.	50

Table XVI. (cont) Statistics on Variables Used in Correlation and Regression Programs (continued)

Rock Subfile - PJ, UT, LR, BA, MJ, SJ, SL

Variable	Mean	Standard Deviation	Number of Samples
PH (pH)	10.	0.	1
HUE (Munsell Hue)	17.	6.	48
TFE (Total Fe, ppm)	19,600.	23,600.	50
MFE (Mobile Fe, ppm)	9,500.	20,400.	34
TMN (Total Mn, ppm)	1,920.	7,520.	50
MMN (Mobile Mn, ppm)	590.	1,660.	33
VEGCOV (Vegetative cover %)	0.3	1.6	50
B4 (Photometric Band 4)	13.1	2.2	6
B5 (Photometric Band 5)	26.7	11.9	6
B6 (Photometric Band 6)	37.9	16.8	5
B504 (B5/B4)	0.3	0.7	50
B604 (B6/B4	0.3	1.1	50
B605 (B6/B5)	0.2	0.7	50
B5M4 (B5 - B4)	1.6	5.7	50
B6M4 (B6 - B4)	2.2	9.6	50
B6M5 (B6 - B5)	0.6	10.2	50
TFETMN (TFE x TMN)	36,150,000.	143,490,000.	50
TFE2 (TFE^2)	929,900,000.	3,059,700,000.	50
TMN2 (TMN^2)	59,120,000.	403,000,000.	50
MFEMMN (MFE x MMN)	2,905,000.	8,181,000.	50
MMN2 (MMN^2)	2,000,000.	11,800,000.	50
MFE2 (MFE^2)	337,100,000.	1,482,000,000.	50

Table XVII. Correlation Matrix for all Variables in Soil Subfile

	U_3O_8	eU	V	Mo	Org C	Tc	Incrg C	Ca	TiO_2	TFe	MFe	TMn	MMr.	pH	Hue	B4	B5	B6	Veg Cov
U_3O_8	95.	83.	95.	95.	95.	95.	95.	95.	10.	95.	95.	95.	95.	81.	95.	85.	85.	78.	95.
eU	.789	83.	83.	83.	83.	83.	83.	83.	5.	83.	83.	83.	83.	76.	83.	80.	80.	73.	83.
V	.092	.139	95	95.	95.	95.	95.	95.	10.	95.	95.	95.	95.	81.	95.	85.	85.	78.	95.
Mo	.063	-.086	.226	95.	95.	95.	95.	95.	10.	95.	95.	95.	95.	81.	95.	85.	85.	78.	95
OrgC	-.185	-.293	.068	.079	95.	95.	95.	95.	10.	95.	95.	95.	95.	81.	95.	85.	85.	78.	95.
TC	-.112	-.227	.064	.122	.692	95.	95.	95.	10.	95.	95.	95.	95.	81.	95.	85.	85.	78.	95
InorgC	.023	-.016	-.011	-.060	-.136	.380	95.	95.	10.	95.	95.	95.	95.	81.	95.	85.	85.	78.	95.
Ca	.019	.005	.069	-.003	-.026	.615	.657	95	10.	95.	95.	95.	95.	81.	95.	85.	85.	78.	95
TiO_2	-.397	-.124	-.309	-.415	.742	-.526	.113	-.538	10.	10.	10.	10.	10.	10.	10.	9.	10.	10.	10.
TFe	-.049	-.099	.271	.270	.307	.441	.325	.328	.611	95.	95.	95.	95.	81.	95.	85.	85.	78.	95.
MFe	-.012	-.056	.213	.252	.275	.297	.169	.096	.602	.790	95.	95.	95.	81.	95.	85.	85.	78.	95.
TMn	-.065	-.262	-.122	-.014	.062	.437	.194	.444	-.499	.171	.249	95.	95.	81.	95.	85.	85.	78.	95.
MMn	-.118	-.153	-.016	.026	.261	.170	-.117	-.110	.145	.140	.350	.469	95.	81.	95.	85.	85.	78.	95.
pH	.214	.242	.109	.135	-.349	.222	.409	.560	-.787	.236	-.057	.086	-.322	81.	81.	78.	78.	73.	81.
Hue	-.068	.040	.076	.171	.052	.122	.198	.057	.604	.348	.275	-.074	.143	.069	95.	85.	85.	78.	95.
B4	.054	.224	.018	-.052	.079	-.073	-.054	-.085	.421	.309	.276	-.196	-.165	.196	-.004	85.	84.	77.	85
B5	.023	.171	.004	.045	.008	-.050	-.006	-.048	.053	.273	.250	-.066	-.019	.258	-.013	.821	85.	77.	85.
B6	.276	.357	.015	.172	-.090	-.106	-.059	-.051	.019	.127	.235	-.132	-.155	.118	-.005	.623	.701	78.	78.
VegCov	-.076	-.153	-.056	-.102	-.180	-.212	-.098	-.129	.023	-.198	-.153	-.026	.024	-.303	-.051	-.184	-.158	-.091	95.

Upper Triangle -- Number of cases in smallest population for correlation
Lower Triangle -- Correlation Coefficients
Soil Subfile includes CH, CC, LB, NJ, and IN sample sites.

Table XVIII. Correlation Matrix for all Variables in Rock Subfile

	U_3O_8	eU	V	Mo	Org C	TC	Inorg C	Ca	TiO_2	TFe	MFe	TMn	MMn	pH	Hue	B4	B5	B6	VegCov
U_3O_8	48.	16.	48.	48.	41.	47.	48.	48.	14.	48.	33.	48.	32.	0.	47.	6.	6.	5.	48
eU	.752	17.	17.	17.	10.	15.	17.	16.	0.	17.	17.	17.	17.	1.	16.	6.	6.	5.	17.
V	.770	.497	50.	50.	42.	48.	50.	49.	14.	50.	34.	50.	33.	1.	48.	6.	6.	5.	50.
Mo	.054	.175	.198	50.	42.	48.	50.	49.	14.	50.	34.	50.	33.	1.	48.	6.	6.	5.	50.
Org C	-.087	-.204	-.152	-.132	42.	42.	42.	42.	14.	42.	26.	42.	25.	0.	41.	5.	5.	5.	42.
TC	-.052	.255	.002	.036	.128	48.	48.	48.	14.	48.	32.	48.	31.	0.	47.	6.	6.	5.	48.
InorgC	-.012	.287	.005	.049	-.101	.950	50.	49.	14.	50.	34.	50.	33.	1.	48.	6.	6.	5.	50.
Ca	.018	.305	-.002	.058	-.085	.911	.947	49.	14.	49.	33.	49.	32.	0.	48.	6.	6.	5.	49.
TiO_2	-.135	--	.263	.222	.129	-.040	-.081	-.126	14.	14.	14.	14.	14.	0.	13.	0.	0.	0.	14.
TFe	-.021	-.119	.181	.035	-.009	-.161	-.175	-.175	.429	50.	34.	50.	33.	1.	48.	6.	6.	5.	50.
MFe	-.045	-.058	.031	-.001	.011	-.181	-.176	-.189	.377	.949	34.	34.	33.	1.	32.	6.	6.	5.	34.
TMn	.075	-.077	-.039	.030	-.172	.507	.008	.512	-.092	-.008	-.068	50.	33.	1.	48.	6.	6.	5.	50.
MMn	.493	.151	-.004	-.014	-.080	.118	-.030	.132	.127	-.017	-.039	.946	33.	1.	31.	6.	6.	5.	33.
pH	--	--	--	--	--	--	--	--	--	--	--	--	--	1.	0.	0.	0.	0.	1.
Hue	.059	-.217	.041	.089	-.030	-.086	-.100	-.003	.441	.001	-.049	-.223	-.173	--	48.	6.	6.	5.	48.
B4	.510	.360	.000	.267	--	.289	.549	.303	--	-.047	-.145	.373	.242	--	.179	6.	6.	5.	6.
B5	-.008	-.269	-.479	-.069	--	-.445	-.385	-.404	--	-.131	.071	-.454	-.410	---	.709	.362	6.	5.	6.
B6	-.602	-.709	-.860	-.420	--	-.627	-.418	-.654	--	-.113	-.062	-.796	-.788	---	.803	-.730	-.230	5.	5.
VegCov	-.058	-.158	-.066	-.108	-.048	-.141	-.128	-.114	--	-.071	-.088	.045	.001	---	.163	-.137	-.030	.767	50.

Upper Triangle -- Number of cases in smallest population for correlation.
Lower Triangle -- Correlation Coefficients
Rock Subfile -- includes RJ, UT, LR, BA, MJ, and SJ sample sites.

It should also be understood that the variable, Munsell hue, relates to only the horizontal dimension of the three-dimensional Munsell color coordinate system and does not incorporate all aspects of color. Quantitative values, rather than location values, were assigned to the variable. These values increase as one moves around the sphere from red to green (all materials observed in the field, fell into the red-green Munsell range). These quantitative values can be better interpreted if considered equivalent to spectral frequency (in the visible range only) rather than actual colors. Low Munsell hue values correspond to low-frequencies and high Munsell hue values correspond to high frequencies. For example, a green object (frequency of 6.7×10^{14}hz) might have a Munsell hue value of 25, whereas, a red object (frequency of 5.3×10^{14} hz) would have a Munsell hue value of 5.

Several associations are apparent from tables XVII and XVIII. U_3O_8 and eU have a strong positive correlation (as stated earlier). V also correlates well with U_3O_8 and eU in the rock subfile. Strong correlation exists among total C, inorganic C, Ca, and pH. This is largely due to the calcite cement of the sandstones. TiO_2, though having a relatively small sample population, shows a positive correlation to both total and mobile Fe, and a negative correlation to total Mn and Munsell hue. Both total Fe and total Mn show a very strong correlation to mobile Fe and mobile Mn respectively. Photometric spectral bands show a positive correlation with one another. This is due to the prevalence of samples that are light or dark in all spectral bands. It is not unusual.

Multiple regression is a statistical technique through which one can analyze the relationship between a dependent (criterion) variable and a set of independent (predictor) variables (Kim and Kohout, 1975). Unlike correlation coefficients, which analyze one-to-one relationships, linear multiple regression techniques analyze multi-variate relationships, and evaluate the contribution of a specific variable or set of variables to find the best linear prediction equation to a given criterion variable. The general form of the regression equation is:

$$Y' = A + B_1 X_1 + B_2 X_2 \ldots B_k X_k$$

Where Y' is the estimated value of the dependent variable Y, X_1 are the independent variables, B_1 are regression coefficients, and A is the Y intercept (a constant).

The proportion of variance of Y explained by each of the variables included in the regression equation (i.e. the goodness of fit of the regression equation) can be evaluated by examining the square of the multiple correlation:

$$R^2 = \frac{\text{Variation in Y explained by the combined linear influence of the independent variables}}{\text{Total variation in Y}}$$

An R^2 value of 1 would indicate that the regression equation produces a perfect fit or prediction of the dependent variable. High confidence can only be placed on the R^2 value if a small number of independent variables are used to fit a curve of the dependent variable which is determined by a large number of samples. If the number of independent variables should approach the number of values defining the curve of the dependent variable, a perfect fit will always be made, and the R^2 values, thus obtained, are meaningless.

Multiple regressions were run for both soil and rock subfiles. Variables listed in Table XV were used selectively as independent variables. Summary tables for multiple regressions using U_3O_8 and Munsell hue as dependent variables are presented in tables XIX and XX. When U_3O_8 was used as a dependent variable, combinations of the radiometric variables Gamma (high energy radiation) and eU yielded an R^2 value of .900 (using three variables to approximate a curve determined by 95 U_3O_8 values) (table XIX A) demonstrating that radiometric uranium values bear the expected close relationship to geochemical uranium values. When only chemical independent variables are regressed against U_3O_8, the picture is much more complicated. For the rock subfile (table XIX C), V, V^2, and mobile Mn explain most variance within U_3O_8 (R^2 = .997, using 3 variables to approximate a curve determined by 48 U_3O_8 values). For the soil subfile (table XIX B), the following variables yield the best predictor equation of U_3O_8 (in order): organic C x total C, V, TiO_2, total C, mobile Mn, and V x Mo. The cummulative R^2 was .989 (using 6 variables to approximate the curve determined by 95 U_3O_8 values). This shows that carbon (especially organic C) and trace elements, such as V, TiO_2, and Mo, are associated with uranium. These results support the chemical zonation predicted by the roll-front model.

In other regressions, Munsell hue is used as the dependent variable against chemical independent variables. The results are difficult to interpret, especially in light of the quantitative values used to represent the Munsell hue variables. For the soil subfile (table XX B), organic C and TiO_2 have a combined R^2 of .715 (when 2 variables are used to approximate a curve determined by 95 Munsell hue values). For the rock subfile (table XX A), the following chemical variables are important (in order): mobile Mn, TiO_2, mobile Fe x mobile Mn, organic C, total Fe x total Mn, Ca x inorganic C, and Mo. The cummulative R^2 for this combination is .995 (using 7 variables to approximate a curve determined by 48 Munsell hue values).

Because TiO_2 has a relatively small population relative to other chemical variables, it is more easily fit into a regression equation. Its high R^2 value in most regressions may be attributed to its low sample number. As a trace element, it probably has a very insignificant relationship to Munsell hue, and its high R^2 values should be disregarded.

Results from these regressions (omitting TiO_2) indicate that color in rocks is a complex combination of Fe, Mn, organic C and $CaCO_3$. Previous experience indicates that all these variables are, indeed, coloring agents. For soils, these results show that organic C has the greatest

Table XIX. Statistical Regressions with U_3O_8 as the Dependent Variable

Soil Subfile (CH, CC, LB, NJ, IN)

Variable	R^2 Change	Cumulative R^2	Simple-R	B	
GAMMA x eU^2	.869	.869	.932	3.634×10^{-8}	A
$GAMMA^2$	.019	.888	.499	1.175×10^{-5}	
GAMMA x eU	.012	.900	.869	-4.584×10^{-4}	
Constant				2.455	

Variable	R^2 Change	Cumulative R^2	Simple-R	B	
Organic C x Total C	.407	.407	-.053	5.491×10^{-8}	B
V	.181	.588	.093	-4.001×10^{-2}	
TiO_2	.157	.745	-.397	-1.192×10^{-2}	
Total C	.142	.887	-.112	-2.317×10^{-3}	
Mobile Mn	.063	.950	-.118	1.675×10^{-2}	
V x Mo	.039	.989	.010	-9.867×10^{-4}	
Constant				60.908	

Rock Subfile (PJ, UT, LR, BA, MJ, SJ, SL)

Variable	R^2 Change	Cumulative R^2	Simple-R	B	
V	.413	.413	.642	1.714	C
V^2	.344	.757	.344	-4.720×10^{-5}	
Mobile Mn	.240	.997	.497	0.557	
Inorganic C	.002	.999	.097	-4.864×10^{-4}	
Constant				-453.275	

Table XX. Statistical Regressions with Munsell Hue as the Dependent Variable

Rock Subfile (PJ, UT, LR, BA, MJ, SJ, SL)

Variable	R^2 Change	Cumulative R^2	Simple-R	B	
Mobile Mn	.449	.449	-.173	1.048×10^{-2}	A
TiO_2	.194	.643	.441	1.053×10^{-2}	
Mobile Fe x Mobile Mn	.156	.799	-.197	-5.705×10^{-7}	
Organic C	.093	.892	-.030	-7.566×10^{-4}	
Total Fe x Total Mn	.067	.959	-.226	-1.300×10^{-7}	
Ca x Inorganic C	.030	.989	.029	5.270×10^{-11}	
Mo	.006	.995	.089	-3.524×10^{-2}	
Constant				-6.500	

Soil Subfile (CH, CC, LB, NJ, IN)

Variable	R^2 Change	Cumulative R^2	Simple-R	B	
TiO_2	.365	.365	.604	4.375×10^{-3}	B
Organic C	.350	.715	.350	-5.627×10^{-4}	
Constant				11.583	

bearing on soil color in the study area. The coloring effects of Fe, Mn, and $CaCO_3$, which are most important in rocks, are apparently reduced relative to organic C by the soil forming process.

CONCLUSIONS

The video image analysis system at the University of Wyoming is a low-cost, fast, effective, and efficient tool which greatly facilitates the development of enhancement techniques suited to a particular situation or location. It greatly aided the identification and mapping of altered sandstone associated with uranium deposits in the Pumpkin Buttes area (plate 2).

Once locations of altered ground are identified, exploratory drilling programs can be directed down-dip in the host sandstone until a roll front has been delineated. Thus, maps of altered sandstone, produced from video enhanced remote sensor data, can be used in conjunction with the roll-front model to reduce the time, costs, and impacts on the surface environment, involved with exploratory drilling for uranium.

The content of this report applies to near-surface deposits only. Future work should include studies on the extent (distance) of alteration from a roll front, and studies on the effect of changing geochemistry with depth, and how it relates to the reliability of using surface alteration as a drilling guide.

Because altered sandstone is often masked by variation in soil and vegetation, image processing and enhancement are essential in order to extract the maximum spectral and spatial information available in remote sensor data. The 7/4 ratio has proven to be most effective for enhanceing altered sandstone at Pumpkin Buttes. This was demonstrated using LANDSAT digital data, airborne scanner data, and field-reflectance spectrometer data. The 6/4 ratio is the best enhancement from color infrared photography (when band 7 is not available). Contrast-stretched color composites do a reasonably good job of enhancing alteration and are especially useful in LANDSAT studies where resolution requirements do not permit the use of ratios. The 5/4 ratio enhances alteration only where there are many rock exposures and vegetative cover is minimal.

Spectral analyses show that ferric iron absorption is apparent at wavelengths of .55 μm and .9 μm only in the spectra of altered ground. These absorption bands effectively limit the reflected light traveling back to the sensor. In the visible range, green light is absorbed at .55 μm, thus allowing a greater proportion of red light to be reflected. This is why altered rocks appear pink to the eye. The ferric absorption band at .9 μm is even more sensitive to iron oxide. However, it is in the near infrared portion of the electromagnetic spectrum, and cannot be detected by photographic systems nor can it be effectively used when incorporated into the broad-band reflectance data provided by LANDSAT. Minor ferrous absorption at 1.1 μm is apparent only in the spectra of unaltered ground. This indicates that reduced iron is more prevalent in unaltered areas. However, surface oxidation and spectral mixing by various materials greatly diminishes the effect of ferrous iron absorption. Most currently available sensor systems cannot detect the minor ferrous

iron absorption band but can readily detect ferric iron absorption. For this reason, altered areas (not unaltered areas) are anomalously visible on the multispectral images.

Field reflectance data indicate that remote sensor bands in the 1.5 μm to 1.8 μm and 2.0 μm to 2.5 μm range can also be useful for discriminating between altered and unaltered ground. Information on rock properties could also be available if the clay (2.2 μm) and carbonate (2.45 μm) absorption bands were sensed. Unfortunately, most currently available remote sensor systems do not sense in these spectral regions.

Geochemical analyses have shown that the following elements associate with particular roll front zones:

> Fe, organic C, TiO_2 are most abundant in unaltered zones.
> Mn, inorganic C, total C are most abundant in altered zones.
> U_3O_8 , V, Mo are most abundant in ore zones.

Equivalent uranium values converted from radiometric measurements in the field correlate well to geochemically derived U_3O_8 values of samples, thus providing a check for the geochemical analysis of uranium. The effect of calcite cement in sandstones of the Wasatch formation is reflected in the good correlation among Ca, inorganic C, total C, and pH. Carbon has a major influence on the geochemistry of soils, as revealed by statistical analyses. The effect of the soil-forming process clearly weakens correlation coefficients among chemical variables. It also weakens the coloring effects of Fe, Mn, and $CaCO_3$, as shown by multiple regressions using Munsell hue as the dependent variable. Once the influence of carbon on soils is taken into account, the results of multiple regressions of U_3O_8 can fit with associations predicted by the roll-front model.

It has been determined by comparing chemical contoured grid sample areas to video enhancements of altered areas, that the major coloring agent of altered sandstone is iron. Spectral analysis shows that altered areas are detectable because of the presence of iron (as an oxide), while geochemical analysis shows that alteration zones can be distinguished from unaltered zones by their lower concentration of iron. This seemingly inverse relationship can be explained by considering altered areas as the barren interior of a roll front. Petrographic studies of thin sections and x-ray diffraction studies have shown that iron is present throughout the host sandstone units, in chemically reduced and ferrous states, as the minerals pyrite and magnetite. As a roll front moves through the sandstone, redox and pH changes occur, allowing iron to become mobilized in the groundwater. Some iron is redistributed or removed from the system while in the mobile state. Remaining iron (in less than original abundance) is re-deposited as an iron oxide stain on sand grains behind the roll front. Thus, the oxidation of ubiquitous magnetite and pyrite result in what is detected as alteration.

Experiments with pure Fe_2O_3 mixtures show that the limit of detectability for iron oxide is near a concentration of 100 ppm, and that spectral absorption for ferric iron increases with greater Fe_2O_3 concentrations. Because the average iron content of altered soil samples collected at Pumpkin Buttes is on the order of 10,000 ppm, there is sufficient iron in the soil to produce a distinctive color anomaly in altered areas.

In order for image analysis techniques on remote sensor data to be successful, several problems must be overcome. First, spectral mixing by all surface materials can effectively reduce or obliterate iron absorption bands (no matter how strong the absorption is). This is why enhancement of alteration in soil is exceedingly difficult in areas with significant vegetative cover. Muting effects of soil moisture and vegetation can be reduced by selecting imagery obtained during a dry period in the fall season when vegetation is senescent.

Spatial resolution is another problem, particularly with LANDSAT data. The size of a pixel is 79 m x 79 m (259 ft x 259 ft) on the ground. Areas smaller than this can, generally, not be resolved on LANDSAT data. Specialized digital processing to enhance edges of objects can enable some smaller objects to be resolved, but spectral contrasts are distorted in the process. Video processing further reduces spatial resolution with each "generation of recording". Detailed alteration mapping must be accomplished using airborne sensor data.

Another problem is that some features are enhanced during image processing which are not related to altered sandstone. For example, the 6/4 ratio enhances red-colored shales and siltstones and areas surrounding stock watering wells, as well as altered areas. Altered sandstones associated with uranium deposits usually have a definite geomorphic expression (ridge formers) which allows them to be discriminated from other similarly colored features.

Another problem often encountered is the aquisition of high-quality imagery. This is extremely important to the success of image analysis. Different image data used in this study contained vignetting, low spectral contrasts, geometric distortion, pronounced scan striping, and processing noise. These defects limited the success of many image enhancements. Processing of images at a large scale can reduce some of these problems, but it is best to start with high-quality imagery.

Field reflectance spectra collected at several uranium districts in Wyoming indicate that in some cases, the alteration enhancement techniques developed at Pumpkin Buttes may be successfully extended to other districts. However, in some areas, the techniques may not be effective. Similar geological environments, surface conditions, and type of alteration and deposit are essential in order to extrapolate enhancement techniques from one district to another. Future work should include studies of both similar uranium districts and unexplored areas in Tertiary basins using techniques developed in this study. The video image analysis system would be an ideal tool for such work because of its speed, efficiency, input flexibility, and low operating costs.

REFERENCES CITED

Abrams, M. J., et. al., 1977, Mapping of hydrothermal alteration in the Cuprite mining district, Nevada, using aircraft scanner images for the spectral region 0.46 to 2.36 μm; Geology, V. 5, No. 12, p. 713-718.

Adler, H. H., and Sharp, B. J., 1967, Uranium ore rolls-occurrence genesis, and physical and chemical characteristics; Guidebook to the Geology to Utah, No. 21, Utah Geological Society, p. 53-77.

Aguilera and Jackson, 1954, Soil Science Society of America Proc., V.18, p. 350.

Aguilera and Jackson, 1953, Soil Science Society of America Proc., V.17, p. 359.

Bailey, R. V., and Childers, M. O., 1977, Applied mineral exploration with special reference to uranium; Westview Press, Boulder, Colorado, 542 p.

Becker, C. F., and Alyea, J. D., 1964, Temperature probabilities in Wyoming; University of Wyoming Agricultural Experiment Station Bull. 415, p. 44-47.

Berner, R. A., 1969, Goethite stability and the origin of red beds; Geochimica et Cosmochimica Acta, V. 33, p. 267-273.

Birkeland, P. W., 1974, Pedology, weathering and geomorphological research; Oxford University Press, New York, p. 3-29.

Blackstone, D. L., 1977, Oral communication.

Boniface, H. J., and Jenkins, R. H., 1975, Coulometric determination of carbon in steel, BISRA Corp. Lab., Br. Steel Corp., London, England, available through National Technical Information Service, PB. Rep. No. 242503.

Breckenridge, R. M., Glass, G. B., Root, F. K., and Wendell, W. G., 1974, Campbell County, Wyoming: Geologic map atlas and summary of land, water, and mineral resources; Geological Survey of Wyoming, County Resource Series No. 3.

Butler, A. P., 1969, Groundwater as related to the origin and search for uranium deposits in sandstone; Contributions to Geology, V. 8, No. 2, p. 81-88.

Centanni, F. A., Ross, A. M., and DeSesa, M. A., 1956, Fluorometric determination of uranium; Anal. Chem., V. 28, p. 1651.

Cheney, E. S., and Jensen, M. L., 1966, Stable isotopic geology of the Gas Hills, Wyoming, uranium district; Econ. Geol., V. 61, p. 44-71.

Childers, M. O., 1974, Uranium occurrences in upper Cretaceous and Tertiary strata of Wyoming and northern Colorado; The Mountain Geologist, V. 11, No. 4, p. 131-147.

Conel, J. E., Abrams, M. J., and Goetz, A. F. H., 1978, A study of alteration associated with uranium occurrences in sandstone and its detection by remote sensing methods; NASA/JPL publication 78-66, DOE report GJBX - 120/78.

Darton, N. H., 1905, Preliminary report on the geology and underground water resources of the central great plains; U. S. Geological Survey Prof. Paper 32, 433 p.

Davidson, D. F., 1953, Distribution of coarse- and fine-grained rocks in the Wasatch Formation and their relationship to uranium deposits, Powder River Basin, Wyoming; U. S. Geological Survey TEM-676, 12 p.

Davis, J. C., 1973, Statistics and data analysis in geology; John Wiley and Sons, Inc., New York, 550 p.

Davis, J. F., 1969, Uranium deposits of the Powder River Basin; Contributions to Geology, V. 8, No. 2, p. 131-141.

Delson, E., 1971, Fossil mammals of the early Wasatchian Powder River local fauna, Eocene of northeast Wyoming; Bull. Am. Museum of Natural History, V. 146, p. 307-364.

DeNault, K. J., 1974, Origin of sandstone type uranium deposits in Wyoming; Ph. D. Dissertation, Stanford University, 352 p.

Denson, N. M., and Pipiringos, G. N., 1969, Stratigraphic implications of heavy mineral studies of Paleocene and Eocene rocks of Wyoming; Wyoming Geological Association Guidebook. V. 21, p. 9-18.

Denson, N. M., Zeller, H. D., and Stephens, J. G., 1956, Water sampling as a guide in the search for uranium deposits and its use in evaluating widespread volcanic units as potential source beds for uranium; U. S. Geological Survey Prof. Paper 300, p. 673-680.

Department of Interior, 1974, Draft environmental impact statement development of coal resources in the eastern Powder River Coal Basin of Wyoming, Bureau of Land Management (principle agency), Cheyenne, p. 1268-1277.

Dooley, J. R., Tatsumoto, M., and Rosholt, J. N., 1964, Radioactive disequilibrium studies of roll features, Shirley Basin, Wyoming; Economic Geology, V. 59, p. 586-595.

Eargle, D. H., and Weeks, A. D., 1961, Possible relation between hydrogen sulfide-bearing hydrocarbons in fault-line oilfields and uranium deposits in the southeast Texas coastal plain; U. S. Geological Survey Prof. Paper 424D, p. D7-D9.

Eastman Kodak Company, 1971, Kodak data for aerial photography; Kodak Pub. 17-29, 80 p.

Fenneman, N. M., 1931, Physiography of western United States; McGraw-Hill Book Co., New York, 534 p.

Fernandez, F. J., 1973, Atomic absorption of gaseous hydrides utilizing sodium borohydride reduction; Atomic Absorption Newsletter, V. 12, p. 93.

Frondel, C., 1958, Systematic mineralogy of uranium and thorium; U. S. Geological Survey Bull. 1064, 400 p.

Geological Society of America, 1975, Rock-color chart; Geological Society of America, Boulder, Colorado.

Glassey, T. W., Dunnewald, T. J., Brock, J., Irving, H. H., Tippetts, C., and Rohrer, C., 1955, Soil survey reconnaissance of Campbell County, Wyoming; U. S. Soil Conservation Service, Series 1939, No. 22, 67 p.

Goetz, A. F. H., and staff, 1975, Application of ERTS images and image processing to regional geologic problems and geologic mapping in northern Arizona; Jet Propulsion Laboratory Technical Report 32-1597, 188 p.

Goetz, A. F. H., and Billingsley, G. C., 1973, Digital image enhancement techniques used in some ERTS application problems; Contributions to Geology, V. 12, No. 2, p. 7-21.

Granger, H. C., 1966, Ferroselite in a roll-type uranium deposit, Powder River Basin, Wyoming; U. S. Geological Survey Prof. Paper 550-C, p. C133-C137.

Granger, H. C., and Warren, C. G., 1969, Unstable sulfur compounds and the origin of roll-type uranium deposits; Economic Geology, V. 64, p. 160-171.

Gruner, J. W., 1956, Concentration of uranium in sediments by multiple migration-accretion; Economic Geology, V. 51, No. 6, p. 495-520.

Grutt, E. W. Jr., 1971, Prospecting criteria for sandstone-type uranium deposits; Uranium Prospecting Handbook, The Institution of Mining and Metallurgy, London, p. 47-78.

Grutt, E. W. Jr., 1957, Environment of some Wyoming uranium deposits; 2nd Nuclear Engineering and Science Conference, Paper No. 57-NESC-69, in Advances in Nuclear Engineering, Am. Soc. of Mech. Eng., p. 513-525.

Harshman, E. N., 1970, Uranium ore rolls in the United States; Proc. of a Panel on Uranium Exploration Geology, Int. Atomic Energy Agency, Vienna, p. 219-232.

Harshman, E. N., 1968A, Uranium deposits of the Shirley Basin, Wyoming; Ore Deposits of the United States 1933/1967; American Institute of Mining and Metallurgical Engineers, p. 849-856.

Harshman, E. N., 1968B, Uranium deposits of Wyoming and South Dakota; Ore Deposits of the United States 1967; American Institute of Mining and Metallurgical Engineers, p. 815-831.

Hoffer, R. M., and staff, 1975, Computer-aided analysis of SKYLAB multispectral scanner data in mountainous terrain for land use, forestry, water resource, and geologic applications; Laboratory for Applications of Remote Sensing, Purdue University, LARS Information Note 121275, p. 324-353.

Hostetler, P. B., and Garrels, R. M., 1962, Transportation and precipitation of uranium and vanadium at low temperatures, with special reference to sandstone-type uranium deposits; Economic Geology, V. 57, No. 21, p. 137-167.

Houston, R. S., 1978, Oral communication.

Houston, R. S., 1969, Aspects of the geologic history of Wyoming related to the formation of uranium deposits; Contributions to Geology, V. 8, No. 2, p. 67-79.

Houston, R. S., et. al., 1973, Application of the ERTS system to the study of Wyoming resources with emphasis on the use of basic data products; Proc. of the third Earth Resources Technology Satellite-1 Symp., NASA/Goddard Space Flight Center, Greenbelt, Md., V. 1, Sect. A, p. 595-619.

Hunt, G. R., 1977, Written communication.

Hunt, G. R., Salisbury, J. W., and Lenhoff, C. J., 1971, Visible and near-infrared spectra of minerals and rocks: III. Oxides and hydroxides; Modern Geology, V. 2, p. 195-205.

Jeffery, P. G., 1970, Chemical methods of rock analysis; Pergamon Press, New York, N. Y., p. 172-177.

Kahle, A. B., 1977, A simple thermal model of the Earth's surface for geologic mapping by remote sensing; Journal of Geophysical Research, V. 82, No. 11, p. 1673-1680.

Kaminsky, B., 1977, Correlation of LANDSAT multispectral data to rock reflectance measurements; M. S. Thesis, University of Wyoming, Dept. of Geology, 55 p.

Kim, J., and Kohout, F. J., 1975, Multiple regression analysis: subprogram regression; in Statistical Package for the Social Sciences, 2nd edition, Nie, N. H., et. al., ed., p. 320-367.

Knight, D. H., Hill, R. J., and Harrison, A. T., 1976, Potential Natural Landmarks in the Wyoming Basin; Report Prepared for the U. S. Dept. of Interior, National Park Service, Contract No. 9900X20047, p.1-56.

Kober, C. L., and Procter-Gregg, H. D., 1977, Discrimination of uranium alteration zones in selected areas by use of LANDSAT MSS imagery; U. S. Dept. of Energy Open File Report GJBX-4(77), 88 p.

Küchler, A. W., 1964, Potential natural vegetation of the conterminous United States; Amer. Geol. Soc. Special Publication 36.

Langen, R. E., and Kidwell, A. L., 1974, Goology and geochemistry of the Highland uranium deposit, Converse County, Wyoming; The Mountain Geologist, V. 11, No. 2, p. 85-93.

Langmuir, D., 1978, Uranium solution-mineral equilibria at low temperatures with applications to sedimentary ore deposits; Geochimica et Cosmochimica Acta., V. 42, p. 547-569.

Langmuir, D., and Applin, K., 1977, Refinement of the thermodynamic properties of uranium minerals and dissolved species, with application to the chemistry of ground waters in sandstone-type uranium deposits; U. S. Geological Survey Circular 753, p. 57-60.

Law, B. E., 1976, Large-scale compaction structures in the coal-bearing Fort Union and Wasatch Formations, northeast Powder River Basin, Wyoming; Wyo. Geol. Assoc., Guidebook to 28th Annual Field Conference, p. 221-229.

Levinson, R. A., Marrs, R. W., and Grantham, D. G., 1976, Rapid, low-cost image analysis through video processing; U. S. Dept. of Energy (formerly ERDA) Open File Report GJBX-37(76), 54 p.

Love, J. D., 1978, Oral communication.

Love, J. D., 1977, The Pumpkin Buttes Formation; Unpublished report.

Love, J. D., 1952, Preliminary report on uranium deposits in the Pumpkin Buttes Area, Powder River Basin, Wyoming; U. S. Geological Survey Circular 176, 37 p.

Marrs, R. W., et. al., 1973, Color anomalies, minerals, and ERTS imagery; Contributions to Geology, V. 12, No. 2, p. 105-110.

Marrs, R. W., and King, J. K., 1978, Demonstrations of video processing of image data for uranium resource assessments; final report on ERDA Contract E(05-1)-1648, 59 p.

Masursky, H., 1962, Uranium bearing coal in the eastern part of Red Desert area, Wyoming; U. S. Geological Survey Bull. 1099-B, 152 p.

McGrew, P. O., 1971, The Tertiary history of Wyoming; Wyo. Geol. Assoc. Guidebook, V. 23, p. 29-33.

Meschter, D. Y., 1958, Study of concretions as applied to geology of uranium deposits; Geological Society of America Bull., V. 69, p. 1736-1737.

Morris, W. A., 1977, Uranium hydrogeochemical and stream sediment reconnaissance of the northern part of the Powder River Basin, Wyoming; Los Alamos Scientific Laboratory Informal Report LA-6654-MS, 80 p.

Mrak, V. A., 1958, Uranium deposits in the Tertiary sediments of the Powder River Basin, Wyoming; Wyoming Geol. Assoc. Guidebook, V. 13, p. 233-240.

National Aeronautics and Space Administration, 1976, LANDSAT data users handbook; Document No. 765D54258, Goddard Space Flight Center, Greenbelt, Md.

Offield, T. W., Raines, G. L., and Sawatzky, D. L., 1977, Computer-enhanced images and geologic studies, southern Powder River Basin, Wyoming (abstr); U. S. Geological Survey Circ. 753, p. 27-29.

Piech, K. R., and Walker, J. E., 1974, Interpretation of soils; Photogrammetric Eng. and Remote Sensing, V. 40, No. 1, p. 87-94.

Rackley, R. I., 1972, Environment of Wyoming Tertiary uranium deposits; Am. Assoc. of Petroleum Geologists Bull., V. 56, No. 4, p. 755-774.

Rackley, R. I., and Johnson, R. L., 1971, Geochemistry of uranium roll-front deposits with a case history from the Powder River Basin; Econ. Geol., V. 66, p. 202-209.

Raines, G. L., 1974, Evaluation of multiband photography for rock discrimination; Remote Sensing Report 74-2, Dept. of Geology, Colorado School of Mines, Golden, Colorado, 86 p.

Raines, G. L., and Lee, K., 1975, In-situ rock reflectance; Photogrammetric Eng. and Remote Sensing, V. 4, No. 2, p. 189-198.

Riley, J. P., 1958, The rapid analysis of silicate rocks and minerals; Analytica Chimica Acta., V. 19. No. 4, p. 413-428.

Rosholt, J. N., Zartman, R. E., and Nkomo, I. T., 1973, Lead isotope systematics and uranium depletion in the Granite Mountains, Wyoming; Geological Society of America Bull., V. 84, p. 989-1002.

Rowan, L. C., et. al., 1974, Discrimination of rock types and detection of hydrothermally altered areas in south-central Nevada by the use of computer-enhanced ERTS images; U. S. Geological Survey Prof. Paper 883, 35 p.

Rubin, B., 1970, Uranium roll front zonation in the southern Powder River Basin, Wyoming; Wyo. Geol. Assoc. Earth Science Bull., V. 3, No. 4, p. 5-12.

Salmon, B. C., and Pillars, W. W., 1975, Multispectral processing of ERTS-A (LANDSAT) data for uranium exploration in the Wind River Basin, Wyoming; Environmental Research Institute of Mich., Report for Contract GJO-16351, 129 p.

Salmon, B. C., and Vincent, R. W., 1974, Surface compositional mapping in the Wind River Basin, Wyoming by multispectral techniques applied to ERTS-1 data; Proc. 9th Int. Symp. on Remote Sensing of Environment, V. III, Ann Arbor, Mich., p. 2005-2012.

Schafer, R., 1977, Christensen Ranch joint venture uranium deposit, Campbell and Johnson Counties, Wyoming; Joint Geology Conference of the Dept. of Geology, University of Wyoming, Wyoming Geological Assoc., and Wyoming Geological Survey, April 29-30, Laramie, Wyoming.

Schultz, B. C., 1941, The pipy concretions of the Arikaree; Bull. of the University of Nebraska State Museum, V. 2, No. 8, p. 69-82.

Seeland, D. A., 1976, Relationship between early Tertiary sedimentation patterns and uranium mineralization in the Powder River Basin, Wyoming; Wyo. Geol. Assoc. Guidebook, V. 28, p. 53-64.

Shapiro, L., and Brannock, W. W., 1962, Rapid analysis of silicate, carbonate, and phosphate rocks; U. S. Geological Survey Bull. 1144-A, 56 p.

Shapiro, L., and Brannock, W. W., 1956, Rapid analysis of silicate rocks; U. S. Geological Survey Bull. 1036-C, 37 p.

Shapiro, L., and Brannock, W. W., 1952, Rapid analysis of silicate rocks; U. S. Geological Survey Circular 165, 17 p.

Sharp, W. N., 1955, Geologic investigations of radioactive deposits, Pumpkin Buttes Area, Powder River Basin, Wyoming, U. S. Geological Survey TEI 540, p. 118-120.

Sharp, W. N., and Gibbons, A. B., 1964, Geology and uranium deposits of the southern Powder River Basin, Wyoming; U. S. Geological Survey Bull. 1147-D, 60 p.

Sharp, W. N., and Gibbons, A. B., 1957, Geologic investigations of radioactive deposits, southern Powder River Basin, Wyoming; U. S. Geological Survey TEI-690, p. 246-257.

Sharp, W. N., McKay, E. T., McKeown, F. A., and White, A. M., 1964, Geology and uranium deposits of the Pumpkin Buttes area of the Powder River Basin, Wyoming; U. S. Geological Survey Bull. 1107-H, p. 541-638.

Sharp, W. N., McKeown, F. A., McKay, E. J., and White, A. M., 1956, Geology and uranium deposits of the Pumpkin Buttes area, Powder River Basin, Wyoming; U. S. Geological Survey Prof. Paper 300, p. 371-374.

Sharp, W. N., and White, A. M., 1957, Preliminary geologic map of the Pumpkin Buttes area, Campbell and Johnson Counties, Wyoming showing location of uranium occurrences; U. S. Geological Survey MF98.

Shawe, D. R., 1956, Significance of roll ore bodies in genesis of uranium-vanadium deposits on the Colorado Plateau; U. S. Geological Survey Prof. Paper 300, p. 239-241.

Shockey, P. N., Rackley, R. I., and Dahill, M. P., 1968, Source beds and solution fronts; Remarks to Wyoming Metals Section, American Institute of Mining and Metallurgical Engineers, 8 p.

Singleton, P. C., and Cline, A. J., 1976, Detailed descriptions of soils and miscellaneous land types mapped on the Black Thunder Mine site; Final Report Environmental Assessment for the Black Thunder Mine Site; Campbell County, Wyoming, Supplement 1, 210 p.

Smedes, H. W., and Prostka, H. J., 1972, Stratigraphic framework of the Absaroka Volcanic Supergroup in the Yellowstone National Park region; U. S. Geological Survey Prof. Paper 729-C, 33 p.

Spirakis, L. S., and Condit, C. D., 1975, Preliminary report on the use of the LANDSAT-1 (ERTS-1) reflectance data in locating alteration zones associated with uranium mineralization near Cameron, Arizona; U. S. Geological Survey Open File Report 75-416, 23 p.

Steidtmann, J. R., 1978, Oral communication.

Strackless, J. S., Bunker, C. M., Bush, C. A., Doering, W. P., and Scott, J. H., 1977, Geochemical and petrological studies of a uraniferous granite from the Granite Mountains, Wyoming; Journ. of Research U. S. Geological Survey, V. 5, No. 1, p. 61-81.

Taylor, D. W., 1975, Early Tertiary mollusks from the Powder River Basin, Wyoming-Montana, and adjacent regions; U. S. Geological Survey Open File Report 75-331, p. 1-32.

Townsend, T., 1979, Descrimination of alteration in the Crooks Gap, Wyoming uranium district using laboratory and LANDSAT spectral reflectance data; U. S. Geological Survey Open File Report 79-765, 47 p.

Troyer, M. L., McKay, E. J., Soister, P. E., and Wallace, S. R., 1954, Summary of investigations of uranium deposits in the Pumpkin Buttes area, Johnson and Campbell Countles, Wyoming; U. S. Geological Survey Circ. 338, 17 p.

United States Geological Survey, 1959, Savageton Quadrangle, 15-minute series topographic map.

Vincent, R. K., 1977, Uranium exploration with computer-processed LANDSAT data; Geophysics, V. 42, No. 3, p. 536-541.

Vincent, R. K., 1973, Ratio maps of iron ore deposits Atlantic City District, Wyoming; Symp. on Significant Results Obtained from the Earth Resources Technology Satellite, V. 1, Sect. A, p. 379-386.

Waters, A. C., and Granger, H. C., 1953, Volcanic debris in uraniferous sandstones and its possible bearing on the origin and precipitation of uranium; U. S. Geological Survey Circ. 224, 26 p.

Water Resource Research Institute, 1974, Mean annual precipitation map, base period 1941-1970; Laramie, Wyoming.

Webb, M. D., 1969, Stratigraphic control of sandstone uranium deposits in Wyoming; Contributions to Geology, V. 8, No. 2, p. 121-129.

Wegemann, C. H., Howell, R. W., Dobbin, C. E., 1928, The Pumpkin Buttes coal field, Wyoming; U. S. Geological Survey Bull. 806, p. 1-14.

Ziemans, G. M., and Walker, D. N., 1977, Archeology of the eastern Powder River Basin, Wyoming; prepared for Bureau of Land Management, Contract No. YA-512-RFP6-104, p. 26-37.

APPENDICES

THIS PAGE

WAS INTENTIONALLY

LEFT BLANK

APPENDIX A

Descriptions of sample sites in the Pumpkin Buttes study area.

Christensen Grid (CH)

02	soil	over	unaltered	siltstone
03	soil	over	unaltered	siltstone
04	soil	over	unaltered	siltstone
05	soil	over	unaltered	siltstone
12	soil	over	unaltered	alluvium
13	soil	over	altered	limestone
14	soil	over	altered	sandstone
15	soil	over	unaltered	siltstone
18	soil	over	ore-bearing	sandstone
22	soil	over	unaltered	alluvium
23	soil	over	altered	sandstone
24	soil	over	altered	sandstone
25	soil	over	unaltered	siltstone
32	soil	over	unaltered	siltstone
33	soil	over	altered	sandstone
34	soil	over	altered	sandstone
35	soil	over	unaltered	siltstone
41	soil	over	unaltered	siltstone
42	soil	over	unaltered	sandstone
43	soil	over	altered	sandstone
44	soil	over	altered	siltstone
45	soil	over	unaltered	siltstone
51	soil	over	unaltered	siltstone
52	soil	over	unaltered	siltstone
53	soil	over	altered	sandstone
54	soil	over	altered	sandstone
55	soil	over	unaltered	siltstone
61	soil	over	unaltered	siltstone
62	soil	over	unaltered	siltstone
63	soil	over	altered	sandstone
64	soil	over	unaltered	siltstone
65	soil	over	unaltered	siltstone
70	soil	over	unaltered	sandstone
71	soil	over	altered	sandstone
72	soil	over	unaltered	siltstone
73	soil	over	unaltered	siltstone
74	soil	over	altered	sandstone
75	soil	over	unaltered	siltstone
80	soil	over	unaltered	siltstone
81	soil	over	altered	sandstone
82	soil	over	altered	sandstone
83	soil	over	altered	sandstone
84	soil	over	unaltered	siltstone
85	soil	over	unaltered	siltstone

Colorado Christensen Grid (CC)

11	soil	over	unaltered	sandstone
12	soil	over	altered	sandstone
13	soil	over	unaltered	siltstone
14	soil	over	unaltered	siltstone
21	soil	over	unaltered	sandstone
22	soil	over	altered	sandstone
23	soil	over	ore-bearing	sandstone
24	soil	over	unaltered	siltstone
25	soil	over	altered	sandstone
31	soil	over	unaltered	siltstone
32	soil	over	unaltered	sandstone
33	soil	over	unaltered	sandstone
34	soil	over	unaltered	siltstone
35	soil	over	altered	sandstone
41	soil	over	unaltered	siltstone
42	soil	over	altered	sandstone
43	soil	over	altered	sandstone
44	soil	over	unaltered	sandstone
45	soil	over	altered	sandstone
52	soil	over	unaltered	sandstone
53	soil	over	altered	sandstone
54	soil	over	altered	sandstone
55	soil	over	unaltered	siltstone
63	soil	over	unaltered	sandstone
64	soil	over	altered	sandstone
65	soil	over	altered	sandstone
66	soil	over	unaltered	sandstone

Jeannette Pit Transect (PJ)

01	altered	pink	sandy soil
02	unaltered	gray	sandstone
03		white	calcite vein
04	altered	yellow	sandstone
05	altered	red	sandstone
06	unaltered	gray	shale
07	altered	pink	sandy soil
08	altered	red	sandstone
09	altered	red	conglomerate
10	unaltered	gray	conglomerate
11	unaltered	gray	sandstone
12	purple	ironstone	fossil wood
13	purple	ironstone	fossil wood

Lauby Transect (LB)

Surface Samples

01	soil	over	unaltered	siltstone
03	soil	over	altered	sandstone
05	soil	over	altered	sandstone
07	soil	over	unaltered	siltstone
09	soil	over	unaltered	siltstone
11	soil	over	unaltered	siltstone
13	soil	over	altered	sandstone

Samples collected at a depth of 15 cm (6 in)

02	soil	over	unaltered	siltstone
04	soil	over	altered	sandstone
06	soil	over	altered	sandstone
08	soil	over	unaltered	siltstone
10	soil	over	unaltered	siltstone
12	soil	over	unaltered	siltstone
14	soil	over	altered	sandstone

Utah Mine Transect (UT)

01	altered	yellow	sandstone
02	altered	yellow	sandstone
03	ore-bearing	brown	sandstone
04	ore-bearing	green	sandstone
05	altered	red	sandstone
06	altered	red	conglomerate
07	unaltered	brown	sandstone

Innes Transect (IN)*

01	soil	over	unaltered	marlstone
02	soil	over	unaltered	sandstone
03	soil	over	unaltered	marlstone
04	soil	over	unaltered	siltstone
05	soil	over	unaltered	siltstone

*IN is located 5 km (3.3 mi) north of mineral district.

North Jeannette Transect (NJ)

01	soil	over	unaltered	shale
02	soil	over	unaltered	shale
03	soil	over	ore-bearing	sandstone
04	soil	over	altered	sandstone
05	soil	over	unaltered	shale

Jeannette Spectrometer Sites (SJ)

01	altered	pink	sandy soil
02	unaltered	red	sandstone
03	altered	red	sandstone
04	unaltered	gray	sandstone
05	altered	yellow	sandstone
06	altered	red	sandstone
07	altered	red	sandstone
08	altered	red	sandstone
09	unaltered	gray	shale
10	altered	pink	sandy soil

Mid Jeannette Transect (MJ)

01	unaltered	gray	sandstone
02	gray	ore-bearing	sandstone
03	altered	red	sandstone

Laur Mine Transect (LR)*

01	unaltered	gray	sandy soil
02	unaltered	gray	sandstone
03	unaltered	gray	sandstone
04	altered	yellow	sandstone
05	altered	red	sandstone
06	unaltered	gray	sandstone
07	unaltered	gray	shale

*LR is located 11.3 km (7 mi) south of the study area.

Blowout Anomaly #119 Transect (BA)

01	unaltered	gray	sandy soil
02	unaltered	gray	sandstone
03	unaltered	gray	sandstone
04	unaltered	gray	sandstone
05	ore-bearing	yellow	sandstone
06	altered	yellow	sandstone
07	unaltered	gray	sandstone
08	altered	yellow	sandstone
09	altered	yellow	sandstone
10	altered	red	sandstone

Spot Sample Locations (SL)

01	gray sandstone, White River fm.
02	coal (lignite), Wasatch fm.
03	soil over unaltered siltstone, Wasatch fm.
04	soil over unaltered siltstone, Wasatch fm.
05	Uraninite ore from BA pit, Wasatch fm.
06	Carnotite ore from BA pit, Wasatch fm.
07	Uraninite ore from BA pit, Wasatch fm.

Spot Sample Locations from Chimney Hill Area (CM)*

01	gold-colored limestone, Wasatch fm.
02	unaltered buff sandstone, Wasatch fm.
03	unaltered buff sandstone, Wasatch fm.

*CM is located 5 km (3.2 mi) north of mineral district

APPENDIX B

Results of geochemical analyses for sample transects.

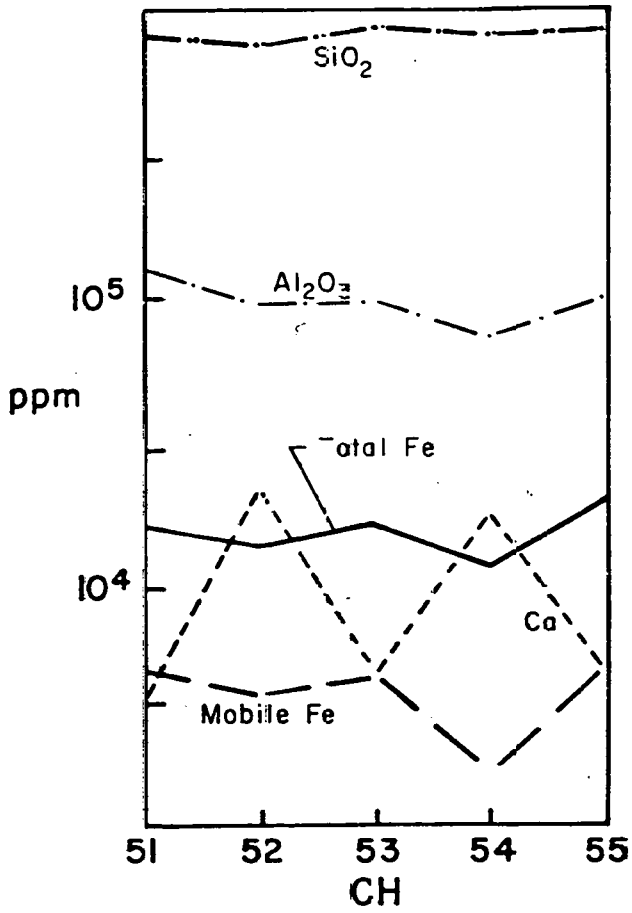
SiO2
Al2O3
10^5
ppm
Total Fe
10^4
Ca
Mobile Fe
51
52
53
54
55
CH

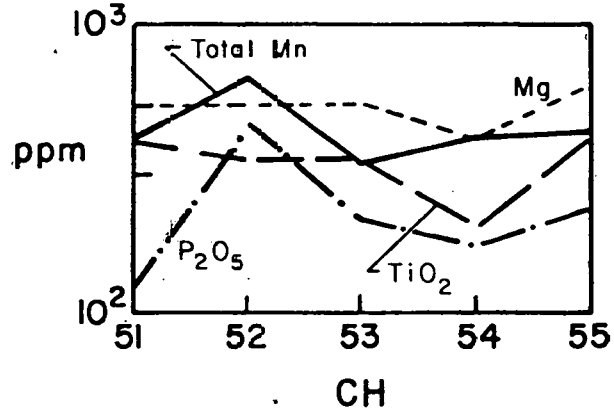
10^3
Total Mn
Mg
ppm
P2O5
TiO2
10^2
51
52
53
54
55
CH

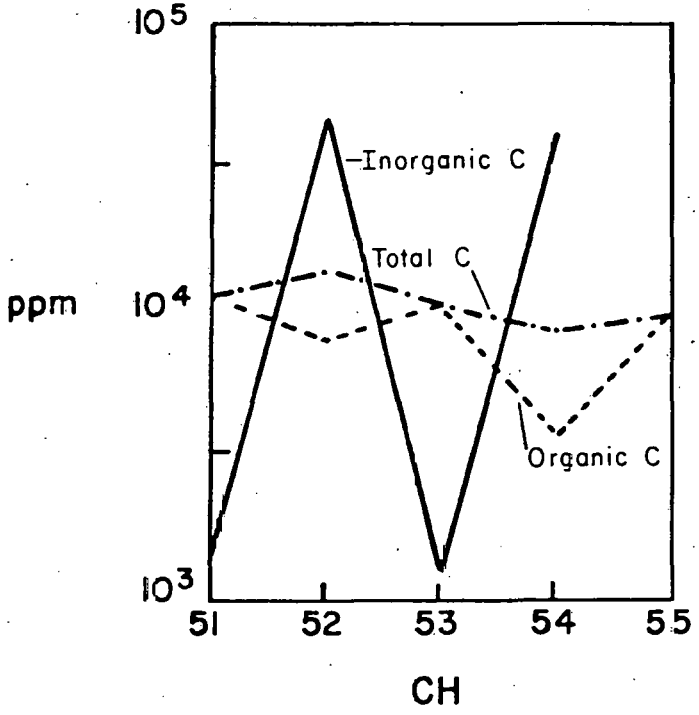
ppm
10^5
10^4
10^3
Inorganic C
Total C
Organic C
51
52
53
54
55
CH

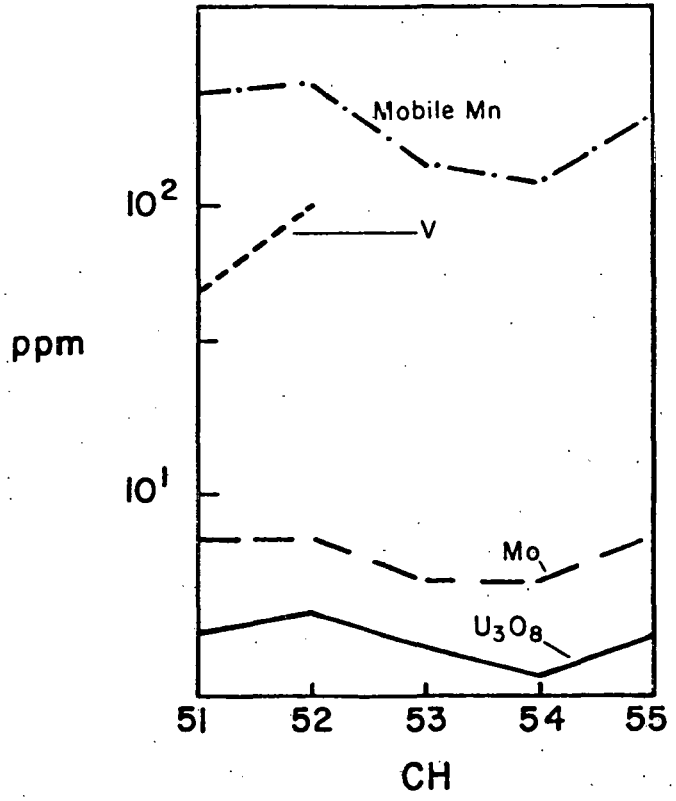
ppm
10^2
10^1
Mobile Mn
V
Mo
U_3O_8
51
52
53
54
55
CH

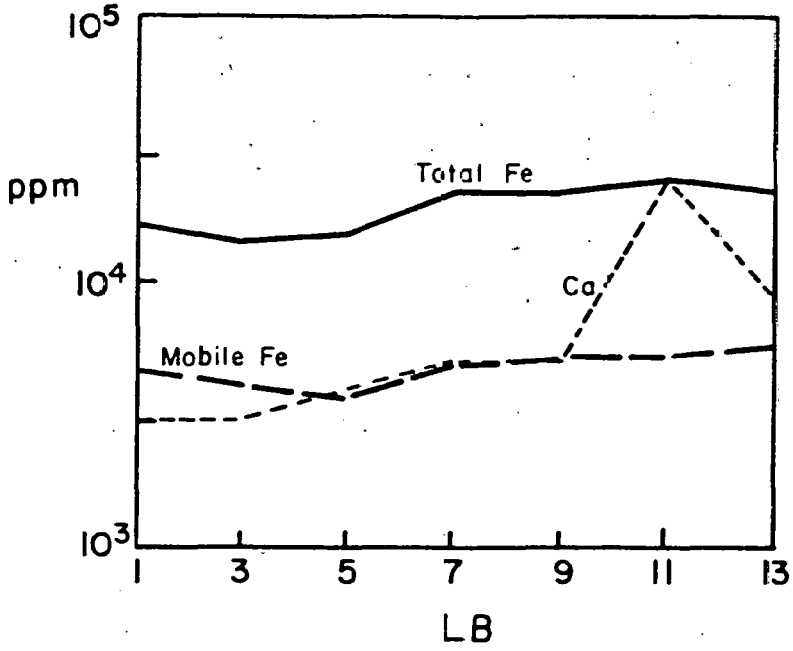
10^5
ppm
10^4
10^3
Total Fe
Ca
Mobile Fe
1
3
5
7
9
11
13
LB

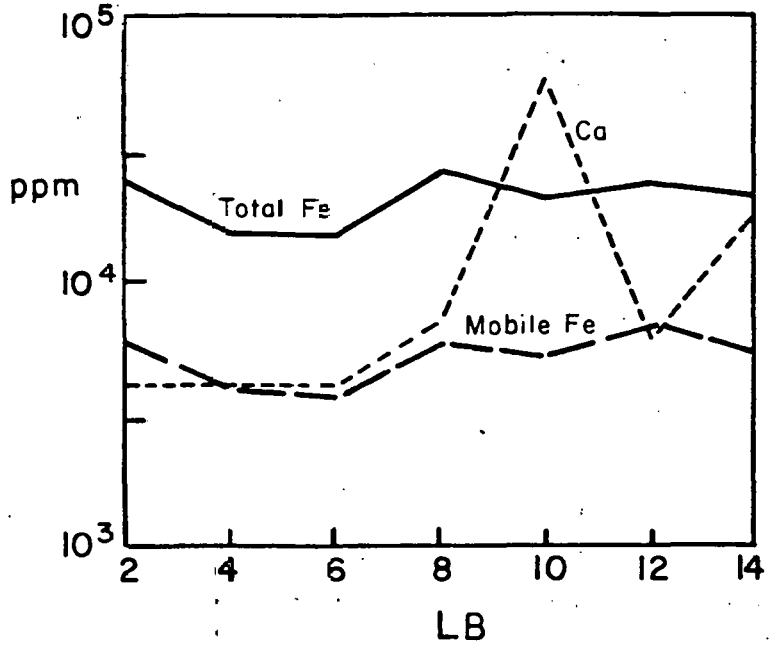
10^5
ppm
10^4
10^3
Ca
Total Fe
Mobile Fe
2
4
6
8
10
12
14
LB

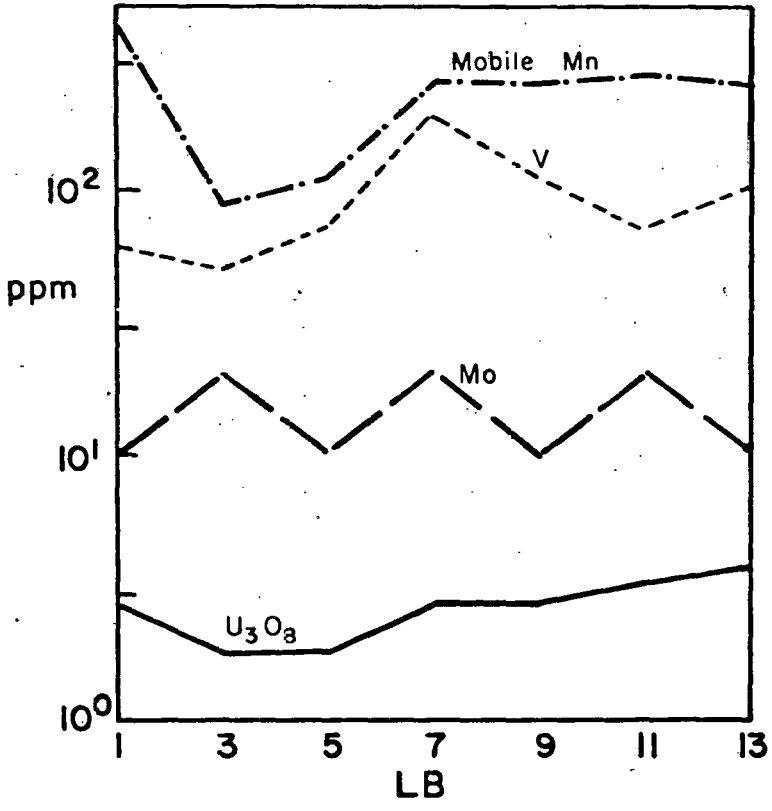
Mobile Mn
V
Mo
U_3O_8
ppm
10^2
10^1
10^0
1
3
5
7
9
11
13
LB

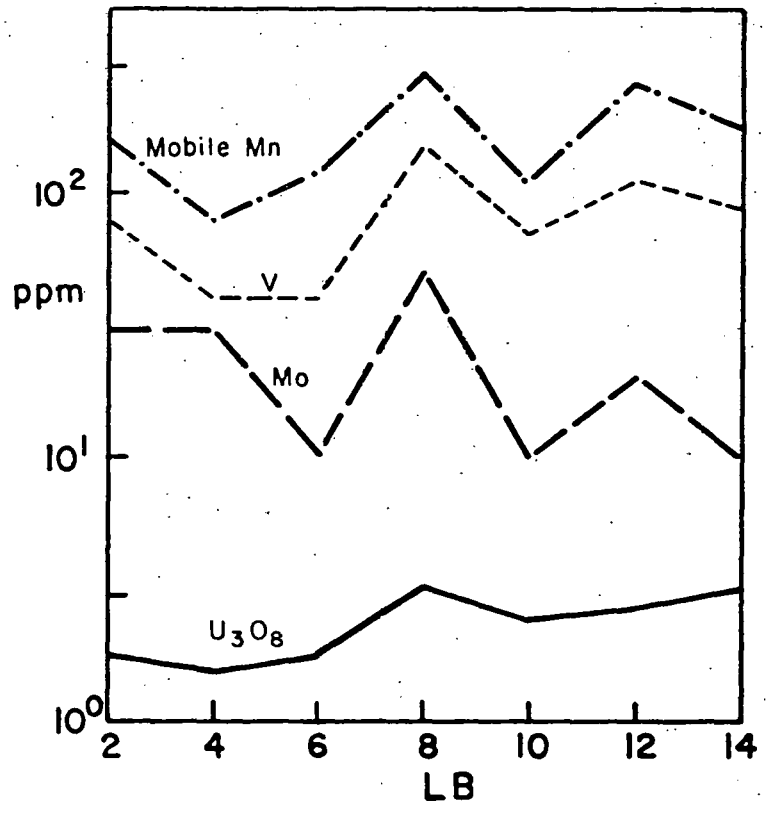
Mobile Mn
V
Mo
U_3O_8
ppm
10^2
10^1
10^0
2
4
6
8
10
12
14
LB

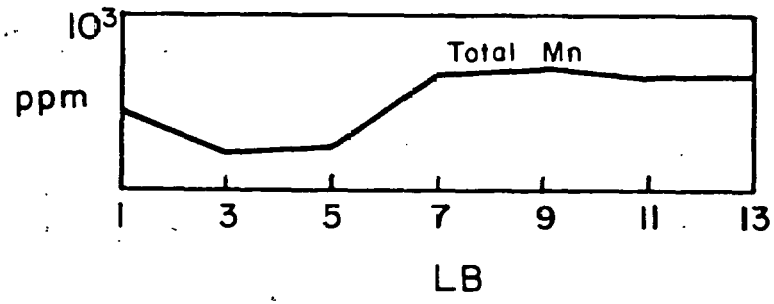
10^3
ppm
Total Mn
1
3
5
7
9
11
13
LB

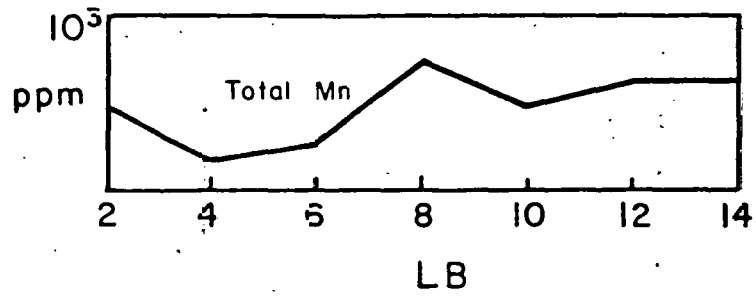
10^3
ppm
Total Mn
2
4
6
8
10
12
14
LB

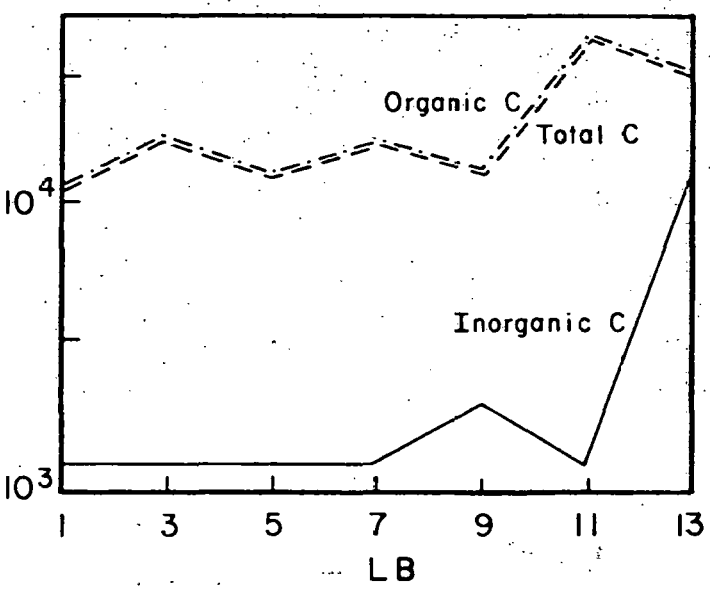
ppm
10^4
10^3
Organic C
Total C
Inorganic C
1
3
5
7
9
11
13
LB

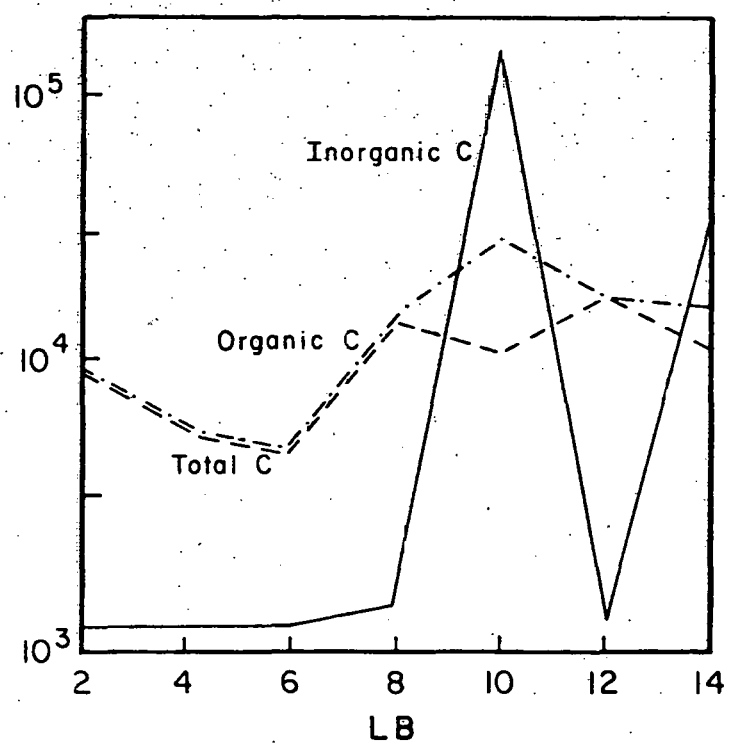
10^5
10^4
10^3
Inorganic C
Organic C
Total C
2
4
6
8
10
12
14
LB

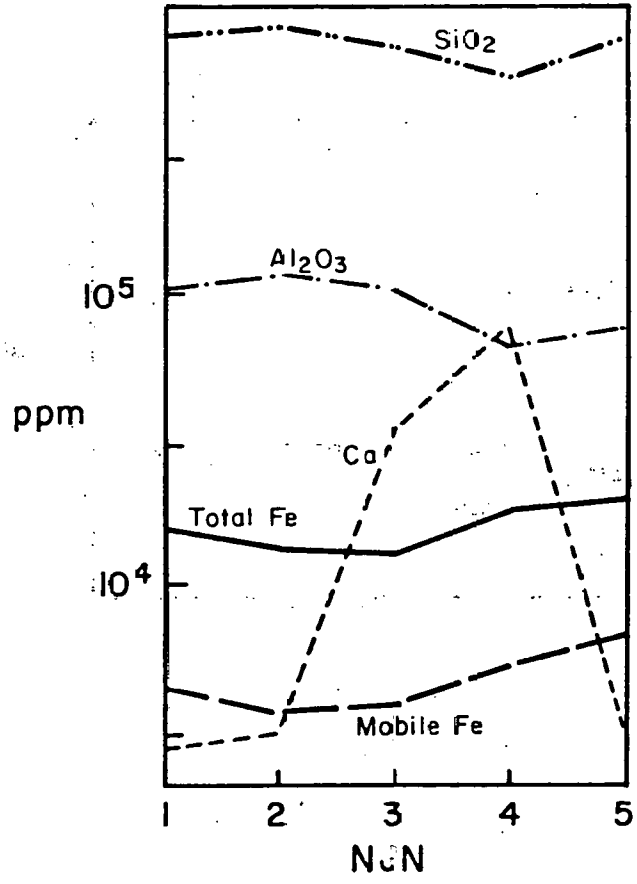
SiO2
Al2O3
10^5
ppm
Ca
Total Fe
10^4
Mobile Fe
1
2
3
4
5
NJN

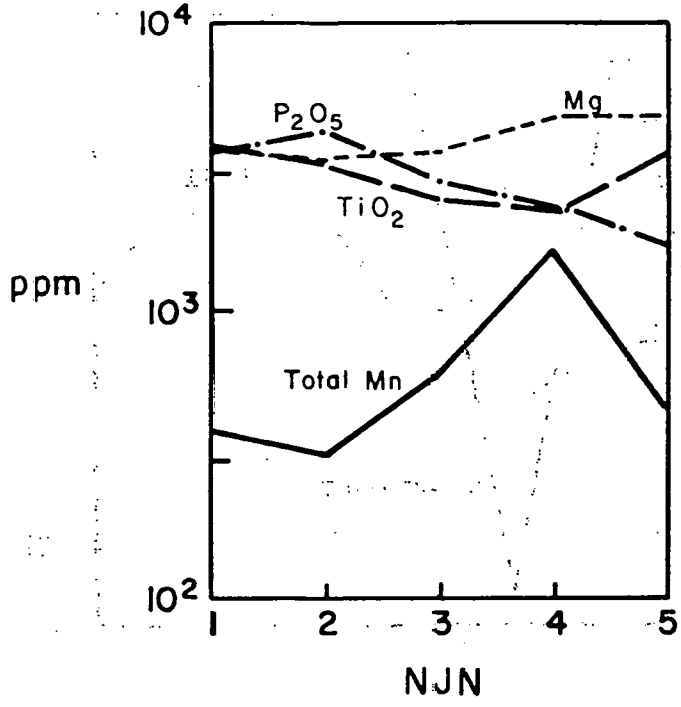
10^4
P2O5
Mg
TiO2
ppm
10^3
Total Mn
10^2
1
2
3
4
5
NJN

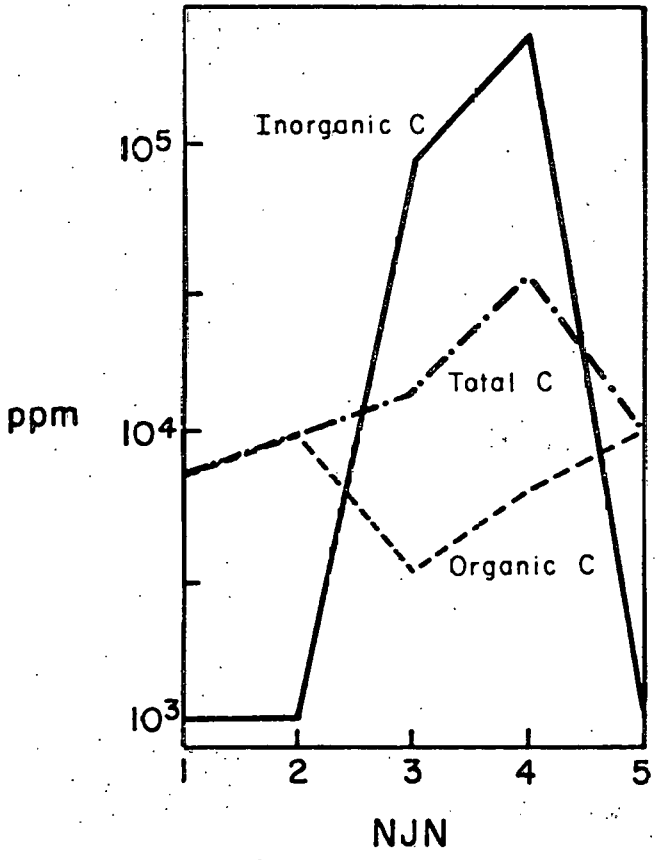
Inorganic C
Total C
Organic C
ppm
10^5
10^4
10^3
1
2
3
4
5
NJN

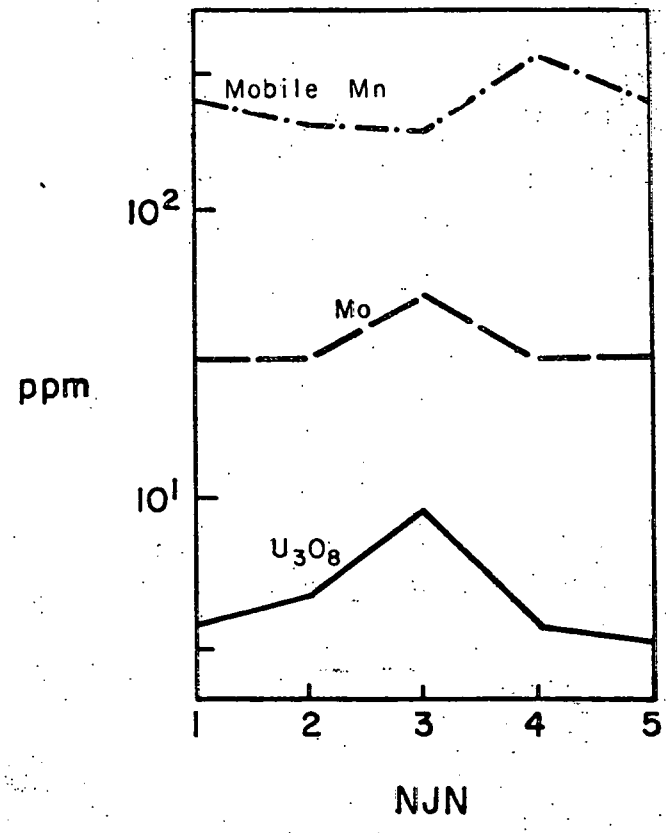
Mobile Mn
Mo
U_3O_8
ppm
10^2
10^1
1
2
3
4
5
NJN

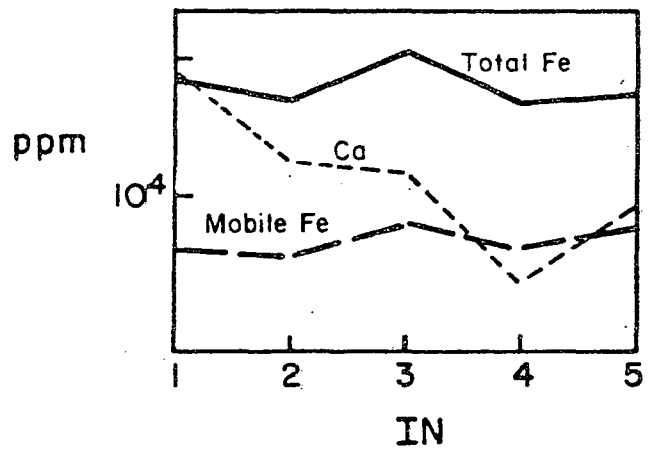
ppm
Total Fe
Ca
Mobile Fe
10^4
1
2
3
4
5
IN

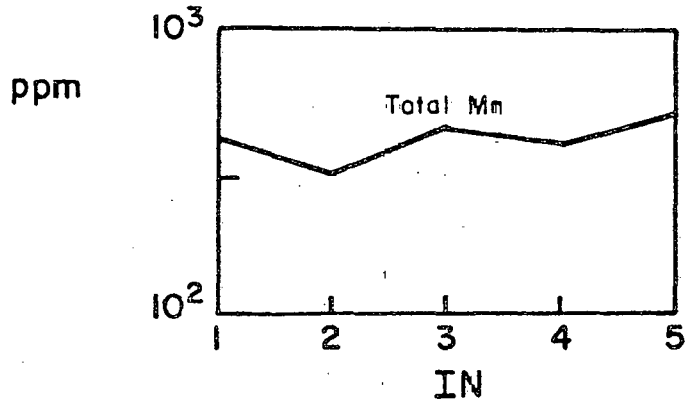
ppm
10^3
Total Mn
10^2
1
2
3
4
5
IN

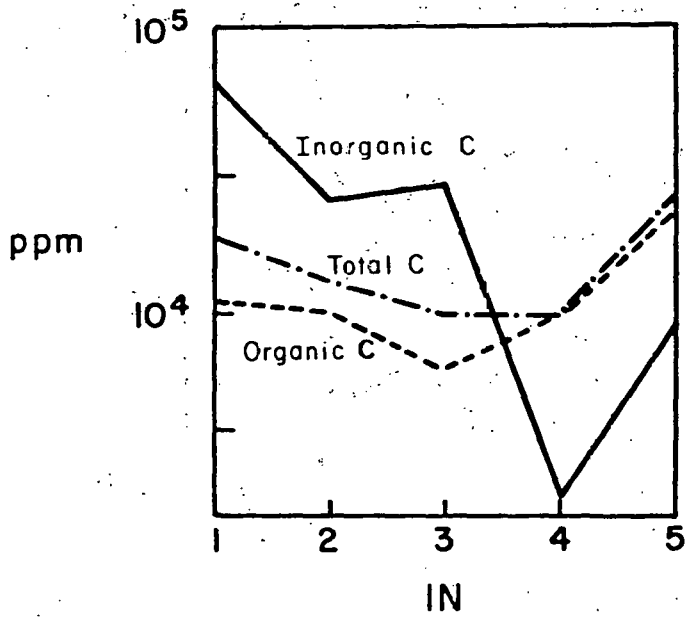
10^5
ppm
10^4
Inorganic C
Total C
Organic C
1
2
3
4
5
IN

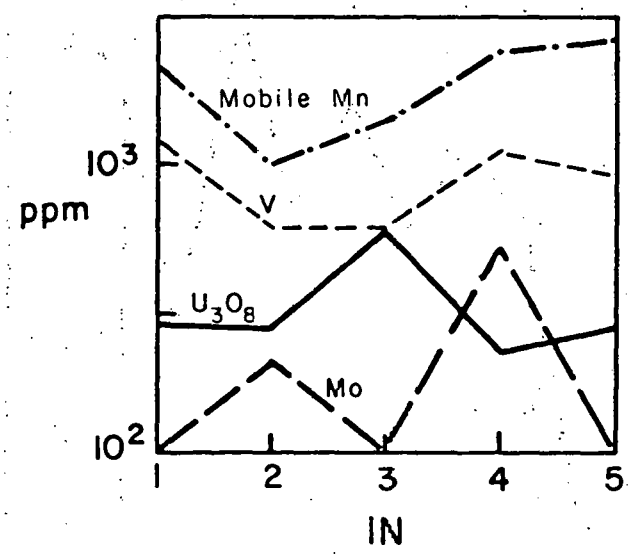
Mobile Mn
10^3
ppm
V
U_3O_8
Mo
10^2
1
2
3
4
5
IN

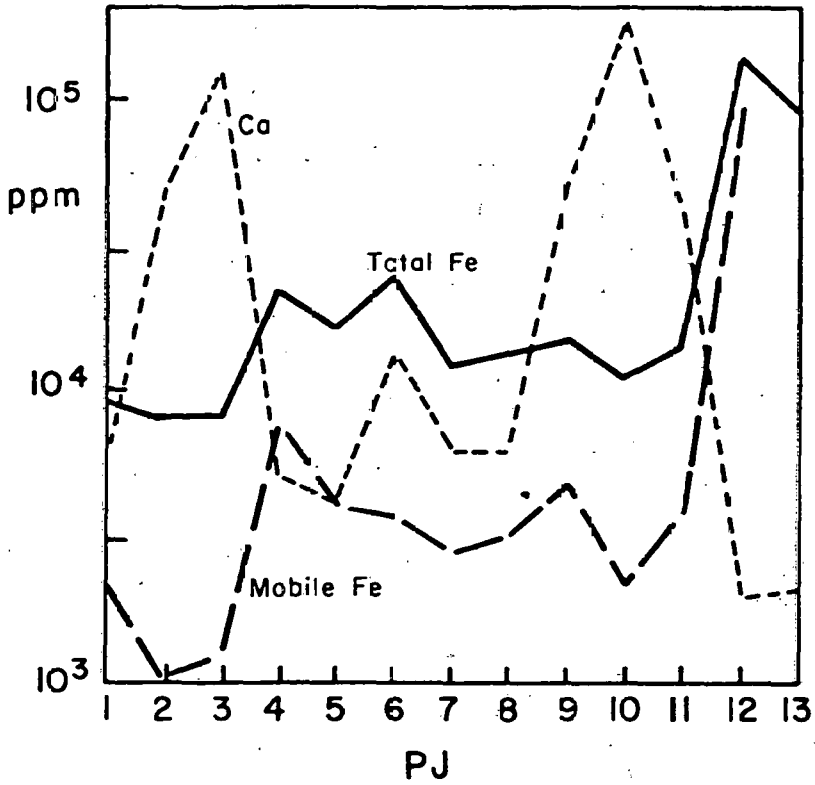
10^5
ppm
10^4
10^3
Ca
Total Fe
Mobile Fe
1 2 3 4 5 6 7 8 9 10 11 12 13
PJ

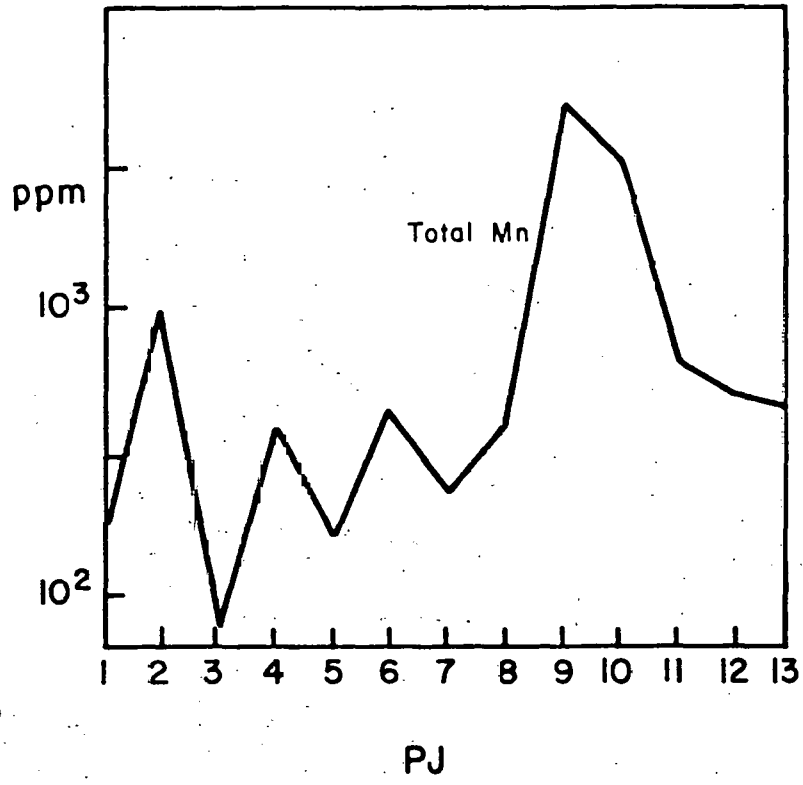
ppm
10^3
10^2
Total Mn
1 2 3 4 5 6 7 8 9 10 11 12 13
PJ

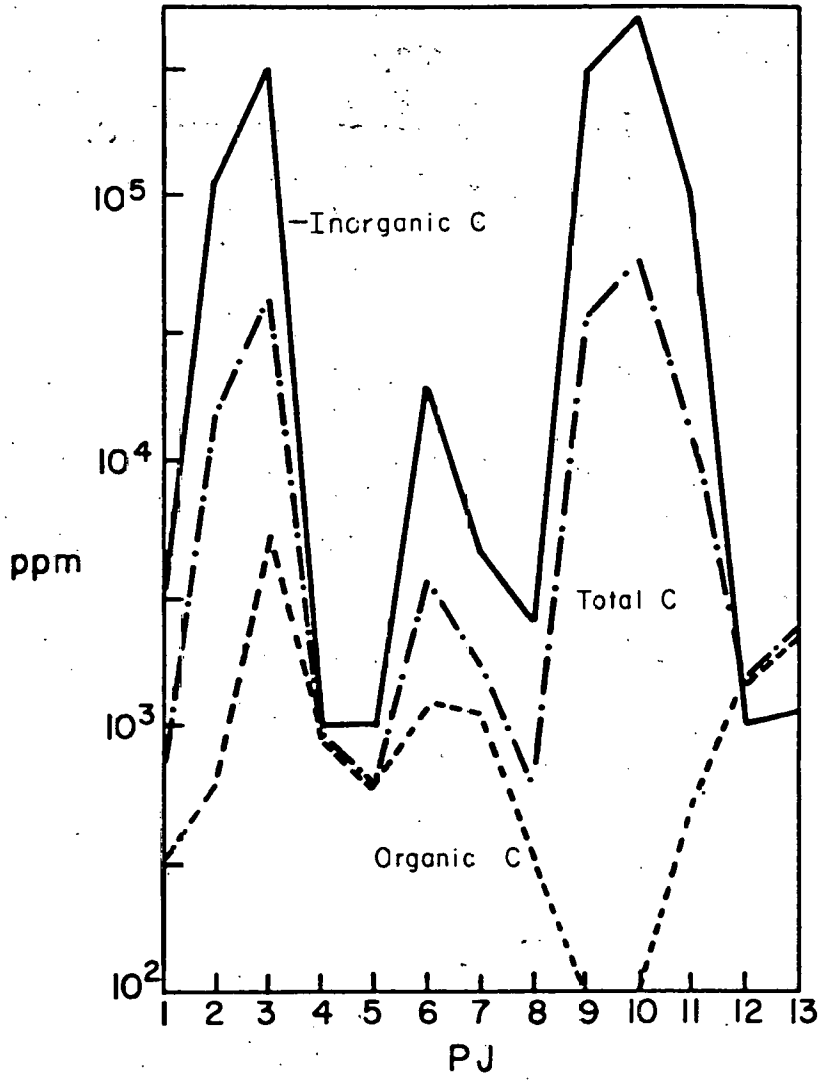
ppm
10^5
10^4
10^3
10^2
Incrganic C
Total C
Organic C
1 2 3 4 5 6 7 8 9 10 11 12 13
PJ

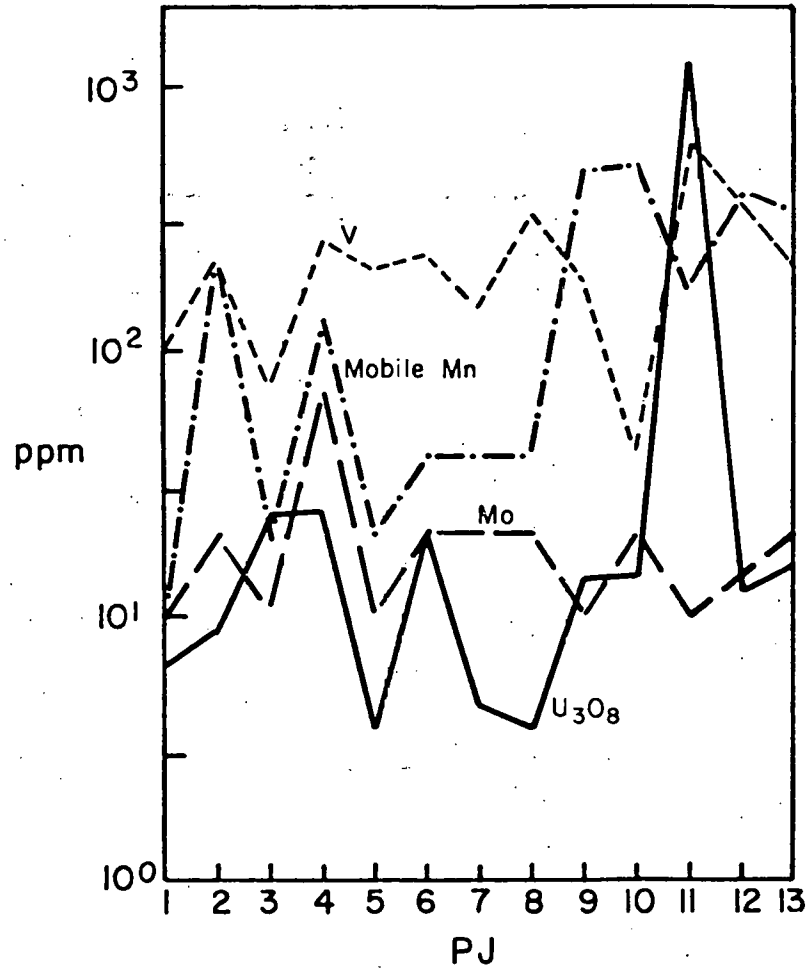
ppm
10^3
10^2
10^1
10^0
V
Mobile Mn
Mo
U_3O_8
1 2 3 4 5 6 7 8 9 10 11 12 13
PJ

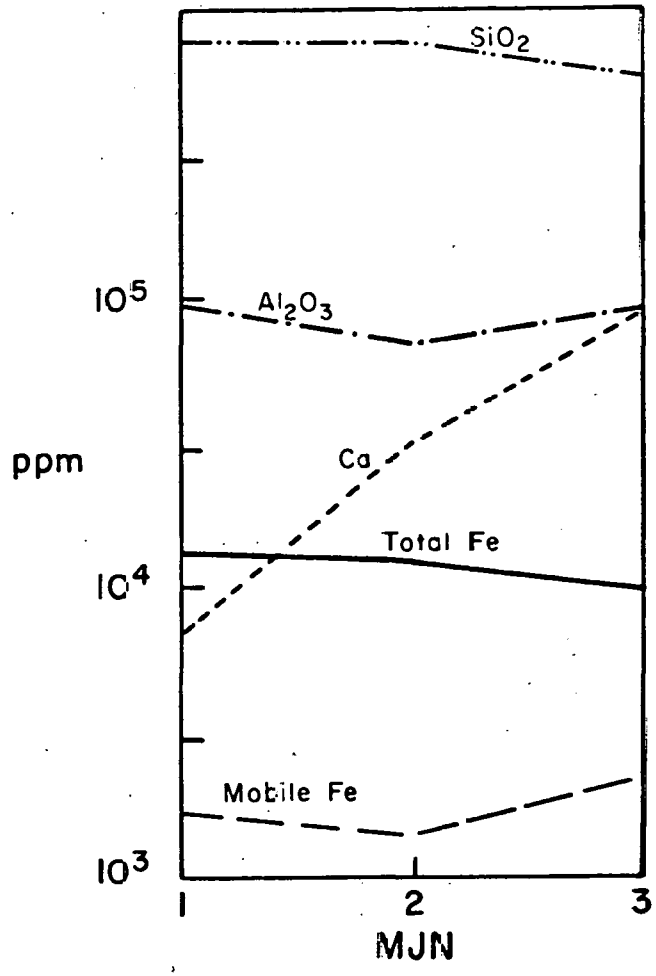
SiO2
Al2O3
Ca
Total Fe
Mobile Fe
ppm
10^5
10^4
10^3
1
2
3
MJN

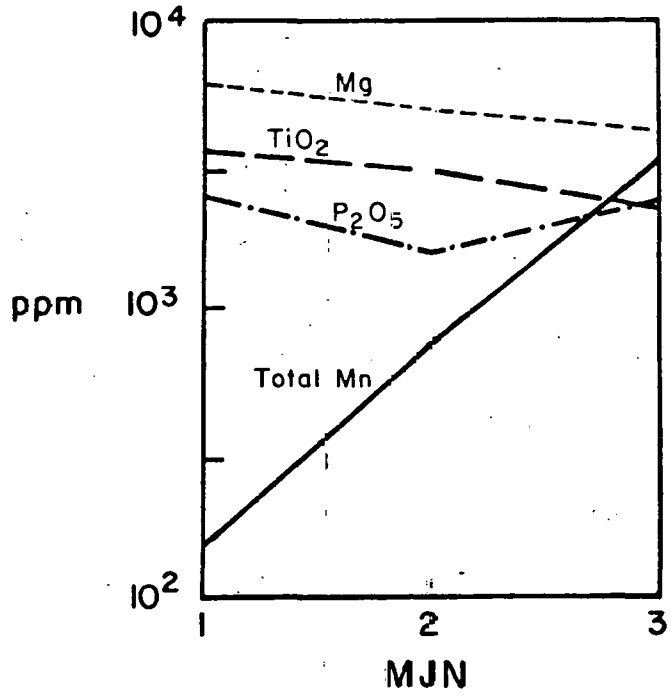
Mg
TiO2
P2O5
Total Mn
ppm
10^4
10^3
10^2
1
2
3
MJN

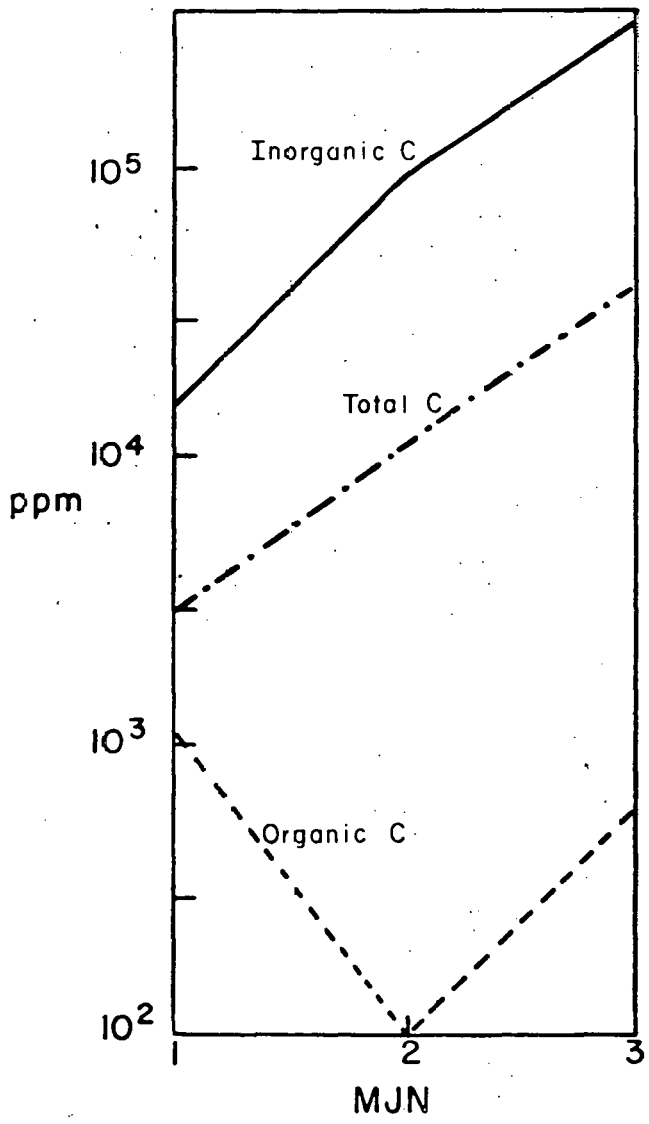
Inorganic C
Total C
Organic C
10^5
10^4
10^3
10^2
ppm
1
2
3
MJN

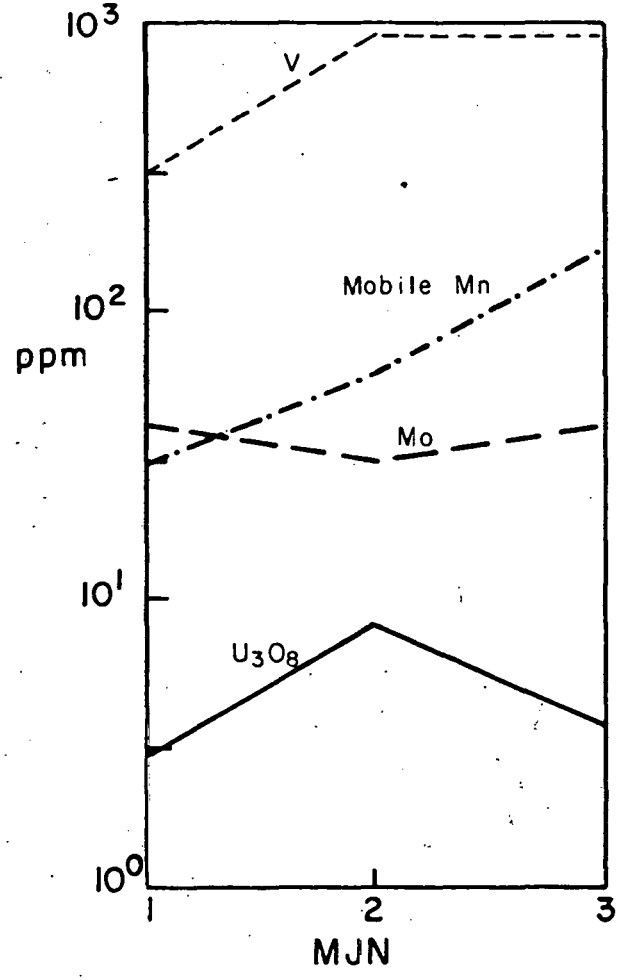
V
Mobile Mn
Mo
U_3O_8
10^3
10^2
10^1
10^0
ppm
1
2
3
MJN

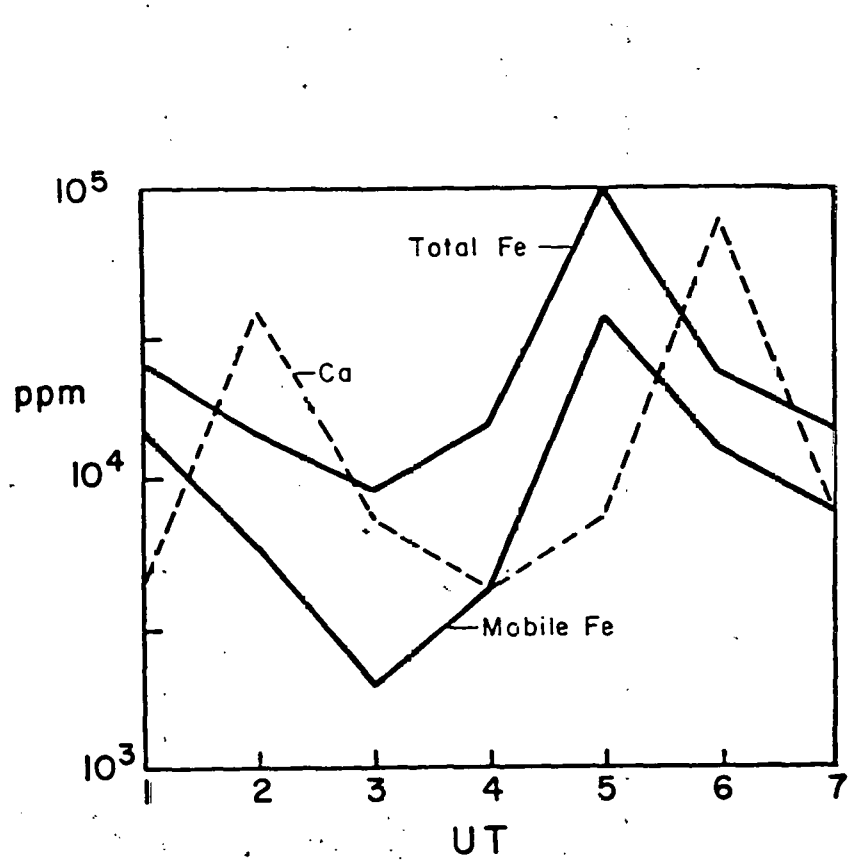
10^5
10^4
10^3
ppm
Total Fe
Ca
Mobile Fe
1
2
3
4
5
6
7
UT

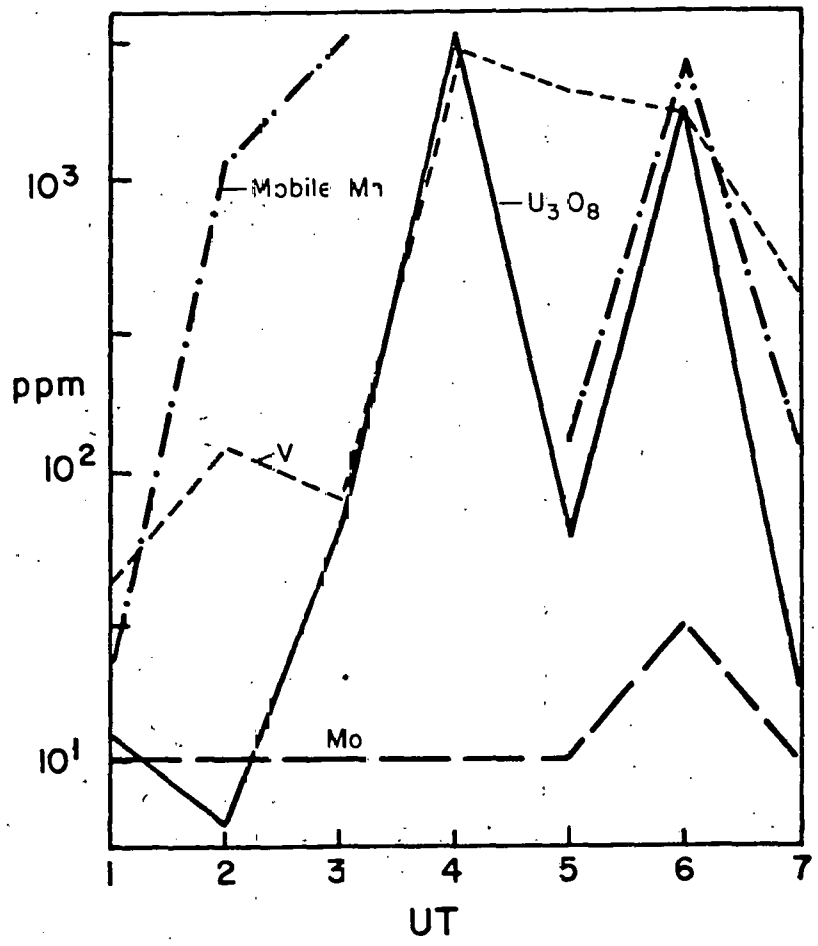
10^3
10^2
10^1
ppm
Mobile Mn
U_3O_8
V
Mo
1
2
3
4
5
6
7
UT

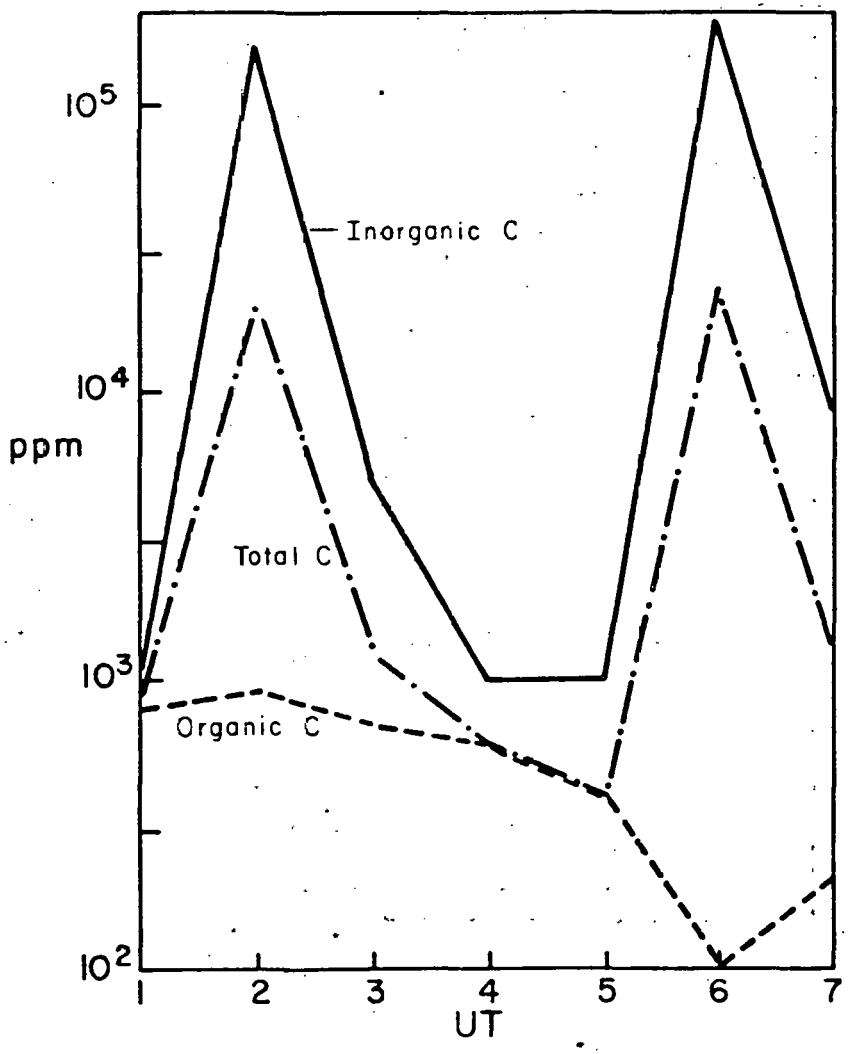
10^5
10^4
10^3
10^2
ppm
Inorganic C
Total C
Organic C
1
2
3
4
5
6
7
UT

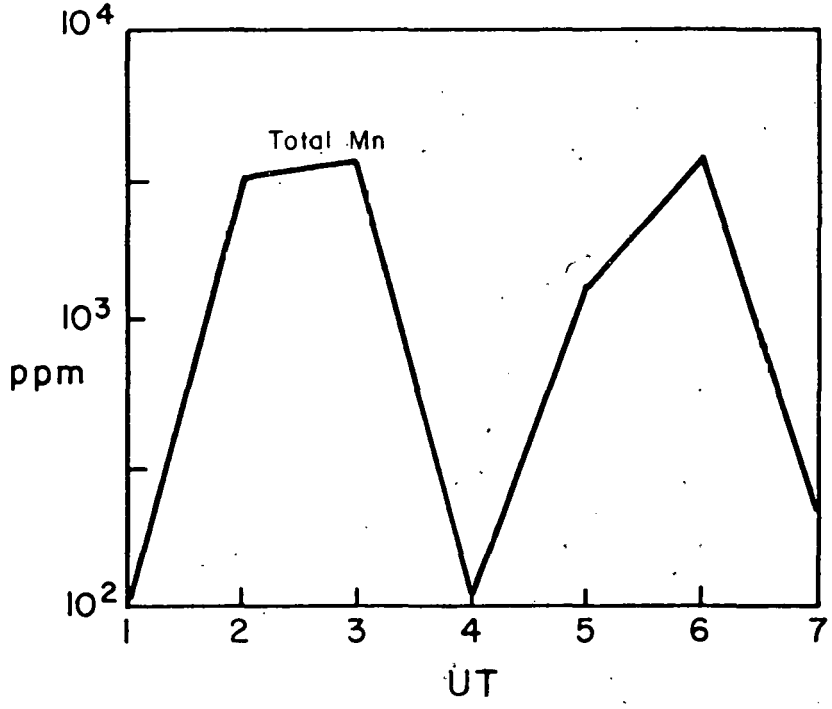
10^4
10^3
10^2
ppm
Total Mn
1
2
3
4
5
6
7
UT

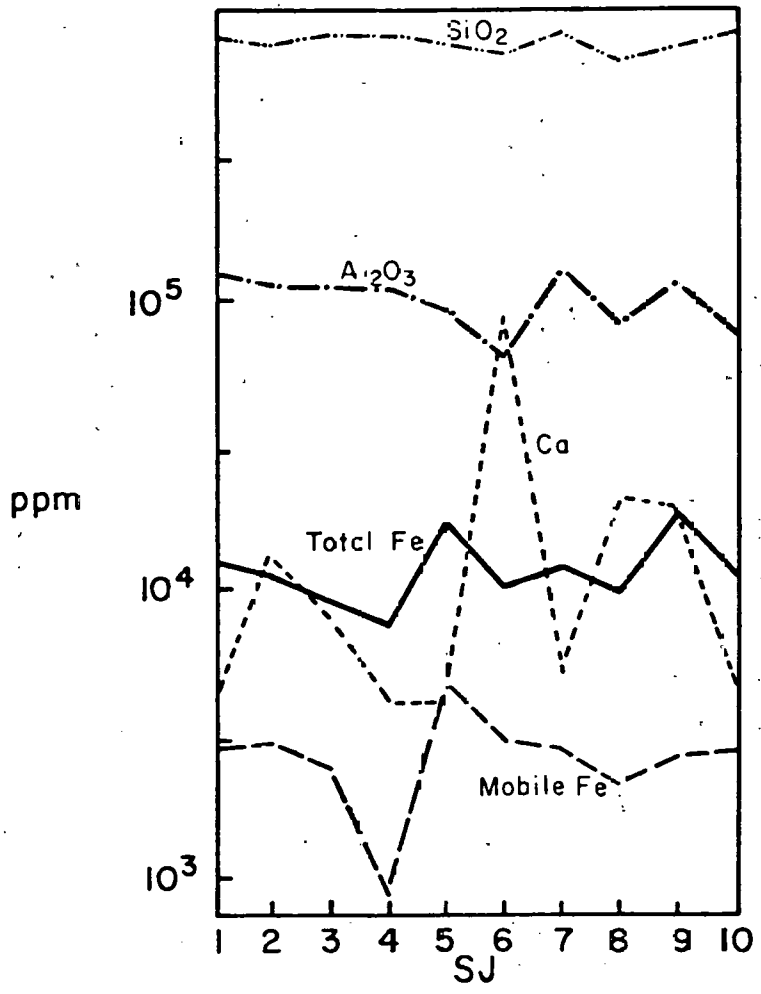
SiO2
Al2O3
Ca
Totcl Fe
Mobile Fe
ppm
10^5
10^4
10^3
1 2 3 4 5 6 7 8 9 10
SJ

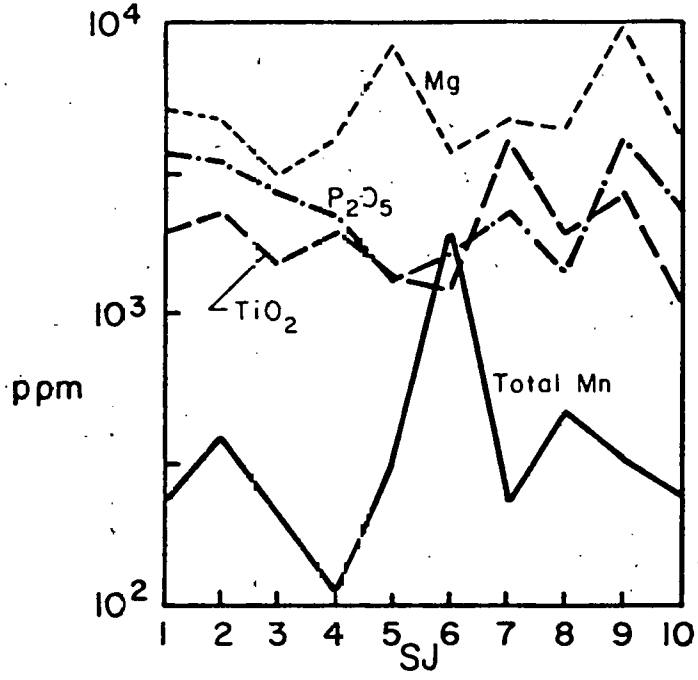
Mg
P2O5
TiO2
Total Mn
ppm
10^4
10^3
10^2
1 2 3 4 5 6 7 8 9 10
SJ

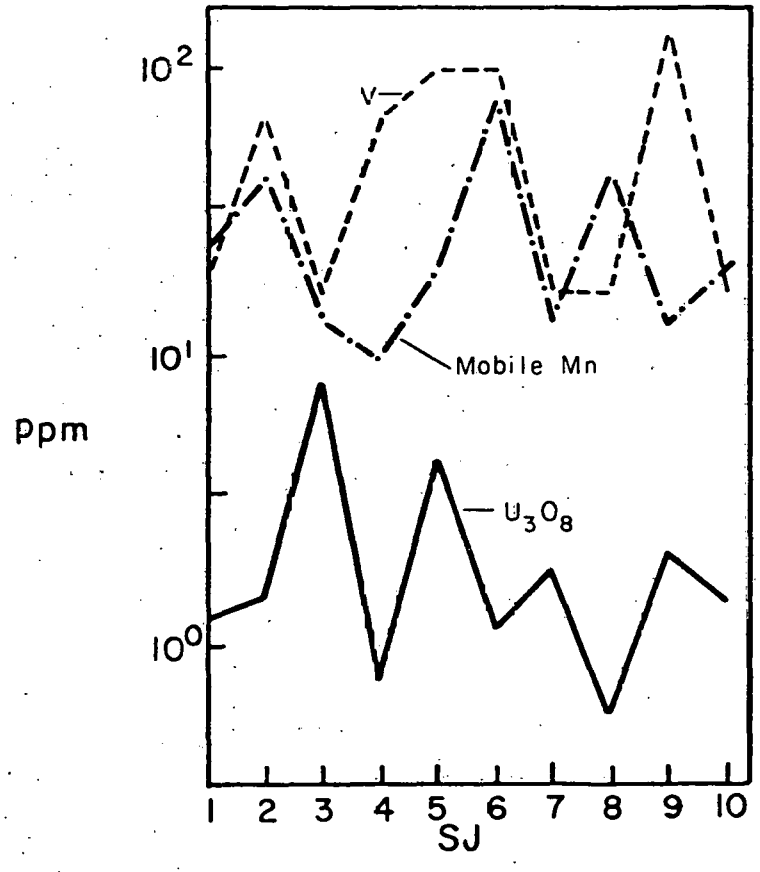
10^2
10^1
10^0
ppm
V
Mobile Mn
U_3O_8
1 2 3 4 5 6 7 8 9 10
SJ

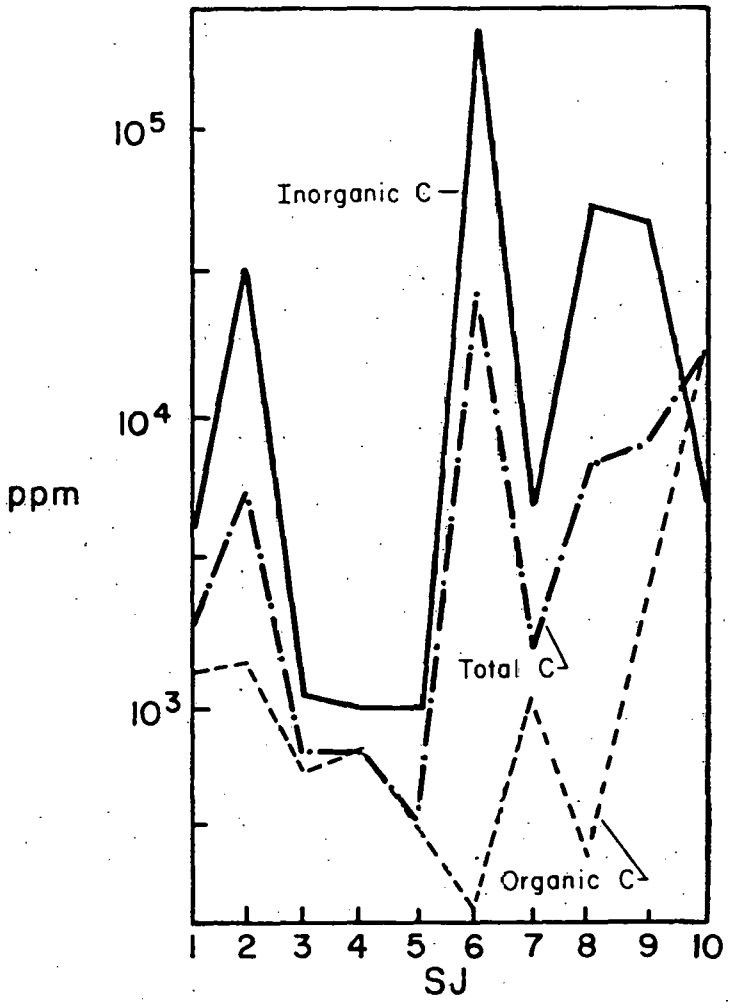
10^5
10^4
10^3
ppm
Inorganic C
Total C
Organic C
1 2 3 4 5 6 7 8 9 10
SJ

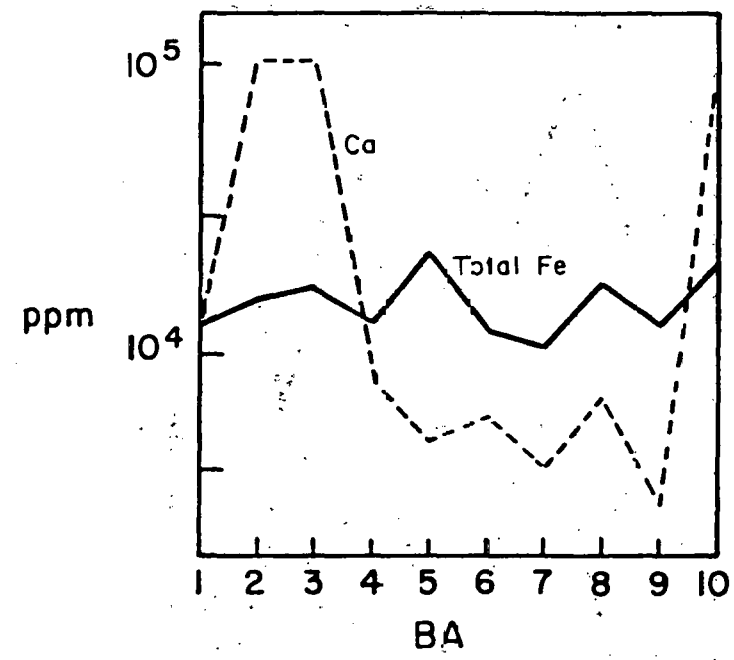
10^5
10^4
ppm
Ca
Total Fe
1 2 3 4 5 6 7 8 9 10
BA

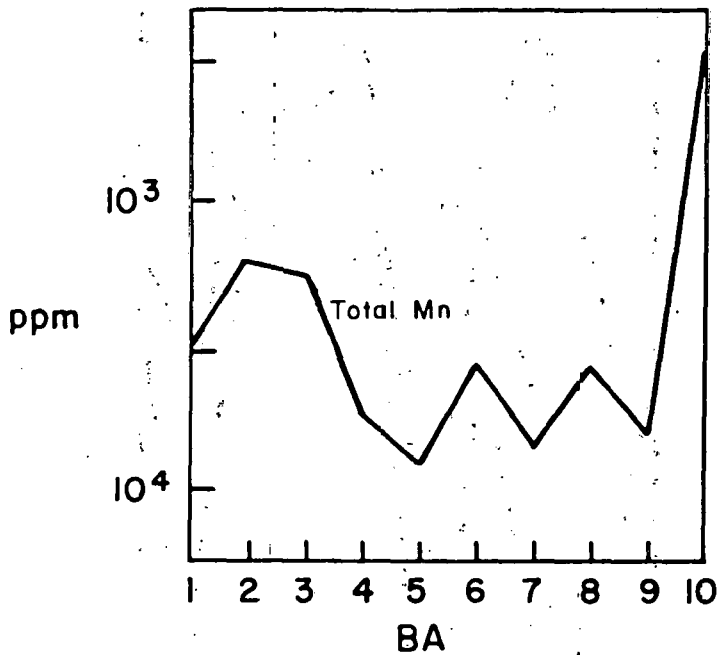
10^3
10^4
ppm
Total Mn
1 2 3 4 5 6 7 8 9 10
BA

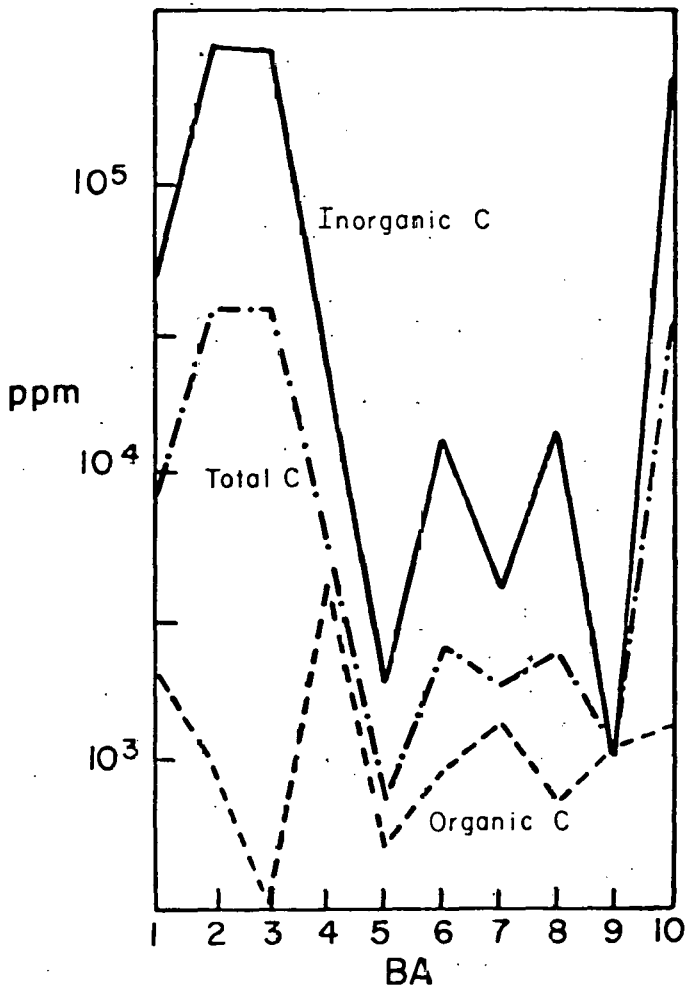
10^5
Inorganic C
ppm
10^4
Total C
10^3
Organic C
1 2 3 4 5 6 7 8 9 10
BA

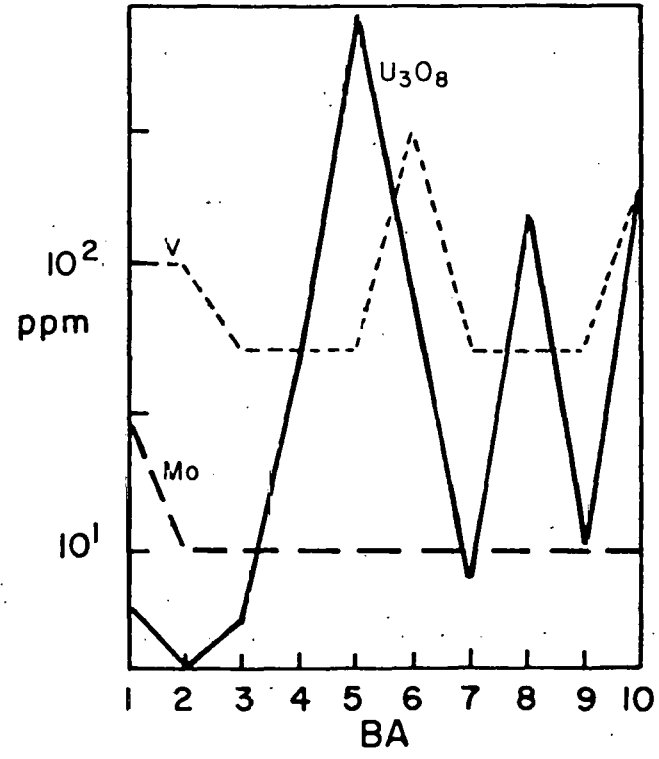
U_3O_8
10^2
V
ppm
Mo
10^1
1 2 3 4 5 6 7 8 9 10
BA

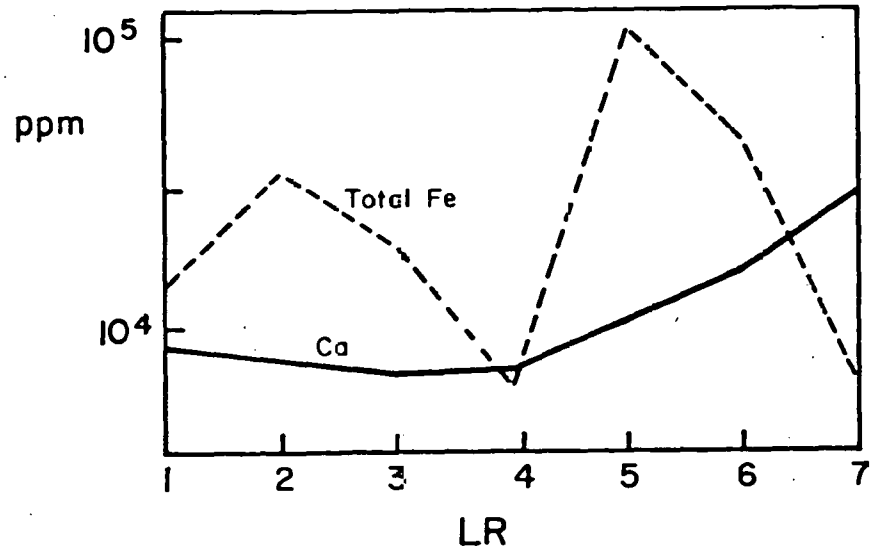
10^5
ppm
Total Fe
10^4
Ca
1
2
3
4
5
6
7
LR

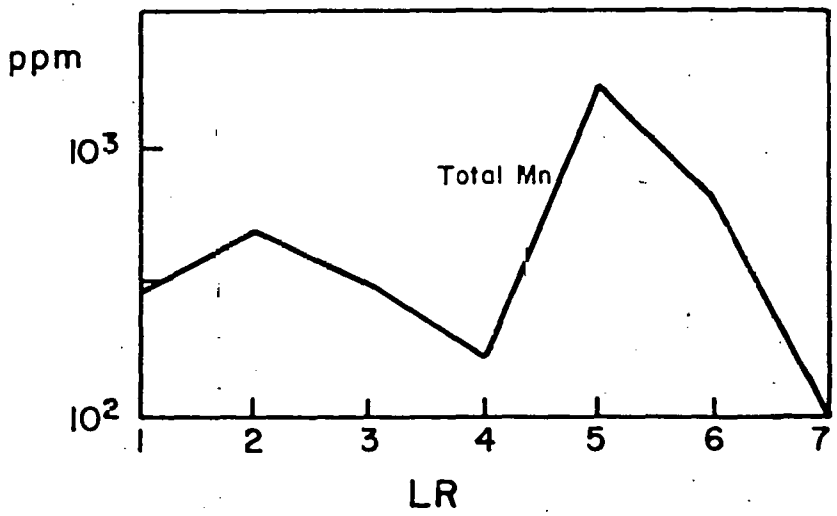
ppm
10^3
Total Mn
10^2
1
2
3
4
5
6
7
LR

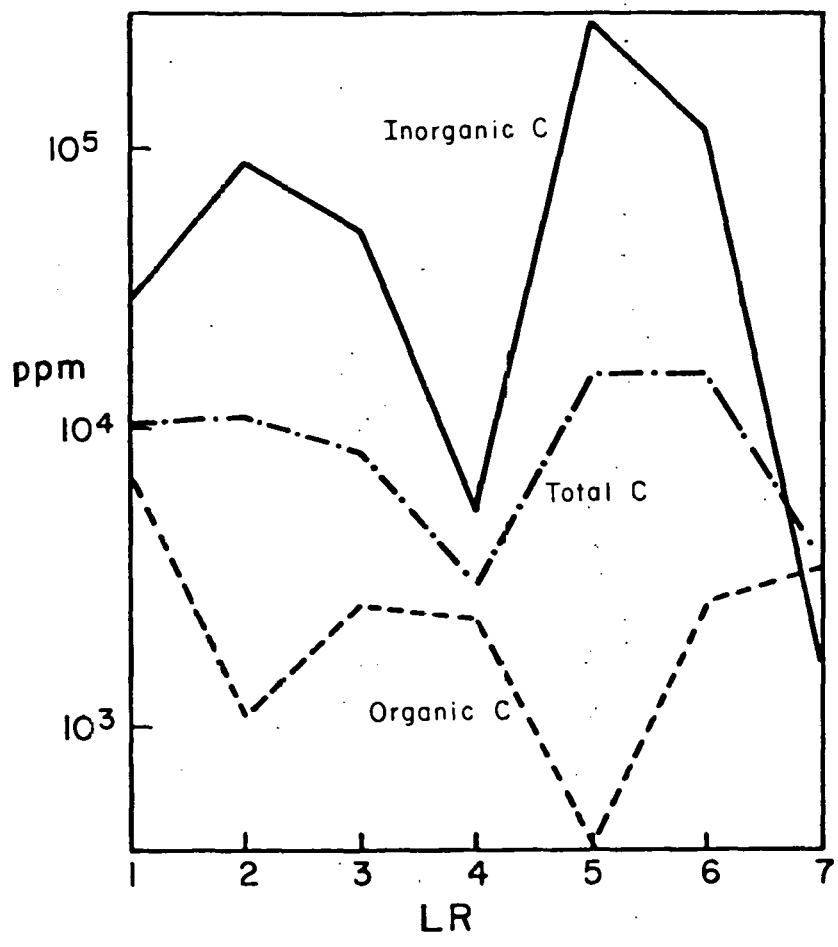
Inorganic C
Total C
Organic C
ppm
10^5
10^4
10^3
1
2
3
4
5
6
7
LR

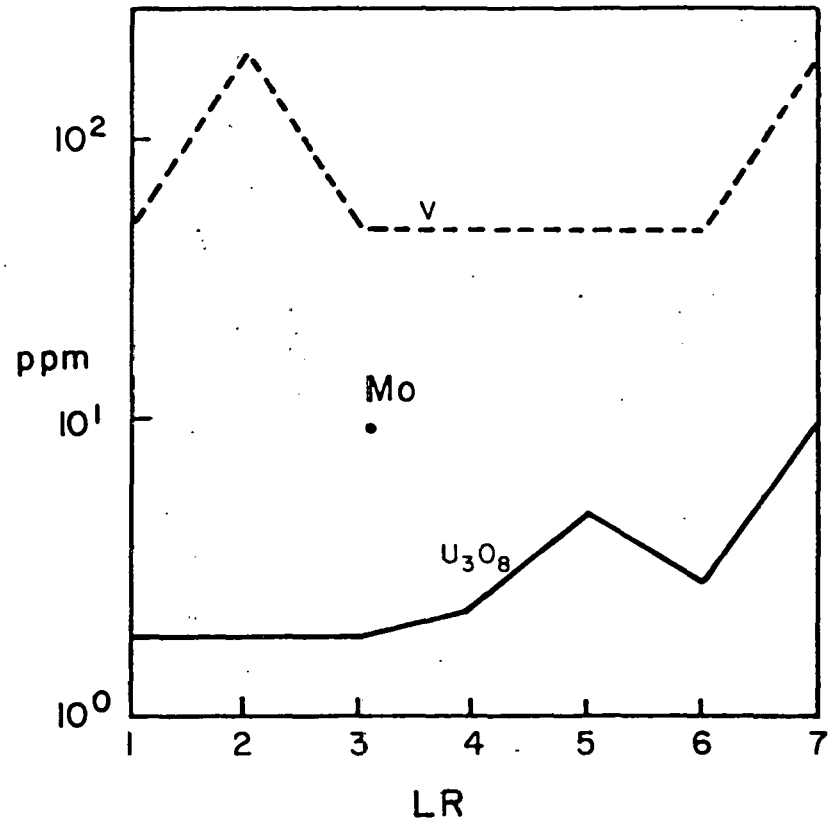
V
Mo
U_3O_8
ppm
10^2
10^1
10^0
1
2
3
4
5
6
7
LR

APPENDIX C

Results of geochemical analyses and photometric measurements for sample grids.*

*Computer contour plots courtesy of Phillips Petroleum Company.

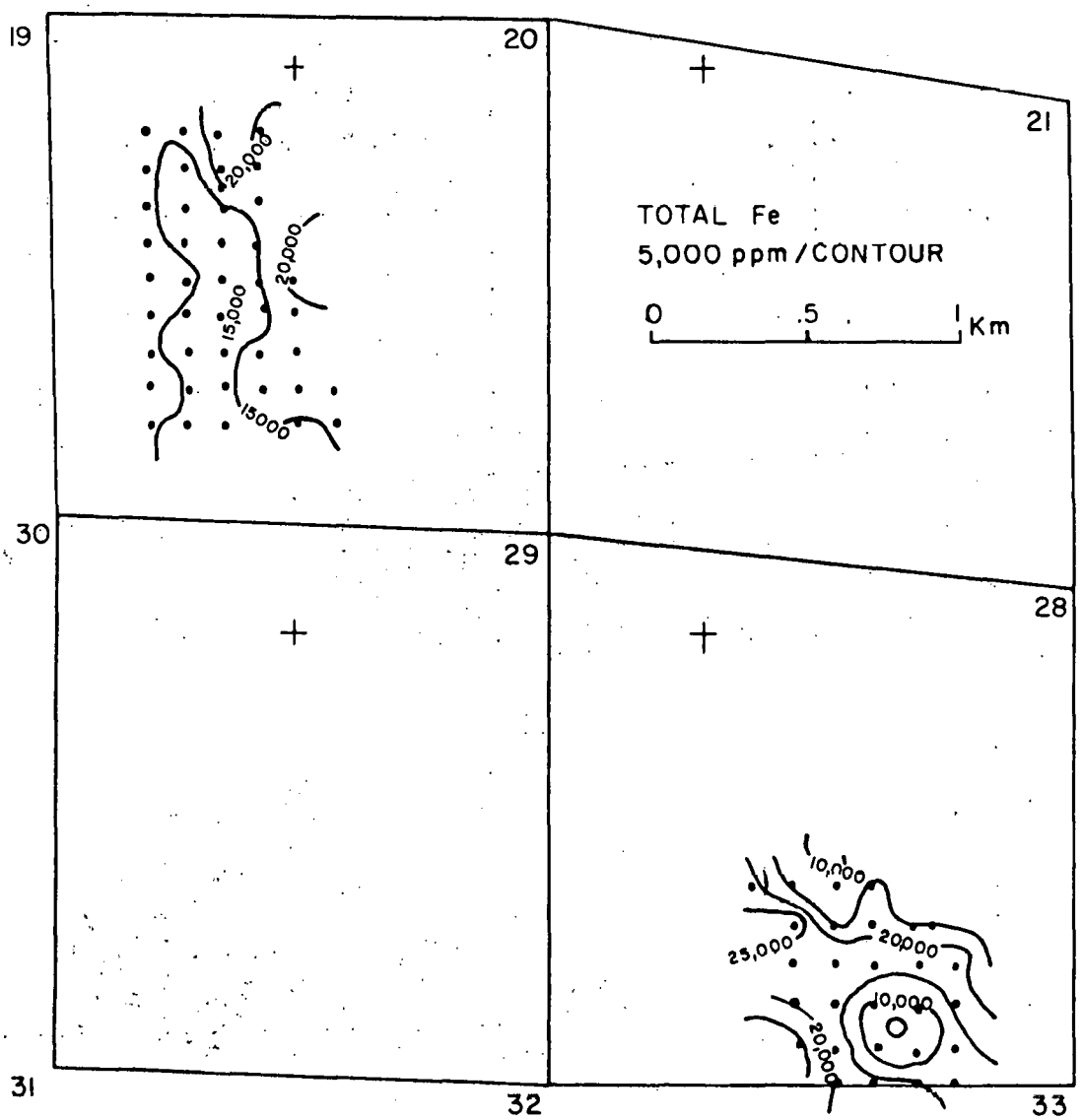
19
20
21
30
29
28
31
32
33
TOTAL Fe
5,000 ppm / CONTOUR
0
.5
1 Km
20,000
20,000
15,000
15000
10,000
25,000
20,000
10,000
20,000

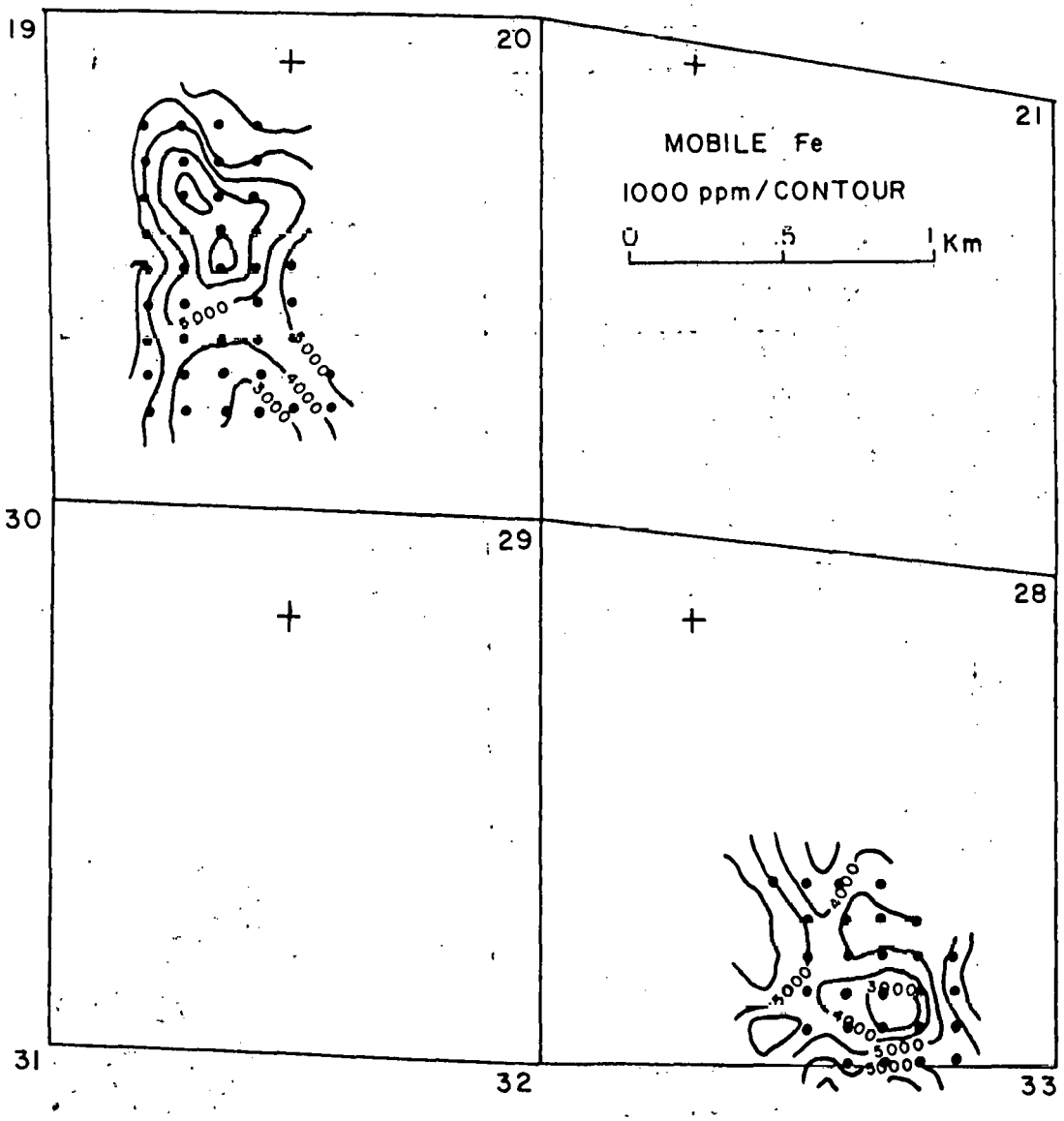
19
20
21
30
29
28
31
32
33
MOBILE Fe
1000 ppm/CONTOUR
0
.5
1 Km
5000
5000
4000
3000
4000
3000
5000
4000
5000
3000

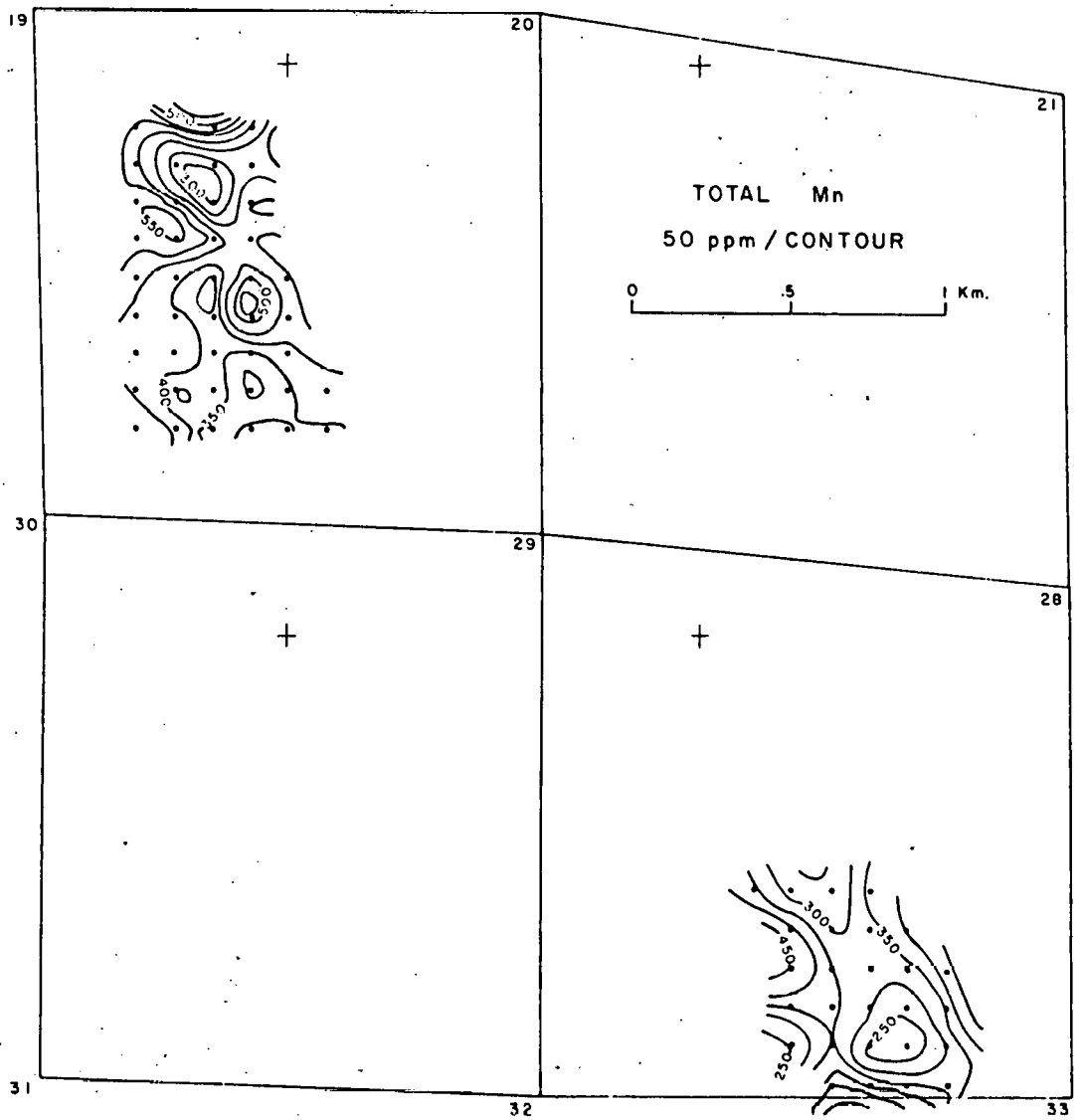
19
20
21
30
29
28
31
32
33
TOTAL Mn
50 ppm / CONTOUR
0
.5
1 Km.
500
550
400
450
300
350
250
250

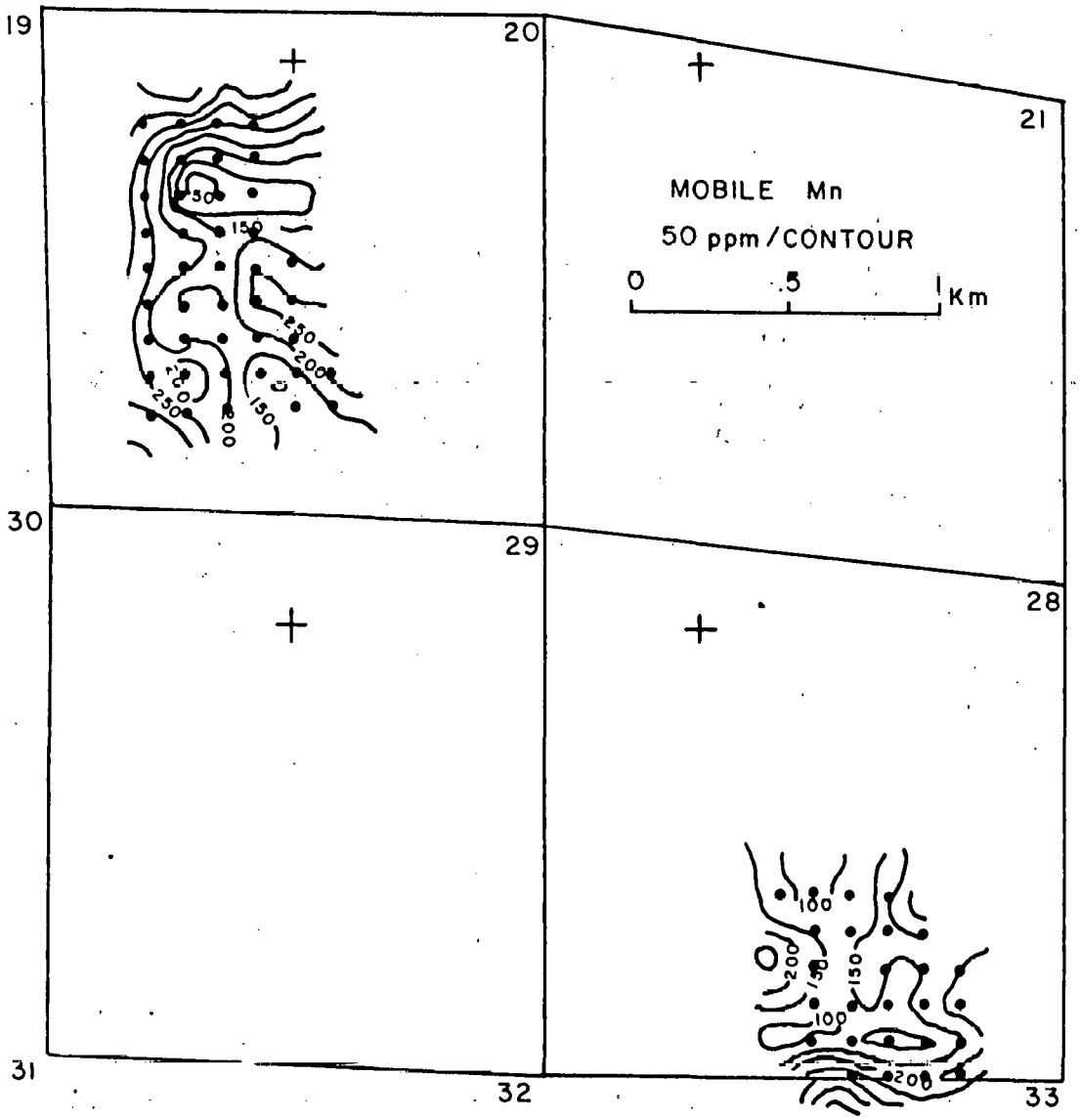
19
20
21
30
29
28
31
32
33
MOBILE Mn
50 ppm / CONTOUR
0
.5
1 Km
50
150
200
250
100
150
100
200
150
100
200

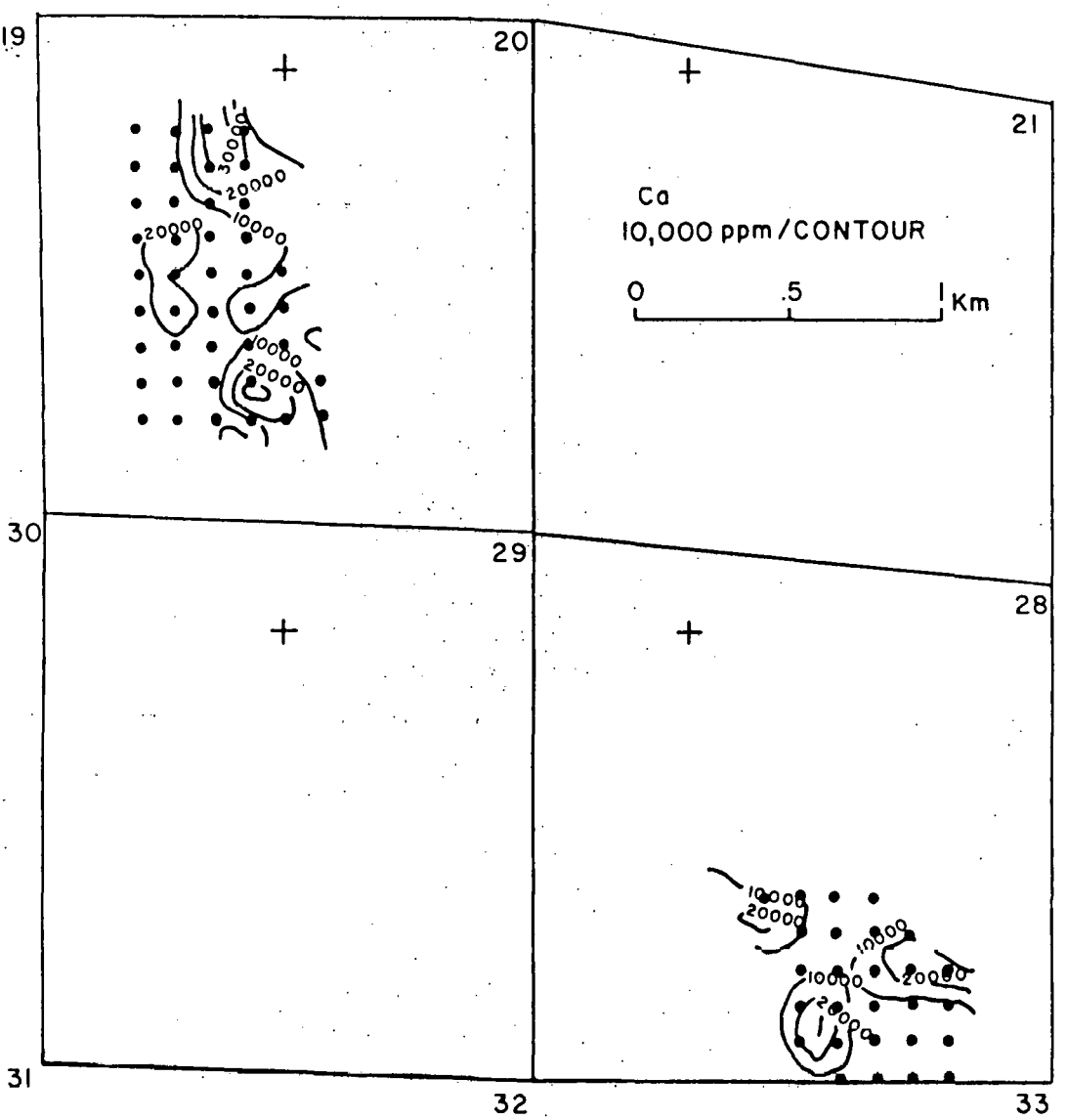
19
20
21
30
29
28
31
32
33
Ca
10,000 ppm / CONTOUR
0
.5
1 Km
10000
20000
30000

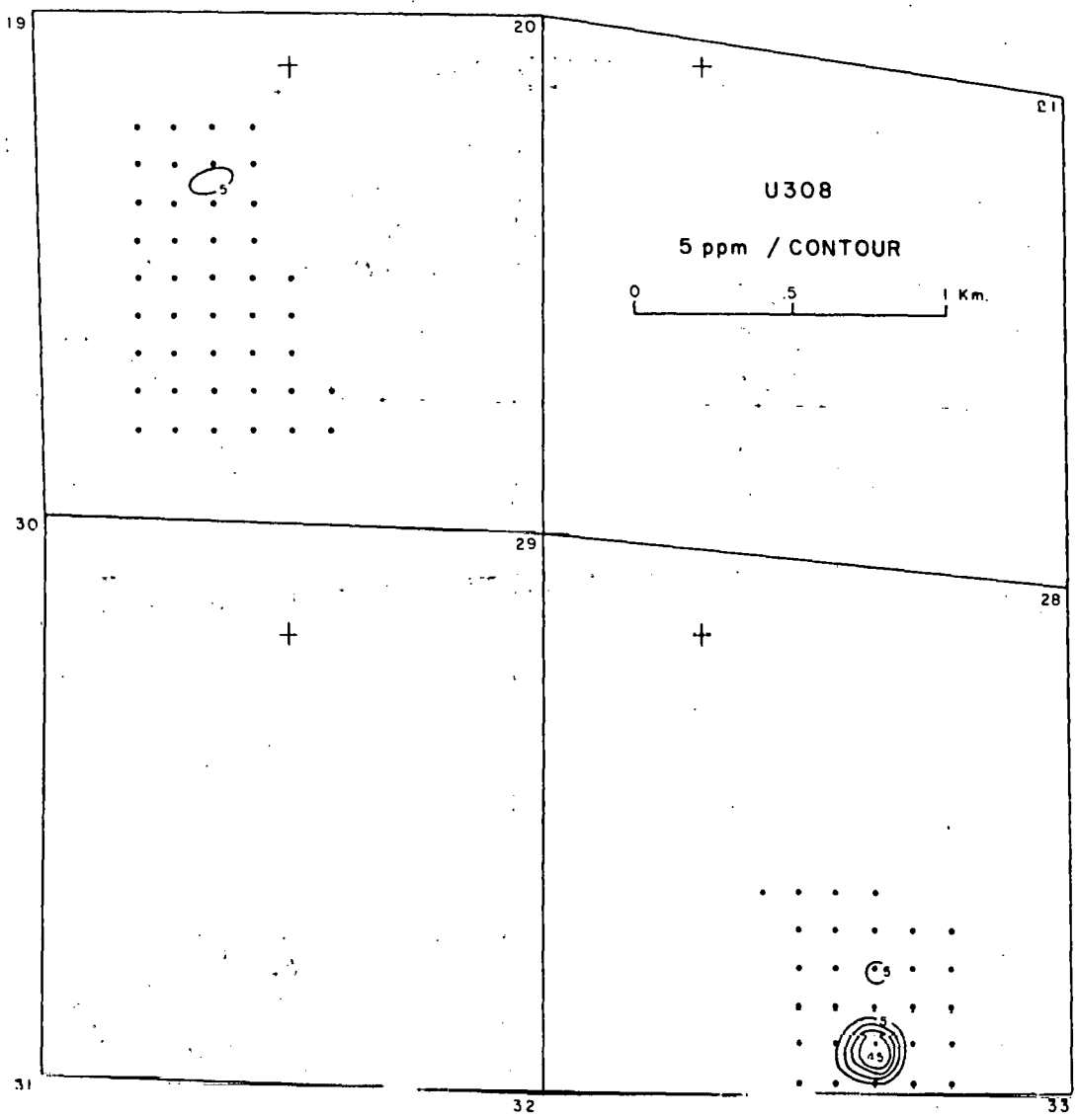
19
20
21
U308
5 ppm / CONTOUR
0
.5
1 Km.
30
29
28
31
32
33

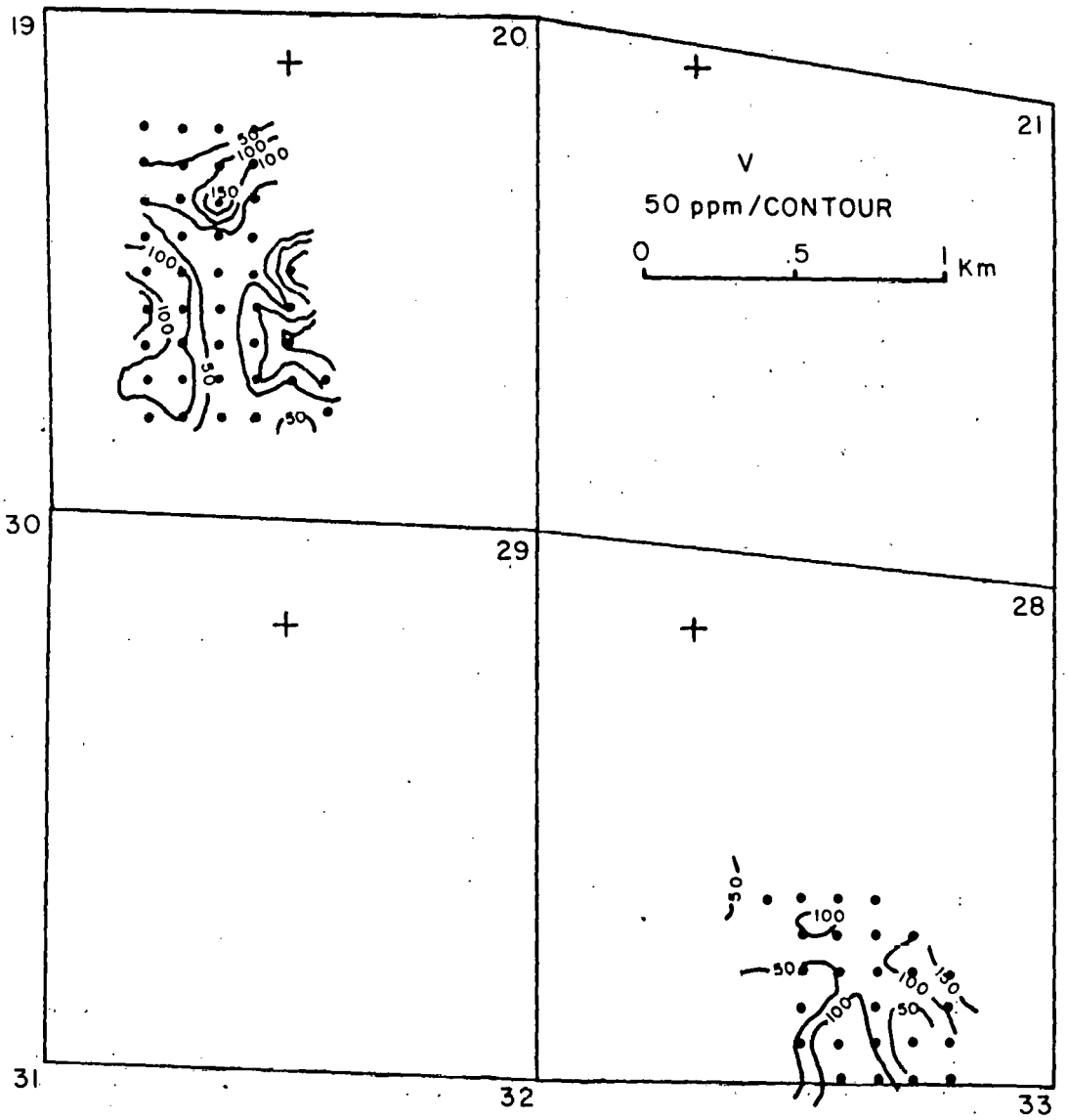
19
20
21
V
50 ppm/CONTOUR
0
.5
1 Km
30
29
28
31
32
33
50
100
150

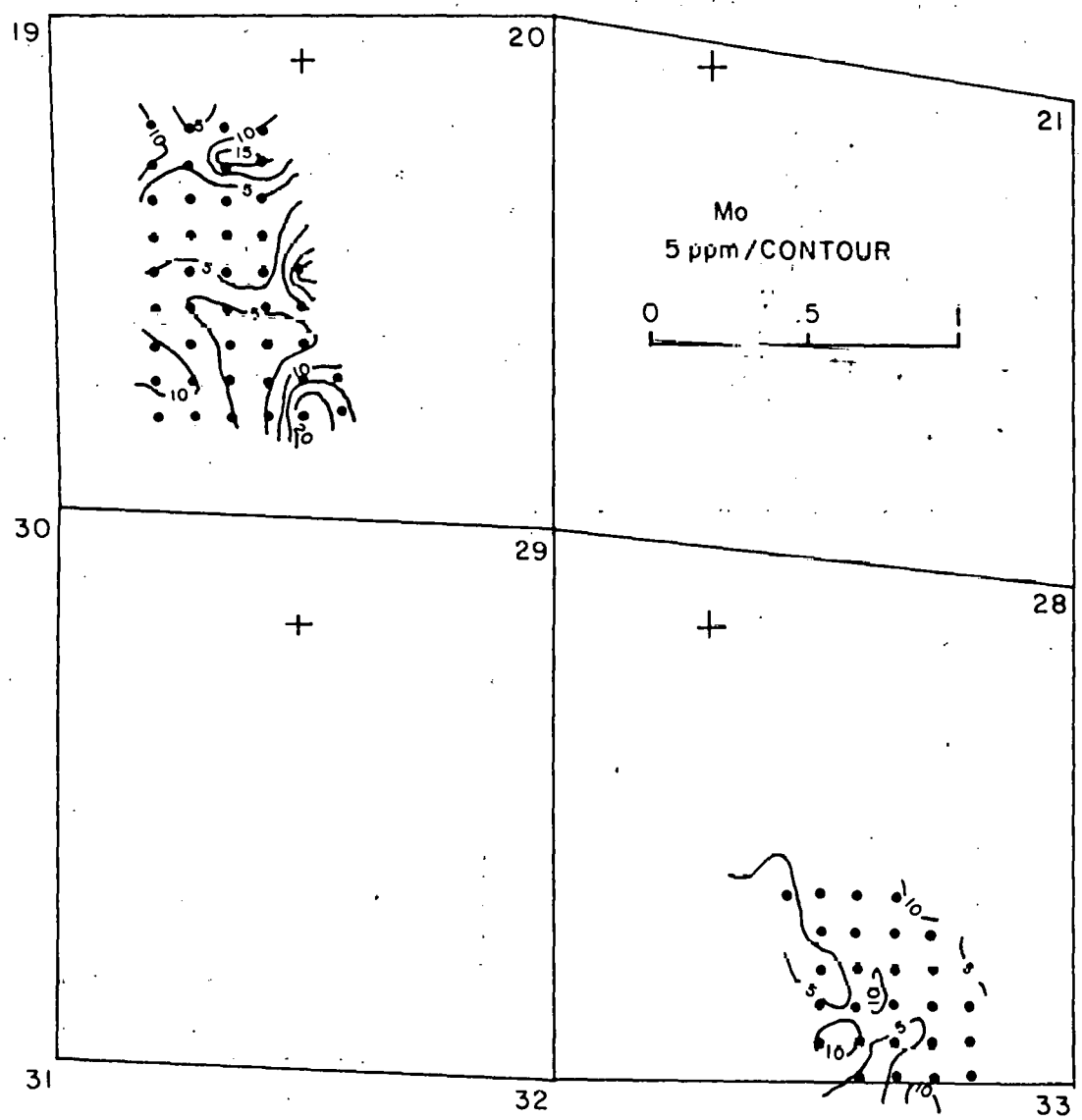
19
20
21
30
29
28
31
32
33
Mo
5 ppm/CONTOUR
0
.5
1

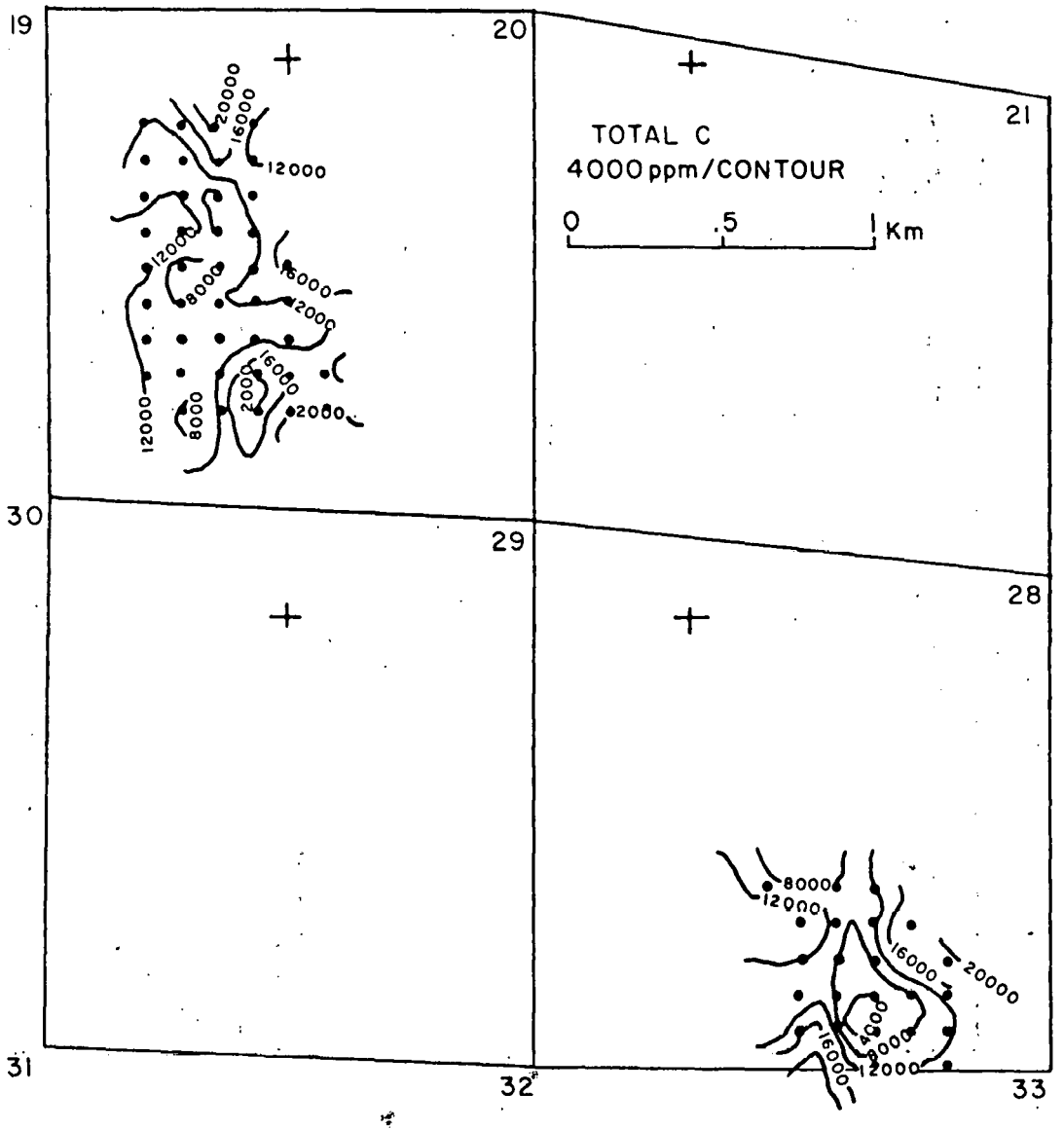
19
20
21
30
29
28
31
32
33
TOTAL C
4000 ppm/CONTOUR
0
.5
1 Km
20000
16000
12000
8000
2000

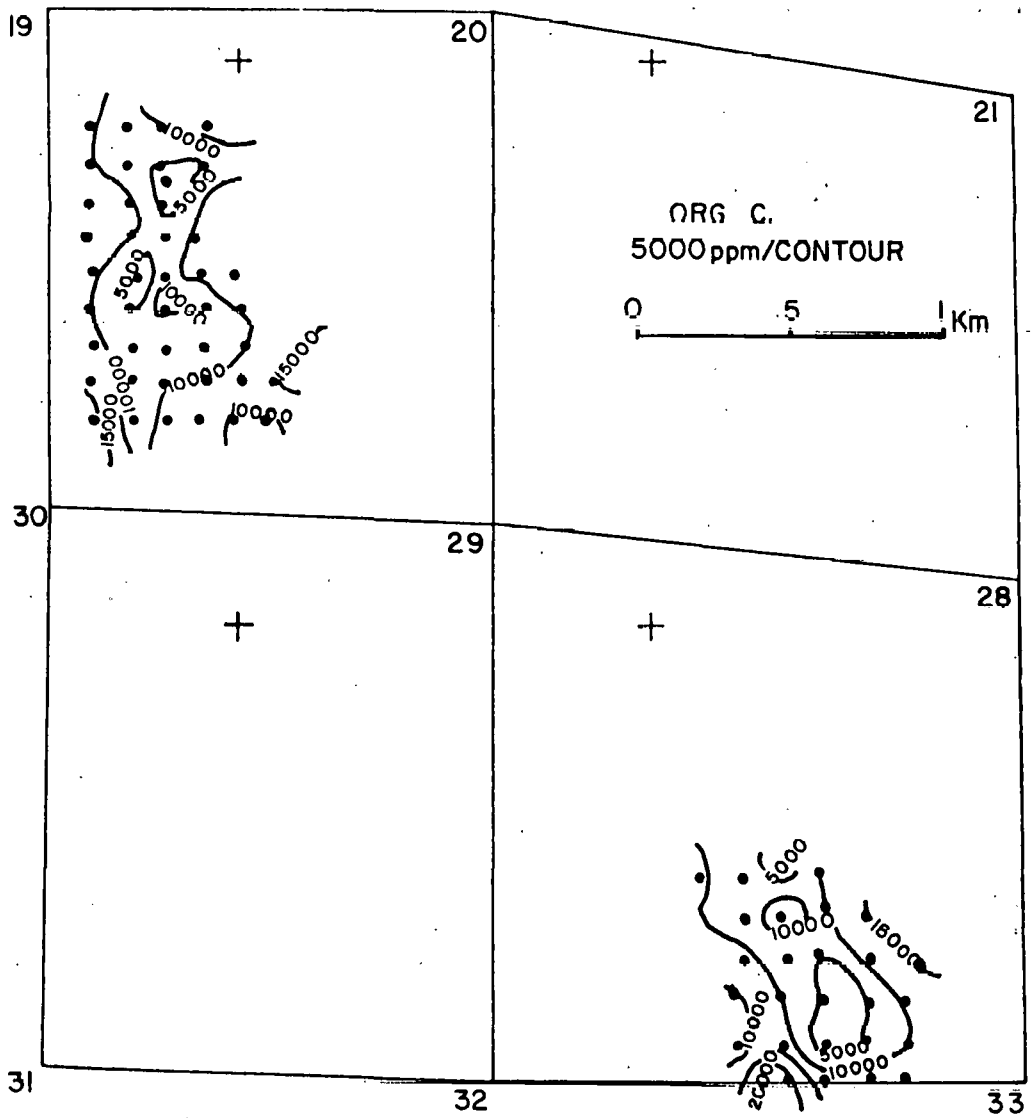
19
20
21
30
29
28
31
32
33
ORG C.
5000 ppm/CONTOUR
0
5
1 Km
10000
5000
15000
5000
10000
15000
10000
10000
5000
10000
18000
10000
5000
10000
2000

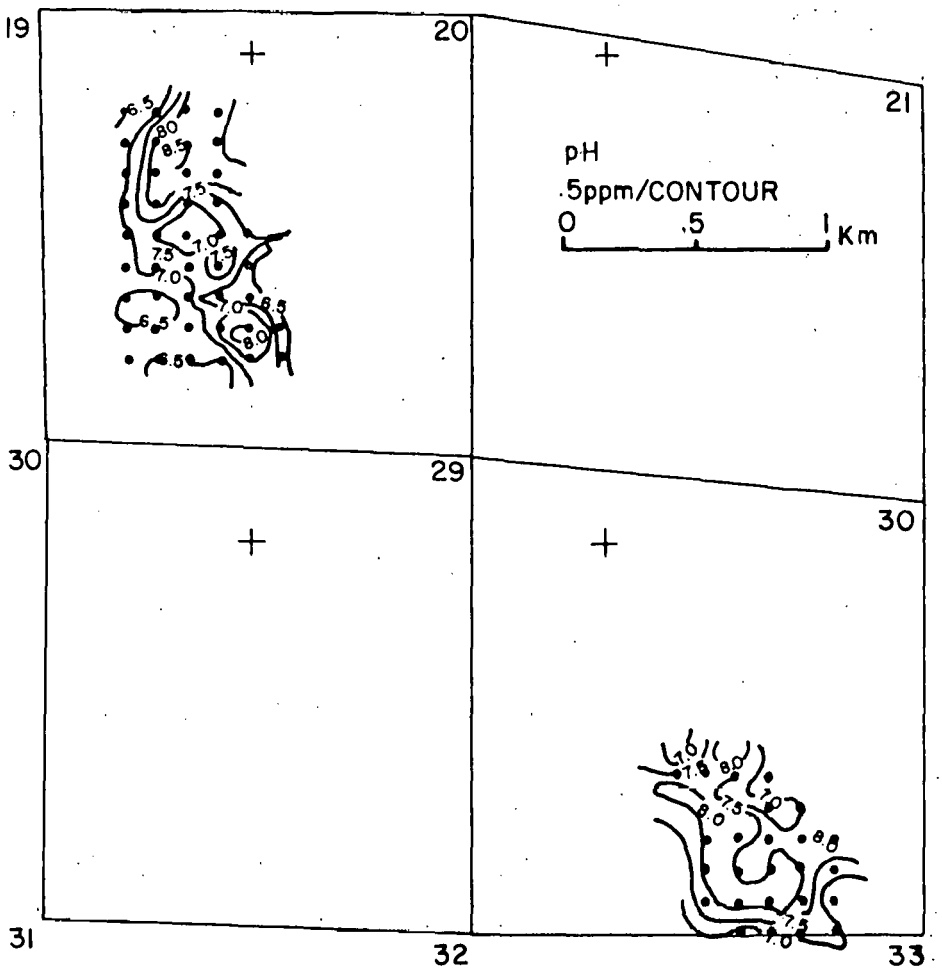
19
20
21
pH
.5ppm/CONTOUR
0 .5 1 Km
30
29
30
31
32
33

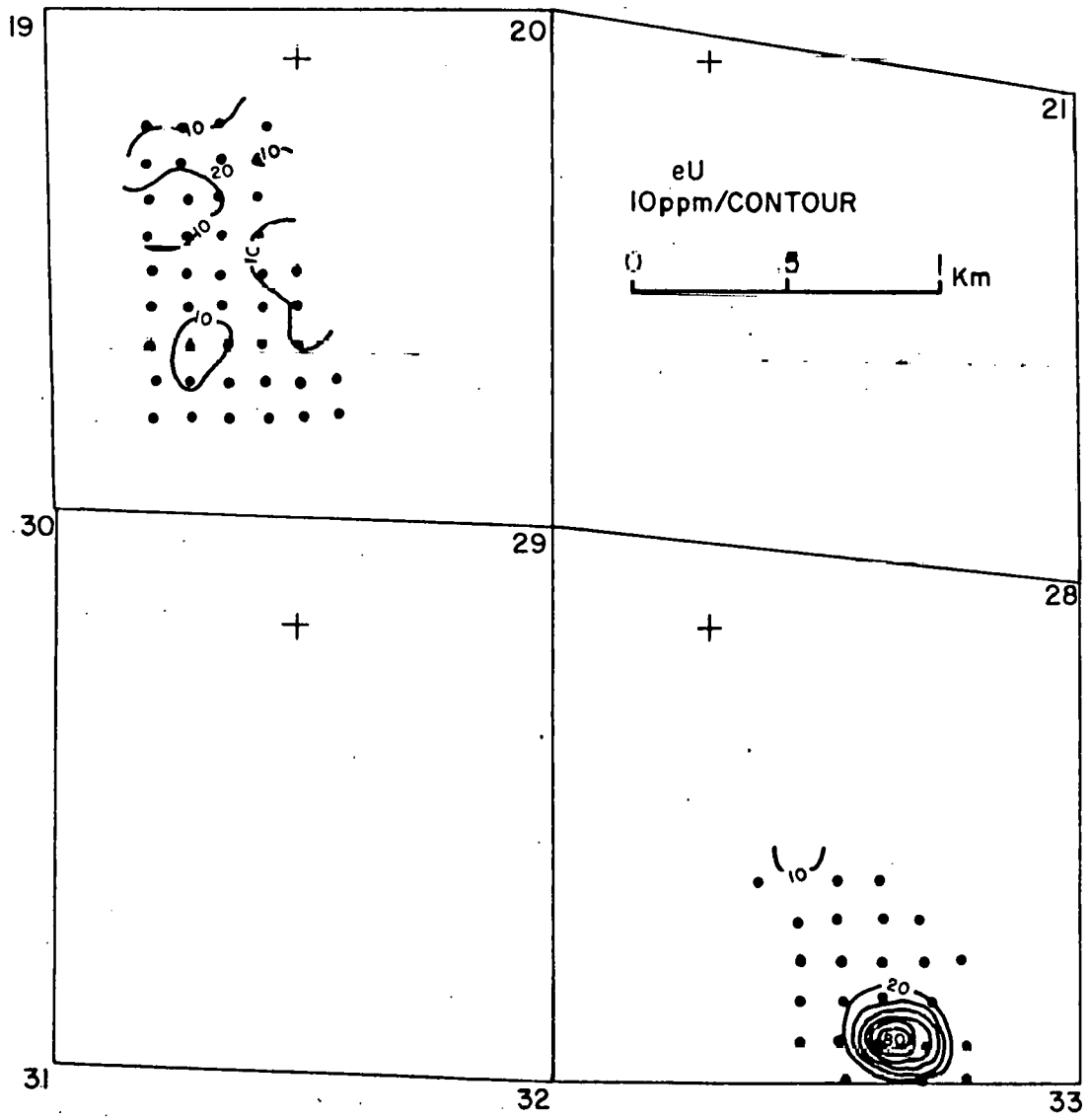
19
20
21
30
29
28
31
32
33
10
20
10
10
10
10
20
30
eU
10ppm/CONTOUR
0
5
Km

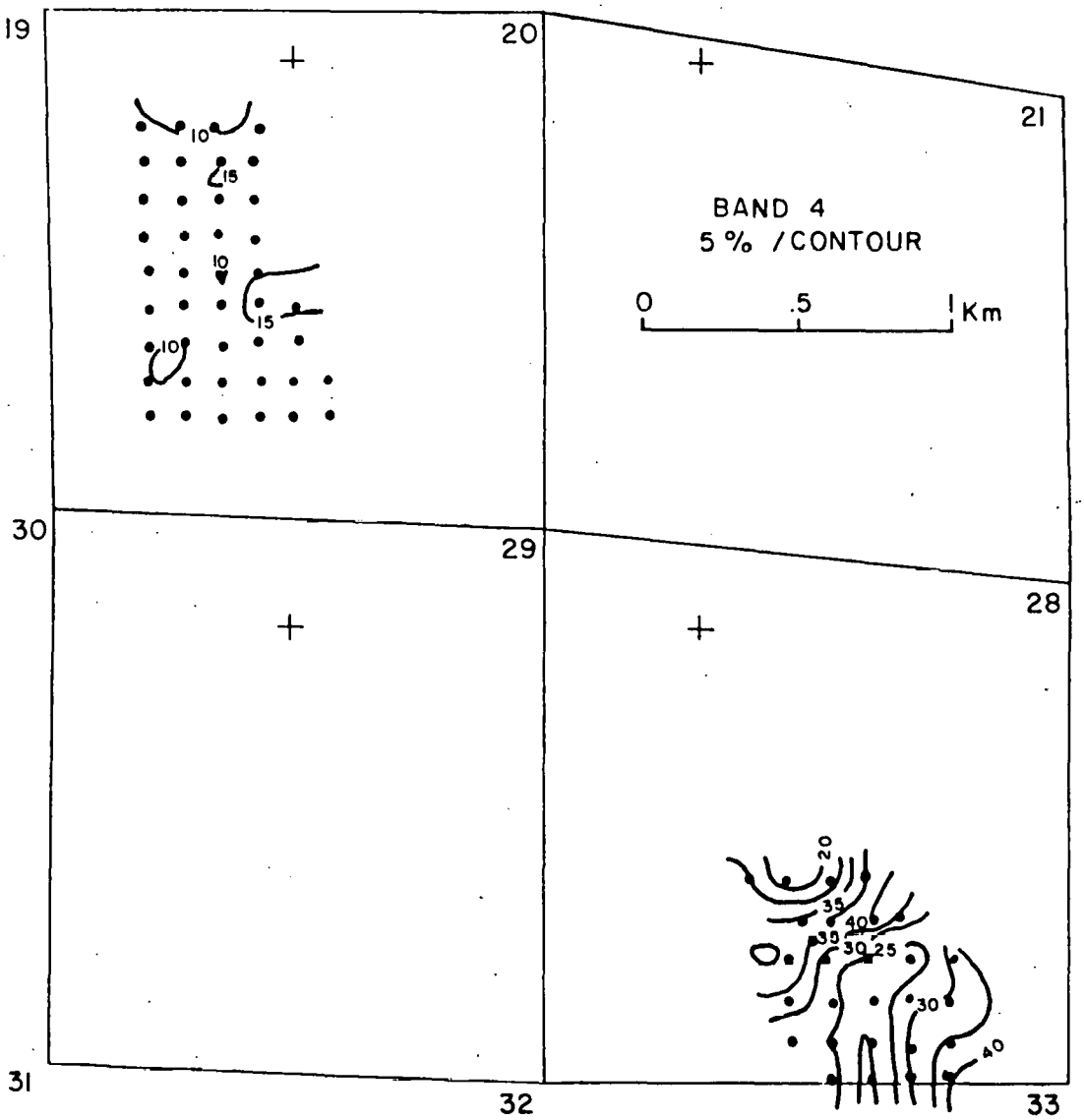
19
20
21
30
29
28
31
32
33
10
15
10
15
10
BAND 4
5 % /CONTOUR
0
.5
1 Km
20
35
40
35
30
25
30
40

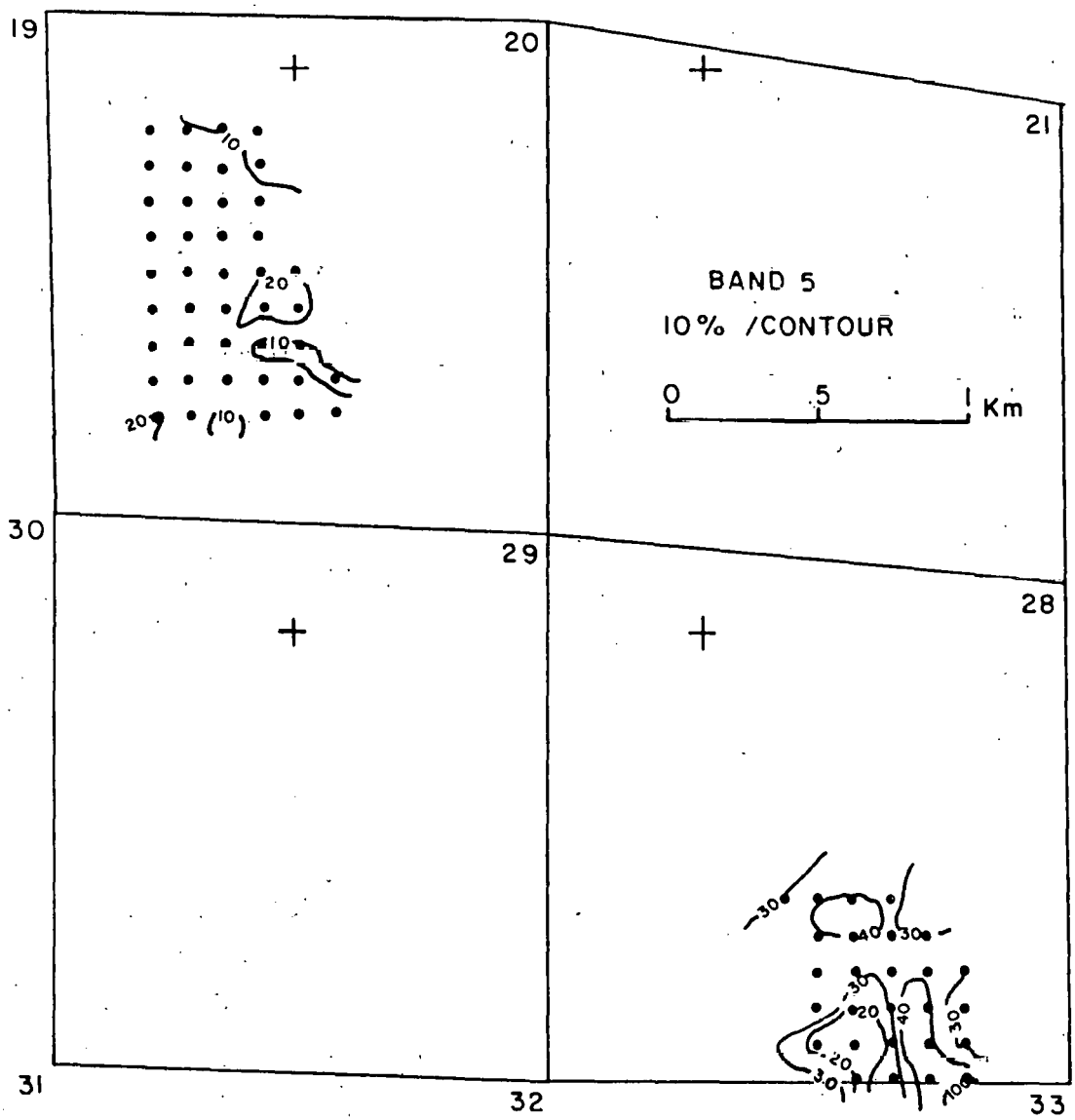
19
20
21
30
29
28
31
32
33
BAND 5
10% /CONTOUR
0
5
1 Km
10
20
10
20
(10)
30
40
30
30
20
40
30
20
30
40

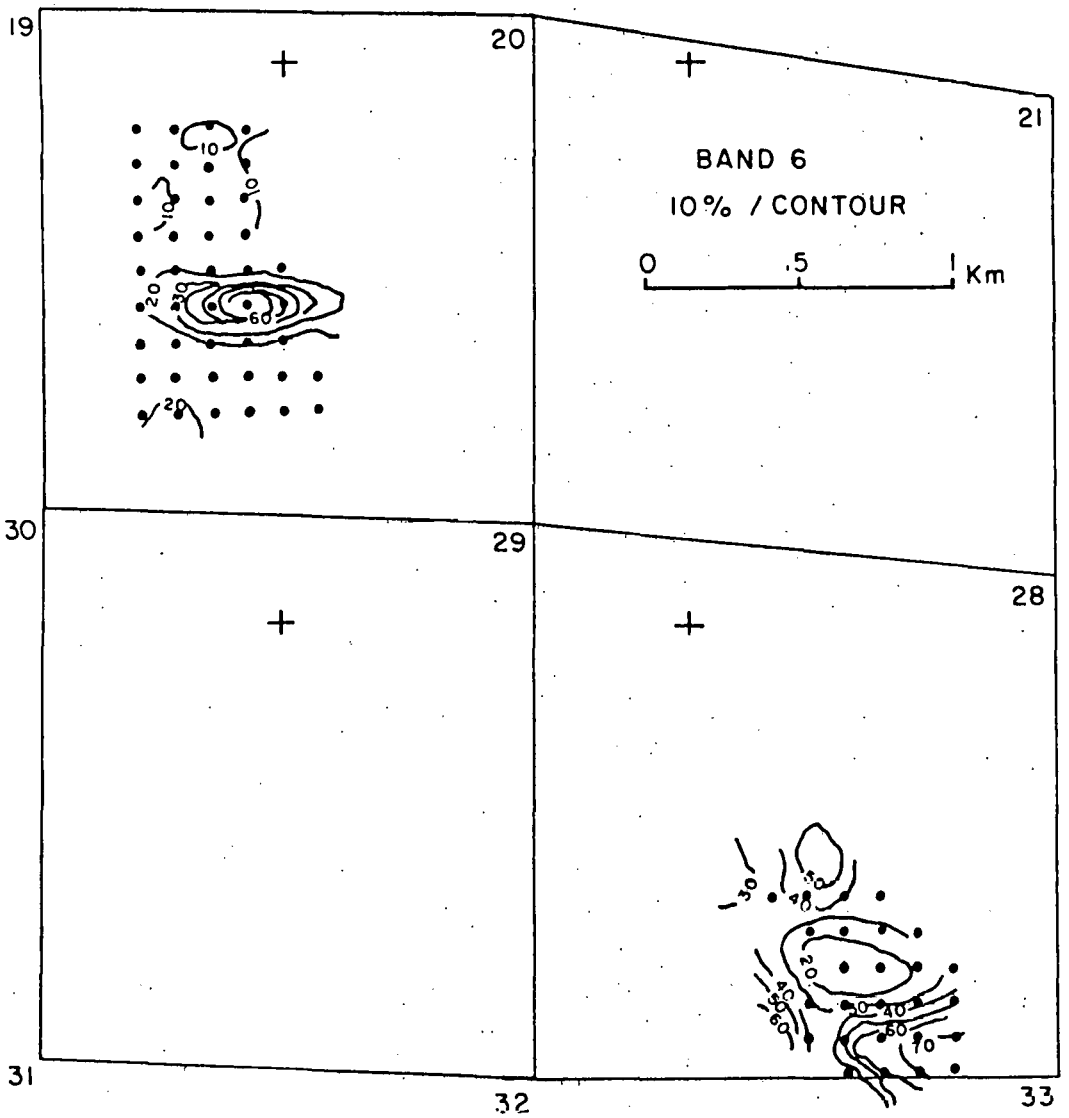
19
20
21
BAND 6
10% / CONTOUR
0
.5
1
Km
30
29
28
31
32
33

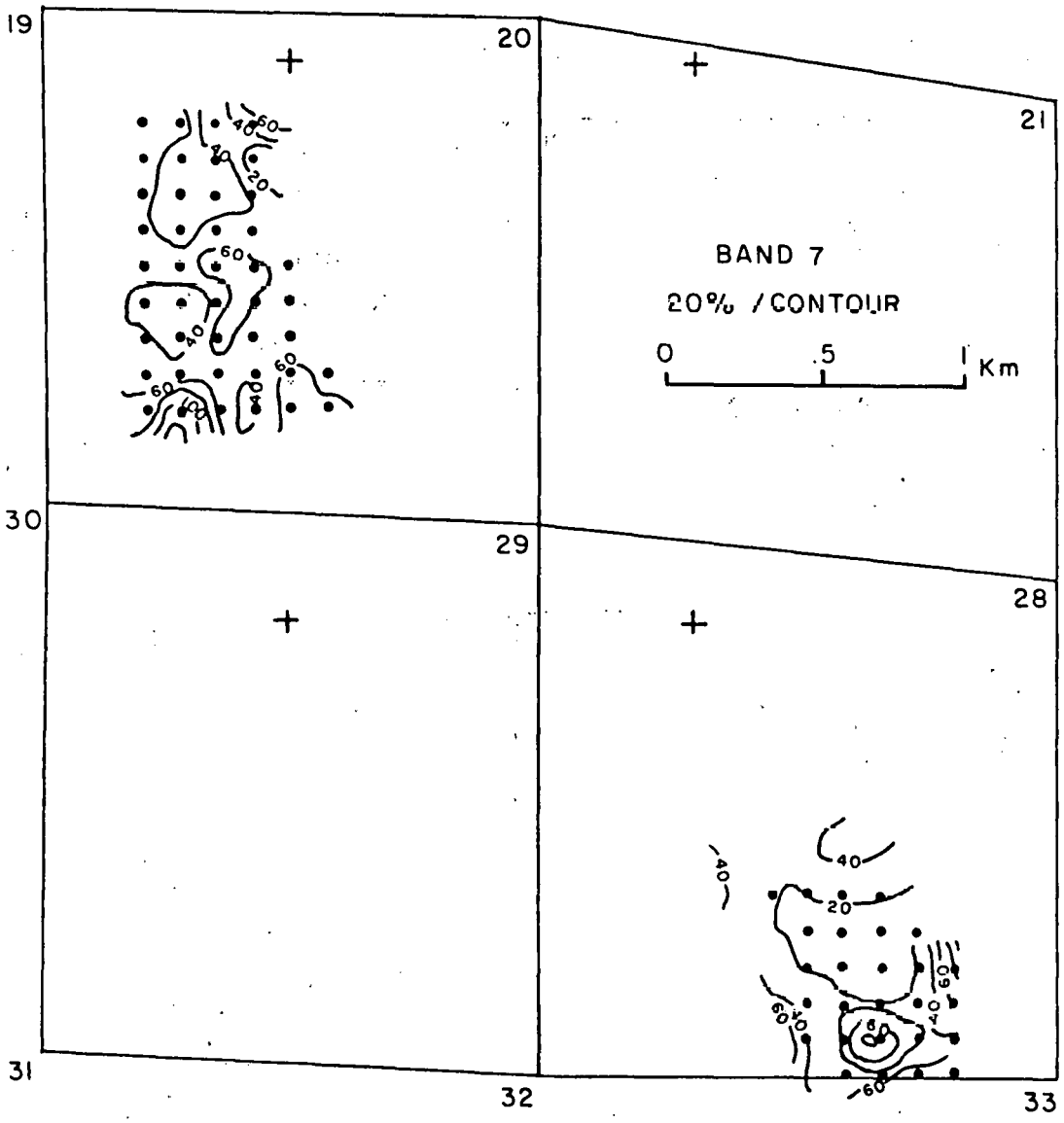
19
20
21
30
29
28
31
32
33
BAND 7
20% / CONTOUR
0
.5
1 Km

APPENDIX D

Spectral curves collected in the Pumpkin Buttes area with the Portable Field Reflectance Spectrometer* (PFRS) and geological sketch maps and cross-sections of spectrometer sample areas.

*PFRS developed by and made available through NASA/JPL.

GEOLOGIC SKETCH MAP
AND
CROSS-SECTION OF THE BLOWOUT ANOMALY #119
NE 1/4, SE1/4, Sect. 11, T45N, R75W, CAMPBELL CO., WYOMING

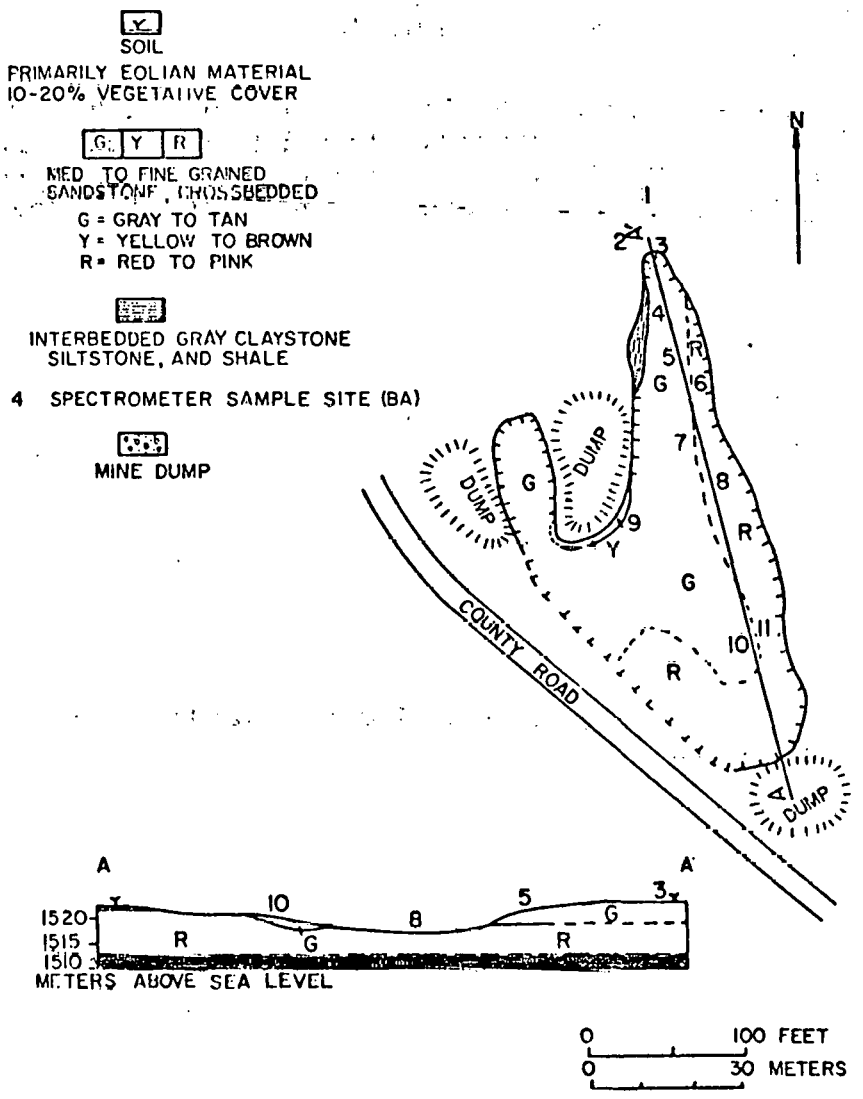

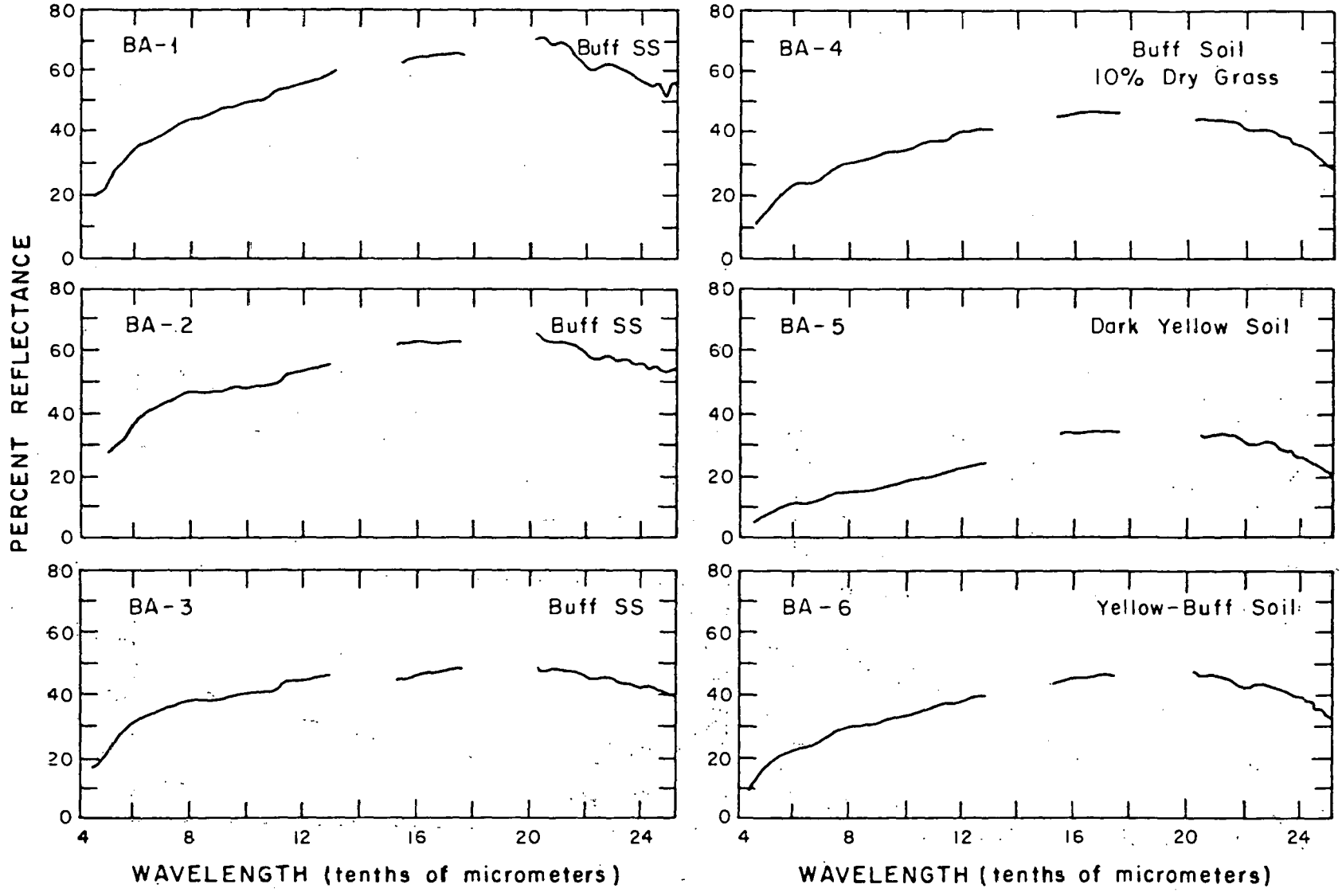
BA-1
Buff SS
BA-2
Buff SS
BA-3
Buff SS
BA-4
Buff Soil
10% Dry Grass
BA-5
Dark Yellow Soil
BA-6
Yellow-Buff Soil
PERCENT REFLECTANCE
0
20
40
60
80
4
8
12
16
20
24
WAVELENGTH (tenths of micrometers)
WAVELENGTH (tenths of micrometers)

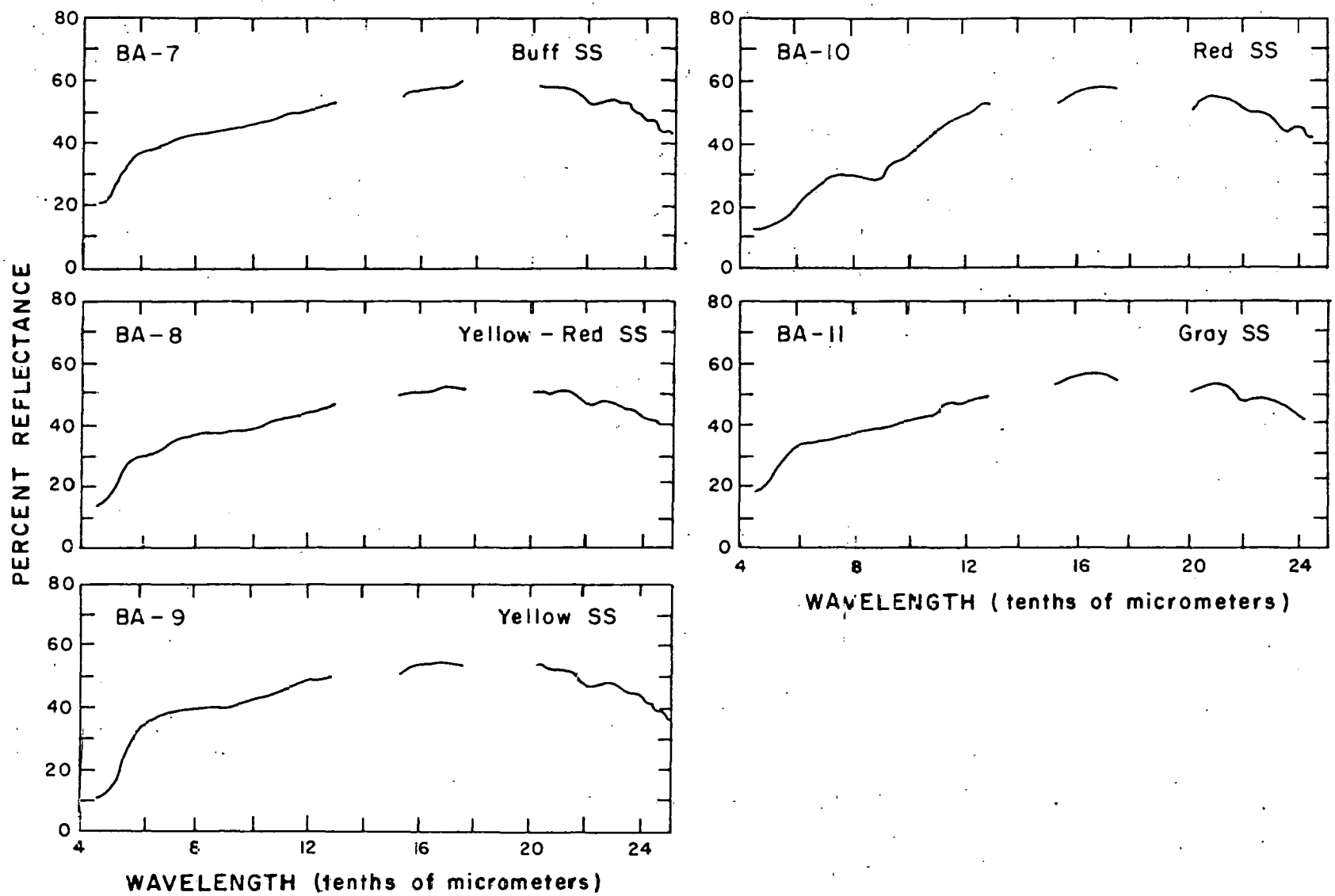
BA-7
Buff SS
BA-8
Yellow - Red SS
BA-9
Yellow SS
BA-10
Red SS
BA-11
Gray SS
PERCENT REFLECTANCE
0
20
40
60
80
4
8
12
16
20
24
WAVELENGTH (tenths of micrometers)

GEOLOGICAL SKETCH MAP AND CROSS-SECTION OF JEANNETTE I MINE
SE 1/4, NE 1/4, Sect. 22, T45N, R75W, CAMPBELL CO., WYOMING

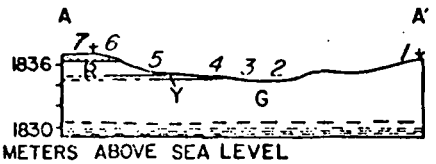

METERS ABOVE SEA LEVEL

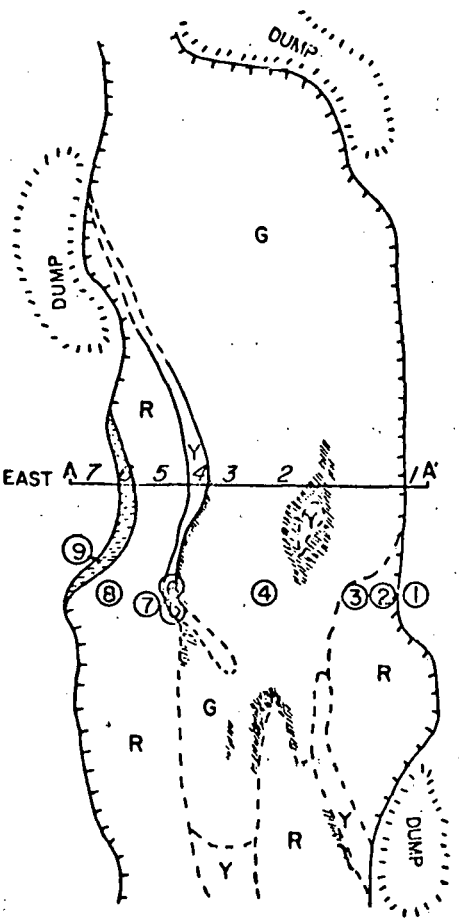

SOIL
PRIMARILY EOLIAN MATERIAL

G | Y | R

SANDSTONE
MEDIUM TO FINE GRAINED, CROSSBEDDED
G GRAY TO TAN
Y YELLOW TO BROWN
R RED TO PINK

SILTSTONE
GRAY, SHALEY IN PARTS

URANIUM MINERALIZATION
GREATER THAN 50 GAMMA COUNTS/SECOND

3 TRANSECT SAMPLE SITE (PJ)

④ SPECTROMETER SAMPLE SITE (SJ)

0 40 FEET
0 10 METERS

N

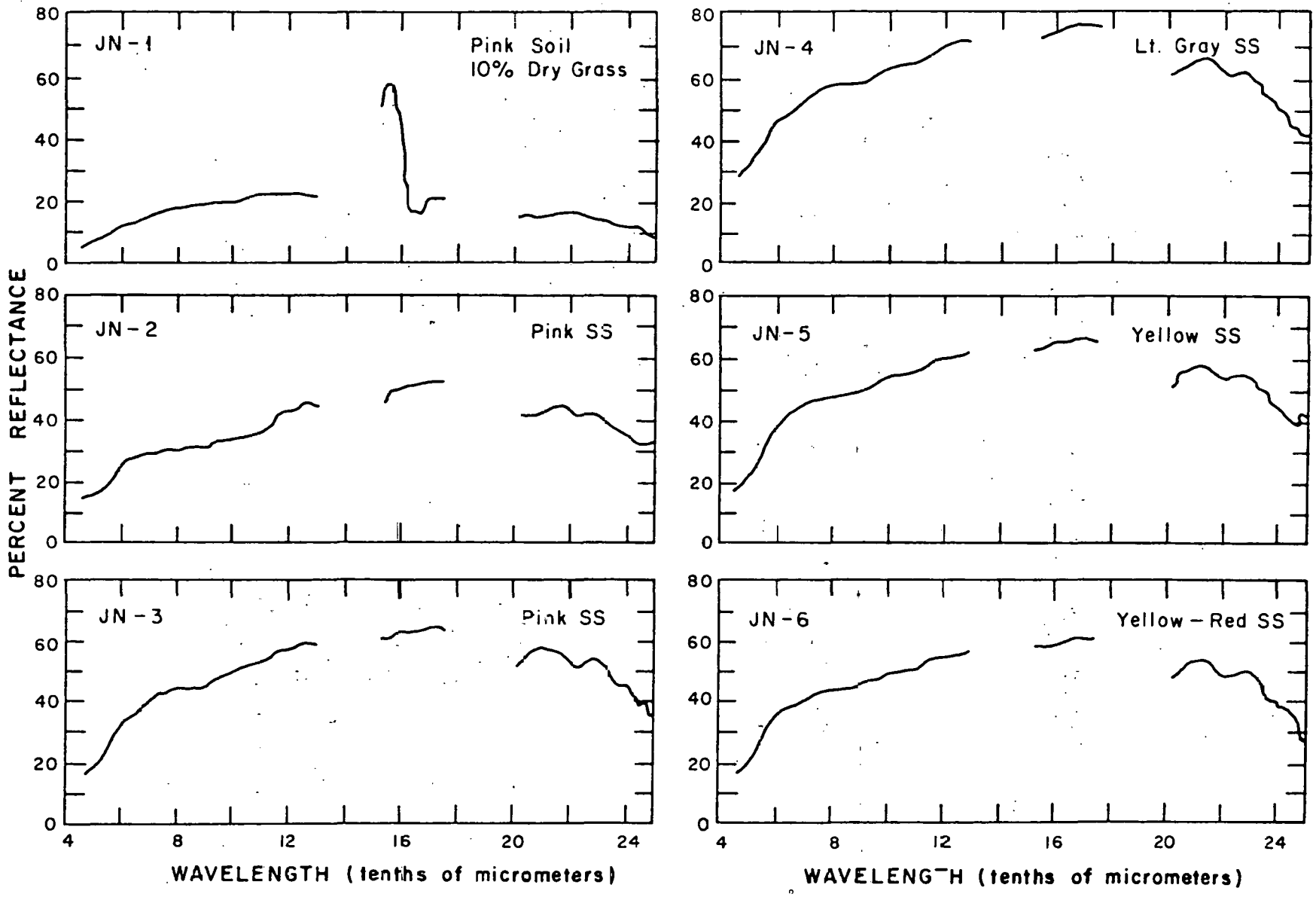
JN-1
Pink Soil
10% Dry Grass
JN-2
Pink SS
JN-3
Pink SS
JN-4
Lt. Gray SS
JN-5
Yellow SS
JN-6
Yellow-Red SS
PERCENT REFLECTANCE
0
20
40
60
80
4
8
12
16
20
24
WAVELENGTH (tenths of micrometers)
WAVELENGTH (tenths of micrometers)

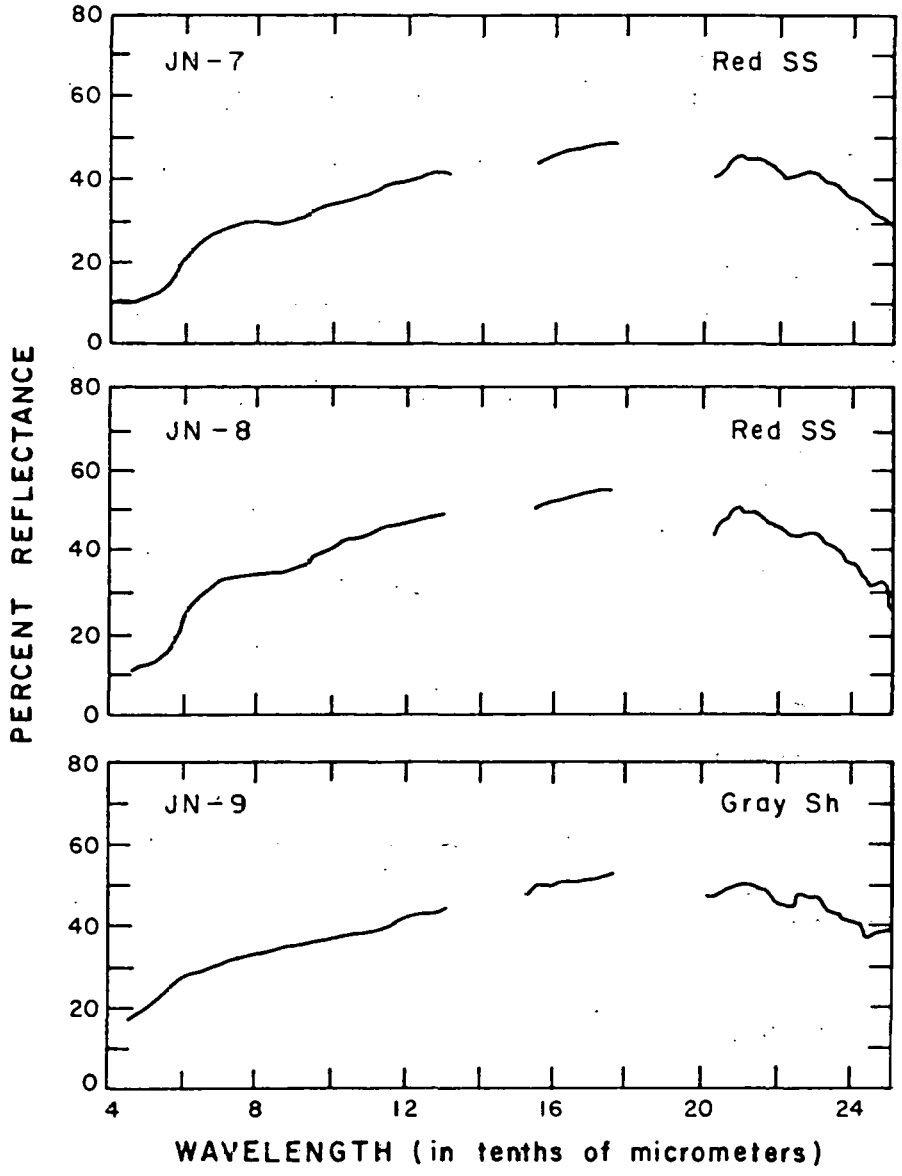

JN-10 Not Available

JEANNETTE SERIES

Spot Locations

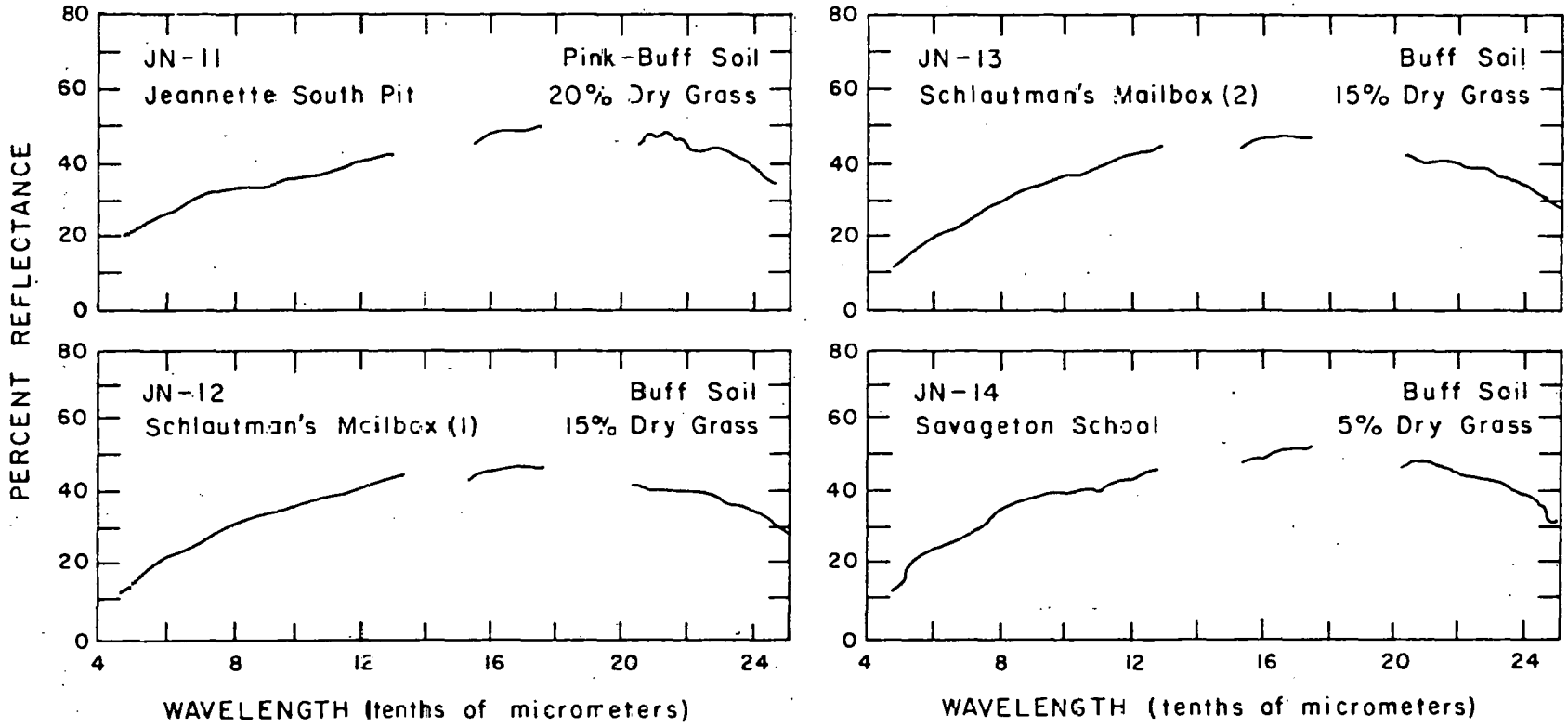

GEOLOGICAL SKETCH MAP AND CROSS-SECTION
OF THE LAUR MINE

SE 1/4, SW 1/4, SEC. 31, T. 43 N., R. 74 W.
CAMPBELL COUNTY, WYOMING

THE RESIDUAL SOIL
10-20% VEGETATIVE COVER

G | Y | R — MEDIUM TO COARSE GRAINED SANDSTONE, ROUNDED, MODERATE TO POORLY SORTED FRIABLE
G= GRAY COLOR Y=LIMONITE STAIN
R= HEMATITE STAIN

INTERBEDDED GRAY CLAYSTONE, SILTSTONE AND SHALE

MINE DUMP

4 SPECTROMETER SAMPLE SITE (LR)

0 40 FEET
0 12 METERS

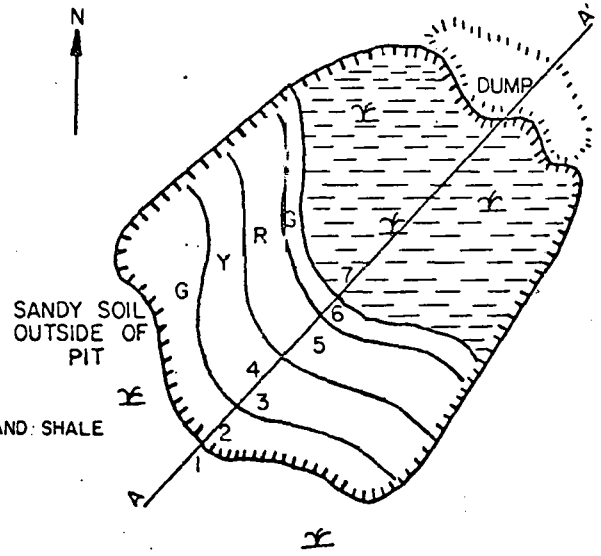

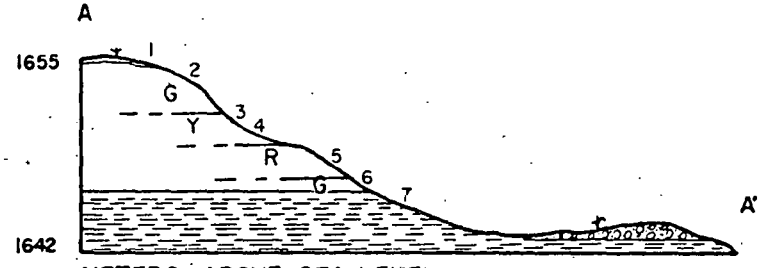

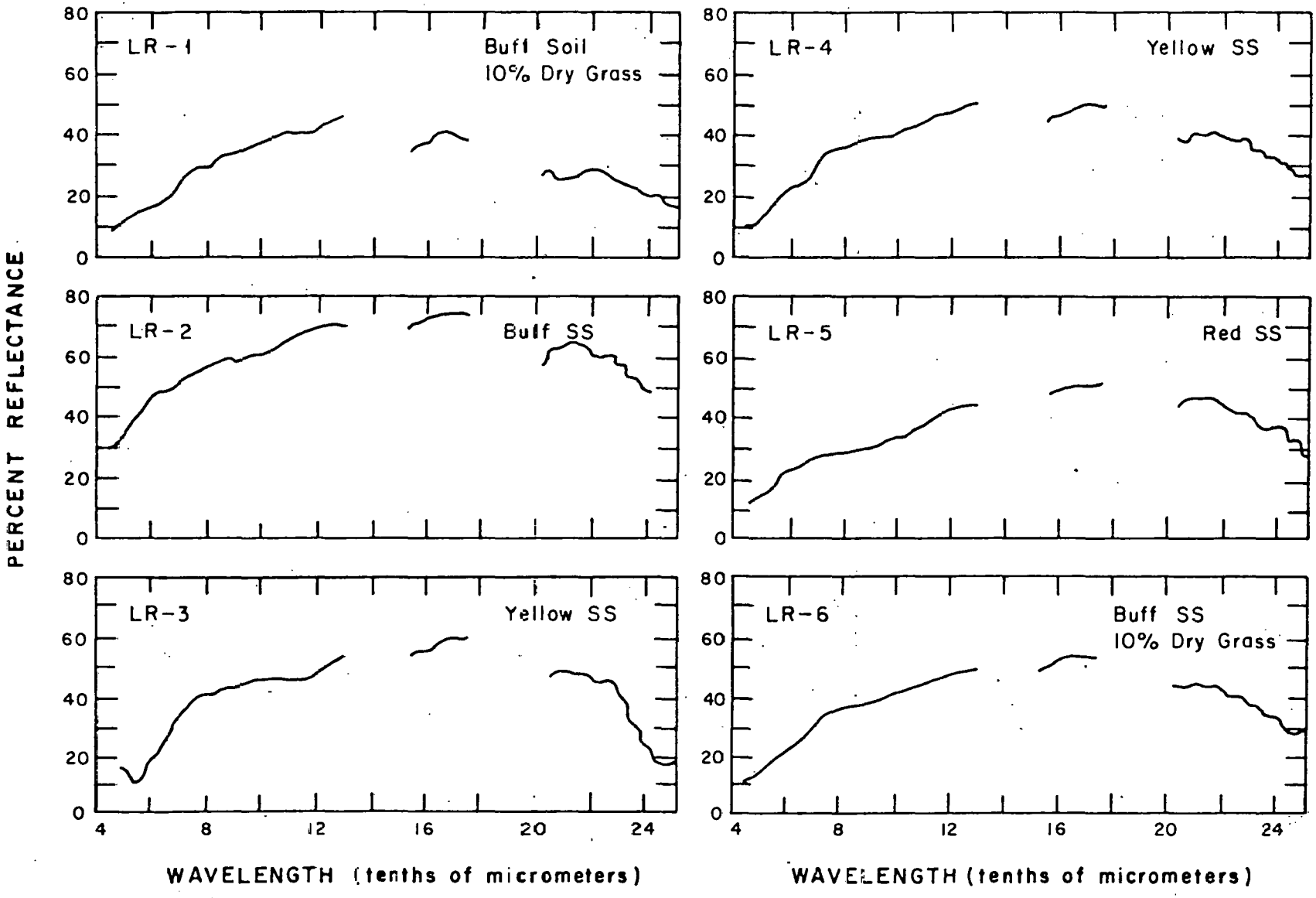
LR-1
Buff Soil
10% Dry Grass
LR-2
Buff SS
LR-3
Yellow SS
LR-4
Yellow SS
LR-5
Red SS
LR-6
Buff SS
10% Dry Grass
PERCENT REFLECTANCE
0
20
40
60
80
4
8
12
16
20
24
WAVELENGTH (tenths of micrometers)
WAVELENGTH (tenths of micrometers)

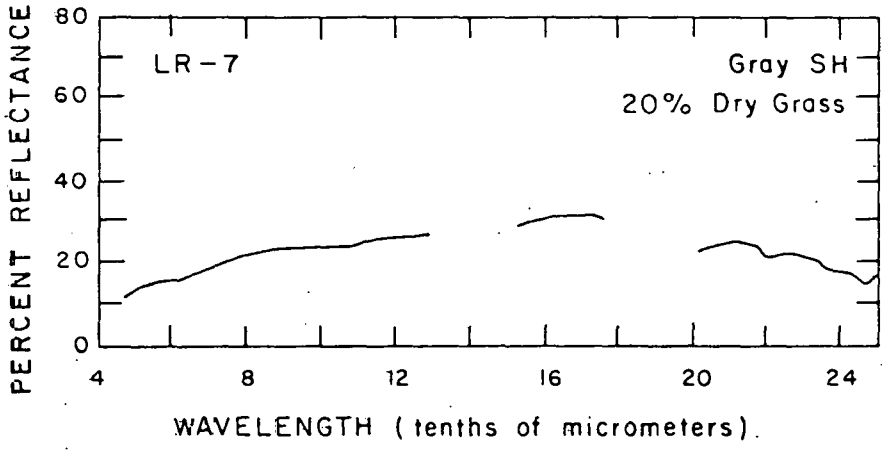
LR-7
Gray SH
20% Dry Grass
PERCENT REFLECTANCE
80
60
40
20
0
4
8
12
16
20
24
WAVELENGTH (tenths of micrometers)

APPENDIX E

Descriptions of petrographic thin sections, x-ray diffraction analysis, and mineral abundance estimates.

Petrographic thin sections were cut from twenty-two rock samples collected at the Jeanette and Colorado Christensen uranium mines and at other locations throughout the Pumpkin Buttes study area. Thin sections were analyzed on a polarizing petrographic microscope. The percentages of major mineral constituents were obtained by averaging ten estimates of mineral abundances from different areas on each thin section. The thin sections were analyzed both in transmitted and reflected light. A mineralogic description was prepared for each thin section (see following pages) which includes mineral descriptions, percentage estimates and textural characteristics. A portion of each rock sample was ground to a fine powder and analyzed by standard x-ray diffraction procedures and equipment. The results of these analyses are also included in the mineralogic descriptions. The major minerals identified from the x-ray curves are reported along with the relative heights of the major diffraction peak. The major diffraction peaks were plotted against the percent estimates of mineral constituents (from the thin section analyses). The resulting plots indicate no strong dependence between mineral percentages and the intensity of the x-ray diffraction. Consequently, we must conclude that the intensity of the diffraction peak is not a reliable indicator of the mineral abundance.

Thin Section #1

North Butte, White River Formation Black Sandstone

Quartz 42%	Most shows undulatory extinction
Feldspar 12%	Plagioclase (9%) Some fresh but most show some dusting of clay. A few grains are very intensely argilized. Some grains have well-developed twinning (albite, carlsbad, pericline). Microcline (3%) Is mostly fresh. Has gridiron twinning.
Cristobalite 13%	Cement. Colloform textured.
Unknown 28%	(Petroleum) Black. Opaque in condensed light, reddish brown slightly at edges. In some areas stains silica cement. Occurs mostly in discrete rounded areas.
Chert fragments 1%	More rounded than silicate grains.
Lithic fragments 1%	Clay cemented silicates. Brownish, little change from plane light to crossed polars.
Biotite <<1%	
Muscovite 1%	Discrete grains.
Epidote <1%	Discrete grains.
Calcite <<1%	Discrete grains.
Amphibole <1%	

Texture: Angular to subangular grains up to about 2 mm.

X-ray results: Quartz (215), Plagioclase (54), K-feldspar (47), Zeolite (38)

Thin Section #2

North Butte, White River Formation Pink sandstone

Quartz 45%	Fresh. Slight to mosaic undulatory extinction. A few larger grains partly replaced by secondary quartz. A few grains have graphic intergrowths.

Thin Section #2, continued

Feldspar 31%	Microcline (12%) Mostly fresh. Well-developed gridiron twinning. May contain veinlets of cristobalite. Plagioclase (19%) Some grains partly replaced by quartz. Usually contain dusting of clay (some heavily argilized). Some grains have sericite inclusions. A few grains partly replaced by cement along microfractures. Contains pericline and albite twinning.
Lithic fragments 3%	Different types. Quartz and epidote (subfounded) (~2 mm). Clay balls (sub-rounded). Fragments may appear pale orange or brown. Some grains may be held together by clay cement and incorporated into the silica cement.
Cristobalite 19%	Cement and fibrous fan-like clusters in cement. Does not appear to extensively replace grains but does fill many microfractures.
Muscovite <1%	Nonpleochroic, colorless.
Epidote <1%	Inclusions in lithic fragments.
Amphibole <<1%	Hornblende? Pleochroic colorless to light green.
Goethite <1% Hematite	From alteration of magnetite. Sometimes occurs mixed with silica cement.
Pyrite? <<1%	Inclusion in rounded feldspar grain. May be marcasite or pyrrhotite. Also occurs as veinlets in altered silicate grains.
Magnetite <<1% Ilmenite	Small discrete grains in silica matrix. Is often somewhat pitted and weathered looking.

Texture: Angular to subangular. Fair sorting. 3 mm to <.01 mm.

X-ray results: Quartz (390), K-feldspar (44), Plagioclase (43), Cristobalite (20), Illite (5).

Thin Section #3

North Butte, White River Formation Yellow-red sandstone

Quartz 39%	Mostly fresh, slight to mosaic undulatory extinction. Almost entirely discrete grains but a little occurs in lithic fragments.

Thin Section #3, continued

Feldspar 24%	K-feldspar (9%) Microcline. Well-developed gridiron twinning. Mostly fresh. Plagioclase (15%) albite. Usually some clay alteration. Many grains intensely argilized. Albite and pericline twinning. Some contains inclusions of sericite. Microfractures may be filled by goethite.
Cristobalite 21%	Cement, colloform texture near grain boundary. Is latest phase, surrounds everything.
Lithic fragments 6%	Muscovite rich fragments, sub-rounded. Chert or fine-grained quartz fragments. Sub-rounded clay fragments with goethite filled fractures.
Muscovite <1%	As discrete grains and as alteration of plagioclase.
Epidote <1%	As discrete grains and in lithic fragments.
Amphibole <1%	Hornblendes? Pleochroic colorless to green.
Magnetite <<1% Ilmenite	Inclusions in chert (?) fragments.
Goethite 4% Hematite	Reddish brown, almost opaque. Fibrous, often shows parallel extinction. Occurs as cement and as discrete grains (~.2 mm in diameter). Colloform texture is developed around goethite grains and cement. Some grains surrounded by goethite and later surrounded by cristobalite. Often surrounds plagioclase.
Biotite <<1%	Discrete grains, mostly altered to chlorite.
Chlorite <<1%	Mostly from alteration of biotite.
Void 3%	

Texture: Angular. Not very well-sorted. Grain size up to about 1 mm.

X-ray results: K-feldspar (>100), Plagioclase (>100), Quartz (>100), Goethite (9), Cristobalite (9).

Thin Section #4

North Butte, West Point. White River Formation Buff sandstone

Quartz 39%	Very angular grains. Some show undulatory extinction.
Feldspar 4%	Plagioclase (1%) is generally fresh but some shows slight dusting of clay. K-feldspar (3%) is mostly fresh. Some has good gridiron twinning (microcline). Some grains of orthoclase (?).
Cristobalite 35%	Colorless, colloform texture near grain boundaries, layered everywhere else.
Chert fragments 16%	Mottled looking. Some contain a light yellow staining.
Lithic fragments 6%	Light tan to brown. Sub-rounded.
Biotite <1%	Pleochroic light tan to light brown. Some grains altered to chlorite with separation of opaque mineral (leucoxene?). Many grains are fibrous looking.
Muscovite <1%	Fresh colorless discrete grains.
Epidote <1%	
Magnetite <1% Ilmenite	Small (.1 mm) discrete grains. Some grains contain rough edges and may be altered to Fe^{+++} mineral.
Goethite <1%	Discrete grains. Brown in condensed light.
Pyrite <<1%	Small (.05 mm) discrete grains in cristobalite cement. Some may be altered somewhat.

Texture: Angular, fine-grained (.1 to .05 mm), very well sorted. Elongate grains are aligned.

X-ray results: Quartz (275), Plagioclase (47), Cristobalite (28), K-feldspar (16), Illite (4).

Thin Section #5

North Butte, White River Formation Sandstone near spring below gate

Quartz 41%	Mostly fresh. Slight to mosaic undulatory extinction. 2V as much as about 5°.
Feldspar 32%	Microcline (21%). Mostly fresh but with some slight clay alteration. Some grains contain gridiron twinning. Plagioclase (11%). Usually somewhat argilized. Some grains contain sericite inclusions. Albite and pericline twinning. Some grains intensely argilized.
Cristobalite 10%	Cement. Forms a thin colloform rim on most grains. Rim (~.05 mm) occurs where grains are in contact with "matrix". Some pieces of cristobalite are "floating" free in void space.
Zeolite 5%	Brown in plane light. Contains a few small (up to .5 mm) quartz inclusions. May only be lithic fragments. No variation in birefringence with rotation of stage. In places forms around other grains.
Goethite 2% Hematite	Usually occurs along grain boundaries or as cement, but also as discrete grains. All hematite is surrounded by silica cement. May replace feldspar or quartz. Appears to be from alteration of magnetite in some places.
Lithic fragments <1%	Mostly small quartz grains cemented by silica cement.
Epidote <<1%	Enclosed in silica cement.
Clay <1%	Mostly from alteration of silicate minerals.
Sericite <1%	As inclusions in plagioclase. Very light blue in plane light.
Magnetite <1% Ilmenite	Usually as discrete grains. May be somewhat altered to hematite.
Unknown <1%	Black opaque material with no reflectance at all. Rims some void areas. May be petroleum.
Void 7%	

Thin Section #5, continued

Texture: Angular to subangular. Fair sorting. Largest grains about 2mm.

X-ray results: Quartz (315), Plagioclase (53), K-feldspar (43), Zeolite (17).

Thin Section #6

Badlands Ridge, Wasatch Formation Marlstone

Quartz	∿49	Small (<.1 mm) angular fragments in matrix of calcite. Slight to very pronounced undulatory extinction. Partly replaced in by calcite at outside edges of grains. Some grains entirely replaced by calcite.
Calcite	∿49	Cement and as discrete grains in calcite cement.
Biotite	<1%	Pleochroic light tan to green.
Muscovite	<1%	
Zeolite or glass shard	<1%	Brown, sparkly, no change under crossed polars.
Unknown	<1%	Isotropic, green, non-pleochroic, moderate relief, anhedral, perhaps being replaced by calcite (green stain out into surrounding calcite). (about .1 mm).
Hematite	<1%	
Magnetite Ilmenite	<1%	Discrete fresh grains. Some grains are perhaps being replaced by calcite. Many tiny (<.05 mm) grains floating in calcite.

Very difficult to estimate percent in this thin section because of small grain size.

Texture: Angular to subangular grains in calcite matrix. Grains generally <.2 mm. Most grains completely surrounded by calcite.

X-ray results: Quartz (82), Calcite (78), Dolomite (6).

Thin Section #7

Chimney Hills, Wasatch Formation Marlstone

Calcite 74%	As cement and in veinlets as much as 1 mm wide. Veinlets contain pieces of marlstone and a few large (∿.5 mm) quartz grains. Quartz may have precipitated into open space in veinlet. Calcite grains as much as ∿.7 mm occur in center of veinlets but near edges grain size is much less (.1 mm).
Clastic grains 25%	Mostly very small (<.1 mm) quartz grains. Muscovite, calcite, biotite, and Fe-oxide are also present. Grains are floating in a matrix of calcite.
Magnetite <<1% Ilmenite	A few discrete grains. Some are partly altered to goethite (?) and some are fresh.

Texture: Fine-grained (most grains less than .1 mm). Angular. Well sorted. In thin section rock has yellowish tinge.

X-ray results: Calcite (124), Quartz (72), Illite (11), Dolomite (8), K-feldspar (6), Kaolinite-?(3).

Thin Section #8

Chimney Hills, Wasatch Formation Sandstone (unaltered)

Quartz 31%	Some replacement by calcite. Undulatory extinction (2V ∿5°) on some grains. Oriented perpendicular to C axis at one end of slide.
Calcite 45%	Cement. Replaces quartz and feldspar locally.
Lithic fragments 4%	Brown. More rounded than other grains.
Feldspar 9%	Microcline, plagioclase and untwinned feldspar (biax(-)). Plagioclase may be entirely replaced by calcite (twinning preserved).
Chert? fragments 8%	May show slight replacement by calcite. More rounded.
Clay 1%	Mostly from alteration of silicate minerals.
Biotite <1%	Pleochroic light tan to brown. Some altered to chlorite with separation of opaque oxides. Often bent. Interlayered calcite.

Thin Section #8, continued

Muscovite	<<1%	Fresh. Occasional quartz inclusion. Colorless.
Epidote	<<1%	Rare.
Chlorite	<1%	From alteration of biotite. Sometimes contains interlayered calcite. Also occurs as discrete grains.
Magnetite Ilmenite	<1%	Usually as small discrete grains. A few grains are slightly altered to Fe^{+++} oxide (goethite ?).
Hematite Goethite	<1%	From alteration of magnetite.
Void	<<1%	

Texture: Angular. Moderately well sorted (grains .2mm or less).

X-ray results: Calcite (290), Quartz (138), Plagioclase (23), K-feldspar (19), Illite (7), Kaolinite (6).

Thin Section #9

Colorado Christiansen Mine, Wasatch Formation Buff sandstone

Quartz	53%	Slight to pronounced undulatory extinction.
Calcite	32%	Cement and discrete grains.
Biotite	3%	Some appears to be replaced by calcite. Pleochroic colorless or light brown to green or dark brown. Some altered to chlorite with separation of opaque oxides.
Clay	1%	Mostly from alteration of silicate minerals.
Feldspar	1%	Microcline (<1%). Mostly fresh. Plagioclase (<1%). Most is fresh. Albite twinning.
Goethite Hematite	1%	Yellowish brown with condenser in. From alteration of magnetite.
Zeolite ?	1%	Brown under plane light and crossed polars. Red (with condenser in) rectangular, opaque, inclusions.
Epidote	<<1%	A few scattered discrete grains.

Thin Section #9, continued

Muscovite	<1%	Colorless, Non-pleochroic. Discrete grains.
Zircon	<<1%	Rare scattered discrete grains.
Magnetite Ilmenite	<1%	Discrete grains. Usually slightly, sometimes largely altered to hematite or goethite. Some grains are aligned to give the appearance of a veinlet.
Lithic fragments	<1%	Chert fragments mostly.
Amphibole	<<1%	A few scattered grains.
Chlorite	<1%	Mostly from alteration of biotite.
Void	6%	

Texture: Angular to subangular. Fair sorting. Grain as much as .5 mm.

X-ray results: Quartz (230), Calcite (73), Illite (6).

Thin Section #10
Colorado Christiansen Grid 33, Wasatch Formation Pink sandstone schmoo

Quartz	28%	Mostly fresh. Slight to pronounced undulatory extinction. May also occur in clusters of grains (perhaps from veinlets). Edges may be slightly replaced by calcite.
Calcite	39%	Cement. May completely replace some feldspar grains. Large area several mm often has same optical (crystallographic) orientation.
Feldspar	14%	Microcline has gridiron twinning. It may contain several rounded quartz inclusions. May be replaced by calcite. Some K-feldspar grains have needlelike tourmaline (?) inclusions. Plagioclase has albite twinning and sometimes is replaced by calcite.
Lithic fragments	6%	Brown nearly opaque with inclusions of silicate minerals. Some grains have opaque layers with interstitial quartz(?). Often rounded, some contain hematite grains.
Chert fragments	2%	May contain other (dark brown) lithic fragments.
Clay	2%	Some grains completely replaced by highly birefringent clay.

Thin Section #10, continued

Hematite Goethite	1%	As discrete grains, cement in very localized areas, and as clusters of small (.05 mm) discrete grains with goethite?? cement. Also occurs in lithic fragments. Discrete grains may be (.25 mm) and may have chert(?) inclusions. Most is from alteration of magnetite.
Tourmaline(?)	<<1%	Needlelike inclusions in K-feldspar. Pleochroic pale green to dark green.
Pyroxene	<<1%	Biaxial (+), partly altered to epidote.
Epidote	<1%	Discrete grains or alteration of plagioclase. May occur as cluster of grains with quartz.
Biotite	1%	Mostly unaltered discrete grains. Contains opaque inclusions. Pleochroic tan to brown or brown to dark brown.
Muscovite	<1%	Some grains contain quartz inclusions.
Magnetite Ilmenite	<<1%	Up to .25 mm large. As discrete grains almost always associated with and partly altered to hematite. Many grains are entirely altered to hematite.
Apatite	<<1%	Rare, small inclusions in quartz.
Chlorite	<1%	Pleochroic colorless to light green.
Void	5%	

Texture: Angular, a few grains (quartz) rounded. Calcite cement.

X-ray results: Quartz (275), Calcite (88), Plagioclase (37), K-feldspar (18), Illite (6).

Thin Section #11

Colorado Christiansen grid 54, Wasatch Formation Red sandstone

Calcite	36%	Cement. Discrete portions encompassing several grains goes extinct at same time (not entire slide at once).
Quartz	33%	Fresh, even to mosaic extinction. Sometimes occurs in clusters in lithic fragments.

Thin Section #11, continued

Feldspar 4%	Microcline is mostly fresh, gridiron twinning. Some plagioclase is altered to clay, albite twinning. About equal abundance.
Chert fragments 10%	May contain grains of quartz with pronounced undulatory extinction and occasional opaque inclusions (in quartz). Often yellow or reddish brown.
Clay 1%	Some silicate grains completely altered to clay. Some clay has low first order colors and some clay has second order colors.
Lithic fragments 6%	Mostly brown, nearly opaque. Usually more rounded. May contain quartz and feldspar grains. Some lithic fragments largely replaced by calcite. Some contain small discrete grains of magnetite and/or ilmenite.
Biotite 2%	Often compressed by compaction. Pleochroic tan to brown. May be almost opaque brown.
Muscovite 1%	Seldom compressed by compaction.
Silica fragment <1%	Possibly cristobalite.
Unknown <1%	Biaxial (+), high first order colors, 2V>50°, high relief, R.I. <calcite, colorless, non-pleochroic, cleavage? 90°?, non=parallel extinction.
Magnetite <1% Ilmenite	Often partly altered to hematite, sometimes entirely altered. A few grains are fresh.
Epidote <1%	Discrete grains and as clusters of tiny grains.
Garnet <<1%	Isotropic, colorless, high relief.
Pyroxene <1%	Discrete grains, slight replacement by calcite. Biaxial (-) 2V∿60°, non-pleochroic.
Hematite <1%	Probably mostly from alteration of magnetite. May completely surround silicate grains. Locally cements silicate grains.
Chlorite <1%	
Unknown 2 <1%	Uniax (-), 90° cleavage, moderately high relief, non-parallel extinction, grain ∿.5 mm. Nearly centered figure, interference color gray to black.

Thin Section #11, continued

Unknown 3	<1%	Reddish brown, uniax (-), high relief, first order colors, nearly centered figure, non-pleochroic concoidal fracture. No color rings in interference figure, uneven extinction. (Biotite?????)
Void	3%	

Texture: Angular, fair sorting. Generally little diagenetic change. Calcite cement. Grain size generally .5 mm or less. Grain boundaries are generally sharp.

X-ray results: Quartz (320), Calcite (200), K-feldspar (32), Plagioclase (28).

Thin Section #12

Colorado Christiansen grid 24, Wasatch Formation Red sandstone finger

Quartz	35%	Fresh. Even to undulatory extinction.
Calcite	34%	Cement. May occur in some altered biotite grains. Many small grains, whole sections do not go extinct at one time.
Chert fragments	12%	Discrete angular grains.
Lithic fragments	10%	One large (∿1.5 mm) lithic fragment contains silica and Fe-oxide cement. Generally more rounded. One fragment (∿3.0 mm) contains hematite and silica cement biotite, quartz, second order birefringent clay, feldspar, silica appears to be later than Fe-oxide cement.
Feldspar	3%	Microcline is mostly fresh, gridiron twinning.
Hematite Goethite	∿2%	Coats most grains and forms cement in some places. Extensively stains the rock.
Clay	1%	Some grains completely altered to second order birefringent clay.
Biotite	<1%	Pleochroic brown to very dark brown. May have low first order colors.
Epidote	<1%	From alteration of plagioclase and as discrete grains.

Thin Section #12, continued

Magnetite Ilmenite	∿1/4%	Always partly or completely altered to hematite. A few grains contain very little alteration.
Muscovite	<1%	Discrete, fresh, grains.
Amphibole	<1%	A few small discrete grains.
Pyroxene	<1%	A few discrete grains.
Silica	<1%	Cement in lithic fragments.
Silica (glass)? shards	<1%	
Void	<1%	

Texture: Generally angular. Calcite cement. Largest grains ∿.5 mm, rather small. Difficult to estimate percentage of minerals because of small grain size.

X-ray results: Quartz (230), Calcite (120), Plagioclase (13), K-feldspar (6).

Thin Section #13

Powder River Breaks, Wasatch Formation northwest of North Butte. Red sandstone

Quartz	41%	Fresh angular to subrounded grains. Some quartz grains may have some overgrowth of later quartz. Slight to pronounced undulatory extinction.
Calcite	27%	Cement.
Chert fragments	24%	Some are iron stained.
Hematite Goethite	3%	Surrounded by calcite. Goethite is brown and more translucent, uniaxial (-), occurs as veinlets, grain coatings, and as discrete grains (.75 mm). Some hematite grains .75 mm. A few hematite cemented fragments present.
Feldspar	2%	Microcline (1%) is mostly fresh, well developed gridiron twinning. Plagioclase (1%).
Magnetite Ilmenite	<1%	Mostly altered to Fe^{+++} minerals. Some relatively fresh grains do exist. Usually surrounded by Fe^{+++} minerals.

Thin Section #13, continued

Amphibole << 1%	Partly altered to calcite.
Muscovite < 1%	
Biotite < 1%	Some is altered to chlorite.
Chlorite < 1%	From alteration of biotite.
Epidote << 1%	
Garnet (?) < 1%	
Void 1%	Perhaps just holes in slide caused by preparation.

Texture: Angular to subangular. Fair sorting. Grain size as much as about .75 mm.

X-ray results: Quartz (265), Calcite (69), K-feldspar (13), Plagioclase (10), Illite (3).

Thin Section #14

Hill west of Colorado Christiansen grid Wasatch Formation Hematite stained nodules

Goethite 70%	Cement.
Silicate minerals 30% Quartz and Feldspar	Angular to subangular fragments in a sea of goethite. Feldspar is angular to subangular fragments in a sea of goethite.
Muscovite <<1%	Rare flakes.
Magnetite? << 1% Ilmenite	A few tiny (.05 mm) scattered fresh grains of what appears to be magnetite or ilmenite.

One edge of thin section has rim of silicate grains (up to about .5 mm) in goethite and hematite cement. Silicate grains generally have about .1 to .01 mm rim of goethite with the remainder of the cement being hematite.

Very difficult to estimate percentages because of small grain size of silicates.

Texture: Small (as much as .1 mm) angular to subangular silicate (mostly quartz) fragments in extensive goethite matrix.

X-ray results: Quartz (47), Goethite (19).

Thin Section #15

Mid-Jeanette, Wasatch Formation Buff sandstone

Quartz 55%	Undulatory extinction slight to strong. Often has what look like exsolution lamellae (thin aligned wormlike streaks). Occasional large (1.5 mm) grains.
Feldspar 8%	K-feldspar (5%) usually fresh, microcline mostly. Plagioclase (3%) often has dusting of clay.
Lithic fragments 10%	A few are calcite cemented quartz fragments. Mostly mud fragments.
Biotite ∿ 3%	Pleochroic light brown to brown. Biax (-) 2V about 0°. Many flakes parallel to plane of thin section. Often partly altered to chlorite with separation of opaque.
Clay 3%	Interstitial to grains. Also occurs in lithic fragments but only the percentage of interstitial clay was estimated. Some from alteration of feldspar.
Chlorite ∿ 1%	Probably from alteration of biotite. Pleochroic very light green to green. Biax (-). Small 2V.
Hematite <<1% Goethite	Apparently most is from alteration of magnetite.
Amphibole <1%	Pleochroic light tan to green biaxial (-). Cut by quartz veinlets. Second order interference colors.
Epidote <<1%	Scattered discrete grains and from alteration of plagioclase.
Calcite < 1%	Common grains. In a few places occurs interstitial to silicate grains.
Muscovite <1%	Birdseye extinction. Some grains contain quartz veinlets parallel to cleavage.
Magnetite < 1% Ilmenite	Discrete grains often slightly altered to hematite. A few grains are almost totally altered to hematite.

Thin Section #15, continued

Void 18%

Texture: Angular to subrounded. Moderately well sorted. Individual grains often cut by quartz veinlets (<.1 mm) but silica is not the cement. Clay appears to be the cement but rock is probably poorly consolidated. There are a lot of void spaces around grains.

X-ray results: Quartz (610), K-feldspar (60), Plagioclase (31), Smectite (18), Illite (10), Amphibole (5).

Thin Section #16

Mid-Jeanette, Wasatch Formation Buff sandstone (ore)

Quartz 50%	Fresh. Does not appear to be replaced by calcite. Most shows undulatory extinction.
Lithic fragments 21%	Most are fine-grained. Some contain quartz cemented muscovite grains (<.1 mm). Clay cemented quartz, feldspar and amphibole grains are also present.
Calcite 16%	Cement. Occurs in irregular patches which make up about 2/3 of the rock (the rock is not 2/3 calcite).
Biotite 2%	Biaxial (-) 2V∿5°. Pleochroic, most is light brown to brown but much less abundant colorless to green variety (2V 10°) is also present (possibly glauconite). Partly altered with separation of leucoxene(?).
Chlorite 2%	May be mostly from alteration of biotite. Biaxial (-) 2V>50°. Non-pleochroic.
Clay ∿ 1%	From alteration of feldspar.
Feldspar 2%	Mostly microcline (1%), fresh, well developed gridiron twinning. Some plagioclase (<1%), some has dusting of clay, some completely altered to clay.
Goethite < 1% Hematite	Hematite mostly as alteration product of magnetite. A few discrete grains of goethite.
Muscovite < 1%	Some grains contain interlayered calcite.

Thin Section #16, continued

Amphibole	< 1%	Biaxial (-), second order colors. A few scattered grains. Not being replaced by calcite.
Magnetite Ilmenite	<1%	(∿1/4%) Sometimes very slightly altered to goethite. A few grains are completely altered to Fe^{+++} minerals. Discrete grains. Calcite surrounds Fe^{+++} oxide as well as magnetite therefore is later.
Opaque	<< 1%	Discrete grains aligned for ∿ 2 mm.
Garnet	<1%	Colorless, high relief.
Void	4%	

Texture: Fairly well sorted, grains as much as 1.5 mm but most less than .2 mm. Angular. Irregular patches of calcite cement.

X-ray results: Quartz (400), Calcite (122), K-feldspar (62), Plagioclase (38), Illite (15), Smectite (14), Amphibole (10).

Thin Section #17

Middle Jeanette, Wasatch Formation Pink sandstone

Quartz	41%	Fresh. Slight to distinct undulatory extinction.
Calcite	32%	Cement.
Feldspar	5%	Microcline (2%) is fresh. Well developed grid-iron twinning. Plagioclase (3%). Some large (∿1.5 mm) grains present with sericite inclusions. Mostly fresh, some grains are extensively altered to clay and some have sericite inclusions.
Chert fragments	8%	Slightly less angular than silicate grains.
Lithic fragments	7%	More rounded, look like clay balls. Brown.
Biotite	∿1%	Some altered to chlorite. Pleochroic light tan to brown or colorless to green.
Hematite Goethite	2%	Small (1 mm) veinlets in calcite cement. Sometimes forms grain coatings. Some but doubtful that all is from alteration of magnetite. In a few places forms cement for a few silicate grains.

Thin Section #17, continued

Clay ∿ 1%	Mostly from alteration of feldspar. Some grains completely argilized
Mica? < 1%	2V∿10°, Biaxial (-), colorless, moderate-high relief, second to third order colors (mostly yellow), Phologopite? Two fair cleavages at 90° to each other.
Muscovite < 1%	Discrete grains and a few inclusions in plagioclase.
Chlorite < 1%	Probably mostly from alteration of biotite.
Magnetite < 1% Ilmenite	Discrete grains. Often with alteration rim of hematite and some grains are completely altered.
Epidote < 1%	Mostly replacement of plagioclase.
Amphibole ? < 1%	Discrete grains. Possibly pyroxene.
Void 1%	

Texture: Angular. Several large grains 1-2 mm but most of sample < .5 mm.

X-ray results: Quartz (325), Calcite (140), K-feldspar (36), Plagioclase (21), Illite (9), Smectite (5).

Thin Section #18

West Jeanette, Monument Peak, Wasatch Formation Pink sandstone

Quartz 35%	Even extinction to pronounced undulatory extinction.
Calcite 34%	Cement.
Chert fragments 18%	In some places appears to be interstitial to grains. Does not appear to be replacing any minerals.
Feldspar 3%	Microcline (1%). Plagioclase (2%) may be almost entirely altered to clay. Some grains are very fresh looking. Albite twinning.
Biotite ∿2%	Pleochroic light to dark brown. Some altered to chlorite.

Thin Section #18, continued

Clay	2%	Some silicate grains entirely altered to clay.
Hematite Goethite	2%	Hematite occurs as thin grain coating in most of the slide and as interstitial cement (?) locally. Calcite is later than grain coatings. Most Fe^{+++} is in hematite, very little goethite. Locally hematite occurs as veinlets in calcite cement.
Muscovite	∿ 1%	Colorless, some grains .5 mm long. Discrete grains.
Chlorite	< 1%	Probably from alteration of biotite.
Lithic fragments	<1%	Brownish. Mostly clay.
Pyroxene ?	<1%	Perhaps amphibole.
Epidote	< 1%	Rare discrete grains.
Magnetite Ilmenite	< 1%	Always partly or entirely altered to hematite.
Void	< 1%	

Texture: Angular to subangular grains up to ∿.5 mm. Some grains are more rounded.

X-ray results: Quartz (285), Calcite (120), K-feldspar (9), Plagioclase (8), Aragonite ? (5).

Thin Section #19

West Blowout Anomaly, Wasatch Formation Buff sandstone

Quartz	22%	Mostly fresh. Some cut by sericite veinlets. Even to pronounced undulatory extinction.
Calcite	50%	Cement, replaces (partially) some grains.
Chert fragments	6%	Slightly more rounded than mineral grains. Appear to contain slightly larger quartz grains than chert in other thin sections.
Feldspar	8%	Some microcline and plagioclase is partly replaced by calcite.

Thin Section #19, continued

Biotite	2%	Pleochroic colorless to green. Some altered to chlorite. Some partly replaced by calcite. Some altered with separation of opaque oxide.
Clay	2%	Some grains completely altered to clay, probably smectite.
Lithic fragments	∿1%	More rounded, small silicate grains.
Chlorite	< 1%	Probably from alteration of biotite.
Muscovite	< 1%	Discrete grains up to .5 mm long.
Hematite Goethite	< 1%	Usually as discrete fairly small areas. Hematite coats a few grains but Fe^{+++} minerals are generally not abundant. Hematite is surrounded by calcite.
Amphibole	< 1%	A few scattered discrete grains.
Magnetite Ilmenite	< 1%	Generally less abundant than in other thin sections of Wasatch Formation. Grains are generally fresh but commonly contain slight hematite alteration. At least one grain was partially replaced by calcite.
Pyrite	? << 1%	Tiny grains in lithic fragment.
Void	7%	

Texture: Angular to subangular. Grains up to ∿1 mm. Calcite cement. Fair sorting.

X-ray results: Quartz (205), Calcite (122), K-feldspar (26), Illite (8), Plagioclase (7).

Thin Section #20

Black Butte, White River Formation Red sandstone float

Quartz	38%	Even to pronounced undulatory extinction. Some quartz grains contain aggregate of quartz grains. Some grains contain rough looking centers.
Feldspar	23%	Microcline has gridiron twinning, mostly fresh. Plagioclase has albite twinning. Is often somewhat altered to clay. Some feldspar grains rather rounded. Rim of Fe-oxided inclusion of feldspar.

Thin Section #20, continued

Calcite	3%	About all is hematite stained and the percentage estimate is a real shot in the dark. Seems to form cement in some areas. Hematite stained calcite may form most of the cement.
Hematite Goethite	12%	Both minerals may be present. Hematite is by far more abundant. Hematite is the cement, surrounds most grains, and occurs as veinlets. Hematite shows a polygon type fracturing similar to mud cracks. Hematite may replace silicate grains.
Lithic fragments	1%	Some as large as 2 mm, argilized and intensely fractured minerals cut by quartz veinlet, quartz veinlet shows good undulatory extinction. Many lithic fragments appear to be mostly clay and are rounded. Magnetite and/or ilmenite occurs in some quartz rich lithic fragments.
Chert fragments	1%	Many are iron stained or have inclusions (?) of Fe-oxide possibly from alteration of pyrite or magnetite.
Amphibole	< 1%	Sometimes several grains together as lithic fragment. Some grains have quartz (?) inclusions.
Epidote ?	< 1%	Sometimes intermixed with hematite.
Muscovite	< 1%	Discrete grains.
Biotite	< 1%	Pleochroic light tan to brown.
Isotropic mineral	<1%	Partly altered to highly birefringent (second order) clay. Very low relief, no cleavage, possibly quartz.
Magnetite Ilmenite	<< 1%	A few fresh grains, some are surrounded by calcite. Tiny grains occur in some lithic fragments.
Void	20%	

Texture: Grain size is .5-2 mm for most of thin section. Angular to subangular, fair sorting. Fe-oxide cement. Cement replaces feldspar in several places. Some silicate grains somewhat rounded (sub-round).

X-ray results: Quartz (154), Calcite (24), K-feldspar (13), Plagioclase (11).

Thin Section #21

North Butte Amphitheatre, Wasatch Formation Metallic sandstone

Pyrite 52%	Cement. Most pyrite is fine-grained groundmass but some grains as much as .25 mm are present.
Quartz 36%	Even to pronounced undulatory extinction.
Feldspar 2%	Microcline and plagioclase.
Chert fragments 6%	Angular not rounded like in other thin sections.
Lithic fragments 1%	Appear to be mostly clay.
Biotite 1%	Pleochroic light tan to brown and colorless to green.
Chlorite < 1%	Sometimes occurs in lithic fragments and from altered biotite.
Muscovite < 1%	Discrete grains.
Epidote << 1%	Rare discrete grains.
Hematite < 1% Goethite	Discrete areas, some are perhaps lithic fragments. Seem to be enclosed by pyrite cement.
Clay < 1%	Completely replaces some grains. Highly (second and third order) birefringent.

Texture: Angular silicate grains (<.5 mm) are floating in a sea of pyrite.

X-ray results: Quartz (77), Pyrite (58), K-feldspar (5), Plagioclase (4).

Thin Section SL105-2

Blowout Anomaly, Wasatch Formation Small, 1" high roll front

Quartz 43%	Distinct to slight undulatory extinction. Contains a few zircon inclusions.
Feldspar 6%	Plagioclase (3%) Some fresh, some intensely argillized, a few sericite inclusions. K-feldspar (3%) Microcline has good gridiron twinning. Usually fresh. Some is altered to epidote.

Thin Section SL105-2, continued

Lithic fragments 12%	Generally orangish brown in thin section. Subangular usually. Very fine grained but sometimes contain larger silicate grains. Color changes very little when polars are crossed.
Chert fragments 15%	Generally very fine grained. Grains are generally subangular.
Clay 2%	Second order colors, some is from alteration of plagioclase.
Magnetite < 1% Ilmenite	Discrete grains usually slightly, occasionally almost entirely, altered to hematite or less commonly goethite. Some grains may be pyrite altering to hematite.
Apatite <<1%	Inclusions in biotite.
Muscovite < 1%	Birdseye extinction. Grains as much as ∿1 mm long.
Zircon <<1%	Inclusions in biotite and quartz.
Chlorite ? < 1%	From alteration of biotite (brownish) and detritial (greenish).
Biotite < 1%	Pleochroic light tan to dark brown or green. Partly altered to chlorite (?) with separation of opaque (red) oxides. Some has small zircon inclusions. May occur in sunbursts. Some biotite contains apatite and zircon inclusions.
Pyroxene < 1%	Biaxial (+), high 2V, pleochroic very light green to green, two cleavages at 45°, high relief, first order colors. Occasional discrete grains. Occasionally contain center of quartz.
Chlorite < 1%	Some discrete grains. Some probably from alteration of biotite.
Epidote < 1%	A few discrete grains. Some appears to be from alteration of feldspar.
Garnet << 1%	High relief, colorless, angular.
Pyrite ? <<1%	Possibly a few grains in a lithic fragment. Possibly some grains that appear to be magnetite altering to hematite are pyrite.

Thin Section SL105-2, continued

Hematite	< 1%	Both minerals occur throughout slide. They appear to be somewhat more abundant at top & bottom (altered areas). In unaltered area magnetite grains may be somewhat less altered but this is rather speculative. There is no distinct difference between altered and unaltered areas on slide.
Goethite		

Void 19%

Texture: Angular, fair-good sorting. Very poorly cemented, perhaps a little clay cement. Maximum grain size is generally .5 mm. Sediment has been compacted, biotite grains bent around other grains.

X-ray results: Quartz (<<100), K-feldspar (41), Plagioclase (14).

Thin Section SL105-2 stained, continued

Description of two areas that show slight radioactivity from autoradiograph.

Area 1 (slight amount of radioactivity detected (two spots)).

Area contains abundant hematite. Hematite contains abundant opaque inclusions. Some opaques associated with biotite. Yellowish brown rims on most silicate grains; this is true of silicate grains in the general area but rims are more intense in area #1. Some hematite may be from altered pyrite, small discrete six-sided subhedral grains. Some silicate grains completely altered to clay.

Area 2 (very slight amount of radioactivity detected (one spot)).

Area contains common opaque grains which do not appear to be hematite. Grains look more brownish (goethite?). Some hematite is present however, occurs as small red grains in a lithic fragment. Silicate grains do not have oxide coating. Some silicate grains completely altered to clay.

Thin Section SL105-1

Description is similar to SL105-2. Three areas of slight radioactivity were detected by autoradiograph.

Area 1 (one lightly exposed spot on film)

Area contains small amount of opaque material. Grains do not contain hematite coating. Exposed spot on film may be due to zircon in biotite grain. One cluster of possible hematite after pyrite is present. Some feldspar grains completely replaced by clay.

Area 2 (two light exposed spots)

Abundant brownish red hematite (or perhaps goethite) grains and cement. One area (1.2 mm) contains abundant hematite cement. Some opaque material does not have red rim under condensed light and may be anhedral pyrite. Some cement may be pyrite. The source of the radiation is not apparent.

Area 3 (two lightly exposed spots)

Opaque material is common, biotite is abundant. Most of the opaque does not appear to be hematite. Some opaque grains are inclusions in lithic fragments. Some silicate grains completely altered to clay. A few hematite grains appear to be present. Source of radioactivity is not apparent.

Stratigraphic Sections Measured on North Butte

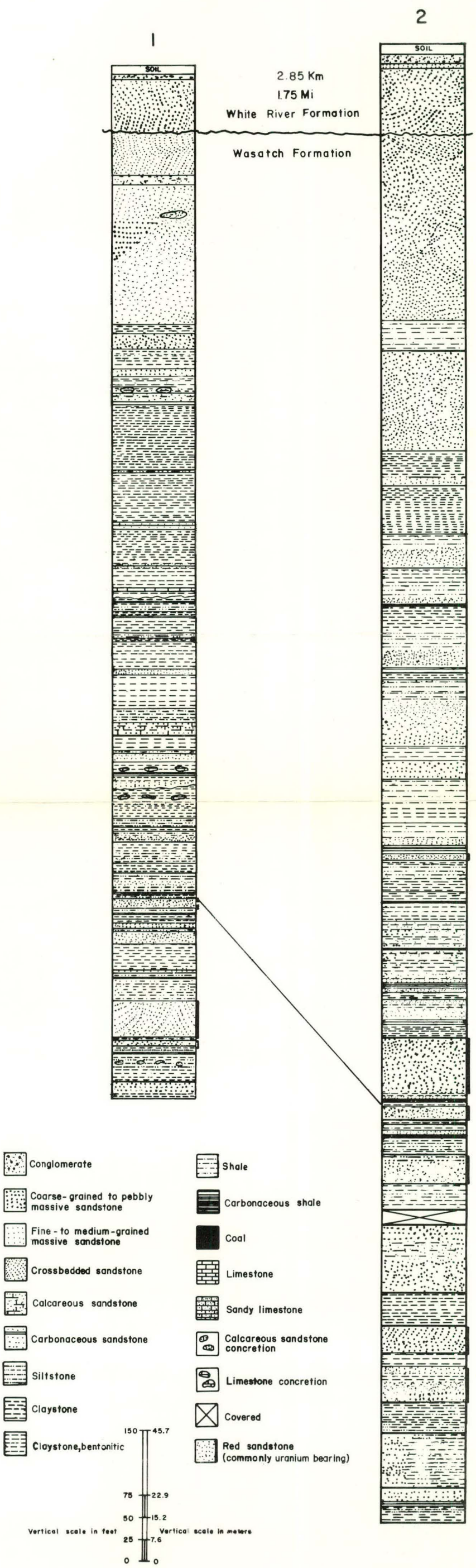

Plate 1

Adapted From Love, 1977, Unpublished Report

URANIUM ALTERATION MAP

INTERPRETED FROM ENHANCED AERIAL PHOTOGRAPHY

R 76 W R 75 W R 74 W

T46N

T45N

T46N

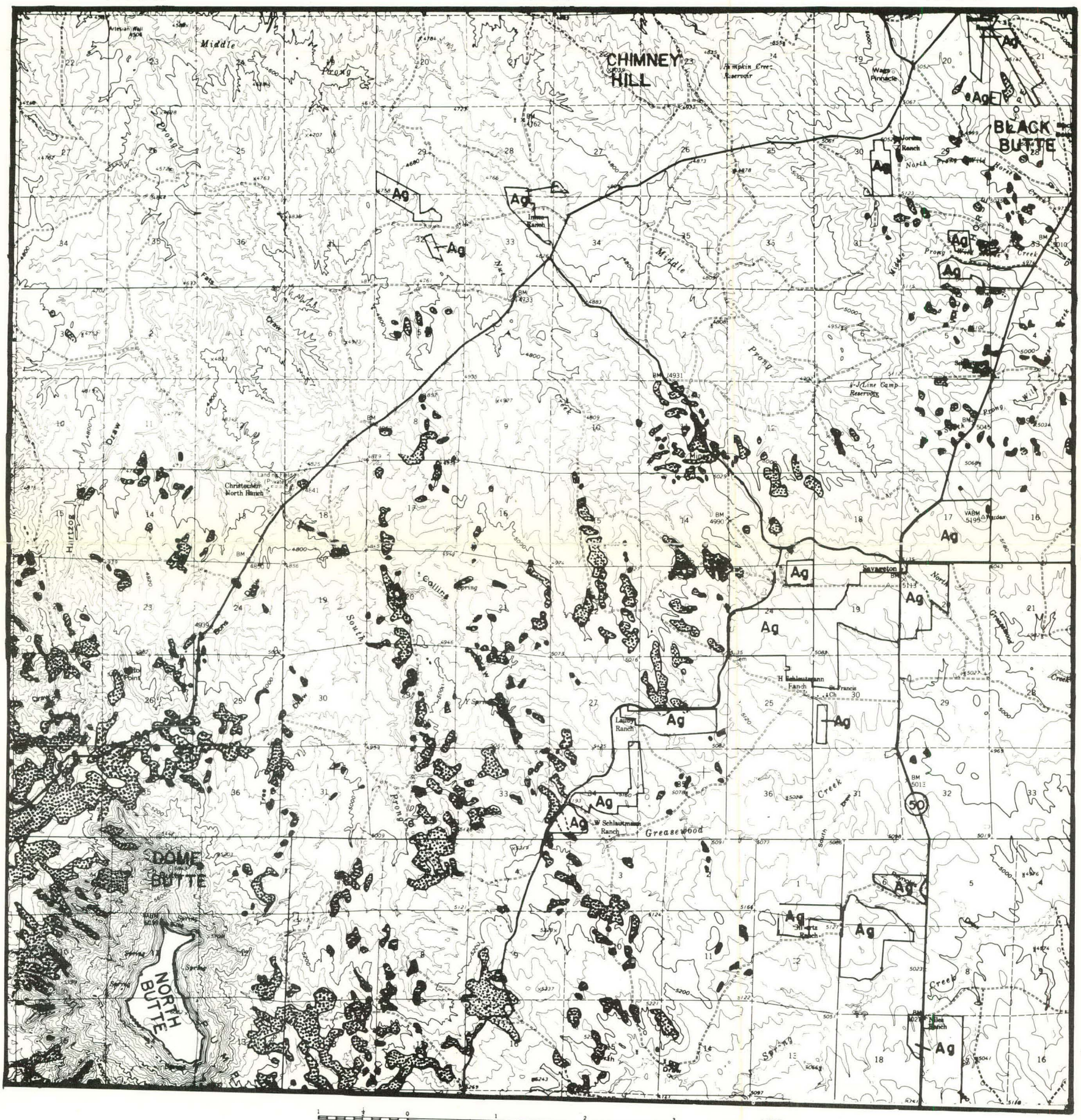

URANIUM ALTERATION
Ag AGRICULTURE

Plate 2
R. Levinson, 1979

APPROXIMATE MEAN DECLINATION, 1959
15°
TRUE NORTH
MAGNETIC NORTH

4 MILES
21000 FEET
5 KILOMETERS

CONTOUR INTERVAL 40 FEET
DATUM IS MEAN SEA LEVEL

Base and Topographic Contours from Savageton, Wyo. Quadrangle USGS 15 Minute Series Topographic Map

WYOMING
QUADRANGLE LOCATION

ROAD CLASSIFICATION
Light-duty ——— Unimproved dirt - - - - - -

Interpreted from Video Enhanced Aerial Photograph NASA MISSION 72-138 Line C-D, FRAME 4736 August 11, 1972, Color Infrared